Numerical Prediction of Ship Manoeuvring in Regular Waves by a 2.5D Approach

by

Shi He

A thesis submitted in fulfillment of the requirements for the degree of

Doctor of Philosophy

Department of Naval Architecture & Marine Engineering

Universities of Glasgow and Strathclyde

May, 2017

This thesis is the result of the author's original research. It has been composed by the author and has not been previously submitted for examination which has led to the award of a degree.

Signed: Date:

Abstract

This thesis intends to study the manoeuverability of a single ship advancing in regular waves which is believed to be important for ship navigation safety as the situation is much more common experienced by a seagoing ship in real seaways instead of the calm water environment for traditional manoeuverability analysis.

For this purpose, a so called two time scales model is applied to study the problem, according to the difference of the motion frequencies between the two involved sub-problems. That is to say, the total ship motions are consist of two parts, namely the wave induced motions analysed in a rapidly varying time scale system and the manoeuvring motions associated with a slowly varying time scale system. The two systems exchange data with each other at specific time intervals to reflect the interaction between two sub-motions. By this means, the analysis for an advancing ship executing a maneuver in waves can be achieved.

To make concrete analysis of the sub-problems, a boundary element method (BEM) based on the 2.5 dimensional (2.5D) potential flow theory is adopted to solve the 5 degrees of freedom (DOF) rapidly varying wave induced motions, i.e., the seakeeping problem of slender ships advancing at speeds from moderate to relatively high is determined by interactively solving the discrete boundary integrate equation, kinematic and dynamic boundary conditions on the free surface in cross sections from bow to stern in time domain. Besides, this method is also used for the estimation of the manoeuvring derivatives required by the manoeuvring analysis. A numerical scheme called Multi-Transmitting Formula (MTF) is imposed on an artificial boundary to satisfy the radiation condition. The lift force, regarded as a consequence of the 3 dimensional (3D) flow effect which is important to manoeuvring motions but normally be neglected in the 2.5D theory, is taken into account for the evaluation of the total hydrodynamic forces acting on the ship during lateral motions. Furthermore, Non-Uniform Rational B-Spline (NURBS) is used for modelling the body plans of the ship and expressing the unknown quantities on the boundary elements to give more accurate and smoother solutions for the boundary value problems (BVP). To validate

the established numerical tool, computations are carried out on a WigleyIII hull, a Series 60 hull and a container ship S175 hull respectively. The results are compared with the available experimental data.

Regarding the manoeuvring motion simulations, the model is established based on the modular concept proposed by the Japanese Mathematical Modelling Group (MMG). The forces and moments induced by the propulsion system, the rudder system and the nonlinear viscous effect are estimated separately by empirical formulae or directly obtained from experimental measurements. The mean second order wave drift force is determined by direct pressure integration depending on the solved linear velocity potential from the seakeeping module. Simulations of the standard free running maneuvers, namely turning circle motion and Zig-zag motion, are carried out on the S175 ship in calm water and different regular waves successively. The results are compared with experimental measurements for validation which demonstrates that the present numerical tool can reasonably predict the manoeuvring motions of a slender ship in regular waves.

Key words: manoeuvring in waves; two time scales; 2.5D theory; NURBS; MMG

Acknowledgement

First of all, my deepest gratitude goes to my supervisor, Prof. Atilla Incecik, who gave me the opportunity to study in this famous department with the longest history in our field. This thesis is finished under his constant encouragement and guidance with strong support academically and financially, especially in the final writing up stage. Moreover, he is an example of hard working that every student in our department should follow.

Secondly, special thanks also go to Prof. Zao-jian Zou who led me into this research field in my master stage. He and his research group have kept on giving me advice and academic support on my subject through the years.

Thirdly, I want to extend my acknowledgment to all colleagues of the department, particularly Dr. Zhi-liang Gao, Dr. Wei Jin, Dr. Zhi-ming Yuan and Dr. Ai-jun Wang, for their valuable suggestions towards the specific problems of my subject after innumerable discussions as well as their sincere friendships with me in my daily life.

In addition, as the second most important staff next to our supervisors, Mrs. Thelma Will has given her meticulous care and assistance to every postgraduate student for any issues regarding our studies since the application stage even before we came to Glasgow. Many thanks also go to Ms. Susan Pawson who has done a very good job as well after Mrs. Thelma Will's retirement.

Finally, this thesis is dedicated to my father Prof. Renyi He and my mother Mrs. Shuping Mao, who brought me to this wonderful world and always accompany with me to overcome any difficulties without a word of complaint.

This work was funded by CSC of the Chinese government. I gratefully acknowledge this financial support.

Table of Contents

List of figures

List of tables

Nomenclature

General Rules

- Symbols are generally defined where they first appear in the text.
- Only the most used symbols are listed here.
- Sometimes the same symbol is used to indicate different things in different cases..
- Vectors are represented by introducing a right arrow above the symbols.

Abbreviations

2D	Two dimensional
2.5D	Two and a half dimensional
3D	Three dimensional
BEM	Boundary Element Method
BVP	Boundary Value Problem
CAD	Computer Aided Design
CFD	Computational Fluid Dynamics
COB	Center of Buoyancy
COG	Center of Gravity
DOF	Degree of Freedom
MMG	Mathematical Modelling Group
MTF	Multi-Transmitting Formula
NURBS	Non-Uniform Rational B-Spline
RAO	Response Amplitude Operator

Subscripts

H, P, R, W	Hull, propeller, rudder, wave, respectively
i	Serial number of the control point in NURBS expression
$j = 0;1,...6;7$	Mode of the 6-DOF motions; 0 denotes no hull exists, 7 denotes the hull constrained
kj	Correspond to the variable in k-th direction due to the motion in j-th mode
x, y, z	Spatial derivative in the corresponding direction

Superscripts

$p-1, p, p+1$	Time index
0	Initial values for time $t = 0$
$(0),(1),(2)$	Zero, first and second order magnitude

Roman Symbols

A	Incident wave amplitude
A_R	Rudder area
A_W	Water plane area
A_{kj}	Added mass of the whole ship in the k-th direction per unit oscillatory displacement in the j-th mode
a_H	Rudder force increase factor
a_{kj}	2D sectional added mass in the k-th direction per unit oscillatory displacement in the j-th mode $(k, j = 2,3,4)$
B	Ship breadth
$B(x)$	Local sectional beam
B_{kj}	Damping coefficient of the whole ship in the k-th direction per unit oscillatory displacement in the j-th mode

B_{44_e}	Equivalent roll damping coefficient
b_{kj}	2D sectional damping coefficient in the k-th direction per unit oscillatory displacement in the j-th mode $(k, j = 2,3,4)$
C_A	Aftermost cross section
C_B	Block coefficient
C_M	Midship section coefficient
C_P	Prismatic coefficient
C_{angle}	Prefixed heading angle difference limit
C_f	Friction coefficient
C_{kj}	Restoring coefficient in the k-th direction per unit oscillatory displacement in the j-th mode $(k, j = 3,4,5)$
D	Ship draft
D_P	Diameter of the propeller
$\vec{F}$	Total hydrodynamic force
F_D	Diffraction force
F_I	Froude-Kriloff force
F_R	Radiation force
F_S	Hydrostatic restoring force
F_N	Rudder normal force
F_n	Froude number $U/\sqrt{gL}$
$f_{2.5}$	Correction ratio factor for 2.5D approach result
f_α	Rudder lift gradient coefficient
$\overline{GM_L}$	Longitudinal metacentric height
$\overline{GM_T}$	Transverse metacentric height
g	Acceleration of gravity

H_R	Rudder height
H_{kj}	Hydrodynamic force in the k-th direction per unit oscillatory displacement in the j-th mode
I_{xx}, I_{yy}, I_{zz}	Moment of inertia of ship with respect to the axis that the subscript shown
J_P	Advanced ratio
K_T	Thrust coefficient
$L\left(L_{PP}\right)$	Ship length (between perpendiculars as default value)
L_{WL}	Length of the design waterline
m	Ship mass
m_x, m_y, J_{xx}, J_{zz}	Added masses and added moment of inertia in manoeuvring motions with respect to the axis that the subscript shown
$\vec{n}$	Boundary normal vector positive outward the fluid
n_P	Propeller revolution, rps
$(O-xyz)$	Cartesian right-handed hydrodynamic coordinate system
$(O'-x'y'z')$	Cartesian right-handed manoevuring body fixed coordinate system
$(O_0-x_0y_0z_0)$	Cartesian right-handed Earth fixed inertial coordinate system
P	Propeller pitch; field point
p	Hydrodynamic pressure; roll rate
$\tilde{p}$	Amplitude of hydrodynamic pressure
p_a	Atmospheric pressure
p_S	Hydrostatic pressure
Q	Source point on the bounday
$R(u)$	Resistance of the ship in straight moving
r	Yaw rate

r_{ij}	Distance between the source point and field point
S^*	Instantaneous wetted surface
S_0	Mean wetted surface
S_F	Free surface
$S_L \, or \, S_R$	Open boundary surface
$S_x(t)$	Underwater contour of the section corresponding to time t
t	time
t_{p0}	Thrust deduction factor
t_R	Steering resistance deduction factor
U	Mean forward speed
U_R	Resultant inflow velocity to rudder
u	Longitudinal velocity component; parameter of B-spline
v	Lateral velocity component
w_P	Wake coefficient
w_{P0}	Wake coefficient when the ship advancing straightly
w_R	Wake coefficient at rudder position
X, Y, K, N	Surge force, lateral force, roll moment and yaw moment
x_H	Longitudinal coordinate of acting point of the additional lateral force component induced by steering
x_P	Longitudinal coordinate of propeller position
x_R	Longitudinal coordinate of rudder position
x_0, y_0	Global position of the ship
y, z	Coordinates of a field point in cross plane
z_B	vertical coordinate of the center of buoyancy

z_G	vertical coordinate of the center of gravity

Greek Symbols

α	Angle of attack
β	Drift angle of the ship
γ	Vortex distribution
γ_R	Flow straightening coefficient
Δ	Value difference
δ	Rudder angle
ε	Slenderness parameter; ratio of wake friction at propeller and rudder positions
ζ	Free surface elevation in 3D flow
ς	Equivalent free surface elevation in 2D cross section
η	Incident wave angle; ratio of propeller diameter to rudder height
Θ	Downwash angle
θ	Pitch angle; wave propagation direction angle of transverse wave
Λ	aspect ratio of the rudder
λ	Incident wave length
ν	Viscosity coefficient
$\vec{\xi}$	Radius vector from the centroid to an arbitrary point on the hull
ξ_j	Amplitude of the j-th mode motion
ρ	Mass density of the fluid
τ	Brard number defined as $\tau = U\omega_e / g$
Φ	Total velocity potential

Φ_S	Steady flow velocity potential
Φ_T	Time dependent velocity potential
ϕ	Generalized disturbance velocity potential; roll angle
ϕ_D	Diffraction potential
ϕ_I	Incident wave potential
ϕ_R	Radiation potential
ϕ_j	Radiation potential due to unit motion in the j-th direction
φ_j	Equivalent velocity potential in 2D cross section $(j = 2,3,4)$
χ	Ship wave encounter angle
ω_e	Frequency of encounter
ω_0	Incident wave frequency
ψ	Heading angle

Special Symbols

$\lvert\ \rvert$	Absolute value
∇	Displaced volume; vector differential operator
$\times$	Vector product
$[\ ]$	Matrix; closed interval

1 Introduction

1.1 Background and motivation

When designing and building a ship, there are six aspects of navigation performances that need to be evaluated in the framework of hydromechanics, namely, buoyancy, stability, insubmersibility, rapidity, seakeeping and manoeuverability. According to the motion state of the ship, the studies on these hydromechanical problems can be classified into two groups. The former three performances (buoyancy, stability and insubmersibility) of a ship are the subjects of ship hydrostatics depending on the submerged volume of the ship, while ship hydrodynamics dependent on the sailing speed covers the other three (rapidity, seakeeping and manoeuverability). It is generally known that the development of ship hydrostatics has a long history since the advent of the ship in ancient times. Related theories were established step by step based on the Archimedes' principle described in the work, *on floating bodies*, written around 250 BC. To the present, ship hydrostatics has been well developed and relevant methods are mature enough to give satisfactory evaluations of ship's buoyancy, stability and insubmersibility in practice. By contrast, the development in the field of ship hydrodynamics has not progressed to the same extent yet. Therefore, more efforts should be made to the hydrodynamics problems studies since ship's performances in moving state are what we are more concerned about in transportation of passengers and cargoes.

Broken down further, the ship resistance and propulsion deciding ship's rapidity are normally the subjects when the ship is advancing straightly with a constant speed in still water therefore can be considered as steady problems, whereas the seakeeping and manoeuvring problems are regarded as unsteady ones which are generally thought to be more complex. To be specific, seakeeping performance represents the ability of a seagoing ship to carry out particular missions in a given sea condition, speed and heading. The wave environment will not only affect the effectiveness of the ship in attaining its mission, but may also put the ship in danger of structural damage even capsizing. On the other hand, ship's manoeuverability is the ability of a ship to keep

or change its state of motion under the control actions, i.e., keeping the straight ahead course with constant speed for lower fuel consumption purpose, or changing the speed, the course and the position of the ship to avoid obstacles appearing on its routes, according to the intention of the helmsman. By these definitions, it is quite clear that both of the unsteady hydrodynamic performances are vitally important to navigation safety.

Fig. 1.1 Ship seakeeping (internet photo)

(a) *(b)*

Fig. 1.2 Ship manoeuvring (a) Zig-zag; (b) Turning (internet photos)

However, in the past, less attention has been paid to seakeeping and manoeuverability than the other four performances at the draft stage of ship design. This is not only because of the different complexity levels of relevant problems, but also due to the requirements proposed by the ship owners from an economic standpoint. Especially

for the manoeuverability, verification of this performance is often carried out after the design stage, even until the ship has been constructed. Accordingly, the improvement of manoeuverability would be very limited which brings potential risks of collision, etc. For instance, if somehow the manoeuverability is overestimated based on the original construction of the ship, in particular the rudder control and response characteristics, the developed situation may lead to the point of no return in time even if an extreme rudder action is executed.

Looking back through the shipping history, there are spectacular shipwrecks resulting in severe loss of life and property and pollution to the environment, due to deficiency of manoeuverability and improper steering operations. At this point, everyone's first thought would be the most well-known *Titanic* passenger liner who is the largest and most secure cruise at the time she entered service. Although she was claimed to be unsinkable, she went down to the bottom of the North Atlantic Ocean due to colliding with an iceberg on her maiden voyage as reported by Young (1912) 37 days after the sinking. Of the 2224 passengers and crew aboard, more than 1500 died, making it one of the deadliest peacetime maritime disasters in modern history. According to the record, she sailed at her full speed ahead aiming to arrive in New York earlier. Consequently, the collision could not be avoided when the iceberg appeared in front of the ship even the engines were set in reverse to full astern with a tiller order of hard a starboard (an old British Merchant Navy steering order which was not phased out until 1933) directing the helmsman to turn the wheel to port (anti-clockwise) as far as it would go to attempt to clear the iceberg by swinging the ship to her port side. Apart from the lack of telescope and lifeboats, weak iron rivets, and communication barrier which are considered as the major causes to this disaster, it should be noted that the ship's manoeuverability, to some extent, is not good enough to change the course at a relatively high speed in case of emergency.

In the near decades, the deficiency of manoeuverability still threatened the navigation safety. In 1999, a Chinese Ro-Ro ferry *Dashun* capsized after a series of manoeuvers on the way back to the port when encountering severe weather in the Yellow Sea. As cited by Ma (2007), the ferry tried to keep a straight course instead of moving on a Zig-zag route which led to a large amplitude (30 degrees) roll motion around a 15 degrees of heeling angle in the beam sea. Together with the steering engine failure

due to the fire induced by the movements of the vehicles carried inside, the ship finally capsized after letting go port anchor during the drifting in wave. Obviously, unlike the calm sea state the *Titanic* sailed in, this is a typical case of a ship manoeuvring in waves which implies improper steering operations will not only lead to an undesirable course but also result in decrease of seakeeping performance and then further affect the manoeuverability in turn. That is to say, there exists coupling effect between the manoeuvring motion and the wave induced motion which is the main task of the present study and will be described in more detail later. Other more recent shipwrecks, such as the oil tanker *Cosco Busan* collided with the pier of the Bay Bridge resulting in serious oil spill to the sea in 2007 and the sensational Korean motor vessel *Sewol* capsized with nearly 300 people deaths in 2014, are all closely connected to the steering and manoeuvring problems. According to rough statistics given by Xia & Fan (2008), about 40% of shipwrecks are related to the deficiency of manoeuverability.

In order to improve the situation and prevent more disasters occurred in future, the International Maritime Organization (IMO) started to propose the evaluation criteria of ship's manoeuverability since 1982. Relevant guidelines and standards were issued and adopted to make explicit quantitative requirements on ship's manoeuverability in 1985, 1993 and 2002 successively. A questionnaire survey carried out by the Manoeuvring Committee of the 24th International Towing Tank Conference (ITTC) reported that approximately half the respondents regarded the IMO resolution as mandatory for conventional ships. Besides, due to the adoption of IMO manoeuvring standards, the number of cases regarding ship's manoeuverability was increasing rapidly, and 80% among ship builders noticed an increased awareness for manoeuvring issues. On the other hand, Computational Fluid Dynamics (CFD) and Experimental Fluid Dynamics (EFD) techniques have been promptly developed in the recent decade with the usage of more advanced computers and modern experiment equipment, thereby greatly strengthen the research means for designers. In these circumstances, motivation on studying ship's manoeuverability received a big boost and it comes to a conclusion that assessment of manoeuverability should be made at the design stage prior to ship construction as well as other performances.

Traditionally, ship's manoeuverability is evaluated in calm water as the IMO standards based on. Admittedly, this evaluation is essential and valuable, and even enough for a ship navigating in port areas or inland waterways. However, for a seagoing ship, its manoeuvring performance on a given route in the open sea or exposed coastal areas may be significantly affected by the presence of environmental forces due to waves, wind and tidal currents. Recalling the *Dashun* shipwreck mentioned before, these environmental factors did present during the voyage. Hence the ship can be subjected to additional forces which might be of considerable magnitude. Among of them, wave effects are perhaps the most important since moderate values of this phenomenon can result in large magnitude of forces and moments. In this case, corresponding steering operations should be executed to maintain a desired heading in a seaway which may induce large ship motions and a variation of the wetted surface, even the dangerous scenarios such as propeller and rudder emergence. Moreover, due to increasing added resistance in waves and reducing propulsive efficiency, an involuntary speed loss can be experienced during the manoeuvers which is also undesirable from economy aspect. As a consequence, the trajectory of the ship will be quite different from the expected one in calm water. On the other hand, the wave force direction and the encounter frequency are varying with the incident wave angle, thereby the seakeeping performance is also affected during manoeuvers. In a word, a ship navigating in a seaway implies a more complex problem and requires some insight into the fluid phenomena acting upon the ship. The fluid effects involving the viscous and the potential contribution and, the nonlinear behaviour as a result of the rigid body motions, increases the complexity of the problem. The assumptions taken into account for the manoeuvring in calm water and seakeeping analysis might not be applicable, at least not directly. Therefore, in order to solve the ship dynamics while manoeuvring in a seaway, a method must be sought that investigates both performances conjunctly.

In fact, the topic of the manoeuvring motions in waves has been raised and discussed since a few decades ago. However, research on this problem was hobbled due to its much more complexity than the two separate ones and the limit of the discipline level in the early period. With the rapid development of ship hydrodynamics and relevant techniques in recent years, substantial progress has been achieved. And the ITTC has

also put this combined problem in a list of subjects with special care in 2011 and 2014, which means it is a leading edge topic at present.

As long as in the scope of mechanics, the subject can always be studied by conducting experiments, i.e., full scale trials which can provide most accurate results directly. However, these results are the important criterion for the delivery of the newly built ship, thereby does not meet the premise of being carried out prior to the ship construction in the design stage. Therefore, conducting series of model tests is the common option until now even it suffers the so called scale effects which will also be mentioned in the next chapter. In order to further reduce research cost, and to maximum extent eliminate the scale effects and experimental errors during repeating the tests, adopting a numerical approach with the advantage of modern computers is an effective alternative for designers.

Moreover, with the tendency of the demand for high speed vessels, the knowledge and experience of traditional ships of relatively low speed would be not suitable for high speed vessels. Therefore, there is an urgent need to apply a practical method to study the dynamic behaviour of high speed vessels in a seaway.

Finally, in order to integrate with the actual ship construction, applying geometry modelling techniques into the hydrodynamic calculations is another research hotspot nowadays. Among them, Non-Uniform Rational B-Spline (NURBS) is a widely used tool from industrial design field which can fulfill the requirement and connect with Computer Aided Design (CAD) well. The present work is carried out based on the above background.

1.2 **Aims and Objectives**

In brief, the main objective of the present work is to predict the manoeuverability of a single ship advancing in regular waves numerically. The water depth is assumed to be infinite and the navigation area has infinite horizontal extent which means shallow water and bank effect are not taken into account here. Balance between the efficiency of simulation and the accuracy within the engineering practice is pursued in the development.

Specific objectives include the following:

- To establish a systematic model for the simulation of ship manoeuvring in waves which can combine the wave induced motions and the manoeuvring motions in calm water together and capture the interaction between the motions.

- To formulate a numerical approach addressing the seakeeping performance of slender ships advancing in a seaway suitable for application to speed range from moderate to relatively high.

- To connect with CAD in ship structural constuction by applying a practical modelling technique for precisely expressing ship geometry and integrating it into the developed seakeeping analysis tool.

1.3 Outline of the thesis

In Chapter 2, a detailed literature review of previous studies on the seakeeping and manoeuvring problems respectively as well as the combined problem is presented. The review also introduces previous works on the application of spline modelling techniques in the field of hydrodynamic calculations by BEMs.

In Chapter 3, according to the objectives of the present study, the adopted approach is outlined based on the literature review, followed by presenting the innovations.

In Chapter 4, an numerical approach mainly for the seakeeping analysis to determine the hydrodynamic forces acting on an advancing ship with relatively high speed is developed, together with the equations of ship motion responses in regular waves been established. The numerical schemes to solve the boundary value problems are detailed, including discretization formats and processing of deterministic conditions. Besides, viscous correction and solutions for low frequency lateral motions are presented as the obtained hydrodynamic derivatives are required in the manoeuvring analysis. Special attention is also paid to the lift effect generally negligible in vertical motions whereas is important to lateral motions associated with the manoeuvring.

In Chapter 5, an extension of the numerical scheme for the solutions of the BVPs described in Chapter 4 is made by introducing a spline modelling technique to form the contours of the geometries for the purpose of better integrating with ship structural construction and improving the accuracy of the results. Verification and validation of the geometry modelling module are carried out on a circle and several selected ships. Then validations of the completed seakeeping analysis module are carried out on the selected ships by calculating series of hydrodynamic characteristic coefficients and comparing with experimental data or other numerical results available in published literature.

In Chapter 6, a combined mathematical model involving the manoeuvring motions and the wave induced motions is applied for the analysis of a ship manoeuvring in regular waves based on the fact that the manoeuvring and steering control actions typically occur at a much lower frequency than the important linear wave encounter frequencies. The derivation of the motion equations in the established coordinate systems is given in detail. Forces and moments acting on the ship are estimated by proper methods, including the hydrodynamic wave loads dependent on the wave induced motions solved in seakeeping analysis. After that, the flow chart of the whole simulation system for a single slender ship manoeuvring in regular waves is presented. Simulations are carried out on one selected ship and compared with available results for validation, together with the parameter studies to analyse the wave effect on the manoevring motions.

Finally, in Chapter 7, the conclusions drawn from the present work are summerized including the major achievements and conclusions, eventually the perspectives for further studies are proposed.

2 Literature review

As mentioned before, to investigate a single ship manouevring in waves, two sub-problems, namely the low frequency manoeuvring in calm water and high frequency seakeeping problem, should be taken care of in advance. Therefore, in this Chapter, previous work and progress on these two sub-problems will be reviewed successively. Application of the spline modelling technique in the hydrodynamic calculation is also introduced. Finally, an overview of the state of the art relavant to the prediction of the manoeuvring behaviour of ships in a seaway is presented.

2.1 Previous works on manoeuvring problems in calm water

2.1.1 Introduction of manoeuvring prediction

Investigation of ship manoeuverability in calm water conditions was initiated during early 1960s. Norrbin (1960) gave a review of the state of the art of scientific work carried out on manoeuverability of ships in that time. Since then, an increasing attention has been paid on research in this particular field gradually. Consequently, several theoretical and experimental methods have been developed and improved through the use of more refined techniques, comparisons between different methods, and parametric studies. Generally, there are four categories of methods for this prediction at the design stage, which are the method of conducting free running model tests, the estimation method based on data base or regression formulae, computer simulation of manoeuvring motions using mathematical models, and numerical prediction based on CFD technique.

Free running model tests are usually conducted with scaled models in indoor basins or sheltered outdoor lakes, thereby the limited size of water area makes it difficult for manoeuvring tests of high speed vessels at their maximum operating speeds. In the tests, the standard manoeuvers are performed on the model and the parameters evaluating its manoeuvring characteristics are measured from the test records. Hence, this method is the most direct way for prediction and regarded as the most reliable method. For example, in the recently held special workshops on the verification and

validation of ship manoeuvring simulation, SIMMAN (2008, 2014), plenty of free running model tests had been carried out on several ship types, e.g., KCS, KVLCC, DTMB 5415 etc. by different organizations and the measured results can be used as valuable benchmarks for manoeuvring simulations and related comparative studies. Besides, a recommended procedure and guideline for conducting free running model tests was proposed by the manoeuvring committee of the 27th ITTC (2014). However, this method is time consuming and costs a lot of money to build the model after all. And it is inconvenient for application at the design stage since series of model tests are usually needed to be repeated. Moreover, it should be noted that due to the so called scale effects, there usually exists a distinct difference of performance between the model and the full scale ship as pointed out by Qudvlieg &Tonelli (2015).

Similarly, the estimation method based on data base or regression formulae also rely on large number of model tests or full scale trials of similar parent ships, then results are gathered from these tests to derive a data base containing the characterized parameters of manoeuverability or establish regression formulae to estimate these parameters as functions of ship particulars. Representative works can refer to Lyster & Knights (1979) and Haraguchi (2000). Although this method would be very efficient once the data base obtained, it is quite limited for new type ship construction since lack of accurate data.

2.1.2 Computer simulation using mathematical models

With the rapid development of the computer technology and its successful application in ship engineering, the third category of methods, i.e., computer simulation using the mathematical models becomes more and more popular. It provides a convenient way for predicting ship manoeuverability in the design stage. By considering the ship as a rigid body, this category of methods need to establish a dynamic system to simulate the motions under external forces including the components on the hull, the propeller and the rudder, which are collectively known as the manoeuvring hydrodynamic forces. Normally, these hydrodynamic forces are determined indirectly by obtaining a series of corresponding coefficients in the models through experiments or theoretical calculations. Compared to the former two methods, the advantages of this method are it is more convenient to conduct particular model tests to obtain the coefficients and the contribution from each force component to the manoeuvring motion with its

changing rule can be better analysed. There are two main types of mathematical models for the manoeuvrability analysis, namely response models and hydrodynamic models.

In the response models, the motion equations are transformed into the expressions of which the motions are the response to the value of control parameters such as rudder angle. In this way, the coefficients in the transformed motion equations reflect the characteristics of the manoeuvring hydrodynamic forces and can be derived from particular model tests. The initial model of this concept was first proposed by Nomoto et al. (1956). They carried out Laplace transform to derive the transfer function between yaw rate and rudder angle from the linear manoeuvring motion equations established by Davidson & Schiff (1946). After that, Nomoto & Taguchi (1957) summarized the first and second order linear response models respectively. For the first order linear response model, only two parameters K and T are contained which can be easily derived from Zig-zag motion tests. Although this model cannot give precise predictions for large amplitude manoeuvring motions, both of the parameters have definite physical meaning, and can be used to evaluate ship's manoeuverability directly. Thereby they are beneficial for qualitatively predicting and improving ship's manoeuverability. Based on the linear models, several nonlinear response models were developed later, such as Bech (1966), Clarke (1971), Matsumoto & Suemitsu (1981), which have been widely applied in ship control and autopilot design.

In contrast to the response models, the hydrodynamic models keep the original motion equations without transformation and solve the equations directly by obtaining the manoeuvring hydrodynamic forces contained in the equations. To be specific, the existing hydrodynamic models for manoeuvring problems studies can be essentially classified into two groups, which are the whole ship models or common called the Abkowitz models named after the introducer Martin A. Abkowitz, and the modular manoeuvring ship models or the so called MMG models, short for Mathematical Modelling Group, the proposer in the Japanese Towing Tank Conference.

The whole ship models were developed in the early stages of the manoeuvring simulation studies by Abkowitz (1964), Chislett & Strøm-Tejsen (1965) and later revised by Norrbin (1970). This kind of models represents composed manoeuvring

system where the total hydrodynamic forces and moments acting on the combination of hull-propeller-rudder, and are expressed as functions of the kinematic parameters and the rudder angle in a formal way using the perturbation analysis to expand the total hydrodynamic forces and moments into a series of the hydrodynamic derivatives through Taylor expansion of a function of several variables. Although the whole ship model is still very attractive to use due to the relatively simple series representation of the total hydrodynamic forces and moments, its applicability among the manoeuvring simulator facilities worldwide starts to show the limitations during 1980s. The limitations related to the difficulties in the comparison procedures between different modelling approaches led to the second group of mathematical models proposed by Japanese research group, namely the MMG models. Ogawa et al. (1977), Hamamoto (1977), Kasai & Yushitsu (1977) outlined the main concept of these modular manoeuvring simulation models. Afterwards, Kose et al. (1981), Inoue et al. (1981) and Kijima et al. (1990) presented the concrete models based on this concept and further improved them. Recently, Yasukawa & Yoshimura (2015) summarized the previous works and established the standard form of the MMG model with procedure for determining the hydrodynamic force coefficients required by the model to avoid inadaptability of hydrodynamic force data between different models.

The MMG model is a physically motivated model based on the modular concept by decomposing the total hydrodynamic force and moment into three parts, i.e., the parts acting on the hull, the propeller and the rudder respectively and evaluating them through a set of interactively connected modules. Each module is programmed as a separate unit which describes particular force and moment due to the hull, the propeller and the rudder, as well as the environmental forces and moments due to waves, wind and current if exist. The modules are linearly superimposed, so that the complete manoeuvring model in general can be easily modified according to the imposed requirements from a manoeuvring simulation.

2.1.3 Determination of hydrodynamic derivatives

Obviously, as the precondition to carry out the manoeuvring motion simulations, the hydrodynamic derivatives in both the whole ship model and the MMG model should be determined experimentally or theoretically. There are four basic methods for this

purpose, i.e., captive model tests, system identification technique, semi-theoretical and semi-empirical method, and numerical method.

Captive model tests are conducted with a scale model in ship model basins, where the models are forced to move in a prescribed manner. These tests include oblique towing test (OTT) in a conventional long and narrow towing tank, rotating arm test (RAT) in a rotating arm facility, the planar motion test using planar motion mechanism (PMM) in a long and narrow towing tank, and circular motion test (CMT) in a big towing tank or in a seakeeping and manoeuvring basin. By analyzing the forces and moments measured on the model, the hydrodynamic derivatives can be determined. Chislett & Strøm-Tejsen (1965) conducted PMM tests on a mariner vessel to obtain all the hydrodynamic derivatives based on the Abkowitz model, then applied these derivatives to carry out standard manoeuvring simulations on this mariner vessel including turning, Zig-zag and spiral manoeuvers, and the results show good agreement with the full scale trials measurements. Norrbin (1970) also conducted captive model tests such as OTT and RAT to obtain the derivatives based on a whole ship model proposed by himself, then carried out Zig-zag and spiral manoeuvers simulations on a 98000 deadweight ton (DWT) tanker. The results also show satisfied agreement with the full scale trials measurements. On the basis of existing test procedure, Kose & Kijima (1977) gave a recommended procedure for captive model tests based on a MMG model. Inoue (1981) followed the procedure to carry out a series of captive model tests on 10 different types of ships in different ballast conditions, and gave regression formulae for linear hydrodynamic derivatives based on ship's principal dimensions. As the container and ro-ro ships have small transverse metacentric heights which leads to relatively large heeling angles in turning motions, the roll coupling effect on manoeuvring should not be neglected. Son & Nomoto (1982) established a 4-DOF MMG model and carried out captive model tests on a SR108 container to obtain corresponding hydrodynamic derivatives. Simonsen (2004) summarized the procedure for captive model tests and presented a method of uncertainty analysis for the tests. In addition, the previous mentioned workshops SIMMAN (2008, 2014) also provided numerous results of captive model tests on the same selected ship types in free running model tests for manoeuvring simulations.

Although captive model tests are considered to give reliable results of derivatives, special experimental facilities are often unaffordable to many designers, and it should be noticed that captive model tests also suffer scale effects as the free running model tests, so extrapolation corrections are usually needed. For these reasons, several researchers applied system identification techniques to obtain the hydrodynamic derivatives based on full scale trials. For example, Abkowitz (1980) and Hwang (1980) applied Kalman filter technique to obtain the derivatives using the full scale trial results on the *Esso Osaka* oil tanker. Yoon & Rhee (2003) applied a so called estimation before modelling technique to identify the derivatives of the *Esso Osaka* oil tanker and a *113K* oil tanker based on a modified Abkowitz model. Again, since the full scale trials are available after the construction of the real ship which is the obstacle to the studies in design stage, Zou and his research team carried out identification work to determine the derivatives from free running model tests by system identification methods, such as Luo & Zou (2009), Zhang & Zou (2011), Wang et al. (2014). Not only these works obtain valuable hydrodynamic derivatives of ship models, but also provide references for further improvement of the manoeuvring mathematical models and correction due to scale effect.

The hydrodynamic derivatives can also be determined by semi-theoretical and semi-empirical methods, including the methods of data base and the estimation methods using semi-empirical formulae. Systematic captive model tests still need to be conducted, and the data of measured hydrodynamic force and moment are to be gathered, from which a data base or semi-empirical formulae can be derived based on the main particulars and other ship form coefficients. Then the data base and the semi-empirical formulae can be used to estimate the hydrodynamic derivatives in the equations of motion conveniently. Obviously, this method has the same disadvantage as the previous mentioned manoeuvring performance estimation method by data base or regression formulae which is limited to the data of ship types already existed. The common used formulae for linear hydrodynamic derivatives estimation were given by Inoue (1981) and Clarke et al. (1982). Furthermore, Zhou et al. (1983), Kijima & Nakiri (1999), Kijima (2003), Aoki et al. (2006), Furukawa et al. (2008) presented the formulae for the nonlinear hydrodynamic derivatives estimation based on the two widely used hydrodynamic decomposition expressions proposed by Inoue (1981) and

Kijima (1990). Note that there is another recommended hydrodynamic decomposition expression of the 3rd order polynomial function through Taylor series expansion as presented by Yasukawa & Yoshimura (2015) in the MMG model standard procedure. Although this 3rd order polynomial function expression is believed to be superior to the other expressions in the view of estimation accuracy pointed out by Matsumoto & Suemitsu (1980), it is hard to give regression estimation formulae for the nonlinear derivatives since the correlations between the derivatives and ship form coefficients are not prominent.

2.1.4 Numerical methods for manoeuvring prediction

In the aspect of theoretical calculation, simple analytic methods based on potential theory such as such as the low-aspect-ratio wing theory introduced by Bollay (1939) and the slender body theory originated in the field of aerodynamics were applied to ship manoeuvring problems for qualitative analysis in earlier studies by Inoue (1956), Fuwa (1973) and Newman (1977), respectively. For the purpose of improving the accuracy, there is an increasing trend to apply numerical methods in the calculations with the development of computer technology since 1980s. In such a situation, two categories of numerical methods were initiated. Based on the chosen manoeuvring mathematical model, the first category still need to carry out specific simulations of selected forced manoeuvring motions for calculating the hydrodynamic forces and moments acting on the hull and then to determine the corresponding manoeuvring derivatives of the model. Since the viscosity of the fluid is the essence of generating the hydrodynamic forces acting on the ship in manoeuvring motions, it is important to reflect this viscous effect directly or indirectly in the numerical calculations. For instance, Wellicome et al. (1995) developed a method based on the slender body theory applying source elements and discrete vortices together with a vortex shedding model to calculate the sway force and yaw moment on three ships in oblique motion. On the other hand, Nakatake et al. (1990) proposed a panel method by utilizing a Rankine source distribution on the hull surface and a part of the free surface and a distribution of Rankine type vortices on the center plane of the ship to iteratively solve the lifting flow problem of a drifting Wigley hull. A similar method using Rankine singularities was also presented by Zou & Söding (1994) for conventional ships in steady motion at small drift angles. Meanwhile, Yang et al. (1994) developed

a panel method combined with a wake vortex model to calculate the hydrodynamic forces acting on an obliquely sailing ship with helm angle, in which the mutual interaction among hull, propeller and rudder was taken into account. Matsui et al. (1994) continued their work by using the developed panel method to calculate flow around a hull and the hydrodynamic forces upon it in turning motion. Two shapes of free vortex models were examined to discuss the influence on the efficiency and accuracy of the method. Later on, Ando et al. (1997) applied a simple panel method without iterative procedure by distributing source elements on the hull surface and discrete vortex on the center plane of the hull similar to the distribution adopted by Nakatake et al. (1990) to estimate the hydrodynamic forces acting on three ship models in oblique towing. Nakatake et al. (2001) synthesized the methods by Matsui et al. (1994) and Ando et al. (1997) to carry out the calculations on the flow field around ship hulls in oblique and turning motions. In addition, Kijima & Takazumi (2000) utilized a cross flow model to estimate the hydrodynamic forces acting on a hull in lateral motion. Apparently, all the above mentioned approaches based on the potential flow theory approximate the viscous effect indirectly by considering the effects of vortex. More specifically, for small amplitude manoeuvring motions in which the flow separation can be neglected, circulation was introduced in the model to fulfill certain Kutta condition imposed along the trailing edge of the hull, whereas vortex shedding model or cross flow model was applied for large amplitude manoeuvring motions.

In order to take the viscosity into account directly for further improving the accuracy, more advanced methods based on the viscous flow theory were developed to calculate the hydrodynamic forces and moments acting on the ship during selected forced motions by solving the Reynolds Averaged Navier Stokes (RANS) equations, e.g., Finite Volume Method (FVM), Finite Difference Method (FDM), and Finite Analytic Method (FAM), which are often simply referred to as CFD methods. Ohmori & Fujino et al. (1994, 1995, 1996 and 1998) successively reported a series of pioneering works in this field on the ships in oblique and turning motions. Since then, several similar studies were carried out by Hochbaum (1998), Toxopeus (2004), and Zou et al. (2010), etc. with the free surface neglected, whereas Alessandrini & Delhommeau (1998) and Tahara et al. (2002) took the free surface into consideration. Additionally,

the approach of conducting CFD based PMM tests to generate the hydrodynamic derivatives for manoeuvring prediction has been in development for the recent decade represented by Hochbaum (2006) and Simonsen et al. (2006, 2012). Furthermore, the dedicated benchmarking workshops mentioned previously, SIMMAN (2008, 2014), have greatly promoted the application of CFD methods on forced motion simulations.

With the further development of the CFD technique, the second category of numerical methods for manoeuverability prediction appeared which no longer need to carry out series of forced motion simulations for the estimations of the manoeuvring derivatives contained in the chosen mathematical model, but to simulate the flow field around the ship to obtain the hydrodynamic forces and moments acting on the ship in every time step, and then to solve the rigid body motion equations of the free running manoeuvring motions directly. The representative publications of this category were presented by Sato et al. (1999), Hochbaum & Vogt (2002), Carrica et al. (2006), etc. In contrast to the traditional prediction methods of the first category based on the manoeuvring mathematical models, the advantage of this direct CFD based simulation methods is that not only it can take naturally into account the viscous effects of the fluid but also capture the details of the complex flow field of the real time steering manoeuver around the hull with appendages, the wake in the propeller plane, and the nonlinear interaction effects in the hull-propeller-rudder configurations. However, due to the facts that the approaches have relative higher demand on computational resource, and there are still several technical details under further investigations such as the choice of the turbulence model and the accuracy of the simulation results at large drift angles, it makes the approaches still not mature enough for practical applications but mostly confined to the research communities as pointed out by Skejic (2013).

Finally, an overview of the existing manoeuvring predicition methods is illustrated in Fig. 2.1 summarized by ITTC (2005), while the major advantage and disadvantage of the most applied methods are briefly labelled in Table 2.1.

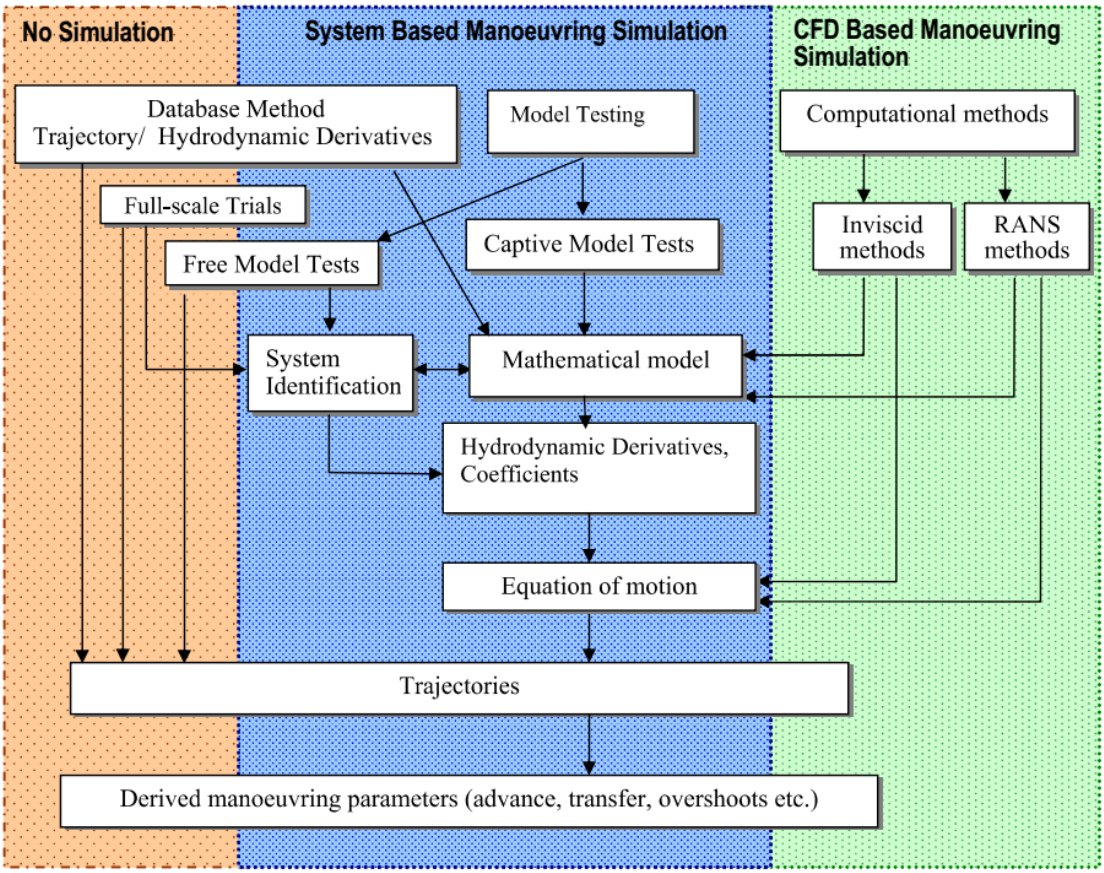

Fig. 2.1 Overview of manoeuvring prediction methods by ITTC (2005)

Table 2.1 Summary of manoeuvring prediction methods

Methods	Advantage	Disadvantage
Free model tests	Most direct	Scale effect; costly
Captive model tests	Systematic	Rely on experiment facility
Empirical	Fast; low cost	Inaccurate
System identification	Reduce scale effect	Rely on number of the tests
Potential flow	Mathematical rigour	Limit to small amplitude manoeuvers
Viscous flow CFD	Close to reality	Computational resource consuming

2.2 **Previous works on seakeeping problems**

For seagoing ships, investigation of ship motions in waves is another classic topic in ship hydrodynamics which people have realized its importance long time ago and tried to reduce the amplitude of ship motions, particularly rolling, by intuitive ways

according to experience. However, theoretical studies on seakeeping performance for a ship in a seaway started from the century before last one, and not much earlier than those on manoeuverability. Fortunately, bigger progress in this field has been made and the applications of theoretical methods are relatively extensive and successful. Therefore, only the related works of theoretical studies will be introduced here, in spite of that experimental methods are also available.

2.2.1 Potential flow theory methods

Since the middle of 19th century, with the advent of steamships without sail to provide sufficient air damping, larger amplitude of roll motion drew designer's attention to study the mechanism of the motion and seek measures for ship stabilization. Froude (1861) and Kriloff (1896) initially started the research work on ship's roll and pitch motions induced by waves respectively. In their works, the assumption, what is now called the Froude-Kriloff hypothesis, neglected the influence on the flow field due to the disturbance by the ship, but only kept the contribution of the exciting force due to the pressure distribution in the undisturbed incident wave. Thereafter, the part of the wave exciting force induced by the undisturbed incident wave is named as the Froude-Kriloff force, F-K force for short in the following. On the other hand, the neglected part of the exciting force is known as the diffraction force.

Series of theories have been developed for seakeeping problems studies gradually since 1940s. Based on the potential flow theory, most of the studies were carried out by establishing and solving the linear boundary value problems of the velocity potential around the ship with the disturbance by the ship been taken into account for more reasonable description of ship motions. It is worth mentioning the work by Haskind (1946) who made use of Green's theorem to construct the perturbation velocity potential due to the presence of a ship and its motions, then solved the resulting integral equation by adopting the thin ship idealization. In his analysis, within the framework of linear theory, the total perturbation velocity potential was decomposed into two components for the first time, which are the radiation potential due to the ship motions in still water and the diffraction potential due to the presence of the ship fixed on its average position. This decomposition was regarded as a classical way for linear seakeeping problems in the following decades until now. At

around the same time, Ursell (1949) also published his work by using a multiple expansion method to determine the hydrodynamic coefficients of semicircular cross sections oscillating in deep water in the frequency domain which marked for the first time a rough estimation could be made of the motions of a ship in regular waves at zero forward speed. Although these pioneering works gave exciting results, no matter the solutions based on the thin ship theory or the studied semicircular cross sections are much different from the actual ship transverse profiles, thus these methods could only be used for qualitative analysis of ship motions.

- ***Strip theories***

Two breakthroughs were achieved in studying the wave induced ship motions in 1950s. The first one is the work presented by St. Denis & Pierson (1953) who first proposed a method to predict the statistics of ship responses to a realistic seaway. Using spectral methods developed in applied mathematics, they established a relationship between the spectral density of ship responses and the input ocean wave spectrum. In this way, the studies of ship motions in regular and irregular waves can be linked to each other which makes the further development of the theories for ship motions in regular wave more meaningful. The second breakthrough is the original strip theory introduced by Korvin-Kroukovsky (1955) from parallel development in aerodynamics. In the theory, the ship is treated as a slender body and can be divided into several transverse strips, typically 20 to 30, which are rigidly connected to each other along the longitudinal direction of the ship. Interactions between the strips are ignored for the zero speed case. Therefore, each strip can be approximately treated as a segment of an infinitely long floating cylinder, and the flow field within each cross section around the strip can be solved by a two dimensional (2D) approach, which means in essence the original three dimensional (3D) problem is simplified and reduced to a set of 2D boundary value problems. Finally, the total hydrodynamic forces and moments acting on the whole ship are obtained by integrating the 2D solutions on each strip over the ship length. Later, Korvin-Kroukovsky & Jacobs (1957) refined the theory by taking the speed effect into account for vertical motions of a ship in head waves, while Tasai (1967) extended the theory to the lateral motions of a ship in oblique waves. In fact, the concept of the strip decomposition was first applied by Lewis (1929) in the study of a hull vibration at high frequency, in which the well-known Lewis two parameters conformal mapping was proposed for

analytical calculating the added mass of ship like sections. Nevertheless, it was Korvin-Kroukovsky's work that applied the strip theory in ship oscillation problem and drew widespread attention.

Since the ordinary strip theory was proposed mostly based on physical intuition without complete and rational derivation, there are some shortcomings in practical applications. For example, in spite of the speed effect been considered by Korvin-Kroukovsky & Jacobs (1957), the hydrodynamic coefficients obtained by this strip method do not fulfill the symmetric relation proved by Timman & Newman (1962). Moreover, in order to satisfy the free surface condition, the theory is limited in low frequency range, that is to say, it is a short wave theory. Even so, as the computation based on the strip theory is relatively simple and the obtained results agree well with experimental ones for ships with length breadth ratio down to about 3.0, especially for the vertical motions in head waves, thus the theory finds popularity amongst naval architects for seakeeping performance analysis.

Since late 1960s, big progress has been made in the development of the strip theory in three aspects. Firstly, in order to make the basis of the theory more rigorous, some improved strip methods with slightly different basic assumptions were developed, e.g., the new strip method by Tasai & Takaki (1969), the rational strip theory by Ogilvie & Tuck (1969), and the famous STF strip theory by Salvesen, Tuck & Faltinsen (1970) which most of today's strip methods are its variations. Results by all of them satisfy the symmetric relation with forward speed mentioned above. The second aspect is the development of approaches for the hydrodynamic calculation in 2D profiles, e.g., the multiple parameters conformal mapping method by Miao (1980) and the close fit method by Frank (1967) to calculate the hydrodynamic forces acting on the real body surface instead of using the resembling ship sections, i.e., Lewis forms, to approximate the contours of the ship which is limited for application at the sections, e.g., the submerged bulbous bow. Up to now, the strip theory has been fully developed and there are several commercial codes based on it, e.g., SEAWAY by Delft University of Technology referring its manual by Journée & Adegeest (2003) and Maxsurf by FormSys, etc.

To remove the limitation of strip theories in low frequency range, the unified theory was developed by Newman (1978) and Newman & Sclavounos (1980). Kashiwagi (1997) described more recent developments of the unified theory. In essence, the theory uses the slenderness of the ship hull to justify a 2D approach in the near field coupled to a 3D flow in the far field, where the flow is generated by distributing singularities along the center line of the ship. The theory can also be regarded as a variation of the strip theory since it turns into the strip theory in the case of high frequency motions or oscillating in short waves, whereas becomes the slender body theory proposed by Newman (1964) in low frequency motions or long waves. Therefore, it is theoretically applicable to all frequencies as its name 'unified'. Despite its better theoretical foundation, the theory failed to give significantly and consistently better results than strip theories for real ship geometries with forward speed as concluded by Sclavounos (1984) and Ronæss (2002), since the near field solution cannot perfectly match with the far field solution to represent the complicated steady wave system around the ship, hence hard to be accepted by practice.

- ***2.5D theory***

Development of the high speed vessels in last decades led to the foundation of another high speed strip theory, which is often called 2.5D or 2D+t theory. In the 2.5D theory, based on the slenderness assumption same as the previous strip theories, the original 3D problem for a ship in waves is approximated by a series of time dependent 2D problems in space fixed cross planes normal to the longitudinal direction of the ship. However, unlike the strip theories, three dimensionality is partly considered as the flow at a cross section is influenced by the flow upstream of this section, but not by the flow downstream of it. In other words, the 2D governing equation and the body condition of the velocity potential are considered in each cross plane with a 3D free surface condition being satisfied in the formation of the theory, thereby its name 2.5D is derived. The calculations start from the bow of the ship and then proceed along the longitudinal downstream direction of the ship. Divergent waves can be described in the 2.5D theory, whereas transverse waves cannot. The consequence is that the sailing speed should be relatively high on the basis of the ship length Froude number usually above 0.4 as claimed by Faltinsen (2005). In addition, it should be noted that an inconsistency happens at a transom stern where the flow separates for high Froude number cases, because the 2.5D theory cannot foresee the flow separation and the

influence from the flow downstream of the transom stern is neglected. This shows an inherent deficiency of the 2.5D theory. In spite of this, the theory has proved to be a very efficient approach for high speed ships.

The concept of the 2.5D approximation was proposed by Munk (1924) in his slender body theory for airships. Tulin (1957) and Ogilvie (1967) applied this idea to slender planing surfaces and displacement hulls. Chapman (1975, 1976) further developed the 2.5D approach together with linear and nonlinear free surface conditions respectively to solve the problem of a surface piercing plate in yaw and sway motions. Since then, many scholars have investigated the application of the 2.5D theory for ship motions by different ways in dealing with the boundary conditions. Yeung & Kim (1981) employed a similar 2.5D approach using linearized free surface conditions to calculate the hydrodynamic forces on an advancing frigate hull in forced heave and pitch motions. Meanwhile, Yamasaki & Fujino (1985) presented a modified 2.5D approach based on Chapman (1975)'s work to study harmonic lateral oscillations of a plate and two ship models with special numerical schemes for the boundary conditions, of which the free surface elevation and velocity potential on the free surface in each station can be given by discretized forms of the free surface conditions through a step procedure. Besides, a more relaxed radiation condition to express the generated wave propagating outwards was imposed at infinity to overcome the numerical jump phenomenon. Later on, Chapman (1976)'s approach was generalized by Faltinsen & Zhao (1991) to study the steady and unsteady motions of a high speed slender ship. They firstly imposed nonlinear free surface conditions to solve the steady flow problem and used a distribution of 2D vertical dipoles with unknown strengths to express the flow far away from the ship, then the velocity potential of the unsteady flow was linearized about the steady flow free surface to take into account the contribution of the steady flow potential. Takaki et al. (1995) presented a comparative study on the estimations of the hydrodynamic forces and motion amplitudes of a high speed ship advancing in head sea by the strip theory, 2.5D theory and 3D methods. They concluded that the 2.5D theory is the most useful and accurate method for the high speed estimation. Similar to Yamasaki & Fujino (1985)'s work, Wang (1999) expressed the free surface kinematic and dynamic boundary conditions along the so called characteristic lines to solve the hydrodynamic problems of two ships in vertical

motions by a 2.5D approach. On the other hand, Duan & He (2001), Davis & Holloway (2003) applied transient free surface Green function to transform the formulation of the 2.5D theory into a boundary integration equation on the body surface of the ship. Due to the fact that linearized free surface condition and radiation condition at infinity can be automatically satisfied by the time domain boundary integration equation, this numerical algorithm is not susceptible to numerical error caused by the stepping procedure for the free surface and radiation condition at infinity, but the method is confined to the linear problems. Moreover, for ships with large flare, numerical divergence problem will be raised as pointed out by Duan (1999). The problem is due to the memory effect term of Green function that oscillates abruptly on the segment with a large inclined angle near the free-surface. This oscillation leads to numerical integration error of memory effect in terms of convolution integral of transient free surface Green function on the segment, then the accumulation of the numerical error causes numerical divergence of the boundary integral equation. In order to avoid this divergence for ships with large flare, Ma et al. (2005) presented a matched boundary integral equation method to solve the formation of the 2.5D theory. More recent relevant works in the application of 2.5D theory should be referred, such as Sun & Faltinsen (2007) studied the gravity influence on the performance of high speed planning vessels, Ma et al. (2012) extended the application to ship motions of trimaran, and Sclavounos & Lee (2013) imposed nonlinear boundary condition on the hull in their solutions to large amplitude ship motions. In addition, Lugni et al. (2004) presented a comprehensive experimental and numerical study of the steady wave elevation around a semi-displacement monohull with transom stern and compared the results of linear 3D and nonlinear 2.5D computations to prove the effectiveness of the 2.5D theory for a large range of high Froude numbers. In the aspect of CFD calculation, Tulin & Landrini (2001) applied the Smoothed Particle Hydrodynamics (SPH) method in a 2.5D approach to investigate the breaking bow waves of slender ships. However, although relevant studies on the 2.5D methods are plenty, commercial codes based on the 2.5D theory are few to the author’s knowledge, only ShipX-VERES by Norwegian University of Science and Technology referring to its manual by Fathi (2004), and MAESTRO by DRS Technologies Inc. used by Zhao & Ma (2016) can be found.

- ***3D methods***

Heretofore, all the mentioned theories for seakeeping performance analysis are based on the assumption of thinness or slenderness, thereby not in general be suitable for the problems of full formed ships which involve blunt bodies and floating structures like offshore platform. Therefore the 3D methods have been developed gradually to treat the corresponding seakeeping problems, with the appearance of high performance computers since 1970s. They can be basically classified into two groups, i.e., the Kelvin-Havelock singularity based methods and the Rankine singularity based methods.

To be specific, the Kelvin-Havelock singularity, or known as the free surface Green function given by Havelock in 1928, can automatically satisfied linear free surface condition and radiation condition at infinity same as that mentioned above in 2D solution, which indicate the velocity potential of the flow around the floating structure can be expressed by the sum of the surface integral of the singularities over the wetted body surface and the line integral along the intersection between the body and free surface. According to the way treating the time varying terms, the free surface Green function can be further classified into two categories in frequency domain and time domain.

The Green function method in frequency domain was studied by many researchers, mainly for zero forward speed offshore structure. Application examples were well established by Faltinsen & Michelsen (1974), Chang & Pien (1976) and Garrison (1978), etc. Besides, Noblesse (1982) and Newman (1985) presented numerical algorithms for the evaluation of the free surface Green function. Here, it is worth mentioning that the well-known program WAMIT developed by Massachusetts Institute of Technology is based on this method referring to its manual by Lee (1995). On the other hand, for a ship advancing with forward speed in a seaway, much less studies can be found by applying the Green function method in frequency domain due to the complexity and time consuming of the evaluation of the Green function, only a few researchers, i.e., Chang (1977), Inglis & Price (1982), Wu & Eatock Taylor (1987) and Chen et al. (2000) presented relevant works. Instead, a preferred alternative is performing the calculations in time domain because the form of the Green function applied in time domain is relative simple regardless of the forward speed. However,

the method is still computationally extensive since the evaluation of the Green function requires the calculation of a convolution integral. By using a transient free surface Green function, Liapis (1986) calculated the added masses and damping coefficients of a Series 60 ship in heave and pitch motions with forward speed. King (1987) further studied the diffraction problem by using this method. Similarly, Bingham (1994) also solved radiation and diffraction problems on a Wigley hull and a Series 60 ship with steady forward speed and carried out motion simulations on these two ships in vertical motions through incident waves.

Here, it should be noticed that the key step to solve the perturbation potiential is the simplification of the governing equations by linearization since the original fully nonlinear problem is difficult to solve. There are mainly two ways for this purpose. The first one is known as the Neumann-Kelvin linearization, N-K for short, proposed by Brard (1972), in which the entire perturbation induced by the body is assumed smaller than that by uniform flow, thus also called uniform flow linearization. It is applicable for a slender body. There is another linearization scheme named the double body linearization which has been applied by Dawson (1977). A basic assumption of the double body linearization is that the flow with waves is a small perturbation of that without waves, thus also called slow ship linearization. A comparative study on these two linearizations are presented by Kim & Kim (2010).

As both linearizations are based on small amplitude ship motions, whereas not suitable for large amplitude motions, Beck & Magee (1990), Lin & Yue (1990), Sen (2002) further imposed exact body condition on the instantaneous wetted surface of the moving body to take account of nonlinear effect while the free surface condition are still linearized. Besides, Lin et al. (1996) improved their method and developed the program LAMP for calculation of the large amplitude ship motions with forward speed. In fact, the LAMP system has several editions due to the combinations of different levels of nonlinearity of the solution, of which the lastest edition LAMP-4 is a totally nonlinear edition as both the perturbation potential and the wave exciting forces are solved over the instantaneous wetted hull surface. In addition, it is worth noting that Lin et al. (1999) further implemented a mixed source formulation into the LAMP which takes advantage of both transient Green function and Rankine source which will be introduced later, to enhance the efficiency of the code.

Although the time domain Green function based method is superior to the frequency domain based one for seakeeping performance analysis with forward speed, there are four main disadvantages in application as pointed out by Dai (1998) and Bertram (2000). Firstly, it is difficult to numerically treat the term of waterline integral in the integral equation, thereby contribution from this term is normally neglected. Secondly, for a ship having a large flare form which means the body surface is not vertically wall sided at the free surface, the difficulty that time stepping calculations give divergent results will be encountered. The greater the flare, the worse the calculated results. Fortunately, Duan & Dai (1999) presented a practical solution to this problem. The third challenge comes from the numerical calculation of the second derivative of the steady flow potential on the average wetted body surface. To overcome this challenge, some researchers used the double body flow model regardless of wave and imposed rigid wall condition on the free surface which is reasonable for low speed case. However, the induced velocity by the steady potential becomes infinite at the non-vertically wall sided intersection, hence violating the assumption of perturbation expansion. That is to say, the original body surface condition on the instantaneous wetted surface cannot be transferred to the one on the average wetted surface which is the burden of the method. Lastly, as the free surface Green function based method only satisfy linear free surface condition, it is hard to apply the method to strong nonlinear problems with nonlinear free surface condition.

For the purpose of avoiding the complexity inherent in the Green function, the Rankine singularity based method, also categorized as the simple Green function method as in the 2D cases mentioned before, was introduced in which the singularities have to be distributed all over the boundaries of the flow field around the structure including the free surface since this kind of Green function does not satisfy any boundary condition in nature. Although this will significantly increase the number of unknowns in the flow domain and put pressure on computer memory, it has greatly broadened the scope of application to nonlinear free surface condition. The basis for the development of the methods using Rankine singularity was given by Gadd (1976) and Dawson (1977) for the steady wave resistance problem. Frequency domain solutions by using the Rankine singularity based method for the unsteady flow problem and the diffraction problem were obtained by Nakos (1990) and Bertram

(1990). Later, the method was extended to time domain by Nakos et al. (1993) and Kring (1994). Based on their works, the code SWAN was the first developed code to be used commercially with different editions in frequency domain and time domain respectively. In the near decade, Chen & Zhu (2010 a b) carried out time domain calculations on a DTMB5512 ship and a 4000 twenty-foot equivalent unit (TEU) container ship by the Rankine source panel method in head wave. Song et al. (2011) considered the nonlinear restoring force in their 3D Rankine source panel method and calculated the motion response on a 6500TEU container ship in waves with different amplitudes. In addition, Kim et al. (2011) developed a program using the 3D Rankine panel method for nonlinear motion responses and wave loads calculations named WISH based on the so called weak scatter hypothesis. More recently, Yuan et al. (2015, 2016) further applied the 3D Rankine source panel method to ship to ship interaction problem studies.

Same as we done in manoeuvring field literature review, the distinguished advantage and disadvantage of the introduced potential theory methods for seakeeping analysis are briefly labelled in Table 2.2.

Table 2.2 Summary of potential flow methods for seakeeping

Methods	Advantage	Disadvantage
Ordinary strip	Simple and fast	Inappropriate with forward speed
STF	More rational	Inappropriate for non-slender body
2.5D	Suitable for high speed	Inappropriate for low speed
3D Green function	Fully consider 3D effect	Limited to linear problem
3D Rankine	Flexible	Computational resource consuming

In spite of developing 3D Rankine singularity based method for different kinds of seakeeping performance analysis is popular nowadays, it is well known that the 3D methods are computationally more demanding and time consuming than the 2D strip theory methods after all. Further, it is not so that the 3D models always represent an improvement over the strip theory calculations for slender high speed vessels which is of interest in this study.

2.2.2 Boundary element method

As numerical tools for computation of potential flow, 2D BEM and 3D BEM (panel method) have been widely used. The original panel method proposed by Hess and Smith (1964) uses large numbers of plane quadrilateral panels to discretize the body surface, and distributes a constant source density on each panel. Similarly, numerous short line segments are used to construct the ship profiles in 2D BEM. In this way, the actual profile or surface of the flow field is represented by a polygon or polyhedron, and the physical quantities on the boundary become discontinuous which violating the continuity condition of the flow field and resulting in poor accuracy if the meshing is coarse. In order to improve the accuracy and efficiency of the method, many efforts have been made on proposing better geometric description of the body surface and smoother singularity density distribution. Webster (1975) applied triangular panels with a linear singularity density distribution on the panel. Willis et al. (2006) used quadratic curved panel with a polynomial distribution in the recent decade. Besides, paraboloidal panel by Hess (1979), hyperboloidal panel by Hsin et al. (1991) were also tried in their developed BEM respectively. In addition, Söding (1993) used point sources instead of source panels in his application. However, all these mentioned approaches have some limitations. Firstly, it is difficult to derive exact normal vector on the body surface if using plane panels. Continuity of the first derivative cannot be ensured at the boundaries between panels even for quadratic curved panels. Secondly, an additional error would be induced by assuming a simple source density distribution on each panel. Thirdly, except for those by Willis et al. (2006) and Söding (1993), large numbers of collocation points have to be set to satisfy the boundary conditions with sufficient accuracy in low order BEM which significantly increases the computational time. On the other hand, in high order BEM, although less collocation points can be used, the position of the collocation points is hard to be chosen. Kouh and Ho (1996) proposed a high order panel method by using the Gaussian points as both the collocation points and the source points to solve this problem.

During the last decade, high order panel methods based on B-spline or NURBS have been developed rapidly. Not only because B-spline and NURBS can give a more precise description of the body geometry and create meshes on the body surface for hydrodynamic calculation easily, but also due to that they can be used to represent the

source density or velocity potential distribution on the panel to ensure the continuity of higher order derivatives of velocity potential on the boundary. Nakos (1990) and Nakos et al. (1993) applied bi-quadratic spline to approximate the distribution of the unknown potential over plane quadrilateral panels in their Rankine source based method. Hsin et al. (1993) developed a 2D higher order panel method, in which the body geometry and the singularity distribution are expressed by B-splines. Maniar (1995) extended the B-spline based panel method to calculate the hydrodynamic force on 3D bodies. Danmeier (1999) used B-spline to represent the velocity potential on the body surface while the body geometry was described by arbitrary mathematical expressions. Kouh & Suen (2001) and Qiu & Hsiung (2002) all used NURBS to describe the body geometry, while the source density distribution was replaced by point sources. Later, Kim & Shin (2003) used NURBS, Datta & Sen (2006) used B-spline to describe the body geometry as well as the velocity potential on the body surface in dealing with radiation and diffraction problems without forward speed. In recent decade, more relevant works such as Wang & Zou (2008), Gao & Zou (2008), Song et al. (2011), Kim et al. (2011) applied B-spline or NURBS for both the body geometry and velocity potential distribution in their 3D Rankine panel methods to carry out the calculations for different kinds of seakeeping problems with forward speed.

2.3 Research progress in manoeuvring in waves

2.3.1 Introduction of the manoeuvring in wave analysis

As mentioned in Chapter 1, a single ship manoeuvring in waves suffers manoeuvring hydrodynamic forces to change its speed, direction and position in horizontal plane and generates 6-DOF oscillation motions due to incident waves. Therefore, it is a combined problem of manoeuvring in calm water and classic wave induced motions.

From the review of the works on these two sub problems, both of them were studied based on the rigid body dynamics. The difference is, the external force acting on the ship in manoeuvring motions is induced by the rudder or other steering devices, while in wave induced motions the wave exciting force is the source. Theoretically speaking, if these two kinds of forces can be fused as a total external force, the motion could be absolutely solved according to the Newton's second law. But, In fact, it is difficult to

implement this fusion since they are essentially different in physical nature. That is, the wave exciting force is dominated by nonviscous force and the main part of it is varying in high frequency, whereas, in contrast, viscous force is the main cause to the manoeuvring motion which is varying slowly. Based on this physical background, most of relevant studies made efforts on finding a reasonable way to take both two kinds of external forces into account simultaneously for the analysis of manoeuvring in waves. According to the report by the ITTC Manoeuvring Committee (2011), different approaches found in the literature have been classified into four categories, namely experimental methods, methods based on two time scales model, methods based on unified theory and methods using CFD.

Experimental methods are still the most reliable to investigate ship manoeuvring and course keeping in waves. Ueno (2003) conducted free running model tests on a VLCC model manoeuvring in regular waves and discussed effects of different wave lengths, encounter angles and loading conditions on the results. Yasukawa (2006, 2008) carried out free running model tests on a SR108 model (typically known as S175 container ship) manoeuvring in regular waves and the measured results become benchmark data for many relevant numerical studies. Similarly, Lee et al. (2009) presented experimental results with a KVLCC model manoeuvring in waves for various wave lengths and wave amplitudes ratios. More recently, Yasukawa et al. (2015) carried out the free running model tests on a KVLCC2 model in irregular waves. In addition, Xu et al. (2007) and Kinoshita et al. (2008) carried out a series of PMM tests in waves and a theory to evaluate wave drift force was summarized.

CFD methods in principle provide an adequate description of all physics. However, same as the situation in calm water, this approach is still highly challenging from a computational point of view, thereby hardly for real time simulation. Moreover, many technical problems need to be further studied mentioned by Skejic (2013), such as how to arrange an appropriate turbulence model which is especially difficult in the highly challenging case of curvilinear motion of a ship, as the flow around the hull is rich in separations, re-attachments, vortex formation and substantial interaction with the rudder and propeller.

2.3.2 The unified theory method

Perhaps the most widely applied methods to deal with manoeuvring in a seaway are methods based on two time scales model and the unified theory. Both of the methods are based on the potential flow theory, whereas different in handling the external force which is to some extent similar to the difference between Abkowitz model and MMG model. The methods based on the unified theory integrate the low frequency manoeuvring motion and the high frequency wave induced motions into a generic set of 6-DOF motion equations to describe the manoeuvring in waves. McCreight (1986) established a nonlinear manoeuvring model in waves, in which the hydrodynamic forces related to the wave induced motion were evaluated in a body-fixed coordinate system by a linear strip method. Ottosson & Bystrom (1991) introduced a more simplified method, where added mass and damping coefficients were assumed to be constant based on mean encounter frequency during manoeuvring motion. Later, Hamamoto (1992) presented a landmark work in which a horizontal body fixed reference frame was proposed to incorporate the standard reference frames used in manoeuvrability, stability and seakeeping, thereby simplify the description of the 6-DOF manoeuvring motions in waves. Based on Hamamoto (1992)'s work, Nishimura & Hirayama (2003) simulated a small vessel manoeuvring in waves by considering the F-K force as the external wave force. Since the inertial forces acting on the ship are varying with the encounter frequency, Bailey et al. (1997) and Fossen (2005) adopted the linear convolution integral formula based on Cummins (1962)'s work to take into account the unsteady memory effects which requires the evaluation of the convolution integral and the impulse response function (IRF) at every time step. Similarly, Ayaz & Vassalos (2003) used the convolution integral approach combined with the evaluation of the first order wave loads on the instantaneous wetted surface of the ship manoeuvring in astern seas. Although this concept of including memory effect seems more reliable, the accurate computation of the convolution integral is not simple as it depends strongly on the asymptotic behaviour and limiting (zero and infinite) values of either the encounter frequency dependent added mass or damping coefficients. Moreover, The first order excitation forces and moments need to be transferred into time domain by means of Fourier transform as they are varying with encounter frequency due to change of ship speed and heading angle. Thereby the evaluation of the IRF will be frequently executed. Consequently this fact together

with direct evaluation of the convolution integrals will increase the CPU time. For example, Ayaz et al. (2006) stored the values of the added mass and the damping coefficients for every 10° heading angle between 0° to 360° and then interpolated for a particular wave heading during simulation. To simplify the convolution integral, Sutulo & Guedes Soares (2006a, 2006b, 2008) employed auxiliary states variables for the approximation of the added mass by a rational function while applying the inverse Fourier transform for the radiation problem. In addition, Fang et al. (2005) developed a less rigorous model by disregarding the convolution integrals but implementing direct evaluation of the hydrodynamic coefficients at instantaneous encounter frequency in time domain. More recent work within this classification were carried out by Lin et al. (2006) and Yen et al. (2010) in which the 3D time domain nonlinear ship motion simulation program LAMP was expanded to study the problem of ship manoeuvring in waves.

A remarkable fact to criticize the methods based on the unified theory is that few of them incorporated the mean second order wave loads which were proved important in context of the manoeuvring ship in waves through model tests by Inoue & Murahashi (1966). In contrast with the short time scale first order wave loads whose mean value over the wave period is zero, the mean second order wave loads are able to produce a long term steady wave effects. These effects will change the average ship manoeuvring trajectory, induce involuntary speed loss, and affect other slowly varying manoeuvring parameters such as drift angle. So the omission of the mean second order wave forces will lead to a wrong prediction of manoeuverability. However, if the incorporation of the mean second order components is sought, it will turn the problem even more complex since it implies a second order expansion of the Volterra series that further increase the difficulty in the estimation of IRF as pointed out by Skejic & Faltinsen (2008). Moreover, even though the second order wave loads can be counted in a few studies, it is impossible to distinguish the contribution from each motion component to the loads due to the motions are considered conjunctly in the unified theory, thereby some approximation has to be introduced and it is hard to guarantee the accuracy of the estimated second order wave loads.

2.3.3 The two time scales model

In contrast to the unified theory model, the two time scales model separates the total motion equations into two sub motions based on the physical assumption of a rapidly varying time scale associated with the wave induced motions and a slowly varying time scale associated with the manoeuvring motion. The independent analysis of each sub motion is solved while including the interaction effects between each other, i.e., the high frequency wave induced motions are determined by the linear first order wave forces according to the kinematic parameters of the ship and the relative incident wave angle derived from the low frequency manoeuvring motion solution, then provide the hydrodynamic forces including the mean second order wave loads back to the next step manoeuvring motion simulation. Hirano et al. (1980) laid a foundation for the development of methods based on two time scales model who first carried out the estimation of manoeuverability by using 3-DOF equations of motion in calm water and computing only wave drift force, but neglecting the wave induced motion. Later, Triantafyllou (1982) gave a systematic derivation of a two time scales model in dealing with the superposition of the high frequency and low frequency motions of moored vessels. Nonaka (1990) generalized the model to the case with forward speed which further demonstrated this concept of separation by time scale difference is reasonable. Thereafter, the two time scales approach has become a popular way for the analysis of manoeuvring in waves. Several recent representative have been presented by Skejic & Faltinsen (2008), Yasukawa & Nakayama (2009) and Seo & Kim (2011). Due to slight difference in implementation, the approach employed by Skejic & Faltinsen (2008) and Yasukawa & Nakayama (2009) can be considered as a sequential evaluation where the seakeeping part is evaluated after the manoeuvring part one by one and repeating the process until the simulation time has been reached, whereas Seo & Kim (2011)'s approach is regarded as the parallel method where the seakeeping is evaluated several times while the manoeuvring runs only one step time. The major difference between referred works are related to the chosen approaches for the seakeeping analysis. Skejic & Faltinsen (2008) and Yasukawa & Nakayama (2009) applied the STF method and 3D panel method respectively in frequency domain in which a quasi-steady behaviour for the time scale of the seakeeping module was considered, while Seo & Kim (2011), on the other hand,

solved directly the seakeeping problem in time domain with their 3D Rankine panel method program WISH.

Regarding the calculation of the mean wave drift loads, there are general two classes of methods, i.e., one class using the conservation of momentum or energy commonly referred as far field methods and the other class using direct pressure integration over the body surface referred as near field methods. Maruo (1960) first developed a 3D far field method using the conservation of momentum to estimate the drift forces acting on a ship with zero forward speed. Similarly, Newman (1967) used the conservation of angular momentum to derive the expressions for the mean second order yaw moment based on the slender body theory. These expressions were simplified by Salvesen (1974) who established the method by using the STF strip method with the so called weak scatter assumption. The method seems to give inadequate estimates of the mean wave loads when the ship is not slender enough. An easy applicable method based on the conservation of energy was presented by Gerritsma & Beukelman (1971) originally valid for head sea. Loukakis & Sclavounos (1978) derived a modification of Gerritsma & Beukelman (1971)'s method by considering the oblique ahead sea. The method was able to predict the mean drift forces, but not the yaw moment. Further, Kashiwagi (1992) improved Newman's (1967) method by taking into account the forward speed and reported that it can be troublesome in the evaluation of the mean yaw moment based on conservation of fluid angular momentum. On the other hand, Pinkster (1980) established a 3D near field direct pressure integration method in which the mean drift loads are derived by integrating the pressure distributed on the instantaneous wetted surface of floating structures without forward speed. The direct pressure integration method for an arbitrary body with forward speed was developed by Faltinsen et al. (1980). Besides, Faltinsen et al. (1980) also proposed an asymptotic theory applicable in cases when the ship experiences short wavelength regular waves. More recently, Kim & Kim (2011) calculated added resistance on a hemi-sphere and a barge floating in waves, and several ship types advancing in waves with forward speed by adopting the formulation given by Joncquez (2009) which is also based on the near field pressure integration. Later, Seo et al. (2013) carried out a comparative study on computation of second order wave drift force and Seo et al. (2014) kept on

their work by proposing new ways to deal with added resistance on ships in short waves which were concluded especially suitable for a slender body.

Back to the mentioned representative works applying the two time scales model for manoeuvring in waves studies, Seo & Kim (2011) adopted the near field method to estimate the mean drift forces and moment, Yasukawa & Nakayama (2009) applied Maruo (1960)'s far field method to estimate the longitudinal added resistance coefficient while also used near field method for lateral drift force and yaw moment estimations. Skejic & Faltinsen (2008) applied four different approaches, i.e., the direct integration pressure method by Faltinsen et al., (1980), Salvesen (1974)'s method, Loukakis & Sclavounos (1978)'s method and the asymptotic theory by Faltinsen et al. (1980), to cover the whole wave-length to ship-length ratios where the ship might operate.

At last, main differences between the methods introduced above on the combined seakeeping and manoeuvring analysis, in the scope of the potential flow theory, are given in Table 2.3 as below.

Table 2.3 Summary of potential flow models for manoeuvring in waves

	Unified theory	Two time scales
Motion equations	Combined	Separated (seakeeping: rapid; manoeuvring: slow)
Time marching	Convolution integral	Data exchange (sequential or parallel)
Wave drift loads	N/A	Far field or near field (far field only valid for mean loads)

3 Adopted approach and innovations

Although one can always claim more accurate results by fully considering every detail of the problem with the help of more powerful computers, a balance should be found between the accuracy of prediction and the consumed computational time in practical application. Therefore, an approach taking the major issues of the problem into account but neglecting the minor ones should be applied which rules out the CFD method and leads to the methods in the scope of the potential theory.

3.1 Adopted approach

Based on the above literature review, the two time scales model method, which has more clear physical explanation and is convenient to consider the second order wave drift loads, will be adopted for the present study following the sequential evaluation approach proposed by Skejic & Faltinsen (2008) instead of the parallel approach to further reduce demand on computational resource. The basic manoeuvring motion will be expressed by a 4-DOF MMG model also due to its more clear physical explanation and capability of modification by parts, while the wave induced motions will be taken care of by a 2.5D approach more suitable for high speed vessels.

In order to improve the accuracy and efficiency of the approach, a NURBS based high order BEM using Rankine type singularities which is more suitable for real ship types and can be extended into nonlinear problems field in the future, will be applied for solving the BVPs of the velocity potential established in the 2D cross sections along the ship, including the low frequency lateral motions. Estimation of the viscous roll damping effects is taken into account by adopting the empirical method given by Himeno (1981). Then 5-DOF (surge neglected) oscillation motions can be solved after deriving the first order hydrodynamic and hydrostatic forces acting on the hull according to the Bernoulli equation. The mean second order wave drift forces will be counted by the direct pressure integration for the purpose of counting other second order force components in the perspective of long term plan. In addition, the lift force associated with the manoeuvring motions neglected in 2.5D approach will be

considered by a special sectional correction factor with the help of the slender wing theory and the low aspect ratio wing theory.

Regarding the propulsive force by the propeller, steering force by the rudder and other nonlinear viscous forces on the hull, empirical or semi-empirical formulae which are commonly used in the manoevuring research field will be applied for estimations in the present simulations, accompanying with several parameters obtained directly from available experimental data. Estimation of the calm water resistance is achieved with the application of a modified Holtrop-Mennen method. The modifications are seen in the application of the Michell's integral for the estimation of the wave resistance.

Finally, for the simulations of the standard manoeuvers in calm water and waves, 4^{th} order Runge-Kutta scheme will be applied as it has been proved stable enough.

3.2 Innovations of the present study

Compard to previous works reviewed in Chapter 2, the innovations of the present study can be outlined as follows.

- Developed a new prediction simulation system for the combined seakeeping and manoeuvring analysis which applying a 2.5D theory based approach suitable for solving wave induced problems at forward speeds from moderate to high.
- A MTF radiation condition originated from the earthquake wave propagation is imposed on the open boundary in the formation of the 2D BEM for the 2.5D theory based approach.
- Indirectly taking the 3D lift effect into account which a 2.5D theory based approach normally can not cover.

4 Seakeeping analysis based on a 2.5D approach

As stated in the review, the seakeeping behaviour of an advancing ship in a seaway can be analysed using the 2D strip theory or the fully 3D approach. Pursuing a certain level of simplicity in present study by using the criteria such as the requirement of minimizing computational resource and accuracy within the engineering practice we will focus our discussion on the 2D strip theory methods.

2D strip methods are the standard tools for the ship seakeeping analysis. In essence, they provide successful simplification of the complex 3D problem of a moving ship in waves by dividing the underwater part of the ship into a number of strips (about 20 to 30). Each strip (ship cross section) formulates a unique 2D boundary value problem due to the particular shape of the cross section. The boundary value problems, once being solved, will provide the values of 2D coefficients. These, integrated over the length of the slender ship, will give an approximation of the 3D coefficients of a ship. This shortly explained concept originated from the work of Korvin-Kroukovsky & Jacobs (1957).

The assumptions on forward speed and wavelength led to the development of numerous variations of strip theories for single ships, e.g., Newman (1978), Maruo (1989). From a broad range of methods which are less or more theoretically rigorous, we need to select a suitable strip theory for the present work. Taking into consideration the objectives of the study which require for seakeeping analysis on an advancing ship at speeds from moderate to relatively high, it is appropriate to choose the 2.5D (2D+t) theory developed by Chapman (1975), also called the high speed strip theory, as an adequate tool to establish following methodology for seakeeping analysis.

4.1 Mathematical description of the problem

The ship is considered to be a rigid body, floating in the surface of an ideal fluid, which is homogeneous, incompressible, irrotational, non-viscosity and free of surface tension. Only the external loads on the underwater part of the ship are considered here and the effect of the above water part will be fully neglected. The above assumptions will hold throughout the whole present study which means that the potential fluid flow theory is assumed. The viscous effects will be introduced when it is necessary to do so like in the example of manoeuvring equations given latter. The discussion will begin with the description of 3D exact BVP, then through the adequate linearization, lead to the formulation of 2.5D theory.

4.1.1 Coordinate system

Assuming a ship advancing with a mean forward speed U in regular waves on a straight line course, 6-DOF oscillation motions will be induced. The flow field and motions of the rigid ship can be described in two Cartesian right handed coordinate systems as shown in Fig. 4.1. An Earth fixed coordinate system $(O_0 - x_0 y_0 z_0)$ with positive z_0 axis pointing upwards vertically is most convenient to express the incident wave and the position of the ship. Normally, the positive x_0 direction is set pointing to the ship bow at initial time. A hydrodynamic frame $(O - xyz)$ whose origin O lays in the plane of undisturbed free surface with positive z axis pointing upwards through the center of gravity (COG) and parallel to the z_0 axis. It moves with the same mean forward speed U as the ship but does not oscillate with the ship. The positive x direction is coincide with the navigation direction. This coordinate system is used to describe the flow field around the ship. The complex amplitudes of six modes of ship motions are defined as $\xi_j (j = 1,...,6)$ refer to surge, sway, heave, roll, pitch and yaw respectively. Besides, ψ is defined as the ship heading angle. The incident wave length is λ and η is the incident wave angle relative to the Earth fixed coordinate system, thereby $\chi = \psi + \eta$ is the encounter heading angle.

According to Fig. 4.1, the transformation between the Earth fixed coordinate system $(O_0 - x_0 y_0 z_0)$ and the seakeeping hydrodynamic frame $(O - xyz)$ is defined as follow.

$$\begin{cases} x_0 = x\cos\psi - y\sin\psi + Ut\cos\psi \\ y_0 = x\sin\psi + y\cos\psi + Ut\sin\psi \\ z_0 = z \end{cases} \tag{4.1}$$

where t is the time variable. It is easy to see that for a zero heading angle $\psi = 0$, the expression (4.1) gives a standard transformation used in the seakeeping analysis.

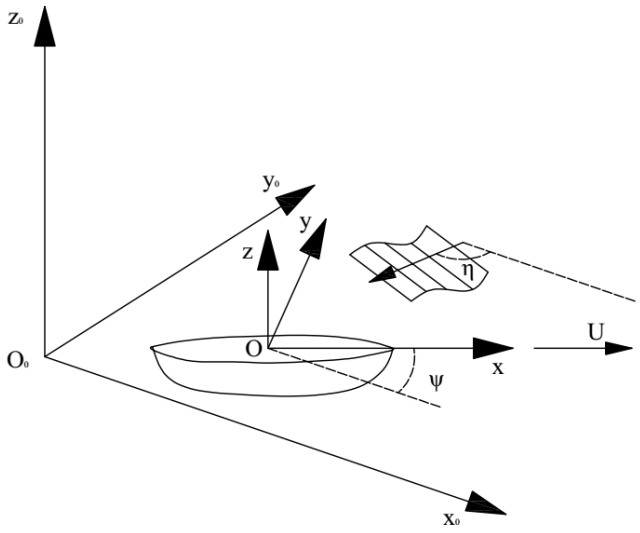

Fig. 4.1 Coordinate systems in seakeeping analysis

4.1.2 Exact expression of the boundary value problem

Based on the assumptions of the fluid stated at the beginning of this section, the fluid velocity can be described by the velocity potential $\Phi(x_0, y_0, z_0, t)$ which satisfies Laplace's equation

$$\nabla^2\Phi = 0 \tag{4.2}$$

in the fluid domain where ∇^2 denotes the Laplace operator.

The fluid pressure follows from Bernoulli's equation

$$p - p_a = -\rho\frac{\partial\Phi}{\partial t} - \frac{\rho}{2}\left|\nabla\Phi\right|^2 - \rho g z_0 \tag{4.3}$$

where $\left|\ \right|$ denotes the absolute value, p_a is the atmospheric pressure, ρ is the fluid density, g is the acceleration of gravity. The fluid domain is bounded with the free surface, the vessel instantaneous wetted surface area $S^*(t)$ and an arbitrary vertical control surface restricting the fluid domain. Further, by assuming a deep water, the fluid domain is infinitely extended in a negative vertical direction, whereas if assuming a water area with limited depth, a flat bottom boundary should also be set.

Next step is to derive the free surface conditions neglecting the surface tension. On the free surface $z_0 = \zeta(x_0, y_0, t)$, the fluid particles remain on the free surface, meaning that the velocity potential Φ needs to satisfy the kinematic free surface condition

$$\frac{D}{Dt}(z_0 - \zeta) = 0 \quad on\ z_0 = \zeta \tag{4.4}$$

Here $D/Dt = \partial/\partial t + \nabla\Phi \cdot \nabla$ is the material substantive derivative, which expresses the rate of change in time if we follow a fluid particle in space. The dynamic free surface condition follows from the equality between the dynamic and atmospheric pressure on the free surface so that

$$\frac{\partial \Phi}{\partial t} + \frac{1}{2}\left|\nabla\Phi\right|^2 + g\zeta = 0 \quad on\ z_0 = \zeta \tag{4.5}$$

Further combing the kinematic free surface condition (4.4) and dynamic free surface condition (4.5) will eliminate the wave elevation ζ and consequently yield the exact free surface condition

$$\frac{\partial^2 \Phi}{\partial t^2} + 2\nabla\Phi \cdot \nabla\left(\frac{\partial \Phi}{\partial t}\right) + \frac{1}{2}\nabla\Phi \cdot \nabla\left(\nabla\Phi \cdot \nabla\Phi\right) + g\frac{\partial \Phi}{\partial z_0} = 0 \ \ on\ z_0 = \zeta \tag{4.6}$$

The boundary condition on the body surface follows from the knowledge that the normal velocity on the body boundary needs to be equal to the surrounding fluid velocity in the same direction. Then it follows

$$\frac{\partial \Phi}{\partial n} = \vec{V} \cdot \vec{n} \quad on\ S^* \tag{4.7}$$

Here, $\vec{V}$ is the local body boundary velocity at the point (x, y, z) on the instantaneous wetted ship surface S^* and $\vec{n}$ is the unit normal vector on the hull boundary with positive orientation pointing out of the fluid domain defined as

$$\vec{n} = (n_1, n_2, n_3), \vec{r} \times \vec{n} = (n_4, n_5, n_6) \tag{4.8}$$

where $\times$ denotes vector product and $\vec{r} = x\vec{i} + y\vec{j} + z\vec{k}$ is the position vector of arbitrary point with respect to the origin of the coordinate system.

In addition to the above conditions the deep water and radiation conditions are needed. The deep water condition simply states that

$$\nabla \Phi \to 0 \ as\ z_0 \to -\infty \tag{4.9}$$

To obtain a unique solution for the velocity potential, it is necessary to define a radiation condition at the borders of the fluid domain. This will ensure a dissipation of the energy from the radiated and reflected waves at an infinite distance from the source of disturbance body.

The above stated boundary conditions with steady state assumption completely describe the exact 3D boundary value problem within the potential flow theory. If the studied flow is unsteady, initial condition should be imposed such as

$$\begin{cases} \zeta(x_0, y_0; 0) = f_1 \\ \dfrac{\partial \zeta(x_0, y_0; 0)}{\partial t} = f_2 \end{cases} \tag{4.10}$$

Or

$$\Phi = 0 \quad at\ t = 0 \tag{4.11}$$

In addition, special attention should be paid to the slender ship in manoeuvring motion or the planning ship sailing at high speed which the hull can be considered as a lifting body seen from overhead view and side view respectively. Therefore, Kutta condition should be imposed on the trailing edge of the ship to keep the conservation of circulation.

4.1.3 Simplification of the BVP

As seen, the exact boundary value problem is mathematically intractable not only because the free surface condition is nonlinear but also both the free surface elevation and the unsteady instantaneous wetted body surface are not known a priori. Some simplifications through linearization should be introduced to solve the problem. By the linearization, it is assumed that all the quadratic terms appearing in the boundary conditions will be neglected. The amplitudes of incident wave and oscillations are all assumed to be small.

In this way, the principle of superposition is applicable in the linearized problems. Then the total velocity potential Φ on the moving body can be separated into a contribution from the uniformly steady incoming flow $-U\vec{i}$, and a disturbance potential ϕ which consist of a steady part and a unsteady time dependent part on the calm water, Φ_S and Φ_T respectively. The stated decomposition can be expressed as

$$\begin{aligned}\Phi &= -Ux + \phi(x,y,z,t) = -Ux + \Phi_S(x,y,z) + \Phi_T(x,y,z,t) \\ &= -Ux + \Phi_S(x,y,z) + \phi_T(x,y,z)e^{i\omega_e t}\end{aligned} \tag{4.12}$$

where $i = (-1)^{0.5}$ is the imaginary unit and ω_e is the encounter frequency defined later. The complex factor $e^{i\omega_e t}$ represents the time component of the harmonic oscillation as the incident wave is regular. $\phi_T(x,y,z)$ is the unsteady spatial velocity potential, which may be further decomposed into three parts, i.e., an incident wave potential ϕ_I, a diffraction potential ϕ_D around the constrained ship and a radiation potential ϕ_R, thus

$$\begin{aligned}\phi_T &= \phi_I + \phi_D + \phi_R \\ &= A(\phi_0 + \phi_7) + \sum_{j=1}^{6} \xi_j \phi_j\end{aligned} \tag{4.13}$$

where A is the incident wave amplitude, ϕ_0 is the incident wave potential with unit wave amplitude, ϕ_7 is the diffraction potential in unit wave amplitude, ϕ_j is the radiation potential due to unit motion in the j-th direction.

According to the wave theory introduced in the book by Newman (1977), the deep water incident wave potential is defined as

$$\phi_0(x, y, z) = \frac{ig}{\omega_0} e^{k_0 z} e^{-ik_0(x\cos\chi + y\sin\chi)} \tag{4.14}$$

where k_0 is the wave number related to the wavelength λ by $k_0 = 2\pi/\lambda$, ω_0 is the circular frequency of the incident wave related to the frequency of encounter ω_e by

$$\omega_e = \omega_0 - k_0 U \cos\chi \tag{4.15}$$

As previous defined in coordinate system, $\chi = \psi + \eta$ is the encounter heading angle, η is the incident wave angle relative to the Earth fixed coordinate system and ψ is the ship heading angle. For zero ship heading angle, i.e., $\psi = 0$, then the encounter heading angle χ is equal to the incident wave angle η, i.e., $\chi = \eta$ with the following definitions: $\chi = 0^o$ is following waves, $\chi = 90^o$ is port beam waves and $\chi = 180^o$ is head waves.

In the next step, linearization has to be performed to simplfy the governing equations. Since the present study is focus on the speed range from moderate to relatively high, say $F_n \geq 0.15$, it is more appropriate to apply the N-K linearization introduced in Chapter 2. The linearization process will be shortly described as follows.

First, we assume $|\nabla\phi| << U$ and keep only linear terms in ϕ in the free surface condition. Then one more time linearization is carried out by using the Taylor series expansion of terms $\partial\phi/\partial t$ and $\partial\phi/\partial z$ around the mean free surface $z=0$, and again keep the linear terms. This gives a linearized form of the free surface condition from (4.6) as shown by Newman (1978).

$$\begin{aligned}&\frac{\partial^2\Phi_T}{\partial t^2}+2\vec{W}\cdot\nabla\frac{\partial\Phi_T}{\partial t}+\frac{1}{2}\vec{W}\cdot\nabla\left(W^2\right)+\vec{W}\cdot\nabla\left(\vec{W}\cdot\nabla\Phi_T\right)\\&+\frac{1}{2}\nabla\Phi_T\cdot\nabla\left(W^2\right)+g\frac{\partial\Phi_S}{\partial z}+g\frac{\partial\Phi_T}{\partial z}=0 \qquad on\ z=0\end{aligned} \tag{4.16}$$

where $\vec{W}$ is introduced to represent the velocity vector of the steady flow, that is

$$\nabla\Phi=\left[-U\vec{i}+\nabla\Phi_S\right]+\nabla\Phi_T=\vec{W}+\nabla\Phi_T \tag{4.17}$$

The linear free surface condition (4.16) is still too complex for practical application. Further simplification of excluding the effect of steady flow potential on the free surface condition is appropriate since the present study's concern is on slender ships. Therefore, the linearized form of the fluid pressure is

$$p-p_a=-\rho\left(\frac{\partial\phi}{\partial t}-U\frac{\partial\phi}{\partial x}\right)-\rho gz \tag{4.18}$$

Similarly, the linearized dynamic free surface condition is

$$\frac{\partial\phi}{\partial t}-U\frac{\partial\phi}{\partial x}+g\zeta=0 \ \ on\ z=0 \tag{4.19}$$

the linearized form of the kinematic free surface condition is

$$\frac{\partial\zeta}{\partial t}-U\frac{\partial\zeta}{\partial x}=\frac{\partial\phi}{\partial z} \ \ on\ z=0 \tag{4.20}$$

Combining (4.19) and (4.20), the single expression of the linearized free surface condition is written as

$$\frac{\partial^2\phi}{\partial t^2} - 2U\frac{\partial^2\phi}{\partial t\partial x} + U^2\frac{\partial^2\phi}{\partial x^2} + g\frac{\partial\phi}{\partial z} = 0 \ \ on\ z = 0 \tag{4.21}$$

With the linearized free surface condition, now we can derive the governing equations of the BVP for the steady flow potential Φ_S and the normalized velocity potential ϕ_j separately. Accordingly, the boundary condition is also satisfied on the mean wetted body surface S_0 now.

$$\begin{cases} \nabla^2\Phi_S = 0 & in\,the\ flow\ field \\ U^2\dfrac{\partial^2\Phi_S}{\partial x^2} + g\dfrac{\partial\Phi_S}{\partial z} = 0 & on\ z = 0 \\ \dfrac{\partial\Phi_S}{\partial n} = Un_1 & on\ S_0 \\ \nabla\Phi_S \to 0 & as\ z \to -\infty \\ radiation\ condition & \end{cases} \tag{4.22}$$

$$\begin{cases} \nabla^2\phi_j = 0 & in\ the\ flow\ field \\ -\omega_e^2\phi_j - 2i\omega_e U\dfrac{\partial\phi_j}{\partial x} + U^2\dfrac{\partial^2\phi_j}{\partial x^2} + g\dfrac{\partial\phi_j}{\partial z} = 0 & on\ z = 0 \\ \dfrac{\partial\phi_j}{\partial n} = \begin{cases} i\omega_e n_j + m_j & (j = 1,...,6) \\ -\dfrac{\partial\phi_0}{\partial n} & (j = 7) \end{cases} & on\ S_0 \\ \nabla\phi_j \to 0 & as\ z \to -\infty \\ radiation\ condition & \end{cases} \tag{4.23}$$

where

$$\begin{aligned} (m_1, m_2, m_3) &= -(\vec{n}\cdot\nabla)\vec{W} \\ (m_4, m_5, m_6) &= -(\vec{n}\cdot\nabla)(\vec{r}\times\vec{W}) \end{aligned} \tag{4.24}$$

are the so called m_j terms derived by Ogilvie & Tuck (1969). $\vec{r}$ is the position vector with respect to the origin of the hydrodynamic coordinate system. It should be noted that the evaluation of the m_j terms can be difficult if the interaction with the steady velocity potential Φ_S is accounted for since involving the second order derivatives of Φ_S.

4.1.4 Formation of 2.5D approach

The governing equation (4.23) for the normalized velocity potential ϕ_j is defined in three dimensional flow field. As mentioned in Chapter 2, most direct and accurate approach would be applying a 3D method no matter based on free surface Green function or Rankine type singularity. However, as we are looking for a more efficient tool which can make better use of the slenderness of the ship to reduce the complexity and computation time without sacrificing much accuracy, the 2.5D theory or 2D+t theory will be applied.

Similar to strip theories, the 2.5D theory assumes the ship hull to be long and slender which means that the draft D and beam B are much smaller than the length L of the ship, and a slenderness ratio $\varepsilon = B/L << 1$ is introduced. Based on this assumption, the original normal vector on the body surface can be approximated by the one on the cross sectional contour.

$$\left(n_1, n_2, n_3, n_4, n_5, n_6\right) \approx \left(0, N_2, N_3, yN_3 - zN_2, -xN_3, xN_2\right) \tag{4.25}$$

$N_j\left(j = 2,3\right)$ is component of inward unit normal vector of one point on the ship's cross sectional contour. Meanwhile， the variation in the x direction is assumed to be much smaller than the variation in the y and z direction, i.e., $\partial/\partial x << \partial/\partial y, \partial/\partial z$. Therefore, the 3D Laplace equation satisfied in (4.23) can be transformed to a 2D Laplace equation by neglecting the term of the order $O\left(\varepsilon^2\right)$. In addition, when the steady flow is approximated by neglecting the steady velocity potential Φ_S, i.e., $\vec{W} \approx -U\vec{i}$, the expression (4.24) gives the following m_j terms:

$$m_j = 0 \ (j = 1,2,3,4),\ m_5 = Un_3,\ m_6 = -Un_2 \tag{4.26}$$

Unlike in the ordinary strip theory, the sailing speed U is defined from moderate to relatively high, e.g., $F_n \geq 0.15$ in present study, and should be kept in the linearized free surface condition in the 2.5D theory. Moreover, no wave is induced ahead of the ship which indicates the Brard number, a product of the Froude number $F_n = U/\sqrt{gL}$ multipling the non-dimensional encounter frequency $\omega_e' = \omega_e \sqrt{L/g}$, should be

$$\tau = \frac{\omega_e U}{g} > \sqrt{\frac{2}{27}} \tag{4.27}$$

as claimed by Chen & Noblesse (1998). This can be understood as the ship is moving faster than the generated wave from physical point of view in brief.

Based on these assumptions, the governing equation (4.23) should be updated as follow.

$$\begin{cases} \dfrac{\partial^2 \phi_j}{\partial y^2} + \dfrac{\partial^2 \phi_j}{\partial z^2} = 0 & \textit{in the flow field} \\ i\omega_e \phi_j - U\dfrac{\partial \phi_j}{\partial x} + g\zeta_j = 0 & z = 0 \\ i\omega_e \zeta_j - U\dfrac{\partial \zeta_j}{\partial x} - \dfrac{\partial \phi_j}{\partial z} = 0 & z = 0 \\ \dfrac{\partial \phi_j}{\partial N} = \begin{cases} i\omega_e N_j + Um_j & (j = 2,...,6) \\ -\dfrac{\partial \phi_0}{\partial N} & (j = 7) \end{cases} & \textit{on } S_0 \\ \phi_j = \dfrac{\partial \phi_j}{\partial x} = 0 & x > x_f \\ \nabla \phi_j \to 0 & \textit{as } z \to -\infty \\ \textit{radiation condition} & \end{cases} \tag{4.28}$$

where ζ_j denotes the complex amplitude of free surface elevation in the j -th direction by the unit radiation and diffraction potential and x_f is the longitudinal position of ship forward perpendicular.

To solve this governing equation, a further transformation has to be performed with the time variables as follow.

$$t = \frac{x_f - x}{U} \tag{4.29}$$

$$\begin{cases} \varphi_j(y,z;t) = \phi_j(x,y,z)e^{i\omega_e t} \\ \varsigma_j(y,z;t) = \zeta_j(x,y,z)e^{i\omega_e t} \end{cases} \tag{4.30}$$

Finally, the BVP becomes

$$\begin{cases} \dfrac{\partial^2 \varphi_j}{\partial y^2} + \dfrac{\partial^2 \varphi_j}{\partial z^2} = 0 & \textit{in the flow field} \\ \dfrac{\partial \varphi_j}{\partial t} + g\varsigma_j = 0 & z = 0 \\ \dfrac{\partial \varsigma_j}{\partial t} - \dfrac{\partial \varphi_j}{\partial z} = 0 & z = 0 \\ \dfrac{\partial \varphi_j}{\partial N} = \begin{cases} \left(i\omega_e N_j + Um_j\right)e^{i\omega_e t} & \left(j = 2,...,6\right) \\ -\dfrac{\partial \phi_0}{\partial N}e^{i\omega_e t} & \left(j = 7\right) \end{cases} & \textit{on } S_0 \\ \varphi_j = \dfrac{\partial \varphi_j}{\partial t} = 0 & t = 0 \\ \nabla \varphi_j \to 0 & \textit{as } z \to -\infty \\ \textit{radiation condition} & \end{cases} \tag{4.31}$$

In this way, the original 3D BVP is successfully changed to a 2D time dependant BVP in a space fixed cross section plane. Then the flow field in the space fixed cross section plane is determined by repeatedly calculating the flow field at various instances after the ship's bow begins to penetrate the plane. Note that different time moment is corresponding to different cross section position. Therefore, the 3D flow field around the ship can be obtained by determining the flow field in a series of space fixed control planes which are placed at equal intervals along the ship's longitudinal direction as shown in Fig. 4.2. Then, the hydrodynamic forces and moments acting on the ship are evaluated by integrating the hydrodynamic pressure over the entire wet surface of the ship. If the ship advances forward for a distance equal to the interval of

the cross planes, then we stop the calculations at the last plane behind the ship and introduce a new plane in front of the ship and initialize the calculation in the new plane because the flow at a cross section is only influenced by the flow upstream of this section, but not by the flow downstream of it which is the key feature of the 2.5D theory. It is worth mentioning that the normal 20 stations division is not enough for calculations to obtain satisfied solution, and the required cross planes is related with the speed, i.e. lower advancing speed needs more planes. According to Ma et al. (2005), 60 sections are needed if the Froude number is lower than 0.2. Therefore, in present study the hull is divided into 80 sections with 81 space fixed control planes for the calculations.

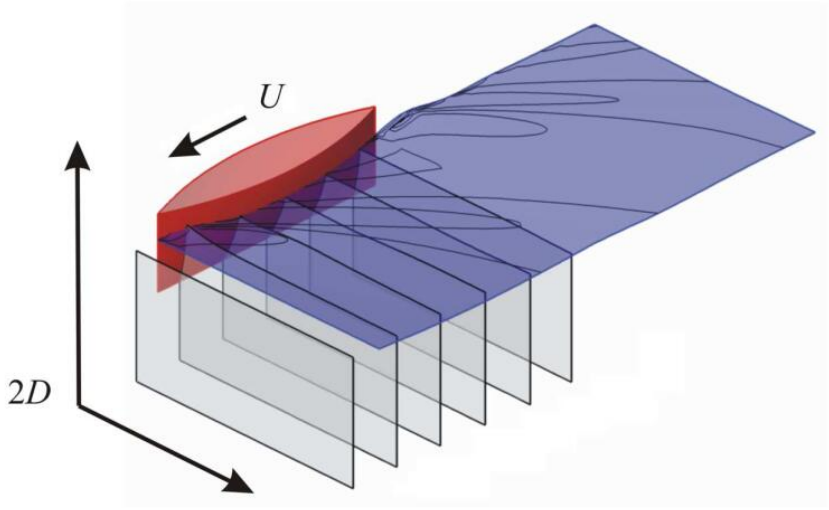

Fig. 4.2 Principle of 2.5D approach drawn by Kreuzer & Sichermann (2005)

The radiation velocity potentials φ_j can be further decomposed into a speed independent and a speed dependent part as follows

$$\varphi_j = \varphi_j^0 + \frac{U}{i\omega_e}\varphi_j^U \tag{4.32}$$

Therefore, the hull boundary condition is divided into the two hull conditions

$$\begin{cases} \dfrac{\partial \varphi_j^0}{\partial n} = i\omega_e N_j e^{i\omega_e t} \\ \dfrac{\partial \varphi_j^U}{\partial n} = i\omega_e m_j e^{i\omega_e t} \end{cases} \tag{4.33}$$

By using the simplified m_j terms (4.26), it follows that the radiation velocity potentials, including the speed dependent contributions, are given as

$$\begin{cases} \varphi_j = \varphi_j^0 \ \ (j = 1,2,3,4) \\ \varphi_5 = \varphi_5^0 + \dfrac{U}{i\omega_e}\varphi_3^0 \\ \varphi_6 = \varphi_6^0 - \dfrac{U}{i\omega_e}\varphi_2^0 \end{cases} \tag{4.34}$$

Therefore, the final BVP is finding the solution to φ_j^0.

Moreover, as the present study is focus on small amplitude oscillation motions, it is appropriate to assume that the free surface conditions satisfied by φ_j in (4.31) may be satisfied along the streamlines on $z = 0$ generated by uniform longitudinal motion, so we should first determine the steady flow potential Φ_S in the 2D control planes by following governing equations transformed from (4.22).

$$\begin{cases} \dfrac{\partial^2 \Phi_S}{\partial y^2} + \dfrac{\partial^2 \Phi_S}{\partial z^2} = 0 & in\,the\ flow\ field \\ U\dfrac{\partial \Phi_S}{\partial x} + g\zeta_S = 0 & on\ z = 0 \\ U\dfrac{\partial \zeta_S}{\partial x} - \dfrac{\partial \Phi_S}{\partial z} = 0 & on\ z = 0 \\ \dfrac{\partial \Phi_S}{\partial n} = Un_1 & on\ S_0 \\ \nabla \Phi_S \to 0 & as\ z \to -\infty \\ radiation\ condition & \end{cases} \tag{4.35}$$

4.2 **Hydrodynamic and hydrostatic forces**

Assuming the velocity potentials have already been obtained, the hydrodynamic pressure acting on the point on the ship mean wetted surface S_0 is

$$p = -\rho\left(\frac{\partial \Phi_T}{\partial t} - U\frac{\partial \Phi_T}{\partial x}\right) = \mathrm{Re}\left(\tilde{p}e^{i\omega_e t}\right),\ \tilde{p} = -\rho\left(i\omega_e\phi_T - U\frac{\partial \phi_T}{\partial x}\right) \tag{4.36}$$

where the atmospheric pressure p_a is set equal to zero.

Due to the linearity of a seakeeping problem, the total pressure can be decomposed into the contributions from incident wave potential, radiation potential and diffraction potential respectively as follow.

$$\begin{aligned}\tilde{p} &= -\rho A i\omega_0\phi_0 - \rho\sum_{j=2}^{6}\left(i\omega_e\phi_j - U\frac{\partial \phi_j}{\partial x}\right)\xi_j - \rho A\left(i\omega_e\phi_7 - U\frac{\partial \phi_7}{\partial x}\right)\\ &= -\rho A i\omega_0\phi_0 - \rho\sum_{j=2}^{6} e^{-i\omega_e t(x)}\frac{\partial \varphi_j}{\partial t}\xi_j - \rho A e^{-i\omega_e t(x)}\frac{\partial \varphi_7}{\partial t}\end{aligned} \tag{4.37}$$

Integrating the pressure over the whole ship, the total hydrodynamic forces $\vec{F}$ and moments $\vec{M}_O$ with respect to the hydrodynamic frame can be derived

$$\begin{cases}\vec{F}(t) = \iint_{S_0} p\vec{n}dS\\ \vec{M}_O(t) = \iint_{S_0} p\left(\vec{r}\times\vec{n}\right)dS\end{cases} \tag{4.38}$$

Or be expressed in matrix form

$$\left\{F(t)\right\} = \iint_{S_0} p(x,y,z,t)\left\{n_k\right\}dS \tag{4.39}$$

Substituting (4.37) into (4.39), and due to the slenderness of the ship, which means $ds = dl\cdot dx$, then

$$\left\{F(t)\right\} = \mathrm{Re}\left[\iint_{S_0} \tilde{p}(x,y,z)\left\{n_k\right\} ds \cdot e^{i\omega_e t}\right] = \mathrm{Re}\left[\left\{F_I(t)\right\} + \left\{F_R(t)\right\} + \left\{F_D(t)\right\}\right] \tag{4.40}$$

where,

$$\begin{cases} \left\{F_I(t)\right\} = -i\rho A\omega_0 \iint_{S_0} \phi_0 \left\{n_k\right\} ds \cdot e^{i\omega_e t} \\ \left\{F_R(t)\right\} = -\rho \sum_{j=2}^{6} \int_L e^{-i\omega_e t(x)} dx \int_{S_x(t)} \frac{\partial \varphi_j}{\partial t} \left\{n_k\right\} dl \cdot \xi_j e^{i\omega_e t} \\ \left\{F_D(t)\right\} = -\rho A \int_L e^{-i\omega_e t(x)} dx \int_{S_x(t)} \frac{\partial \varphi_7}{\partial t} \left\{n_k\right\} dl \cdot e^{i\omega_e t} \end{cases} \tag{4.41}$$

where $S_x(t)$ is the underwater contour of the cross section corresponding to time t.

The F-K force can be directly obtained by substituting (4.14), which is

$$\begin{aligned} \left\{F_I(t)\right\} &= -\rho A i\omega_0 \iint_{S_0} \phi_0 \left\{n_k\right\} ds \cdot e^{i\omega_e t} \\ &= \rho g A \int_L e^{-ik_0 x \cos\chi} \int_{S_x(t)} e^{k_0 z} e^{-ik_0 y \sin\chi} \left\{n_k\right\} dl \cdot e^{i\omega_e t} \end{aligned} \tag{4.42}$$

Regarding the radiation force and diffraction force, from (4.36), they can be expressed as follow.

$$\begin{cases} \left\{F_R(t)\right\} = \left[H\right]\left\{\xi\right\} e^{i\omega_e t} \\ \left\{F_D(t)\right\} = A\left\{H_{k7}\right\} e^{i\omega_e t} \end{cases} \tag{4.43}$$

where,

$$H_{kj} = -i\rho\omega_e \iint_{S_0} \phi_j n_k ds + \rho U \iint_{S_0} \frac{\partial \phi_j}{\partial x} n_k ds \tag{4.44}$$

is the hydrodynamic force and moment in the k-th direction per unit oscillatory displacement in the j-th mode.

By using the variant Stokes' formula, the second term in (4.44) can be rewritten as

$$\begin{cases} \iint_{S_0} U\frac{\partial \phi_j}{\partial x}\vec{n}ds = \iint_{S_0} Un_1\nabla\phi_j ds - U\int_{C_A+wl}\phi_j dl\times\vec{i} \\ \iint_{S_0} U\frac{\partial \phi_j}{\partial x}(\vec{r}\times\vec{n})ds = \iint_{S_0}\left[-U\phi_j\left(-n_3\vec{j}+n_2\vec{k}\right)+Un_1\vec{r}\times\nabla\phi_j\right]ds \\ \qquad\qquad +U\int_{C_A+wl}\phi_j\left(dl\times\vec{i}\right)\times\vec{r} \end{cases} \tag{4.45}$$

where C_A refers to the aftermost cross section or transom stern of the ship, *wl* represents waterline. It should be mentioned that, this transformation assumes the ship to be wall sided at the free surface. When this assumption is neglected, it needs to be adequately modified shown by Ronæss (2002). However, in the continuation of our discussion we will adopt the stated assumption.

For a slender body, the angle between dl at waterline and longitudinal direction is very small, thereby the term involving $\int_{wl}\phi_j dl\times\vec{i}$ can be neglected. At the aftermost cross section, $dl\times\vec{i} = dl\cdot\vec{N}$. Again, due to the slenderness assumption, $n_1 << n_2, n_3$, integrations on the body surface $\iint_{S_0} Un_1\nabla\phi_j ds$, $\iint_{S_0} Un_1\vec{r}\times\nabla\phi_j ds$ can be neglected. Therefore,

$$\begin{cases} \iint_{S_0} U\frac{\partial \phi_j}{\partial x}\vec{n}ds \approx -U\int_{C_A}\phi_j\vec{N}dl \\ \iint_{S_0} U\frac{\partial \phi_j}{\partial x}(\vec{r}\times\vec{n})ds \approx \iint_{S_0} -U\phi_j\left(-n_3\vec{j}+n_2\vec{k}\right)ds - U\int_{C_A}\phi_j\vec{r}\times\vec{N}dl \end{cases} \tag{4.46}$$

Substituting (4.25) and (4.26) into (4.46), we obtain a unified expression for (3.46).

$$\iint_{S_0} U\frac{\partial \phi_j}{\partial x}\vec{n}_k ds = \iint_{S_0} U\phi_j m_k ds - \int_{C_A} U\phi_j N_k dl \tag{4.47}$$

Then, (4.44) can be rewritten as

$$H_{kj} = -i\rho\omega_e \iint_{S_0} \phi_j n_k ds + \rho U \iint_{S_0} \phi_j m_k ds - \rho U \int_{C_A} \phi_j N_k dl \tag{4.48}$$

The radiation force can be further expressed in the form with added mass and damping coefficient.

$$\left\{F_R(t)\right\} = -[A]\left\{\ddot{\xi}\right\} - [B]\left\{\dot{\xi}\right\} \tag{4.49}$$

where,

$$\begin{cases} A_{kj} = \dfrac{1}{\omega_e^2}\mathrm{Re}\left(H_{kj}\right) \\ B_{kj} = -\dfrac{1}{\omega_e}\mathrm{Im}\left(H_{kj}\right) \end{cases} \tag{4.50}$$

'Re' and 'Im' stand for the real and imaginary part of the given expression. The general form of the added mass A_{kj} and damping coefficients B_{kj} for a ship with port starboard symmetry is given by

$$A_{kj}\ \left(or\ B_{kj}\right) = \begin{bmatrix} A_{22} & 0 & A_{24} & 0 & A_{26} \\ 0 & A_{33} & 0 & A_{35} & 0 \\ A_{42} & 0 & A_{44} & 0 & A_{46} \\ 0 & A_{53} & 0 & A_{55} & 0 \\ A_{62} & 0 & A_{64} & 0 & A_{66} \end{bmatrix} \tag{4.51}$$

The hydrostatic forces and moments, also called the restoring forces and moments, follow from the hydrostatic and mass considerations. The hydrostatic pressure acting on the point on the ship mean wetted surface can be expressed as

$$p_S = -\rho g\left(z + \xi_3 - x\xi_5 + y\xi_4\right) \tag{4.52}$$

Integrating the pressure over the wetted surface

$$\left\{F_S(t)\right\} = -[C]\left\{\xi(t)\right\} \tag{4.53}$$

The only non-zero $C_{kj}\left(k,j=1,...,6\right)$ coefficients for a ship with the lateral symmetry plane are

$$\begin{cases} C_{33}=\rho g A_W \\ C_{35}=C_{53}=-\rho g S_y \\ C_{44}=\rho g\nabla\overline{GM_T}=\rho g J_x+\rho g\nabla\left(z_B-z_G\right) \\ C_{55}=\rho g\nabla\overline{GM_L}=\rho g J_y+\rho g\nabla\left(z_B-z_G\right) \end{cases} \tag{4.54}$$

Here, z_G and z_B are the vertical coordinates of the center of gravity and the center of buoyancy, respectively. ∇ is the displaced volume of the ship. A_W is the water plane area. $\overline{GM_T}$ and $\overline{GM_L}$ are the transverse and longitudinal metacentric height, respectively. S_y, J_x and J_y are the static moment with respect to y axis, inertia moments with respect to x axis and y axis, respectively.

4.3 **5-DOF motions response in waves**

With all external forces derived, a differential equation of 5-DOF motions (without surge) can be established as follow.

$$\left(\left[m\right]+\left[A\right]\right)\left\{\ddot{\xi}\right\}+\left[B\right]\left\{\dot{\xi}\right\}+\left[C\right]\left\{\xi\right\}=\left\{f\right\}=\left\{F_I+F_D\right\} \tag{4.55}$$

where $\left\{f\right\}$ is the wave exciting force, $\left[m\right]$ is the generalized mass matrix. For a vessel with the lateral symmetry plane and the arbitrary vertical location of the center of gravity at z_G, the mass matrix is given as follow.

$$\left[m\right]=\begin{bmatrix} m & 0 & -mz_G & 0 & 0 \\ 0 & m & 0 & 0 & 0 \\ -mz_G & 0 & I_{11} & 0 & I_{13} \\ 0 & 0 & 0 & I_{22} & 0 \\ 0 & 0 & I_{31} & 0 & I_{33} \end{bmatrix} \tag{4.56}$$

where m is the mass of the ship, $I_{kj}\left(k, j=1,2,3\right)$, corresponding to roll, pitch and yaw, is the moment of inertia when $k=j$ and is the product of inertia when $k \neq j$. The explicit, exact or approximate (if a vessel mass distribution is unknown), definition of the I_{kj} can be found in the manual by Journèe & and Adegeest (2003). In addition, in the case of a ship with the pointed ends i.e., no transom stern, the terms $I_{13}=I_{31}$ are equal to zero. Furthermore, for a ship with lateral symmetry it also follows that the equation system (4.55) gives one set of the coupled heave-pitch equations and another set of the coupled sway-roll-yaw equations.

If further setting the complex amplitude of the exciting forces and motions as

$$\begin{cases}\{f_a\}=\{f_C\}+i\{f_S\} \\ \{\xi_a\}=\{\xi_C\}+i\{\xi_S\}\end{cases} \tag{4.57}$$

Then the motion equation of the complex amplitudes can be written as

$$\begin{cases}\left(\left[C\right]-\omega_e^2\left[m+A\right]\right)\{\xi_C\}-\omega\left[B\right]\{\xi_S\}=\{f_C\} \\ \left(\left[C\right]-\omega_e^2\left[m+A\right]\right)\{\xi_S\}+\omega\left[B\right]\{\xi_C\}=\{f_S\}\end{cases} \tag{4.58}$$

By solving (4.58), the RAO (response amplitude operator) and the phase can be derived as follow.

$$\frac{\{\xi_a\}}{A}=\frac{\left\{\sqrt{\xi_C^2+\xi_S^2}\right\}}{A},\ \{\angle\xi\}=\left\{\arg\left(\xi_C,\xi_S\right)\right\} \tag{4.59}$$

4.4 **Numerical schemes**

Back to solving the BVPs (4.31) and (4.35), a BEM is adopted by using Green's second identity. The velocity potential at a field point P within the fluid domain can be represented by

$$2\pi\varphi_P = \int_S \left[\varphi_Q \frac{\partial G(P,Q)}{\partial n_Q} - G(P,Q) \frac{\partial \varphi_Q}{\partial n_Q} \right] ds_Q \tag{4.60}$$

where $G(P,Q) = \ln r(P,Q)$ is 2D Green function at field point P due to a source point Q on the fluid boundary, $r(P,Q)$ is the distance between P and Q. The fluid domain is surrounded by a closed boundary S consisting of the body surface S_0, the free surface S_F, the boundary at infinity S_R (right side), the bottom surface S_B (if in shallow water) and the symmetry line boundary below the keel S_K. As seen in Fig. 4.3, only half of the flow domain is taken into account due to the symmetry (vertical motions) or asymmetry (lateral motions) of the flow around the hull. By letting the field point P approach S, an integral equation can be obtained as follow.

$$\varphi_P = \frac{1}{\alpha} \int_{S-S_{(P)}} \left[\varphi_Q \frac{\partial \ln r(P,Q)}{\partial n_Q} - \ln r(P,Q) \frac{\partial \varphi_Q}{\partial n_Q} \right] ds_Q \tag{4.61}$$

where $S_{(P)}$ is a small semicircle around the point P, the internal angle α is equal to π when the surface is smooth, otherwise the angle should be calculated separately.

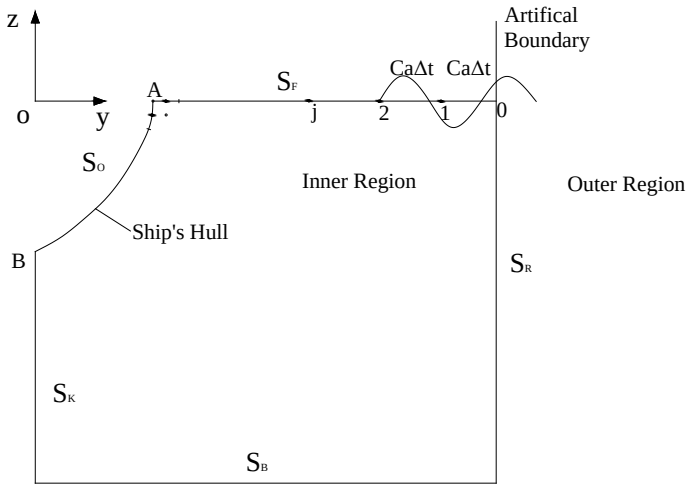

Fig. 4.3 Computational domain of a control plane

In the numerical calculations, the boundary of the domain is discretized into small straight line segments. The velocity potential and its normal derivative are assumed constant over the element and the boundary conditions are satisfied on the midpoint of each element. Equally distributed elements are used on the body surface (40 to 50 elements), the boundary at infinity and sea bottom (if in shallow water). Further, elements varying in size are distributed on the symmetry line boundary. The element closest to the body surface has the same size as its neighboring body surface element. Then the elements are geometrically increasing along the symmetry line boundary, as they are further away from the body. The free surface boundary is divided in two regions. Equal elements are distributed on the first region near the body, while geometrically increasing elements are distributed on the other region far from the body. Usually more elements are distributed on the near-body region than on the other region. The length ratio of these two regions and the number of elements on them can be adjusted. Generally speaking, two rules are followed. The first rule is to use finer elements on regions closer to the body and to use larger elements far away from the body. The other rule is to control that the ratio of lengths of two adjacent elements is around one, so that they have similar size. The boundary at infinity are places 4 to 6 times of beam away from the hull.

By this discretization, the integral equation resulting from (4.61) can be discretized into a set of linear algebraic equations with N_S unknowns which is the total number of the discretized elements on the closed boundary S, of which n_1 on the body surface S_0, n_2 on the free surface S_F, n_3 on the open boundary at infinity S_R, n_4 on the symmetry line boundary below the keel S_K. On boundaries with Dirichlet conditions, φ is known including the free surface, the boundary at infinity and the symmetry line boundary below the keel in lateral motions which is $\varphi = 0$, whereas on boundaries with Neumann conditions, $\partial\varphi/\partial n$ is known including the body surface, the bottom surface (if in shallow water) and the symmetry line boundary below the keel in vertical motions which is $\partial\varphi/\partial n = 0$. One can move the unknown terms to one side and the terms already known to the other side of the equation, hence,

$$\sum_{j=1}^{n_1} D_{ij}\varphi_j - \sum_{j=n_1+1}^{n_1+n_2} S_{ij}\frac{\partial \varphi_j}{\partial n} - \sum_{j=n_1+n_2+1}^{n_1+n_2+n_3} S_{ij}\frac{\partial \varphi_j}{\partial n} + \sum_{j=n_1+n_2+n_3+1}^{n_1+n_2+n_3+n_4} D_{ij}\varphi_j = \sum_{j=1}^{n_1} S_{ij}\frac{\partial \varphi_j}{\partial n} - \sum_{j=n_1+1}^{n_1+n_2} D_{ij}\varphi_j - \sum_{j=n_1+n_2+1}^{n_1+n_2+n_3} D_{ij}\varphi_j \quad \text{Vertical motions} \tag{4.62}$$

$$\sum_{j=1}^{n_1} D_{ij}\varphi_j - \sum_{j=n_1+1}^{n_1+n_2} S_{ij}\frac{\partial \varphi_j}{\partial n} - \sum_{j=n_1+n_2+1}^{n_1+n_2+n_3} S_{ij}\frac{\partial \varphi_j}{\partial n} - \sum_{j=n_1+n_2+n_3+1}^{n_1+n_2+n_3+n_4} S_{ij}\frac{\partial \varphi_j}{\partial n} = \sum_{j=1}^{n_1} S_{ij}\frac{\partial \varphi_j}{\partial n} - \sum_{j=n_1+1}^{n_1+n_2} D_{ij}\varphi_j - \sum_{j=n_1+n_2+1}^{n_1+n_2+n_3} D_{ij}\varphi_j \quad \text{Lateral motions} \tag{4.63}$$

where subscripts i, j now denote the serial numbers of the segments, the matrix coefficients S_{ij} and D_{ij} correspond to integrals of the Green's function and its normal derivative over the length area Δl_j of the j-th segment respectively as

$$S_{ij} = \int_{\Delta l_j} \ln r_{ij}\, dl \tag{4.64}$$

$$D_{ij} = \begin{cases} \int_{\Delta l_j} \dfrac{\partial \ln r_{ij}}{\partial n} dl & i \neq j \\ \pi & i = j \end{cases} \tag{4.65}$$

Applying numerical integrations, e.g., Gauss-Legendre quadrature, to obtain the matrix coefficients S_{ij} and D_{ij}, then algebraic equations (4.62) and (4.63) can be solved by Gauss elimination.

Special care must be taken near the intersection of the body surface and the water surface. The velocity potential is continuous on this intersection. However, the normal velocity is discontinuous because the normal directions at the two sides of the intersection are different. A common treatment to this problem is to assume that the normal velocity should be known on the body surface, but unknown on the free surface. So the normal velocity on the intersection at the free surface side is solved together with the other points on the free surface.

In the following, more details about dealing with the free surface condition and radiation condition are given.

4.4.1 Free surface condition

On the free surface, the following approximations to free surface kinematic and dynamic boundary conditions satisfied by potential φ_j in (4.31) are applied.

$$\begin{cases} \varsigma_j(y+\frac{\Delta y}{2},t+\frac{\Delta t}{2}) = \varsigma_j(y-\frac{\Delta y}{2},t-\frac{\Delta t}{2}) + \Delta t\frac{\partial \varphi_j}{\partial z}(y,0,t) \\ \varphi_j(y+\Delta y,0,t+\Delta t) = \varphi_j(y,0,t) - g\Delta t\varsigma_j(y+\frac{\Delta y}{2},t+\frac{\Delta t}{2}) \end{cases} \tag{4.66}$$

where Δt is time interval of the stepping procedure, and,

$$\Delta y = \Delta t\frac{\partial \Phi_S}{\partial y}(y,0,t) \tag{4.67}$$

This algorithm has been proved stable by Chapman (1976).

Using the initial free surface condition, there is no fluid field disturbance at time $t=0$, we can evaluate the free surface elevation and the fluid potential by

$$\begin{cases} \varsigma_j(y+\frac{\Delta y}{2},\frac{\Delta t}{2}) = \varsigma_j(y,0) + \frac{\Delta t}{2}\frac{\partial \varphi_j}{\partial z}(y,0,0) \\ \varphi_j(y+\Delta y,0,\Delta t) = \varphi_j(y,0,0) - g\Delta t\varsigma_j(y+\frac{\Delta y}{2},\frac{\Delta t}{2}) \end{cases} \tag{4.68}$$

Apparently, the key step prior to (4.66) and (4.68) stepping is determining the steady flow potential first, which can be achieved by solving the BVP of (4.35) using the BEM introduced above together with the following free surface approximations.

$$\begin{cases} \zeta_S(x_{n+1},y) = \zeta_S(x_n,y) + \frac{\Delta x}{U}\frac{\partial \Phi_S}{\partial z}(x_n,y) \\ \Phi_S(x_{n+1},y) = \Phi_S(x_n,y) - g\frac{\Delta x}{U}\zeta_S(x_{n+1},y) \end{cases} \tag{4.69}$$

By substituting the starting conditions at the bow, $\Phi_S = 0, \zeta_S = 0$. Here, the subscript in x_n, x_{n+1} represent the station serial number counting from the bow.

4.4.2 Radiation condition

Regarding the radiation condition, Sommerfeld (1949) gave a brilliant description that is the sources must be sources, not sinks of energy. The energy which is radiated from the sources must scatter to infinity, no energy may be radiated from infinity into the field. To reach this target, several practical treatments have been proposed such as the finite difference technique by Orlanski (1976), the numerical damping beach proposed by Israeli & Orszag (1981) and applied to ship wave problems by Nakos et al. (1994), mismatching technique by moving the source points on the free surface at some distance downstream by Jensen et al. (1986). More recently， Das & Cheung (2012) and Yuan et al. (2014) applied a corrected Sommerfeld radiation condition by taking into account the Doppler shift effect which is available for radiation problem at very slow speed.

Apart from these, Liao (1996) described a general expression of one way wave propagation and developed a system of local non-reflecting boundary conditions using the space-time extrapolation. Its initial aim is to deal with the propagation of earthquake wave out of artificial boundary. In this section, the MTF method about velocity potential φ in water wave problems can be written as follows.

Let y axis be the normal to the artificial boundary S_R and point to the outer region of the model as shown in Fig.4.3. Suppose that the intersection point 0 of the y axis and the artificial boundary is the radiation boundary point on S_R under consideration. 1 and 2 are the points which are away from point 0 along its normal vector to the inner region. The distance between them will be discussed later.

The outgoing waves impinging upon the radiation boundary point may be expressed by their apparent propagation along the y axis,

$$\varphi(y,t) = \sum_i f_i\left(c_{yi}t - y\right) \tag{4.70}$$

where $\varphi(y,t)$ is a function of y and t consisting of arbitrary number of one way waves $f_i(c_{yi}t-y)$, each of them propagates along the y axis with an apparent speed c_{yi}, f_i are arbitrary functions. The apparent propagation of the one way waves in (3.70) is written (neglecting the subscript) as

$$\varphi(y,t)=f(c_y t-y) \tag{4.71}$$

Using (4.71), it is easy to see that

$$\varphi(y,t+\Delta t)=\varphi(y-c_y\Delta t,t) \tag{4.72}$$

where Δt is the time step. Then an artificial wave speed c_a is introduced to replace the physical wave speed c_y. Because c_y is usually unknown, whereas c_a can be chosen flexible in a range between 0.6 and 1.6 times of physical wave speed as suggested by Xu & Duan (2008). The distance between point j and 0 is $jc_a\Delta t$ along the normal vector of point 0 to the inner region. (4.72) is first replaced by

$$\varphi(y,t+\Delta t)=\varphi(y-c_a\Delta t,t)+\Delta\varphi(y,t+\Delta t) \tag{4.73}$$

where the error term $\Delta\varphi(y,t+\Delta t)$ expresses the error introduced by c_a replacing c_y. (4.73) yields

$$\Delta\varphi(y,t+\Delta t)=\varphi(y,t+\Delta t)-\varphi(y-c_a\Delta t,t) \tag{4.74}$$

Substituting (4.71) into (4.74), we may write

$$\Delta\varphi(y,t+\Delta t)=f_1(c_y t-y) \tag{4.75}$$

where f_1 is a function of $c_y t-y$. Following (4.73) the error term may be written as

$$\Delta\varphi\left(y,t+\Delta t\right)=\Delta\varphi\left(y-c_a\Delta t,t\right)+\Delta^2\varphi\left(y,t+\Delta t\right) \tag{4.76}$$

Having replaced y and t in (4.74) by $y-c_a\Delta t$ and $t-\Delta t$, respectively, the first term in the right hand side of (4.76) is written as

$$\Delta\varphi\left(y-c_a\Delta t,t\right)=\varphi\left(y-c_a\Delta t,t\right)-\varphi\left(y-2c_a\Delta t,t-\Delta t\right) \tag{4.77}$$

and the error term in (4.76) is written as

$$\Delta^2\varphi\left(y,t+\Delta t\right)=\Delta\varphi\left(y,t+\Delta t\right)-\Delta\varphi\left(y-c_a\Delta t,t\right) \tag{4.78}$$

Substitution of (4.76) into (4.73) yields

$$\varphi\left(y,t+\Delta t\right)=2\varphi\left(y-c_a\Delta t,t\right)-\varphi\left(y-2c_a\Delta t,t-\Delta t\right)+\Delta^2\varphi\left(y,t+\Delta t\right) \tag{4.79}$$

It is easy to see that $\Delta^2\varphi\left(y,t+\Delta t\right)$ and the higher order error terms are all functions of c_yt-y. Therefore, following the above formulation we can obtain

$$\varphi\left(y,t+\Delta t\right)=\varphi\left(y-c_a\Delta t,t\right)+\sum_{m=1}^{N-1}\Delta^m\varphi\left(y-c_a\Delta t,t\right)+\Delta^N\varphi\left(y,t+\Delta t\right) \tag{4.80}$$

where

$$\Delta^m\varphi\left(y-c_a\Delta t,t\right)=\Delta^{m-1}\varphi\left(y-c_a\Delta t,t\right)-\Delta^{m-1}\varphi\left(y-2c_a\Delta t,t-\Delta t\right) \tag{4.81}$$

$$\Delta^N\varphi\left(y,t+\Delta t\right)=\Delta^{N-1}\varphi\left(y,t+\Delta t\right)-\Delta^{N-1}\varphi\left(y-c_at,t\right) \tag{4.82}$$

Suppose that the origin of the y axis is the boundary point, the coordinates of calculating point are $y=-jc_a\Delta t$ and time $t=p\Delta t$, where integer p represents the time level, the terms of $\varphi\left(y-c_a\Delta t,t\right)$ and $\Delta^m\varphi\left(y-c_a\Delta t,t\right)$ are written as

$$\varphi_j^p = \varphi\left(-jc_a\Delta t, p\Delta t\right) \tag{4.83}$$

$$\Delta^m\varphi_j^p = \Delta^m\varphi\left(-jc_a\Delta t, p\Delta t\right) \tag{4.84}$$

Neglecting the error term of (4.80) and using (4.83) and (4.84), the (4.80) can be written as

$$\varphi_0^{p+1} = \varphi_1^p + \sum_{m=1}^{N-1}\Delta^m\varphi_1^p \tag{4.85}$$

where

$$\Delta^m\varphi_1^p = \sum_{j=1}^{m+1}\left(-1\right)^{j+1}C_{j-1}^m\varphi_j^{p+1-j} \tag{4.86}$$

The binomial coefficients are

$$C_j^m = \frac{m!}{\left(m-j\right)!\,j!} \tag{4.87}$$

Substituting (4.86) into (4.85) can obtain the non-reflecting radiation condition on S_R

$$\varphi_0^{p+1} = \sum_{j=1}^{N}\left(-1\right)^{j+1}C_j^N\varphi_j^{p+1-j} \tag{4.88}$$

N is the order of the MTF. In present study, $N=2$ will be considered. So (4.88) is written as

$$\varphi_0^{p+1} = 2\varphi_1^p - \varphi_2^{p-1} \tag{4.89}$$

(4.89) is the second order radiation condition, where the subscript 0 is the point on the artificial boundary, 1 and 2 are the points which are $c_a\Delta t$ and $2c_a\Delta t$ away from point 0 along its normal vector to the inner region, respectively.

4.4.3 Execution procedure

After all the numerical schemes have been described, the procedure of solving the unsteady velocity potentials is now briefly described here.

Step 1) At $t = 0$, assume that before ship's bow penetrates the space fixed cross plane, the fluid is at rest, thus the potential is equal to zero on the free surface and the open boundary as well. At the boundary under the keel, the potential or its normal derivative is constantly zero because of the asymmetry or symmetry of the flow caused by corresponding motion.

Step 2) At $t = t$, the bow starts to penetrate the cross plane and thereafter, the 2D BVP is solved by using the Rankine singularity based BEM. Thereby, the values of potential on the body surface and the normal derivative on the free surface are calculated.

Step 3) Still at $t = t$, obtain the values of potential at internal points adjacent to the open boundary which is necessary in the treatment of radiation condition according to MTF method. Then obtain the values of potential on the open boundary at following step of $t = t + \Delta t$.

Step 4) Determine the values of steady flow potential first, then stepping the values of unsteady flow potential on the free surface at $t = t + \Delta t$ by using the numerical scheme of the free surface condition.

Step 5) In order to determine the potential on the free surface at $t = t + \Delta t$, the free surface in the vicinity of the hull are again subjected to division since the hull shape at $t = t + \Delta t$ varies from that at $t = t$.

Step 6) Determine the values of potential at the new nodes on the free surface by linear interpolation of the values obtained at step 4.

Step 7) Return to step 2 and repeating the procedure until the whole ship penetrate the plane. Then the time history of the hydrodynamic force acting on the hull section situated in the fixed cross plane can be derived.

Step 8) Integrating the forces in all cross planes along the ship length, the total forces and moment can be obtained for the evaluation of motion responses.

A brief flow chart of the seakeeping analysis module is illustrated in Fig. 4.4.

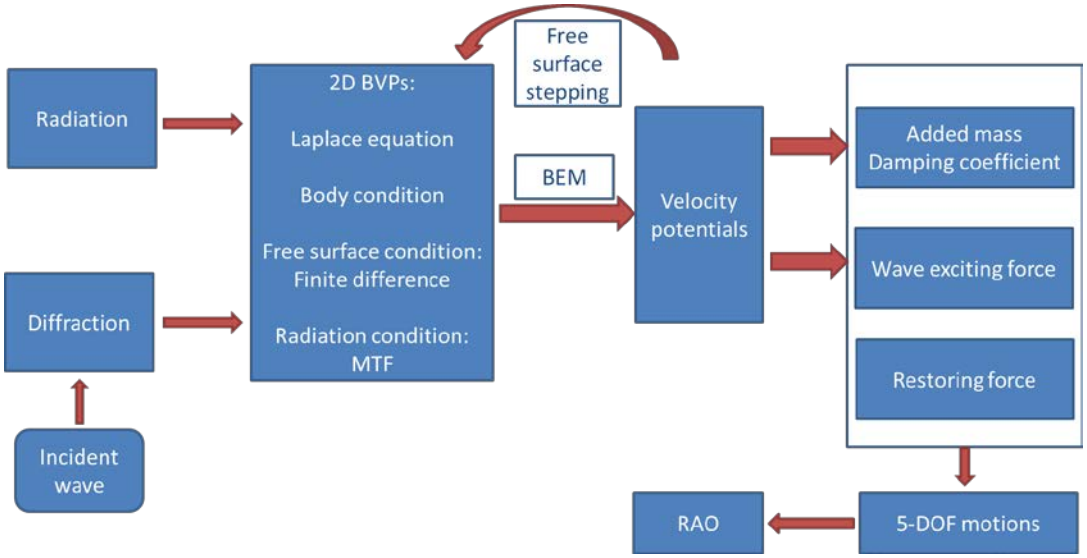

Fig. 4.4 Flow chart of seakeeping analysis

4.5 Additional problems

So far, we have already presented the regular seakeeping analysis of a slender displacement ship in straight moving. In the following, several additional problems which also occur in the scope of seakeeping analysis but usually get less attention will be discussed. They are related to the lateral motions, thereby are to some extent important to the manoeuvring analysis which will be focused on later.

4.5.1 Viscous correction on the roll damping

As known to all, viscous effects should not be neglected in lateral motions. Especially in roll motion, the amplitude of the roll displacement is significantly affected by water viscosity even in the case of a ship without bilge keels. Therefore, it cannot be computed with adequate accuracy if only the roll damping coefficient based on the potential flow theory is accounted for. In fact, there are five components in the equivalent roll damping for a ship, i.e.,

$$B_{44_e} = B_{BK} + B_E + B_F + B_L + B_W \tag{4.90}$$

- B_{BK} due to the bilge keels which consists of the moment due to normal forces on the bilge keels, the moment due to the modification of the fluid flow caused by

the presence of the bilge keels, the moment due to waves generated by the bilge keels.

- B_E due to formation of eddies caused by viscous separation near the sharp corners of the cross sections.
- B_F due to skin friction of the hull in contact with water.
- B_L due to lift forces caused by the angle of attack on the hull when the ship experiences roll.
- B_W due to the waves generated by the rolling ship. Note that this is already estimated by the potential flow theory presented above.

Determination of the roll damping can be carried out by free rolling model tests or empirical methods such as Ikeda et al. (1978). In the present study, a relative simpler empirical estimation method by Himeno (1981) is adopted. The estimation formulae for each components are given in Appendix A.

4.5.2 Inertia forces acting on the hull at low frequency

The BVPs discussed above is for the high frequency wave induced motions which are essential in regular seakeeping analysis. Meanwhile, it is also worth to present the BVPs for low frequency motions, especially in lateral motions as these solutions approaching limiting value of zero frequency can derive the inertia forces acting on the hull in manoeuvring motions in the form of added mass and added moment of inertia.

In this case, the free surface condition in (4.31) can be substituted by a rigid wall as

$$\frac{\partial \varphi_j}{\partial z} = 0 \qquad on \;\; z = 0 \tag{4.91}$$

Therefore, the resulting BVP can be satisfied by using the mirror image of the 2D cross section about the undisturbed free surface plane.

For lateral motions, the velocity potential on the body is an even function of z and the normal velocity has the same value at corresponding points on the body and its mirror

image. So that, for example of the sway motion, the mirror image of the body is in phase with the real body which means that the mirror image moves in the same direction with the swaying body. By the way, the situation is somewhat different for vertical motions such as heave. Although we can still consider having a double body moving in infinite fluid, this double body now experiences a vertical expansion and contraction symmetrical about horizontal plane. A non-existence of the free surface implies that the body cannot generate any free surface waves, which consequently means that the values of the damping coefficients are zero.

The solving of the BVPs for the velocity potentials with the rigid wall free surface condition (4.91) is same as the procedure described previously.

4.5.3 Approximation for lift force

Apart from the above mentioned inertia components, forces due to the viscosity of the fluid is another important component especially in the lateral motions related to the manoeuvring which should not be neglected in estimations. Furthermore, when a ship is advancing at a small drift angle, the linear part of the viscous force is dominant which is often referred as the lift force just like a wing seen from overhead view. Although this is mainly a subject in manoeuvring analysis, discussion will be presented here in advance since it is also vital to a seakeeping analysis as long as the flow around the ship is asymmetry about the center plane such as a ship approaching a bank or two ships overtaking each other. .

Firstly, a brief explanation of the principle of the lift problem is given here by considering a wing moving in unbounded flow field as shown in Fig. 4.5. The angle of attack is α between the moving direction and the chord line from the leading edge to the trailing edge. If we originally establish a BVP without taking the lift effect into account, the streamline will flow round the trailing edge at an infinite velocity until a stagnation point on the leeward side of the wing. This violates the physical phenomena. Moreover, it will lead to a zero total hydrodynamic force on the wing which is known as the *d'Alembert* paradox. In fact, a circulation is created since the wing starts to move from rest. This circulation pushes the stagnation point back to the trailing edge, then the flow leaves the trailing edge in a smooth tangential manner. This may seem to contradict the Kelvin's theorem that the circulation should be

constant about any material contour always containing the same fluid particles. So the constant must equal zero if the motion starts from rest. This apparent contradiction can be resolved by noting that a sufficiently large material boundary surrounding the wing initially and hereafter. The circulation on the wing named as the bound vortex is cancelled by an equal and opposite starting vortex shed from the trailing edge into the wake during the initial acceleration. These two vortices together with the free vortex originating from the ends of the bound vortex along the longitudinal direction form a vortex ring and the region bounded by the vortex ring is called trailing vortex sheet. As the circulation is restricted in the body surface and the trailing vortex sheet, flow field bounded by these surfaces is irrotational thereby still satisfies the Laplace equation. Then a lift force is induced on the wing due to the circulation of the bound vortex. In this way, the BVP around the wing should be revised to account for the circulation and ensure the flow velocity at the trailing edge has a limited value, which is the definition of a Kutta condition imposed on the trailing edge. It holds a general expression as follow.

$$\nabla\phi\big|_{TE} < \infty \tag{4.92}$$

More specific forms can be applied in the numerical processing such as equal pressure on both sides of the trailing edge, equal tangential velocities on both sides of the tailing edge, or zero normal velocity on the extension stream line down from the trailing edge. Further details about the Kutta condition is given by Xu (1998).

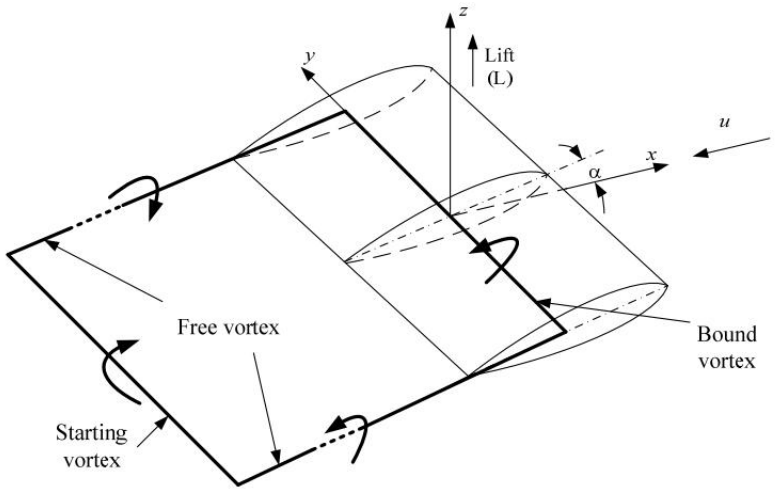

Fig. 4.5 A wing moving at constant speed in unbounded fluid domain

From the above description, we can clearly realize that this lift effect is a total 3D flow effect which represents the influence of the vortex sheet to the hull ahead of it. However, in the 2.5D theory, the upstream effect of the flow is completely neglected which means this trailing vortex cannot be felt by the hull. In order to account for this lift force, an indirect way by using two different methods, i.e., solving the problem asymptotically based on the slender wing theory described by Katz & Plotkin (1991) and the 3D numerical solution by distributing vortex elements based on the low aspect ratio wing theory described by Newman (1977). They are briefly presented as follow.

In the slender wing theory, only the portion of the wing ahead of one cross section will have influence on this section, whereas the influence of the wing sections and the flow field behind this section is negligible. It means the effect of trailing wake is small. The existence of the trailing edge is not felt by the water flow in front of it. Such properties in the slender wing theory are quite similar as those in a 2.5D theory. Considering a wing consisting of the ship and its mirror image about the undisturbed horizontal free surface plane, the pressure jump across the wing can be given as follow from the slender wing theory,

$$\Delta p = 2\rho U(x)\alpha \frac{\partial}{\partial x}\left[U(x)\sqrt{\left(b(x)/2\right)^2 - y^2}\right] \tag{4.93}$$

where $b(x)$ is the local span which actually is twice the ship draft D, and $U(x) = \sqrt{u^2 + (v + rx)^2}$ is the local inflow velocity. By integrating the pressure spanwise, the longitudinal lift force distribution on the ship can be obtained as.

$$\frac{dY_L}{dx} = \frac{\rho\pi U(x)\alpha}{8}\frac{\partial}{\partial x}\left[U(x)b(x)^2\right] \tag{4.94}$$

From this equation, if there is no change in $b(x)$ and no rotation, there will be no lift due to this section.

In the low aspect ratio wing theory, the relation between the lift force and the circulation is given according to the Joukowski theorem as

$$Y_L = \rho U \Gamma \tag{4.95}$$

where Γ is the circulation around the wing due to the bound vortex.

For convenience, an auxiliary body fixed reference is introduced with its origin located at the midpoint of the leading edge and the X axis pointing to the trailing edge. A vortex distribution $\gamma(\xi)$ is imposed on the center plane of the wing with constant value spanwise but varying chordwise, the two parallel free vortices extend to infinity with a downwash angle Θ respect to the wing surface. Then using (4.95), the life force and moment on the wing are given as

$$\begin{cases} Y_L = -\rho U D \int_0^L \gamma(\xi) d\xi \\ N_L = -\rho U D \int_0^L \gamma(\xi)\left(\frac{L}{2} - \xi\right)\xi d\xi = Y_L \frac{L}{2} + \rho U D \int_0^L \gamma(\xi)\xi d\xi \end{cases} \tag{4.96}$$

Therefore, the key problem is to derive the vortex distribution $\gamma(\xi)$.

The Kutta condition gives the vortex strength at the trailing edge as

$$\gamma(L) = 0 \tag{4.97}$$

And the body surface condition should be satisfied which means along the centerline of the wing surface, the normal velocity induced by the bound vortices and free vortices should equal the opposite value of the lateral velocity of the wing which is $-v - (L/2 - X)r$. According to the Biot-Savart Law, the normal velocity induced by the bound vortex element is

$$dV_A = \frac{\gamma(\xi) d\xi}{2\pi(X - \xi)} \cdot \frac{D}{\sqrt{(X - \xi)^2 + D^2}} \tag{4.98}$$

Similarly, the normal velocity induced by the free vortices is

$$\begin{cases} dV_F = \dfrac{\gamma(\xi)d\xi}{2\pi\sqrt{D^2+(X-\xi)^2\tan^2\Theta}}\left[\dfrac{X-\xi}{\cos\Theta\sqrt{D^2+(X-\xi)^2}}+1\right]\cos\mu \\ \cos\mu = \dfrac{D}{\sqrt{D^2+(X-\xi)^2\tan^2\Theta}} \end{cases} \tag{4.99}$$

The downwash angle is chosen approximately as follow.

$$\Theta = 0.5\arctan\left[(v+rx)/u\right] \tag{4.100}$$

Finally, following integration equation can be established for the determination of the vortex distribution.

$$-v-\left(\frac{L}{2}-X\right)r = \frac{1}{2\pi}\int_0^L \frac{\gamma(\xi)}{X-\xi}K(X,\xi)d\xi \tag{4.101}$$

where,

$$K(X,\xi) = \frac{D}{\sqrt{(X-\xi)^2+D^2}} + \frac{D(X-\xi)}{D^2+(X-\xi)^2\tan^2\Theta}\left[\frac{X-\xi}{\cos\Theta\sqrt{D^2+(X-\xi)^2}}+1\right] \tag{4.102}$$

In this way, the total life force and moment together with the lift distribution along the longitudinal direction on the wing can be obtained.

Then, the ratio between the results from these two methods can be used as a sectional 3D correction factor as

$$f_{2.5} = \frac{(dY_L/dx)_{3D}}{(dY_L/dx)_{2D}} \tag{4.103}$$

Subscripts $2D$ and $3D$ denote the solutions by the slender wing theory and the low aspect ratio wing theory respectively. This sectional factor will be multiplied to the force distribution results by 2.5D to make the correction.

4.6 Summary of the chapter

In this chapter, the exact BVP of a slender ship advancing in waves is first established mathematically in 3D flow field according to the physical features of the problem. Then by applying the Neumann-Kelvin linearizationon, the free surface condition is linearized on the calm water and the body surface condition is fulfilled on the mean wetted body surface. Further simplifications based on the slenderness assumption of the ship leads to the transformation of the 3D BVP into a 2D time dependent BVP with the speed effect kept. A 2.5D approach is introduced to solve the problem by applying a Rankine type singularity based BEM. Special numerical schemes are introduced. The free surface condition is implemented in a finite difference expression for time stepping and the radiation condition is fulfilled by a second order MTF scheme. The formulae of the resulting hydrodynamic forces and moments acting on the ship are given according to the Bernoulli equation with the help of the variant Stokes' formula, together with the 5-DOF motions response equations established. At last, additional problems about the viscous correction on the roll damping, BVPs for the low frequency lateral motions are presented. The lift force neglected in the 2.5D approach is taken into account indirectly by multiplying a ratio factor based on the results obtained by the slender wing theory and the low aspect ratio wing theory.

5 BEM based on NURBS

5.1 Introduction of NURBS

Before computers invented, designs were drawn by hand on paper with various drafting tools, i.e., rulers for straight lines, compasses for circles, and protractors for angles. But many shapes, such as the free form curve of a ship's bow, could not be drawn with these tools. Although such curves could be drawn freehand at the drafting board, shipbuilders often needed a life-size version which could not be done by hand. Such large drawings were done with the help of flexible strips of wood, called splines. The splines were held in place at a number of predetermined points, called ducks. Between the ducks, the elasticity of the spline material caused the strip to take the shape that minimized the energy of bending, thus creating the smoothest possible shape that fit the constraints. The shape could be tweaked by moving the ducks.

As computers were introduced into the design process, geometric modelling by mathematical expressions becomes possible and then several kinds of splines or surfaces were developed, e.g., cubic spline and Bezier spline. The physical properties of them have been investigated so that they could be used to model shapes with mathematical precision and reproduced where needed. However, the common disadvantage of these tools is lack of local control to dynamically change curve shapes for design requirements. Take the Bezier spline for example, moving one single control point would lead to the deformation of the whole shape, thus with more control points for higher degree curve, the curve will become unstable. Besides, the curve is relatively far from the control polygon which further make its precision hard to be ensured. For these reasons, the B-spline is invented for its local control characteristic and other advantages like available for degree elevation, knots insertion or elimination and multiple knot technique in free form shape type modelling design.

Although the B-spline is fairly enough for normal traditional ship types modelling, it is unavailable for describing the conics or quadric precisely except parabola or paraboloid which means modern ship types like LNG with special parts would be out

of its range. Therefore, based on B-spline and Non-rational Bezier spline, Non-Uniform Rational B-Splines (NURBS) is developed which can accurately describe any shape from a simple 2D line, circle, arc, or curve to the most complex 3D free-form surface or solid in mathematical representations uniformly which perfectly remedy the above mentioned disadvantage of B-spline. In 1991, the International Standardization Organization (ISO) issued the Standard for The Exchange of Product model data (STEP), and announced NURBS as the unique mathematical description method for the geometry definition of industrial products. Nowadays, NURBS has been widely used in computer aided manufacturing (CAM) and computer aided design (CAD) fields.

Specifically, NURBS geometry has following six important advantages that make it an ideal choice for computer aided modelling.

- Providing a common mathematical form to precisely represent standard analytical shapes, i.e., elementary curve or surface, and free form curve or surface simultaneously which means a unified database can be used to store the shape information of both categories.
- Manipulating control points and the weight factor provides sufficient flexibility for various shapes design.
- Stable and fairly fast calculation.
- Obvious geometric interpretation for designers.
- Powerful geometry processing technologies, e.g., knot insertion and elimination, degree elevation, decomposition, combination, etc.
- Invariant under affine transformations such as scaling, rotation, translation and perspective projection.

Although NURBS still has several disadvantages, e.g., it needs extra storage to define the traditional curve or curved surface, and improper weight factor chosen can lead to very poor parameterization, its application in present study would not be affected by these problems which are beyond the scope of the study and need extra efforts to be made on.

In the following, definition of NURBS will be introduced step by step from Bezier spline and B-spline since they are the basic of NURBS. To be specific, Bezier spline can be considered as a special case of B-spline while B-spline can be categorized into NURBS as shown in Fig. 5.1. Then fundamental algorithms of NURBS applied in the study will be formulated followed by modelling verification on unit circle, mathematical ship types and further validation on real ships. After that, an extension of the BEM presented in Chapter 4 using NURBS will be described. Finally, the developed NURBS based 2.5D seakeeping analysis tool will be validated on several ships by comparing with available experimental data. One more thing to announce is that as the present study is solving 2D BVPs in cross sections, only the 2D NURBS curve is applied though 3D NURBS surface can be used for complete 3D modelling.

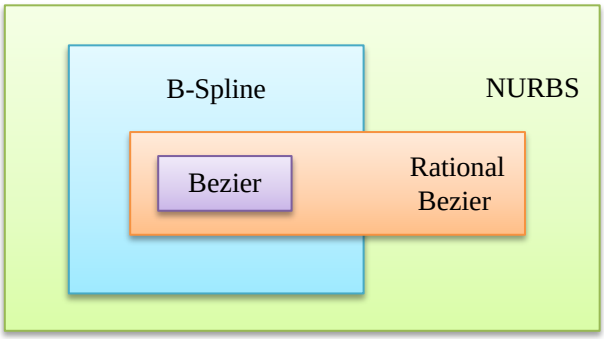

Fig. 5.1 Relations between splines

5.2 Definitions of splines

According to the relations shown in Fig. 5.1, the current section will establish the definitions of Bezier spline, B-spline and NURBS successively which are beneficial to understand the NURBS applied in present study.

5.2.1 Bezier spline

Firstly, let us take a look at a straight line for example. Obviously, there are only two control points which are the endpoints of the line as shown in the top left corner of Fig. 5.2, so points on the line can be derived by following expression.

$$C(u) = (1-u)P_0 + uP_1,\ 0 \le u \le 1 \tag{5.1}$$

where P_0, P_1 are the endpoints, and u is the parameter corresponding to an arbitrary point on the line which can be understood as the proportion of the control point P_1.

Secondly, if we want to draw a curve, three control points are needed as shown in the top right corner of Fig. 5.2. The derivation of the curve follows these steps:

Step 1: Get point A between the control points P_0 and P_1 by formula (5.1).

$$A(u) = (1-u)P_0 + uP_1,\ 0 \le u \le 1 \tag{5.2}$$

Step 2: Likewise, get point B between the control points P_1 and P_2 as well.

$$B(u) = (1-u)P_1 + uP_2,\ 0 \le u \le 1 \tag{5.3}$$

Step 3: Finally, derive the point C on the curve between the new straight line AB.

$$\begin{aligned} C(u) &= (1-u)A(u) + uB(u) \\ &= (1-u)^2 P_0 + 2u(1-u)P_1 + u^2 P_2,\ 0 \le u \le 1 \end{aligned} \tag{5.4}$$

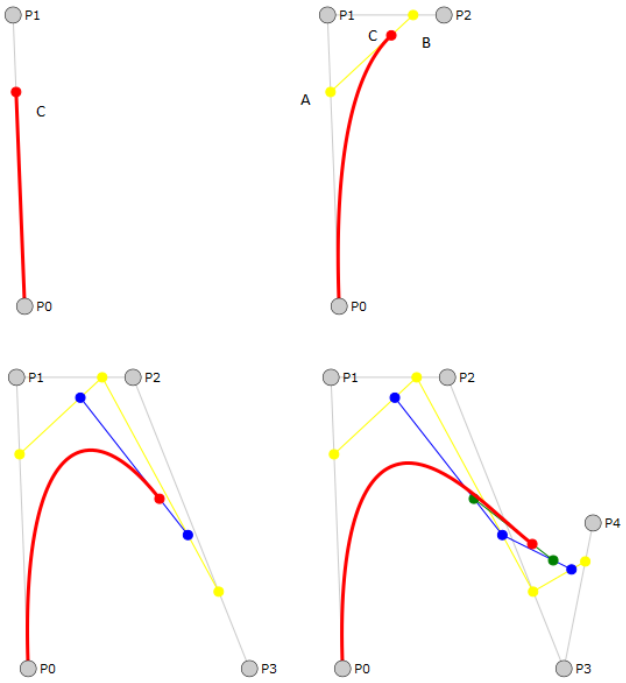

Fig. 5.2 Bezier splines (internet photo)

Further, a Bezier curve with four control points shown in the left bottom view of Fig. 5.2 can be derived by the steps similarly, the expression is established as follow.

$$C(u) = (1-u)^3 P_0 + 3u(1-u)^2 P_1 + 3u^2(1-u)P_2 + u^3 P_3,\ 0 \le u \le 1 \tag{5.5}$$

By that analogy, for an arbitrary number of control points, following the same iterative procedure established above named as *de Castejau* algorithm, the common definition of the Bezier spline can be given consequently referring to the NURBS book by Piegl & Tiller (1997).

Setting the space points $P_i \in R^3 (i = 0,1,\ldots,n)$ as the control points, the expression of the degree n Bezier spline can be given.

$$C(u) = \sum_{i=0}^{n} P_i B_{i,n}(u),\ 0 \le u \le 1 \tag{5.6}$$

here, the space points P_i can also be called Bezier points, and

$$B_{i,n}(u) = c_n^i u^i (1-u)^{n-i} = \frac{n!}{i!(n-i)!} u^i (1-u)^{n-i}, i = 0,1,\ldots,n \tag{5.7}$$

is the Bezier basis function or Bernstein polynomial. Besides, connecting the control points with straight lines form the control polygon of the curve.

The Bezier spline has following properties:

- Property at the endpoints. $C(0) = P_0, C(1) = P_n$ and the curve tangential to the control polygon at the endpoints which means clamped ends.
- Property of derivative. The k-th order derivatives of the curve at the endpoints are only related to the first $(k+1)$ control points counted from the ends.
- Symmetrical. The same Bezier curve shape is obtained if the control points are specified in the opposite order. The only difference will be the parametric direction of the curve. The direction of increasing parameter reverses when the control points are specified in the reverse order.

- A Bezier curve will always be completely contained inside of the convex polygon of the control points.
- Invariant under affine transformation and parameter transformation, but not under projective transformation.
- Variation diminishing property. Any straight line will intersect legs of the control polygon at least as many times as it crosses the Bezier curve itself.
- No local control of shape modification. Every point on the curve with the exception of the first and last ones moves whenever any interior control point is moved. This is the main disadvantage of the Bezier spline.

5.2.2 B-spline

Just due to the last disadvantage of the Bezier spline, B-spline is proposed to remedy it. Similar to the Bernstein polynomial of the Bezier spline which can be considered as a weight value of corresponding control points, the point on a B-spline with parameter u is also set to be the weighted sum of the control points by means of basis functions. However, only a part of the control points should be taken into account here instead of all of them. That is to say for a certain parameter value u, the basis functions for several control points would have no contribution to the point $P(u)$ on the B-spline. This is the local control property of the spline we want.

Having this concept in mind, divide the whole parametric domain into several small domains by a non-descending set of knots, $\boldsymbol{u} = [u_0, u_1, \cdots u_i, \cdots u_m], u_0 \le u_1 \le \ldots \le u_m$. Here u_i denotes the knot, $\boldsymbol{u}$ is the knot vector and the half open interval $\lfloor u_i, u_{i+1} \rangle$ is called i-th knot span. Note that some knots could have a same value such as $u_i = u_{i+1} = \ldots = u_{i+p-1}$, then u_i is a multiple knot with multiplicity p. In addition, the knot vector is usually defined in the close interval $[0,1]$ with $u_0 = 0, u_m = 1$.

Furtherly, a B-spline with degree k means that a point on the curve $P(u)$ is affected by $(k+1)$ control points, then the basis function of the B-spline can be defined according to the *Cox-de Boor* recursion formulae given in the book by Piegl & Tiller (1997).

$$\begin{cases} N_{i,0}(u) = \begin{cases} 1 & if\ u_i \le u < u_{i+1} \\ 0 & otherwise \end{cases} \\ N_{i,k}(u) = \dfrac{u-u_i}{u_{i+k}-u_i} N_{i,k-1}(u) + \dfrac{u_{i+k+1}-u}{u_{i+k+1}-u_{i+1}} N_{i+1,k-1}(u) \\ define \quad \dfrac{0}{0} = 0 \end{cases} \tag{5.8}$$

where $N_{i,k}(u)$ is the normalized B-spline basis function of degree k. Then the completed B-spline expression is established as follow.

$$P(u) = \sum_{i=0}^{n} d_i N_{i,k}(u) \tag{5.9}$$

where d_i now denotes the control point or vertex of the control polygon. Apparently, the B-spline introduced here is categorized into non-rational type.

From the above definition, there are two observations. Firstly, basis function $N_{i,k}(u)$ is nonzero in the interval $\left[u_i, u_{i+k+1}\right)$, or equivalently, $N_{i,k}(u)$ is nonzero in $(k+1)$ knot spans $\left[u_i, u_{i+1}\right), \left[u_{i+1}, u_{i+2}\right), \ldots, \left[u_{i+k}, u_{i+k+1}\right)$. The other one is that in any knot span $\left[u_i, u_{i+1}\right)$, at most $(k+1)$ basis functions of degree k are nonzero, namely $N_{i-k,k}(u), N_{i-k+1,k}(u), \ldots, N_{i,k}(u)$. The relations between control points, knot vector and the corresponding data points on the curve can be illustrated in Fig. 5.3.

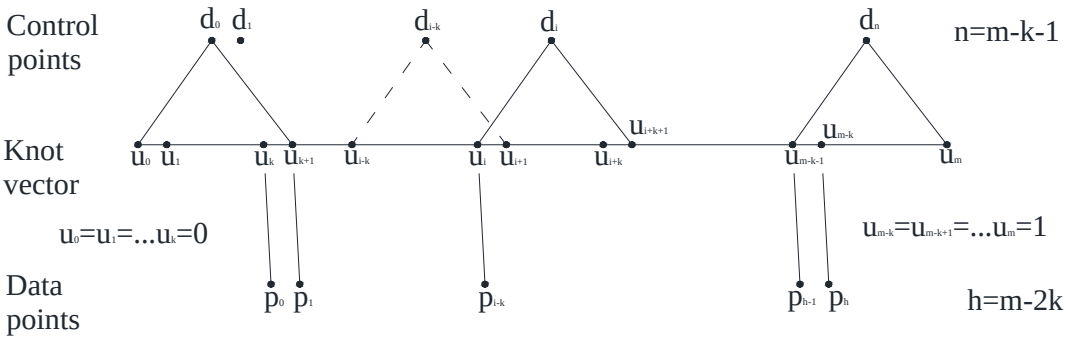

Fig. 5.3 Relations between control points, knot vector and data points

Moreover, the basis function $N_{i,k}(u)$ has following two properties.

- Normative.

$$\sum N_{i,k}(u) = 1 \tag{5.10}$$

- Differentiability.

$$N'_{i,k}(u) = k\left[\frac{N_{i,k-1}(u)}{u_{i+k} - u_i} - \frac{N_{i+1,k-1}(u)}{u_{i+k+1} - u_{i+1}}\right] \tag{5.11}$$

To sum up, B-spline has following properties similar to Bezier spline.

- Invariant under affine transformation, parameter transformation and especially projective transformation.
- Always be completely contained inside of the convex polygon of the control points.
- Variation diminishing property.
- Differentiability. Since the B-spline is piecewise curve, a spline of degree k within each piece are C^{∞}, so called smooth function, while at the knot positions are C^{k-p}, p is the multiplicity of the knot mentioned before.
- The curve would be smoother with higher degree for the same set of control points.

And the most important one,

- Local control property due to the basis function.

5.2.3 NURBS

As mentioned before, in order to precisely represent elementary curves, normal non-rational B-spline is extended to NURBS. From its name, Non-Uniform means the spaces between knots are nonuniform, Rational represents it is a weighted function can be expressed by a rational polynomial and B-Spline denotes that it inherits all the properties of B-spline.

The following piecewise rational polynomial defines a NURBS curve of degree k.

$$Q(x,y,z) = Q(u) = \frac{\sum_{i=0}^{n} w_i d_i N_{i,k}(u)}{\sum_{i=0}^{n} w_i N_{i,k}(u)} \tag{5.12}$$

Note that same nomenclatures are adopted here for the control point d_i and basis function $N_{i,k}(u)$ since they are exactly the same ones defined in B-spline. w_i is the weight factor corresponding to each control point and can be simply understood as the attraction of each control point which is equal to the cross ratio of several specific points on a line constructed by a set of curves with weight factors $w_i = +\infty, 0, 1$ & $w_i \neq 0, 1$ through the control point in fact. Obviously, when the weight factor $w_i = 1$, the NURBS degrades to a normal non-rational B-spline as introduced before.

Actually, there are three equivalent expression forms for NURBS including the most common used expression (5.12) which explicitly indicates that NURBS is an extension of Bezier spline and non-rational B-spline. While the other two forms, expressed by rational basis function and homogeneous coordinates, clearly show the properties and geometric meaning of NURBS respectively. Moreover, the homogeneous coordinate expression of NURBS would be convenient for designers to apply algorithms based on non-rational B-spline in modelling operations due to the invariant property stated previously except for derivatives.

In the homogeneous coordinate system, a NURBS is expressed as follow.

$$Q(u) = H\{P(u)\} = H\left\{\sum_{i=0}^{n} D_i N_{i,k}(u)\right\} \tag{5.13}$$

where $D_i = [w_i d_i, w_i]$ defines the weighted control points corresponding to the original ones d_i, $H\{\ \}$ represents the perspective projection transformation from one dimensional higher Euclidean space to current space, especially 3 dimensional space to 2 dimensional plane in present study as shown in Fig. 5.4. The blue line represented by $P(u)$ is the non-rational B-spline governed by the weighed control points D_i in

the 3D coordinate system $O-XYw$, the red projection line in the projective plane $w=1$ is the defined 2D NURBS curve $Q(u)$. The relation between the coordinates is

$$H\{[X,Y,w]\}=[x,y]=\left[\frac{X}{w},\frac{Y}{w}\right] \tag{5.14}$$

where w coordinate in the 3D space is the weight factor of the corresponding point in the 2D plane.

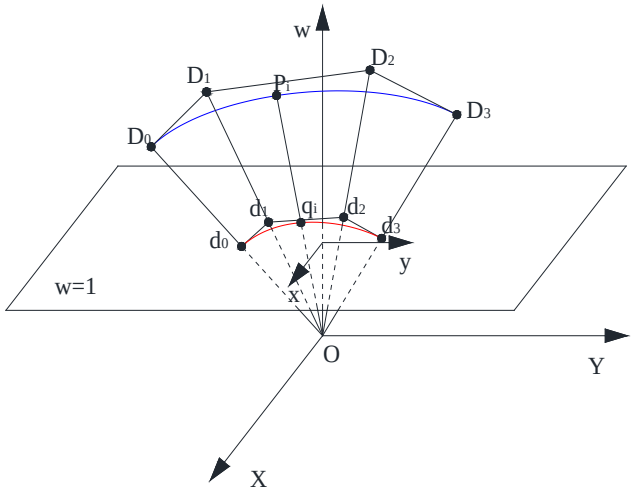

Fig. 5.4 NURBS curve in homogeneous coordinates

5.3 **Construction of complex combined curve**

After introducing the definitions and properties of the splines, we can learn that NURBS is an ideal modelling tool in geometry construction, thereby is chosen for expressing the contours of ships in present study. Fundamental algorithms of NURBS which will be applied in the construction of contour curves are derived in detail in Appendix B.

In general, a complex curve like the contour of a ship's cross section may consist of straight lines, conics and cubic free form curves. Therefore, a uniform NURBS curve of degree 3 is suggested to be applied according to following steps.

Step 1) Express straight lines and conics by NURBS curves of degree 1 and 2 respectively, then raise their degrees to 3.

Step 2) Derive the control points of the free form curves by inverse calculation for interpolation to generate NURBS curves of degree 3.

Step 3) Evaluate the ratios of each curve length to the total curve length according to the chords length of the control polygon constructed by the control points of all generated curves.

Step 4) Divide the knot span by the evaluated ratios and recalculate the knot vectors of each curve.

Step 5) Adjust the multiplicities of the knots at the junctions positions between curves to 3 for differentiability requirement.

Step 6) Construct the new uniform degree 3 NURBS curve with all control points, weight factors and the combined knot vector.

The above procedure only construct the contours of the ship in stations provided, normally 20 stations. In order to construct all the contours in 81 cross sections as stated in Chapter 4, several further steps have to be conducted. That is to say, water plane contours in longitudinal direction at different drafts have to be constructed by using the offset points in all stations at a same draft each time. Finally, contours in all cross sections can be constructed with the new derived offset points on these water plane contours.

It should be pointed out that the weight factors of the data points are usually unknown at the beginning in practical design. In addition, if there is no conic part contained in the curve, the weight factors could all be set as 1 which transforms the construction problem to a normal non-rational B-spline one, and can be adjusted later in the human interaction program.

Actually, research on NURBS modelling is an important but complicated topic in industrial modelling field. There are many other advanced algorithms and techniques have not been presented here, i.e., spline subdivision, control points repositioning and weight modification etc. As they are not needed to be applied and beyond the scope of present study, for further details an interested reader can refer to the book by Piegl & Tiller (1997).

5.4 Modelling verification and validation

For verification of the modelling tool based on the algorithms introduced above, a unit circle and contours at each station of two mathematical ship types, Wigley and WigleyIII, will be plotted and compared with their analytical solutions. After that, real ship types, Series 60 and S175, will also be adopted to model their body plans for validation successively, according to their tables of offsets.

5.4.1 Verification on mathematical profiles

- Circle

In order to express a unit circle by a NURBS of order 3, a convex polygon consists of 9 control points with the first and last ones coincided is applied in the present modelling. The knot vector and the weights of the control points are

$$\begin{cases} \boldsymbol{u} = \left[0,0,0,\frac{1}{4},\frac{1}{4},\frac{1}{2},\frac{1}{2},\frac{3}{4},\frac{3}{4},1,1,1\right] \\ \boldsymbol{w} = \left[1,\frac{\sqrt{2}}{2},1,\frac{\sqrt{2}}{2},1,\frac{\sqrt{2}}{2},1,\frac{\sqrt{2}}{2},1\right] \end{cases} \tag{5.15}$$

Then the circle is plotted in Fig. 5.5 with the 9 control points added.

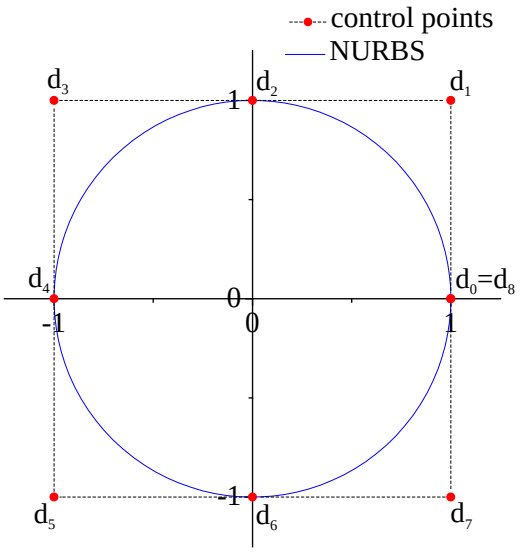

Fig. 5.5 Unit circle by 9 control points

To further check the accuracy of the modelled circle, the perimeter C_{circle} can be calculated numerically by Gauss-Legrendre quadrature and compared with the analytical solution as presented in Table 5.1. The circle is divided into 4 segments corresponding to the 4 quadrants with several sets of Gauss points arranged for numerical integration. Here, the relative error is defined as follow in percentage.

$$relative\ \ error\ (R.E.) = \frac{\left| Present\ \ solution - Analytical\ \ solution \right|}{Analytical\ \ solution} \tag{5.16}$$

Table 5.1 Comparison of the circle's perimeter with same mesh

Analytical	Gauss	Present	R.E. (%)
6.28318531	3 pts	6.28376544	9.233e-3%
	4 pts	6.28316202	3.705e-4%
	5 pts	6.28318624	1.480e-5%
	6 pts	6.28318527	5.795e-7%

From the plotted figure above and data comparison in the table, it is clearly verified that the accuracy of NURBS description for an elementary curve without the parameter π in its expression can reach very high level with relatively large mesh size and few Gauss points to derive its arc length. Also from the table, with adding the Gauss points in each segment, the accuracy climbs extremely fast which is another big benefit in numerical calculation. Because this process would not increase as much computation time as the usual way by simple mesh refinement.

- Wigley and WigleyIII

A standard Wigley ship hull defined by following expression is used for verification.

$$y = \frac{B}{2}\left[1 - \left(\frac{2x}{L}\right)^2\right]\left[1 - \left(\frac{z}{D}\right)^2\right] \tag{5.17}$$

where L, B, D represent ship length, breadth and draft respectively, and fulfill the relations $L/B = 10$, $L/D = 16$, $L = 2m$ is chosen here. Offsets at each station are

calculated by this expression in advance, then the inverse calculation is performed to derive the control points of the curve, finally the NURBS expression of the curve can be established for plotting the contours to compare with the analytical solutions as shown in Fig. 5.6. Note that the weight factors are all set to be 1 as previous stated. And due to the symmetry of the hull, only a quarter of the ship is taken into considered for verification.

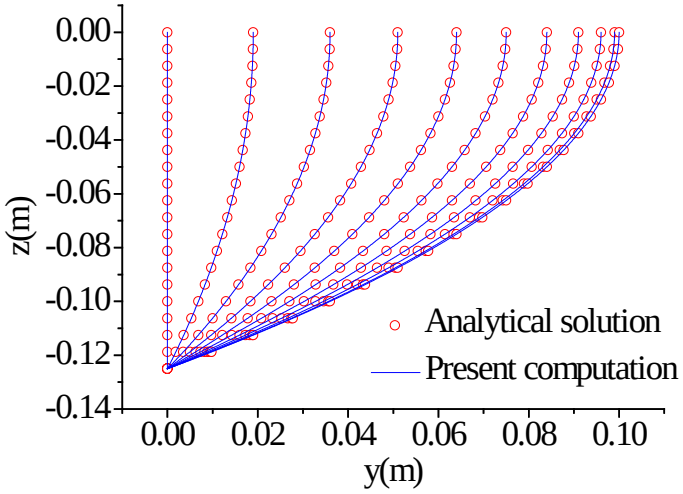

Fig. 5.6 Transverse profiles of the Wigley hull

Besides, the 3D view of the profiles is also presented intuitively in Fig. 5.7.

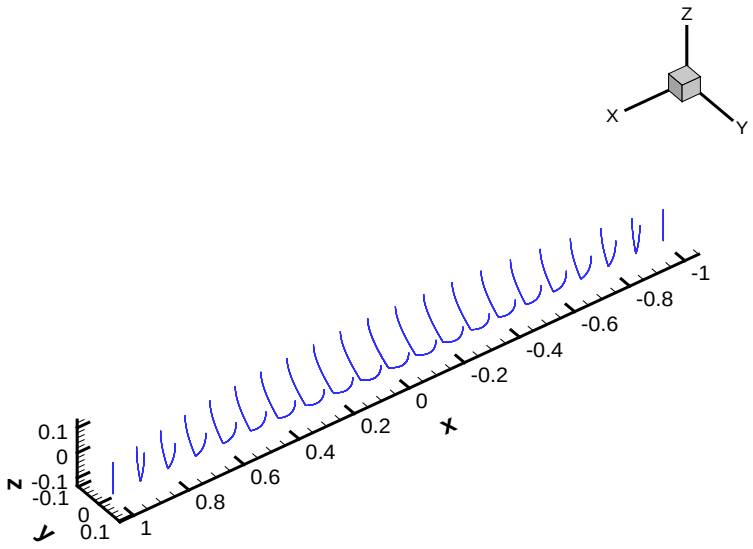

Fig. 5.7 3D view of the Wigley transverse profiles

Similarly, the surface expression for WigleyIII ship hull is also given below.

$$y = \frac{B}{2}\left[1-\left(\frac{2x}{L}\right)^2\right]\left[1-\left(\frac{z}{T}\right)^2\right]\left[1+0.2\left(\frac{2x}{L}\right)^2\right] \tag{5.18}$$

where $L = 3m, B = 0.3m, D = 0.1875m$, volume of displacement $\nabla = 0.078m^3$. Then the contours and their 3D view are shown in Fig. 5.8 and Fig. 5.9 respectively.

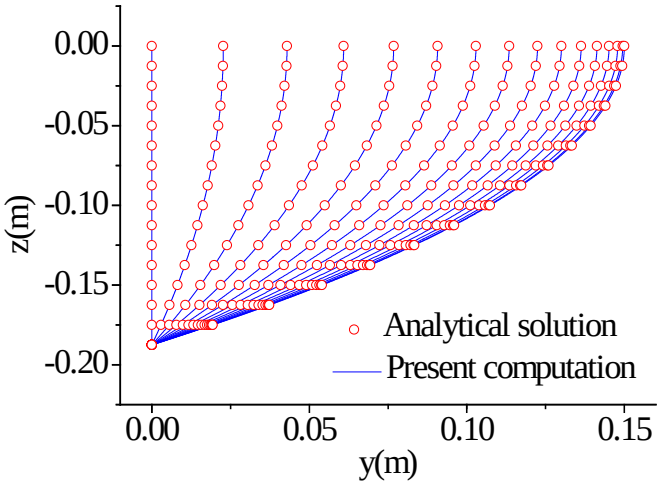

Fig. 5.8 Transverse profiles of the WigleyIII hull

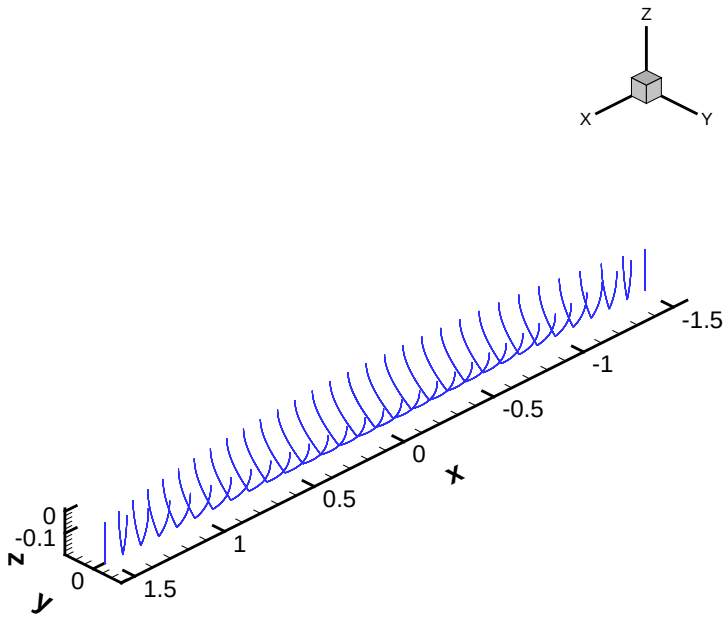

Fig. 5.9 3D view of the WigleyIII transverse profiles

From comparisons of the contours modelled by present NURBS tool with their analytical solutions, it is clearly verified that NURBS can precisely describe the geometries of ships with limited data points provided. Moreover, comparisons of midship section coefficients C_M and the corresponding non-dimensional curve length L_C/L are listed in table 5.2 with 5 segments mesh on half profile and 5 Gauss points arranged on each segment which further verify the high accuracy of the results obtained by present tool. Note that Wigley and WigleyIII share same midship section profiles actually.

Table 5.2 Comparisons of midship parameters

	Analytical	Present	R.E. (%)
C_M	0.66666667	0.66666673	9.752e-6%
L_C/L	0.16671318	0.16671349	1.880e-4%

5.4.2 Validation on real ships

For real ships validation, Series 60 and S175 with their principal particulars given in table 5.3 below are also modelled by the present NURBS tool as shown in Fig. 5.10 and Fig 5.12 respectively. Their 3D views are shown in Fig 5.11 and Fig 5.13 as well.

Table 5.3 Main particulars of Series 60 and S175

Parameters	Series 60	S175
Length, $L(m)$	400	175
Breath, $B(m)$	57.14	25.4
Draft, $D(m)$	22.86	9.5
Block coefficient, C_B	0.7	0.572
Volume of displacement, $\nabla(ton)$	365742	24742
Radius of inertia for roll, k_{xx}	-	$0.33\,B$
Radius of inertia for pitch, k_{yy}	-	$0.25\,L$
Radius of inertia for yaw, k_{zz}	-	$0.269\,L$

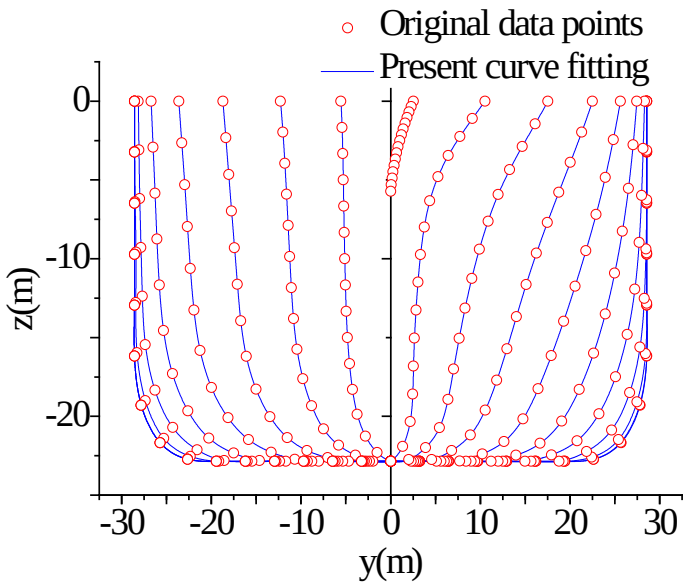

Fig. 5.10 Transverse profiles of Series 60 hull with $C_b = 0.7$

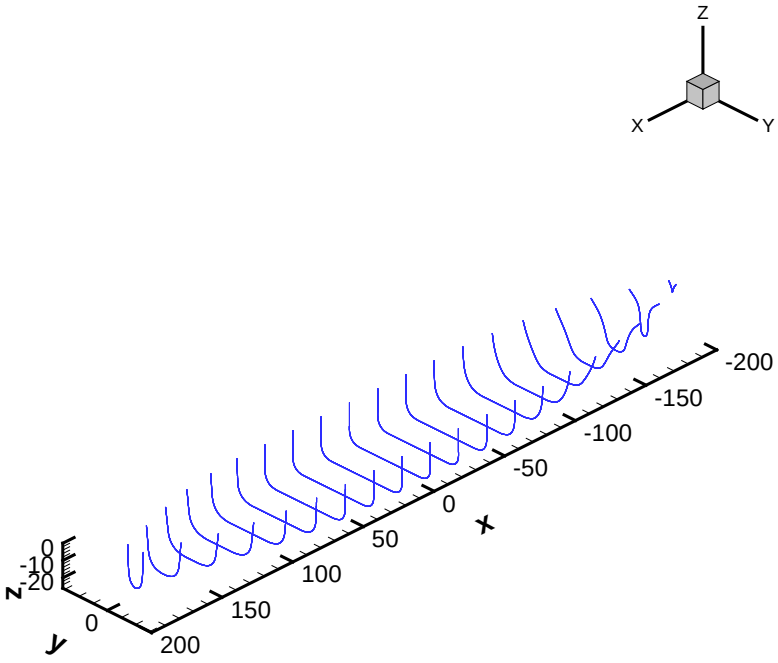

Fig. 5.11 3D view of Series 60 transverse profiles with $C_b = 0.7$

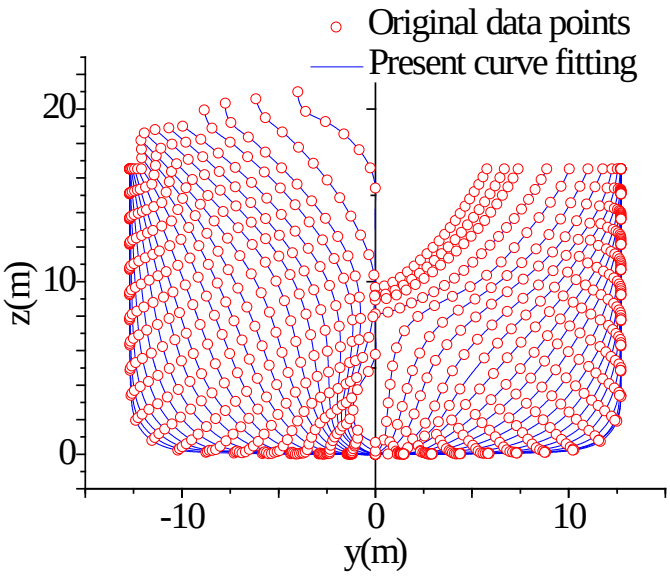

Fig. 5.12 Transverse profiles of S175 hull

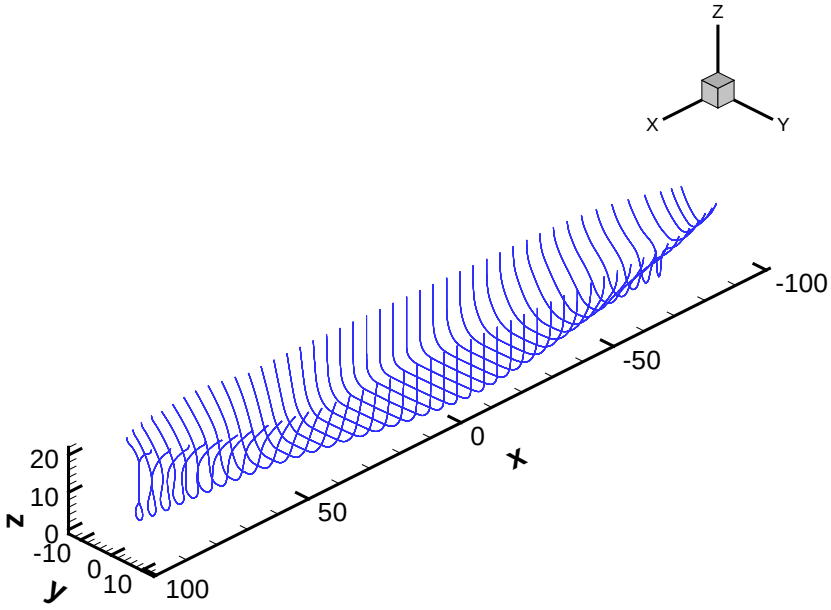

Fig. 5.13 3D view of S175 transverse profiles

As seen from the figures, the interpolated profile curves have satisfied smoothness. Therefore, this tool could be applied for real ships modelling in practical design. Again, since no weight factors are provided, the profiles are non-rational B-splines

actually which are practical enough for profiles without any elementary curve parts. However, the weight factors can be adjusted later if necessary according to the curvature changing of different local areas in human computer interaction program.

5.5 **High order BEM**

Recalling the 2D BEM described in Chapter 4 for solving BVPs, the boundary of the flow field in a cross section plane is discretized into straight line segments with constant values of velocity potential and its derivatives over each segment. As mentioned in the literature review, apart from the discontinuity of the normal derivative at the join points between segments, the main disadvantage of this common applied low order BEM in seakeeping analysis is that large number of segments have to be used for the discretization of the boundary to seek results with satisfactory accuracy. Thus it will consume a lot of computer memories as the coefficient matrix in (4.62) or (4.63) is non-singular. Moreover, when a ship experiencing a wave induced motion at a very high frequency, the wave length of the generated wave would be very small, thereby a denser distribution of elements should be arranged on the free surface.

As is seen from the good geometry modelling results presented in the last sub section, it is appropriate to apply this NURBS tool to represent the distributions of the velocity potential on the boundary as follow.

$$\phi(x,y,z)=\phi(u)=\frac{\sum_{i=0}^{n} w_i\tilde{\phi}_i N_{i,k}(u)}{\sum_{i=0}^{n} w_i N_{i,k}(u)} \tag{5.19}$$

If the weight factors are all chosen as $w_i=1$ since no apparent elementary curve components appear on the boundary contours, the velocity potential and its normal derivative can be described by B-spline as follow.

$$\phi(u)=\sum_{i=0}^{n}\tilde{\phi}_i N_{i,k}(u) \tag{5.20}$$

$$\frac{\partial \phi(u)}{\partial n} = \sum_{i=0}^{n} \left(\frac{\partial \tilde{\phi}_i}{\partial n} \right) N_{i,k}(u) \tag{5.21}$$

Besides, the wave elevation can also be expressed by using the B-spline basis function for free surface stepping.

$$\zeta(u) = \sum_{i=0}^{n_F} \tilde{\zeta}_i N_{i,k}(u) \tag{5.22}$$

In (5.20) and (5.21), the generalized velocity potential ϕ can be Φ_S or φ_j. The elevation ζ is also a generalized one. $\tilde{\phi}_i$, $\partial\tilde{\phi}_i/\partial n$ and $\tilde{\zeta}_i$ denote the control points of the velocity potential, normal derivative and wave elevation respectively. (n_F+1) is the number of control points on the free surface. Similarly, the numbers of control points on body surface, open boundary and symmetry line boundary under the keel are (n_S+1), (n_R+1), (n_K+1) respectively. In the calculations, the order of the spline is chosen as $k=3$ which is quite enough.

Substituting (5.20) and (5.21) into (4.62) and (4.63), the linear algebraic equations of vertical motions and lateral motions, for solving the corresponding values at control points will be derived as follow by (5.23) and (5.24) respectively.

$$\begin{aligned}
&\sum_{j=1}^{n_1} D_{ij} \sum_{s=0}^{n_S} \tilde{\varphi}_{j,s} N_{s,3}(u) - \sum_{j=n_1+1}^{n_1+n_2} S_{ij} \sum_{s=0}^{n_F} \frac{\partial \tilde{\varphi}_{j,s}}{\partial n} N_{s,3}(u) \\
&- \sum_{j=n_1+n_2+1}^{n_1+n_2+n_3} S_{ij} \sum_{s=0}^{n_R} \frac{\partial \tilde{\varphi}_{j,s}}{\partial n} N_{s,3}(u) + \sum_{j=n_1+n_2+n_3+1}^{n_1+n_2+n_3+n_4} D_{ij} \sum_{s=0}^{n_K} \tilde{\varphi}_{j,s} N_{s,3}(u) \\
&= \sum_{j=1}^{n_1} S_{ij} \sum_{s=0}^{n_S} \frac{\partial \tilde{\varphi}_{j,s}}{\partial n} N_{s,3}(u) - \sum_{j=n_1+1}^{n_1+n_2} D_{ij} \sum_{s=0}^{n_F} \tilde{\varphi}_{j,s} N_{s,3}(u) - \sum_{j=n_1+n_2+1}^{n_1+n_2+n_3} D_{ij} \sum_{s=0}^{n_R} \tilde{\varphi}_{j,s} N_{s,3}(u)
\end{aligned} \tag{5.23}$$

$$\begin{aligned}
&\sum_{j=1}^{n_1} D_{ij} \sum_{s=0}^{n_S} \tilde{\varphi}_{j,s} N_{s,3}(u) - \sum_{j=n_1+1}^{n_1+n_2} S_{ij} \sum_{s=0}^{n_F} \frac{\partial \tilde{\varphi}_{j,s}}{\partial n} N_{s,3}(u) \\
&- \sum_{j=n_1+n_2+1}^{n_1+n_2+n_3} S_{ij} \sum_{s=0}^{n_R} \frac{\partial \tilde{\varphi}_{j,s}}{\partial n} N_{s,3}(u) - \sum_{j=n_1+n_2+n_3+1}^{n_1+n_2+n_3+n_4} S_{ij} \sum_{s=0}^{n_K} \frac{\partial \tilde{\varphi}_{j,s}}{\partial n} N_{s,3}(u) \\
&= \sum_{j=1}^{n_1} S_{ij} \sum_{s=0}^{n_S} \frac{\partial \tilde{\varphi}_{j,s}}{\partial n} N_{s,3}(u) - \sum_{j=n_1+1}^{n_1+n_2} D_{ij} \sum_{s=0}^{n_F} \tilde{\varphi}_{j,s} N_{s,3}(u) - \sum_{j=n_1+n_2+1}^{n_1+n_2+n_3} D_{ij} \sum_{s=0}^{n_R} \tilde{\varphi}_{j,s} N_{s,3}(u)
\end{aligned} \tag{5.24}$$

where,

$$\begin{cases} S_{ij} = \int_{\widehat{l}_j} \ln r_{ij}\, dl \\ D_{ij} = \begin{cases} \int_{\widehat{l}_j} \dfrac{\partial \ln r_{ij}}{\partial n} dl & i \neq j \\ \pi & i = j \end{cases} \end{cases} \tag{5.25}$$

It should be noticed that the integral interval in (5.25) is the arc $\widehat{l}_j$ instead of the previous line segment Δl_j. Besides, according to the relation between the control points and data points given in Fig. 5.3, there are only $k+1=4$ nonzero basis functions at each span defined by the space between adjacent knots in the knot vector, the equations (5.23) and (5.24) can be rewritten as follow.

$$\begin{aligned} &\sum_{j=1}^{n_1} D_{ij} \sum_{m=0}^{3} \tilde{\varphi}_{s_j-3+m} N_{s_j-3+m}(u) - \sum_{j=n_1+1}^{n_1+n_2} S_{ij} \sum_{m=0}^{3} \frac{\partial \tilde{\varphi}_{s_j-3+m}}{\partial n} N_{s_j-3+m}(u) \\ &- \sum_{j=n_1+n_2+1}^{n_1+n_2+n_3} S_{ij} \sum_{m=0}^{3} \frac{\partial \tilde{\varphi}_{s_j-3+m}}{\partial n} N_{s_j-3+m}(u) + \sum_{j=n_1+n_2+n_3+1}^{n_1+n_2+n_3+n_4} D_{ij} \sum_{m=0}^{3} \tilde{\varphi}_{s_j-3+m} N_{s_j-3+m}(u) \\ &= \sum_{j=1}^{n_1} S_{ij} \sum_{m=0}^{3} \frac{\partial \tilde{\varphi}_{s_j-3+s}}{\partial n} N_{s_j-3+m}(u) - \sum_{j=n_1+1}^{n_1+n_2} D_{ij} \sum_{m=0}^{3} \tilde{\varphi}_{s_j-3+m} N_{s_j-3+m}(u) - \sum_{j=n_1+n_2+1}^{n_1+n_2+n_3} D_{ij} \sum_{m=0}^{3} \tilde{\varphi}_{s_j-3+m} N_{s_j-3+m}(u) \end{aligned} \tag{5.26}$$

$$\begin{aligned} &\sum_{j=1}^{n_1} D_{ij} \sum_{m=0}^{3} \tilde{\varphi}_{s_j-3+m} N_{s_j-3+m}(u) - \sum_{j=n_1+1}^{n_1+n_2} S_{ij} \sum_{m=0}^{3} \frac{\partial \tilde{\varphi}_{s_j-3+m}}{\partial n} N_{s_j-3+m}(u) \\ &- \sum_{j=n_1+n_2+1}^{n_1+n_2+n_3} S_{ij} \sum_{m=0}^{3} \frac{\partial \tilde{\varphi}_{s_j-3+m}}{\partial n} N_{s_j-3+m}(u) - \sum_{j=n_1+n_2+n_3+1}^{n_1+n_2+n_3+n_4} S_{ij} \sum_{m=0}^{3} \frac{\partial \tilde{\varphi}_{s_j-3+m}}{\partial n} N_{s_j-3+m}(u) \\ &= \sum_{j=1}^{n_1} S_{ij} \sum_{m=0}^{3} \frac{\partial \tilde{\varphi}_{s_j-3+m}}{\partial n} N_{s_j-3+m}(u) - \sum_{j=n_1+1}^{n_1+n_2} D_{ij} \sum_{m=0}^{3} \tilde{\varphi}_{s_j-3+m} N_{s_j-3+m}(u) - \sum_{j=n_1+n_2+1}^{n_1+n_2+n_3} D_{ij} \sum_{m=0}^{3} \tilde{\varphi}_{s_j-3+m} N_{s_j-3+m}(u) \end{aligned} \tag{5.27}$$

where the subscript s is the span index in the knot vector of each boundary with another subscript j to it to indicate the associated panel index j.

Together with the (5.22) been substituted back into the free surface condition (4.66) or (4.69), the wave elevation at the control points to form the free surface profile will also be derived.

$$\begin{cases} \sum_{m=0}^{3} \widehat{\varsigma}_{s_j-3+m}^{p+\frac{1}{2}} N_{s_j-3+m}(u) = \sum_{m=0}^{3} \widehat{\varsigma}_{s_j-3+m}^{p-\frac{1}{2}} N_{s_j-3+m}(u) + \Delta t \sum_{m=0}^{3} \frac{\partial \tilde{\varphi}_{s_j-3+m}^{p}}{\partial n} N_{s_j-3+m}(u) \\ \sum_{m=0}^{3} \tilde{\varphi}_{s_j-3+m}^{p+1} N_{s_j-3+m}(u) = \sum_{m=0}^{3} \tilde{\varphi}_{s_j-3+m}^{p} N_{s_j-3+m}(u) - g\Delta t \sum_{m=0}^{3} \widehat{\varsigma}_{s_j-3+m}^{p+\frac{1}{2}} N_{s_j-3+m}(u) \end{cases} \quad j \in [n_1+1, n_2] \tag{5.28}$$

where the superscript p represents the time index. Noting that in the linear algebraic equations, boundary conditions are fulfilled at the Gauss points on each element instead of at the midpoint of the straight line element in the normal BEM.

5.6 Validation of hydrodynamic coefficients

In this subsection, the frequency dependent hydrodynamic coefficients are computed for a WigleyIII hull and a Series 60 ($C_B = 0.7$) ship forced in vertical motions and lateral motions with forward speed by the NURBS based 2.5D approach described in Chapter 4 & 5. Results are compared with available measured experimental data or numerical results from publications.

5.6.1 Vertical motions

Firstly, added mass and damping coefficients of the WigleyIII in vertical motions are computed and compared with the measured value reported by Journée (1992) in Fig. 5.14 to Fig. 5.17. The Froude numbers F_n used are 0.3 and 0.4. The non-dimensional form of circular frequency of oscillation and hydrodynamic coefficients are defined as

$$\begin{cases} \omega_e' = \omega_e \sqrt{L/g}; \\ A_{kj}' = A_{kj} \Big/ \left(\rho \nabla L^{m_k+n_j} \right); \\ B_{kj}' = B_{kj} \sqrt{L/g} \Big/ \left(\rho \nabla L^{m_k+n_j} \right) \end{cases} \tag{5.29}$$

where, $m_k \text{ or } n_j = \begin{cases} 0 & for\ k, j = 2,3 \\ 1 & for\ k, j = 4,5,6 \end{cases}$.

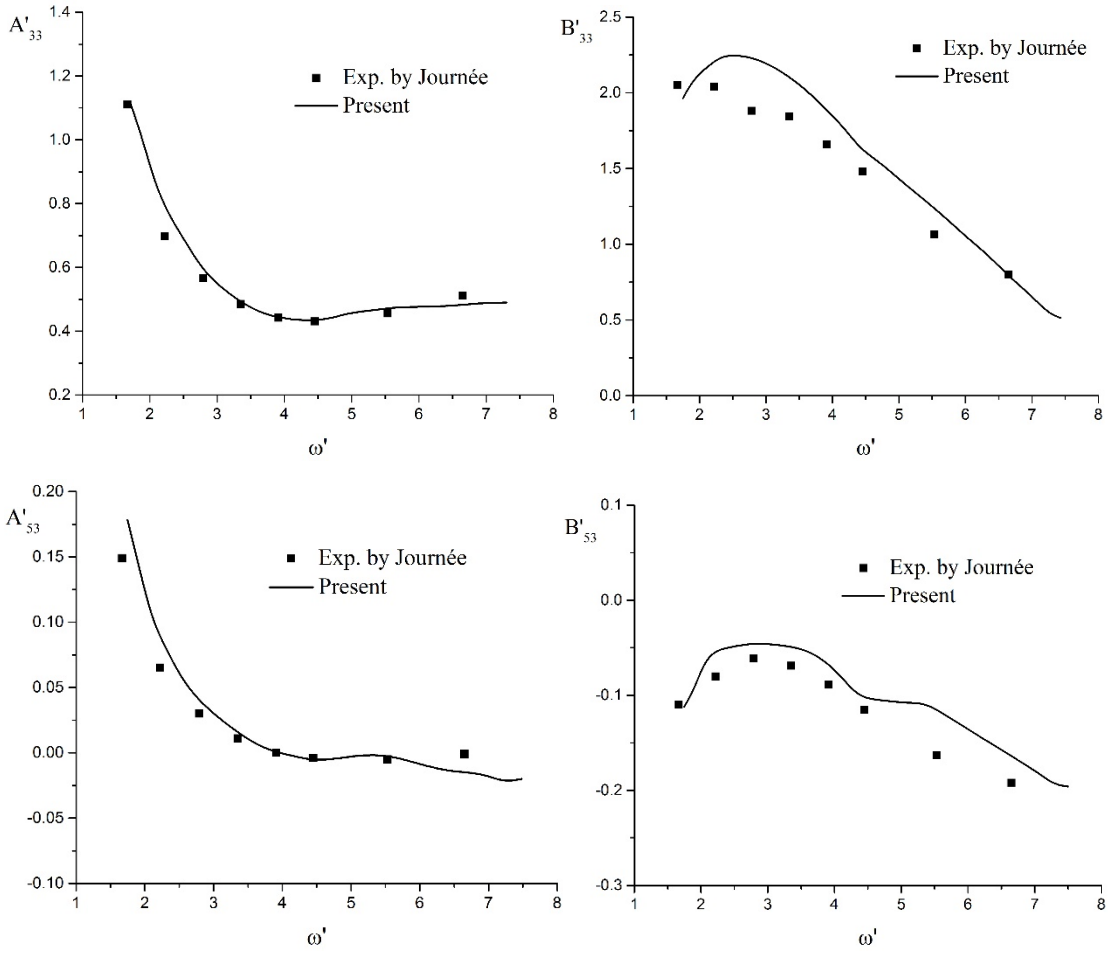

Fig. 5.14 Hydrodynamic coefficients versus ω_e' due to unit amplitude heave motion for the WigleyIII advancing at $F_n = 0.3$

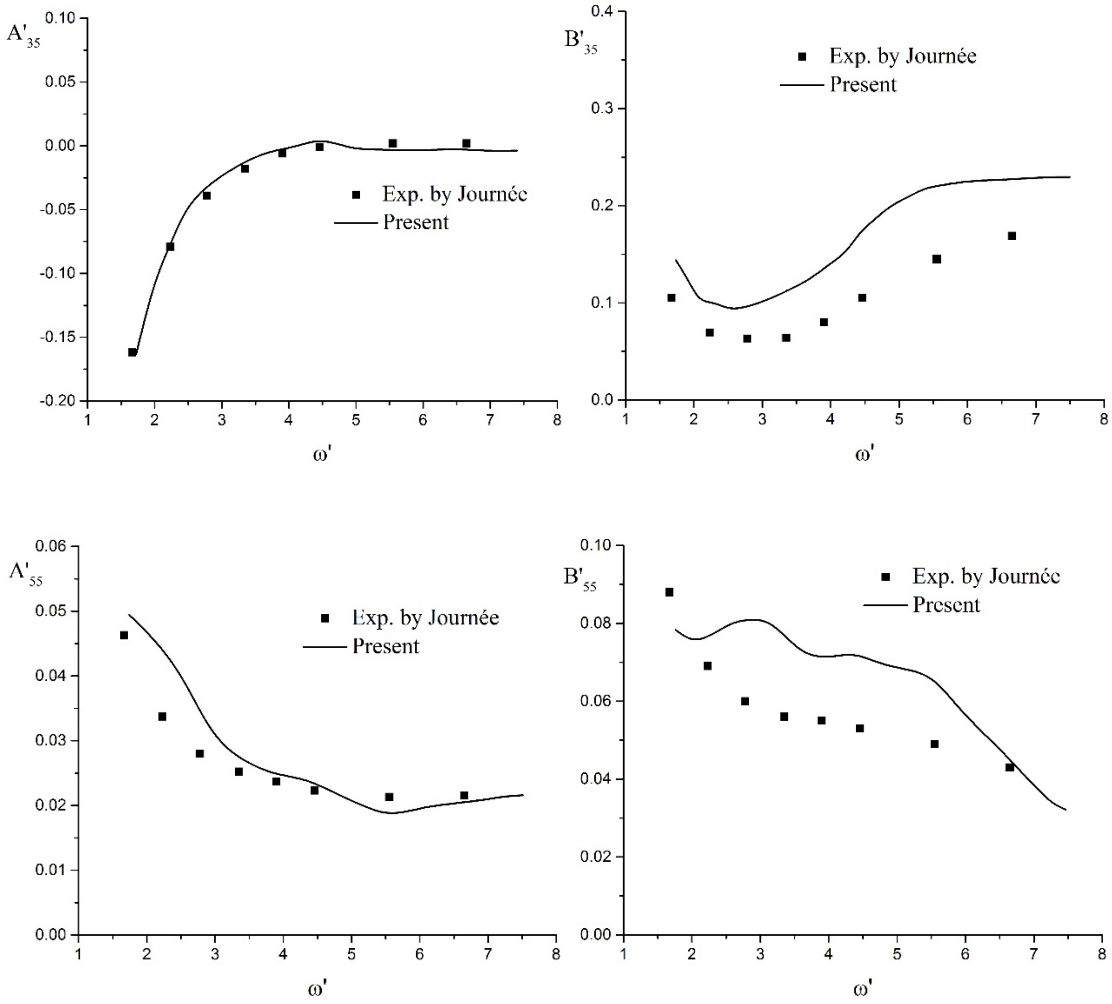

Fig. 5.15 Hydrodynamic coefficients versus ω_e' *due to unit amplitude pitch motion for the WigleyIII advancing at* $F_n = 0.3$

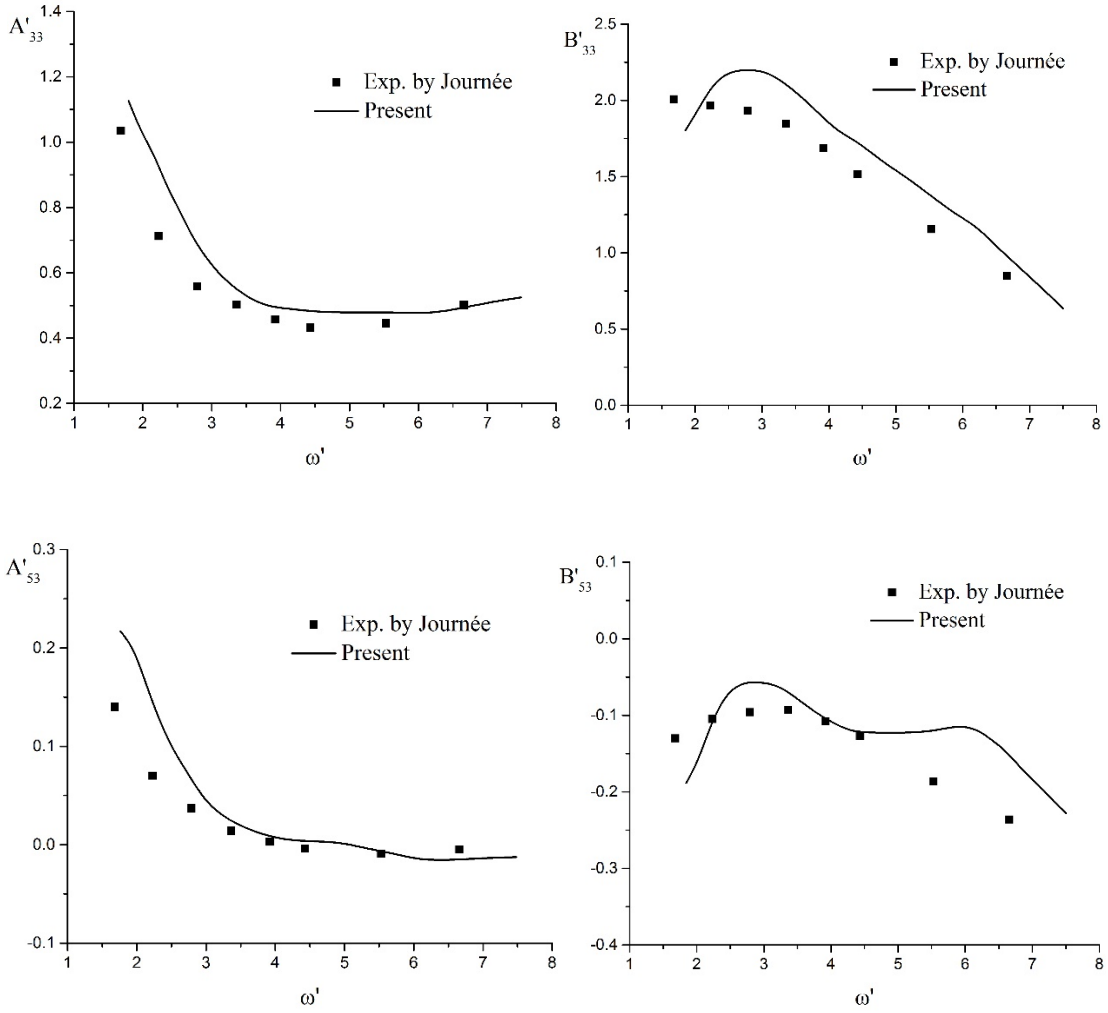

Fig. 5.16 Hydrodynamic coefficients versus ω_e' *due to unit amplitude heave motion for the WigleyIII advancing at* $F_n = 0.4$

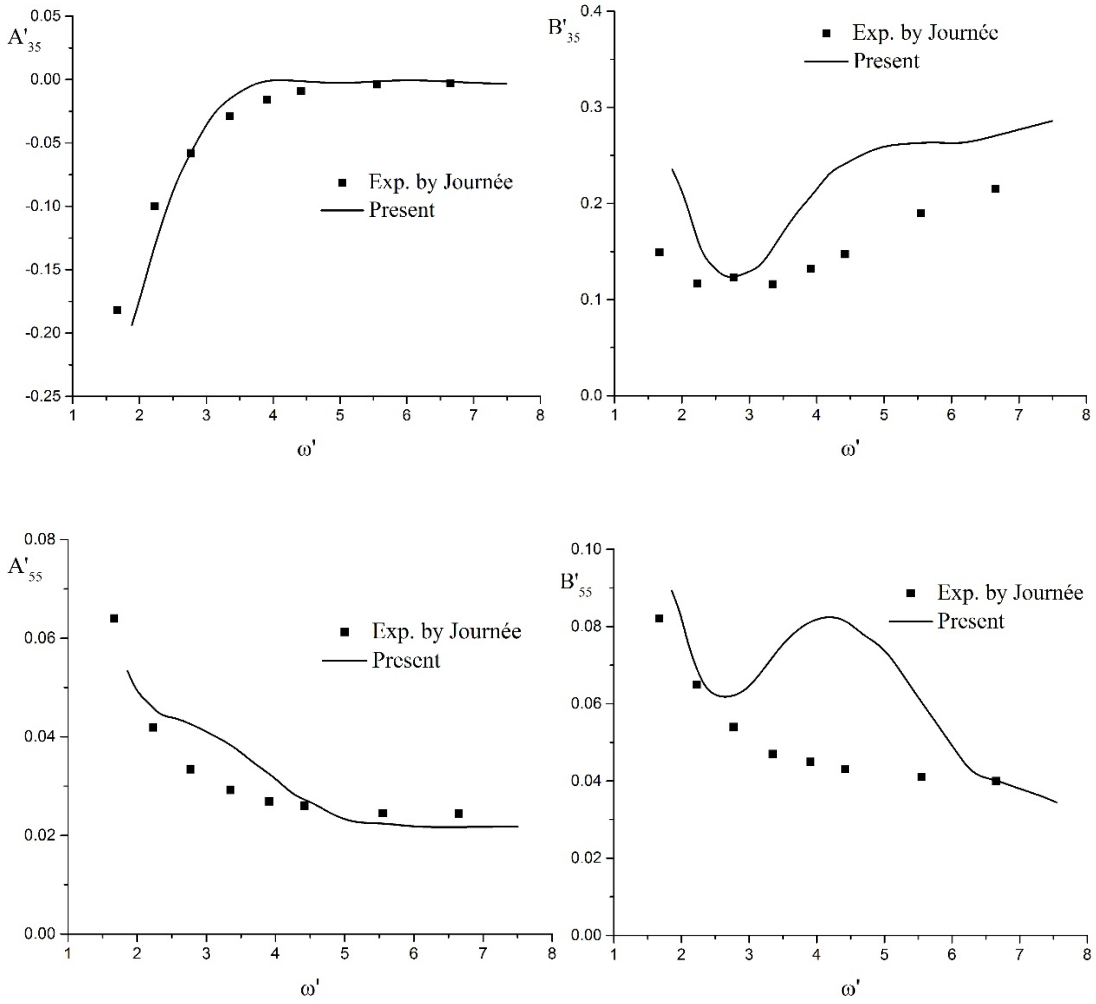

Fig. 5.17 Hydrodynamic coefficients versus ω_e' *due to unit amplitude pitch motion for the WigleyIII advancing at* $F_n = 0.4$

The comparison shows that the heave and pitch hydrodynamic coefficients computed by the present numerical approach are in good agreement with the measured values in general, no matter the forward speed increasing. This normally could not be achieved by using strip theories, as they are based on the assumption of high frequency with zero forward speed or low speed. However, relative big deviations can be observed in the estimations of pitch damping B_{55} which are probably caused by the linearization of the BVP on the free surface condition and body surface condition. Let P_b and P_s represent the exact values of the vertical hydrodynamic pressure on the fore body of the hull and after body respectively. Meanwhile, the nonlinear behaviour of the flow in nature would be much stronger at the bow and stern than that along the midbody of

the hull. So we can assume that the deviation of the pressure only comes from the bow and stern denoted by ΔP_b and ΔP_s as shown in Fig. 5.18. When the hull is in a pitch motion, ΔP_b and ΔP_s would have similar value but opposite direction, thereby cancel each other out in the vertical force estimation. However, they will create a big deviation of moment as the arm of this moment is the ship length thus greatly enlarge the deviation. Moreover, as known to all, the wave damping is related to the energy dissipation. The amplitude of the radiation wave should decay with the wave propagating away from the hull in the real 3D flow field. However, when the problem is transferred into the 2D cross plane, the radiation condition only make sure the wave is radiated into infinity without reflecting but no amplitude decay assumed. Therefore this will result the overestimation of damping force by 2D approaches, and further increase the deviation in the estimation of pitch damping.

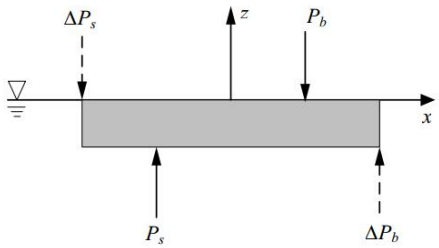

Fig. 5.18 Diagram of the vertical forces on the hull in pitch

Fig. 5.19 and Fig. 5.20 show the computed hydrodynamic coefficients of the Series 60 ($C_B = 0.7$) ship advancing at $F_n = 0.2$. Experimental results reported by Gerritsma (1960) are also shown for comparison.

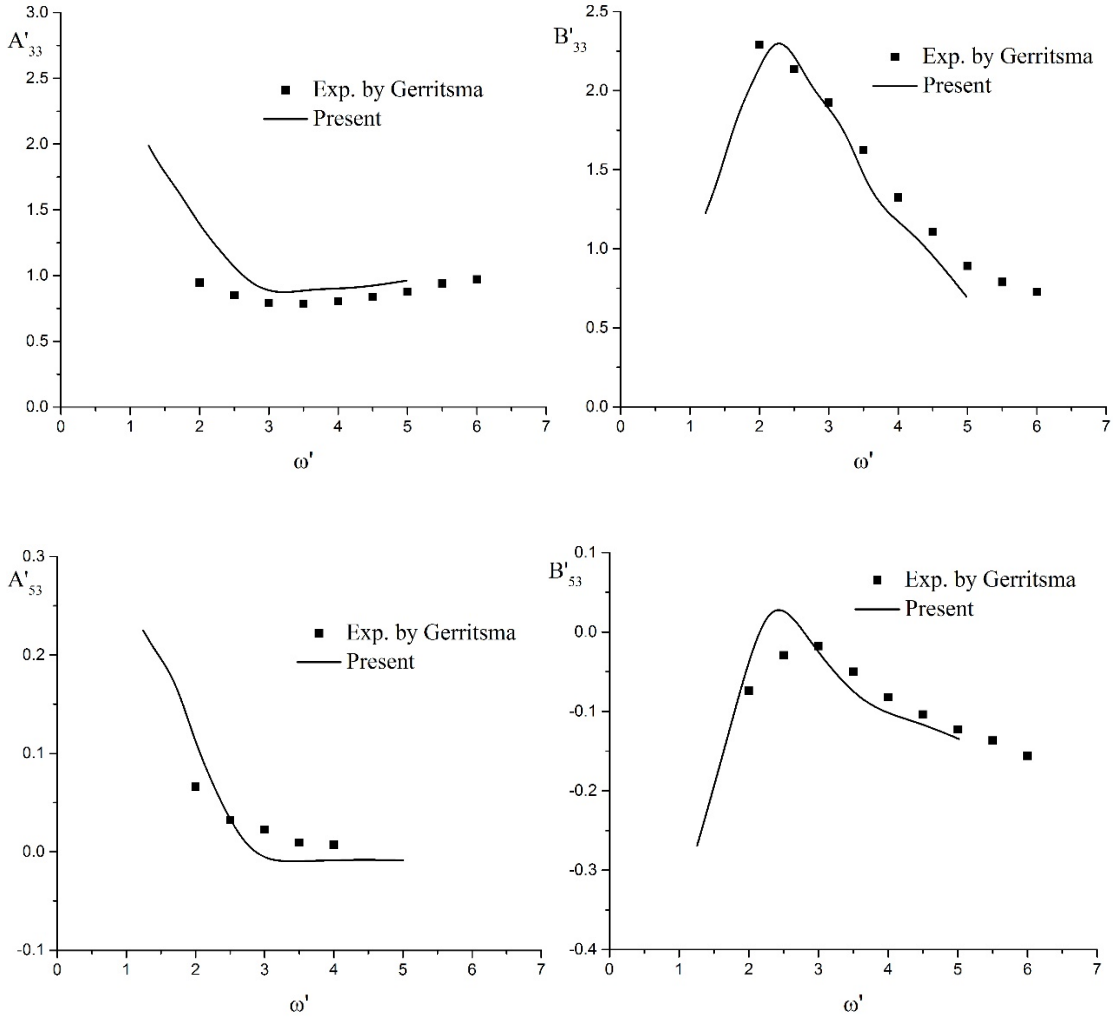

Fig. 5.19 Hydrodynamic coefficients versus ω_e' *due to unit amplitude heave motion for the S60 advancing at* $F_n = 0.2$

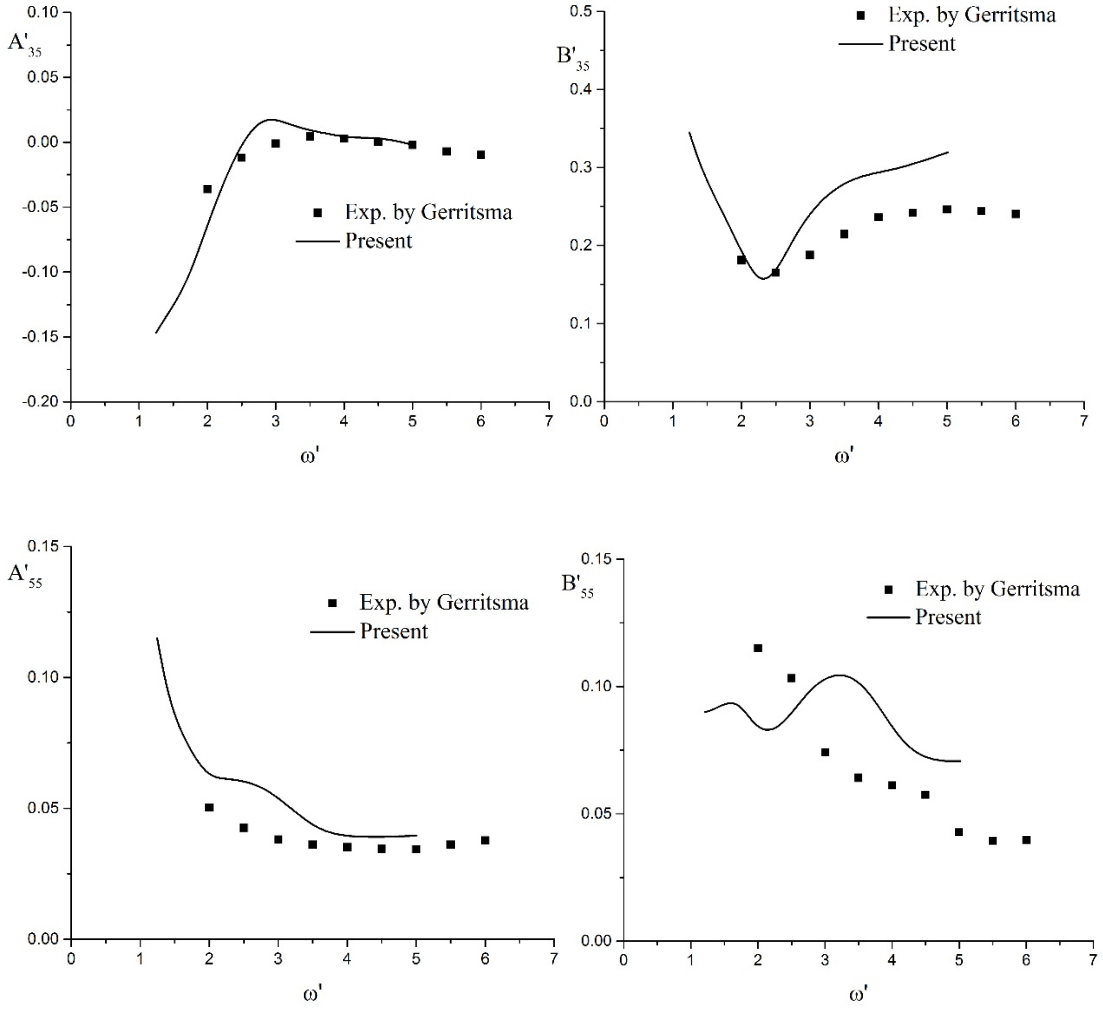

Fig. 5.20 Hydrodynamic coefficients versus ω_e' due to unit amplitude pitch motion for the S60 advancing at $F_n = 0.2$

Again, from the comparison, the results computed by the present approach agree nicely with the experimental results except for the B_{55} due to the probable reason explained before.

5.6.2 Lateral motions

Apart from the hydrodynamic coefficients usually computed for ships advancing in waves coupled with high frequency vertical motions, we are obviously interested in the prediction of the lateral motions in the horizontal plane since our final discussion in the next Chapter will be focused on the manoeuvring analysis. In Fig. 5.21 to Fig. 5.24, hydrodynamic coefficients in the form of manoeuvring derivatives are computed

for the Series 60 ($C_B = 0.7$) advancing with lateral oscillations, together with the experimental results obtained by van Leeuwen (1964). The Froude numbers F_n used are 0.2 and 0.3. The subscript 'dot' in the figures denotes the time derivative product. Noting that the limiting value of these hydrodynamic coefficients at zero frequency can be provided for manoeuvring simulations. Relations between the seakeeping hydrodynamic coefficients and manoeuvring derivatives are presented as follow.

$$\begin{cases} Y_{\dot{v}} = -A_{22}(\omega_e), Y_v = -B_{22}(\omega_e); \\ Y_{\dot{r}} = -A_{26}(\omega_e) + U/\omega_e^2 B_{22}(\omega_e), Y_r = -B_{26}(\omega_e) - UA_{22}(\omega_e); \\ N_{\dot{v}} = -A_{62}(\omega_e), N_v = -B_{62}(\omega_e); \\ N_{\dot{r}} = -A_{66}(\omega_e) + U/\omega_e^2 B_{62}(\omega_e), N_r = -B_{66}(\omega_e) - UA_{62}(\omega_e) \end{cases} \tag{5.30}$$

The non-dimensionalization of the hydrodynamic coefficients will follow the way common applied in manoeuvring analysis, the Prime system, which will also be introduced in next Chapter. Therefore,

$$\begin{cases} Y'_{\dot{v}} = Y_{\dot{v}} \Big/ \left(\frac{1}{2}\rho L^2 D\right), Y'_v = Y_v \Big/ \left(\frac{1}{2}\rho LDU\right); \\ Y'_{\dot{r}} = Y_{\dot{r}} \Big/ \left(\frac{1}{2}\rho L^3 D\right), Y'_r = Y_r \Big/ \left(\frac{1}{2}\rho L^2 DU\right); \\ N'_{\dot{v}} = N_{\dot{v}} \Big/ \left(\frac{1}{2}\rho L^3 D\right), N'_v = N_v \Big/ \left(\frac{1}{2}\rho L^2 DU\right); \\ N'_{\dot{r}} = N_{\dot{r}} \Big/ \left(\frac{1}{2}\rho L^4 D\right), N'_r = N_r \Big/ \left(\frac{1}{2}\rho L^3 DU\right) \end{cases} \tag{5.31}$$

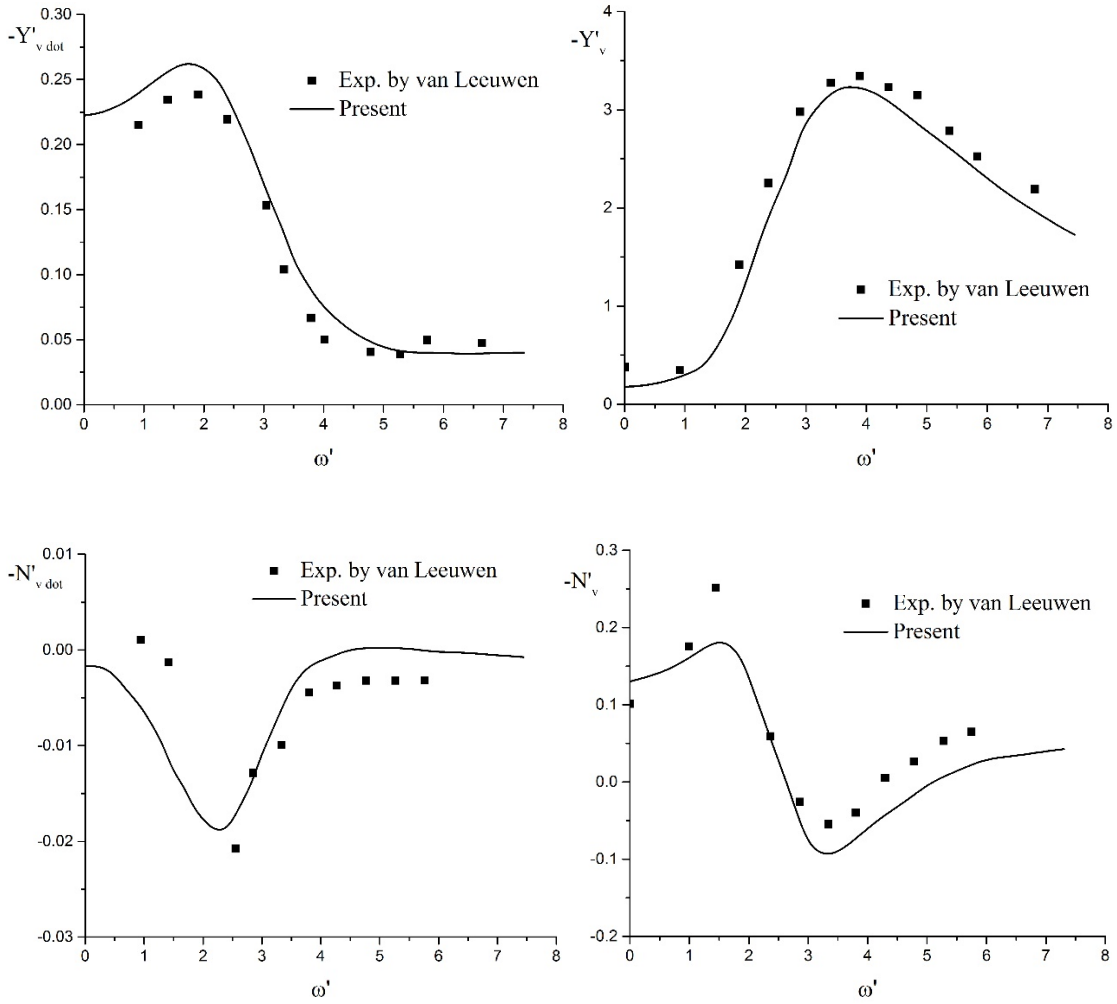

Fig. 5.21 Hydrodynamic derivatives versus ω_e' *due to unit amplitude sway motion for the S60 advancing at* $F_n = 0.2$

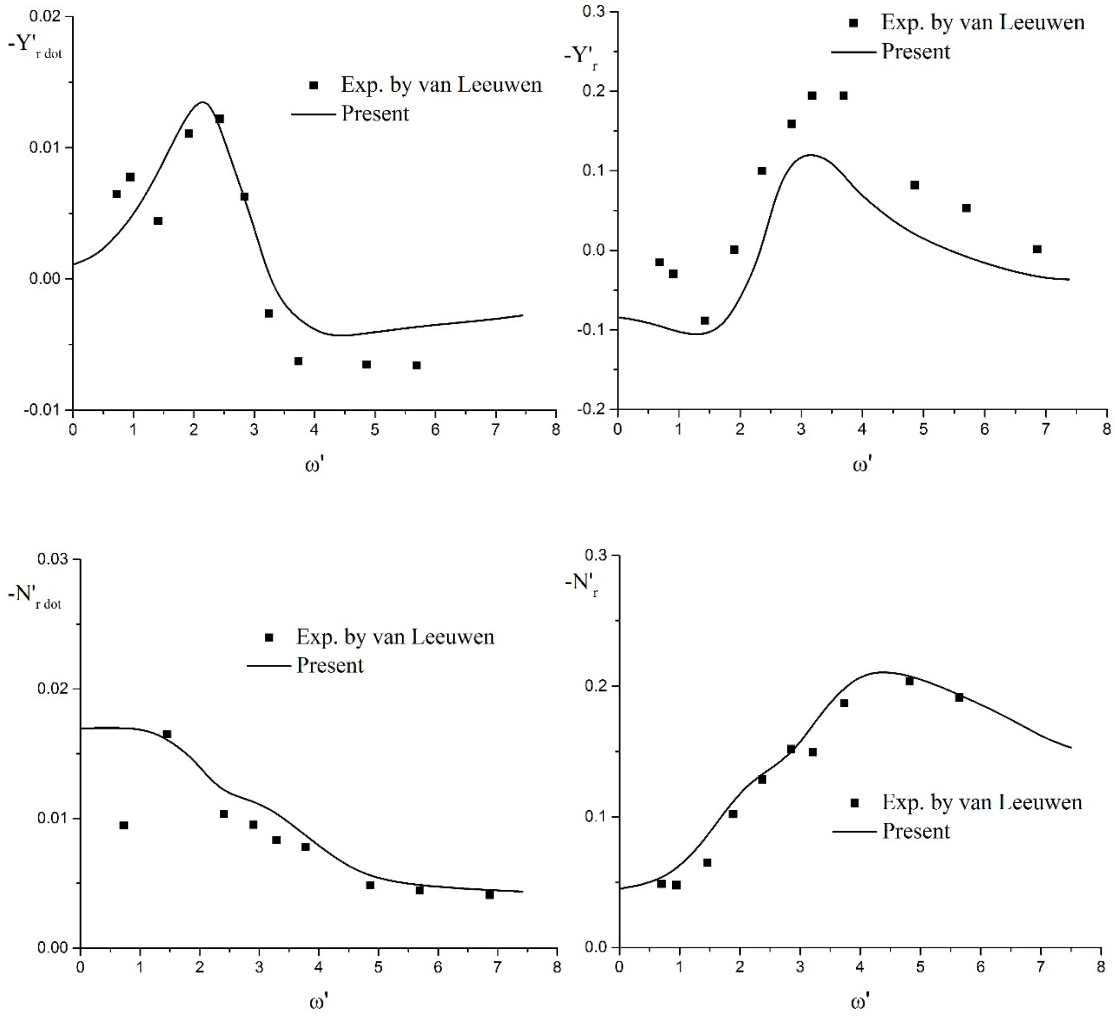

Fig. 5.22 Hydrodynamic derivatives versus ω_e' *due to unit amplitude yaw motion for the S60 advancing at* $F_n = 0.2$

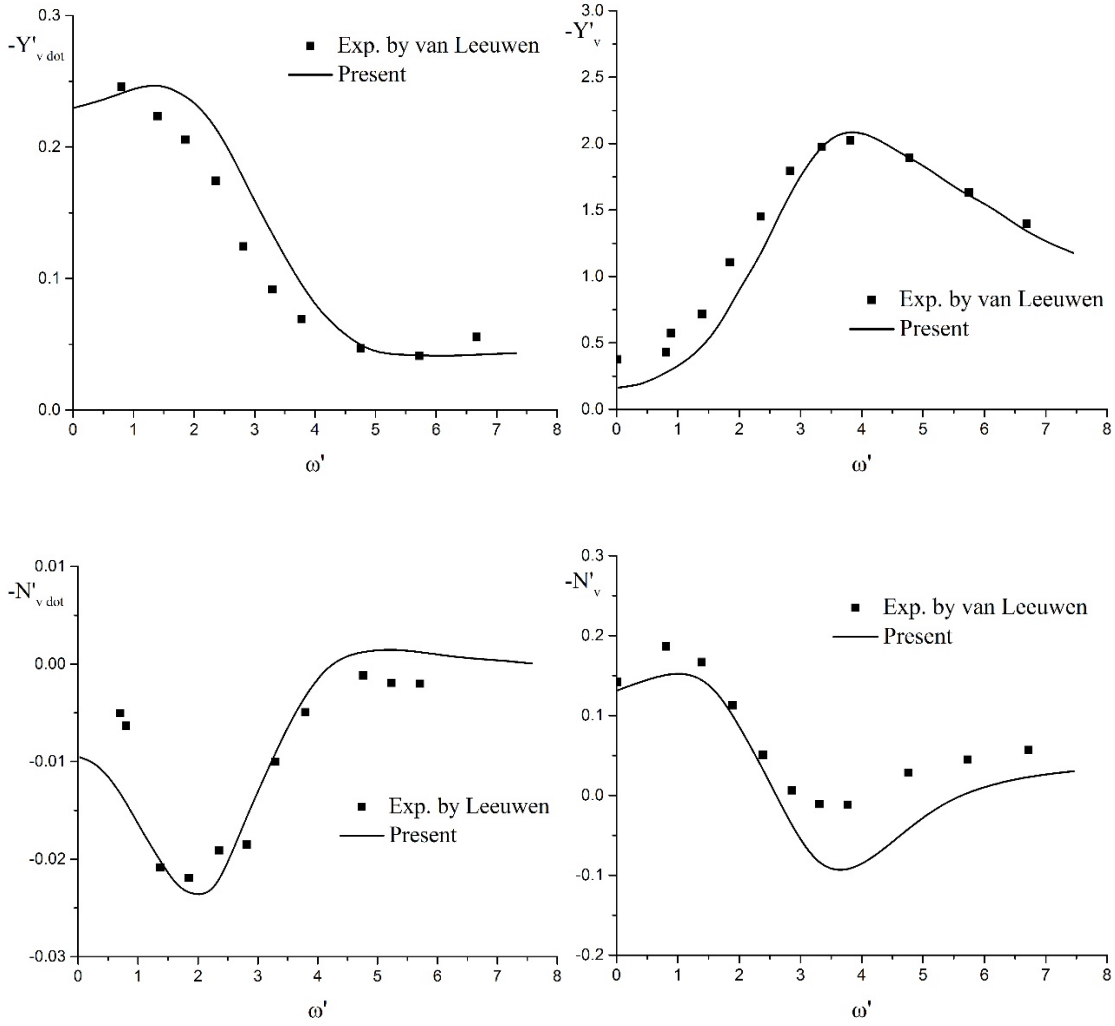

Fig. 5.23 Hydrodynamic derivatives versus ω_e' *due to unit amplitude sway motion for the S60 advancing at* $F_n = 0.3$

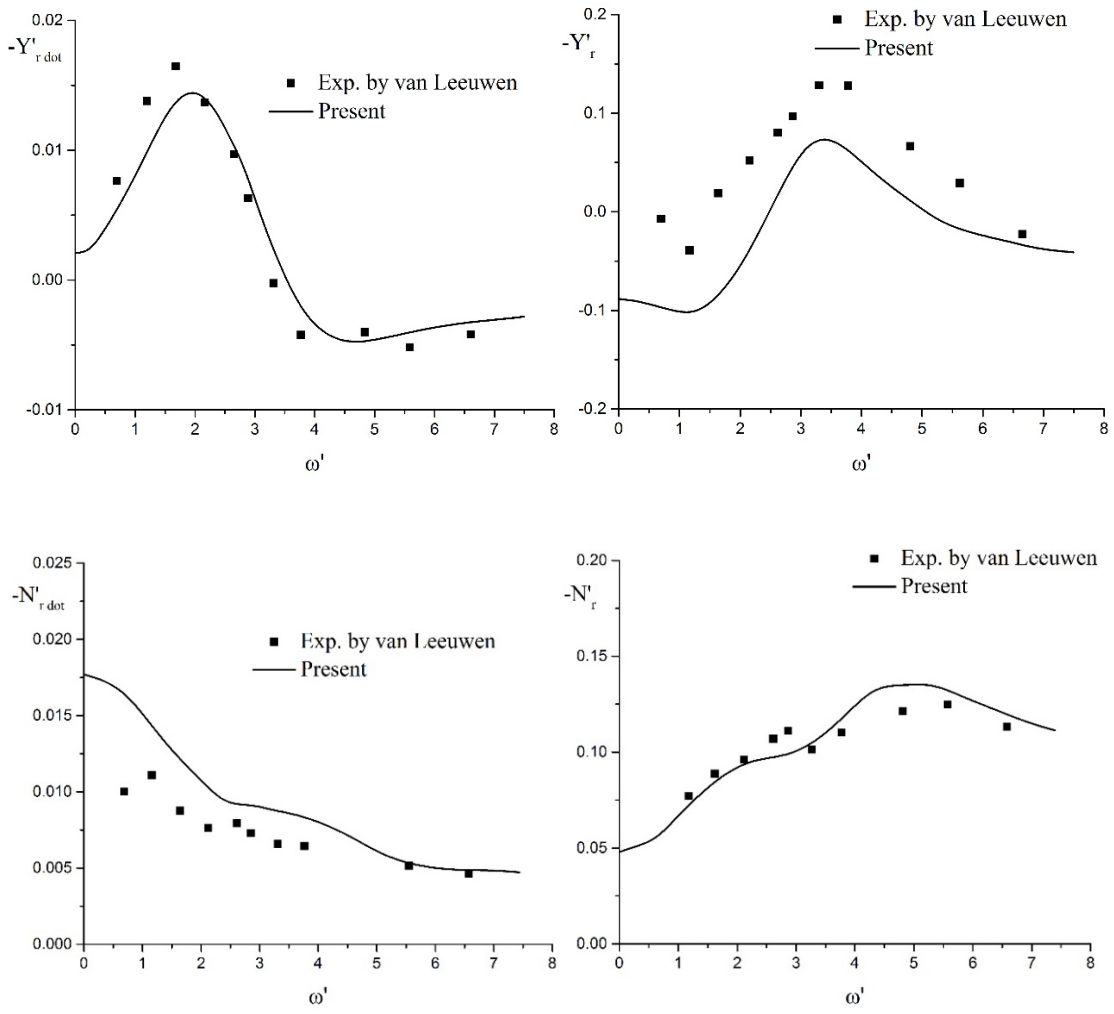

Fig. 5.24 Hydrodynamic derivatives versus ω_e' due to unit amplitude yaw motion for the S60 advancing at $F_n = 0.3$

From comparison, the numerical results obtained by the present approach show significantly positive agreement with the experimental results. The small difference appeared in the limiting value at zero frequency can be explained that in the numerical calculations rigid wall free surface condition is imposed approximately while in fact no such plane is set in experiments.

5.7 **Validation of wave exciting force**

Considering the ship is restrained at its average position advancing in head waves, the following validation of diffraction problems on the Series 60 ($C_B = 0.7$) are presented by showing the magnitude and phase of the wave exciting forces and moments acting

on the hull. The Froude number F_n used is 0.2. Experimental results reported by Gerritsma (1960) and the computed results by the 3D method by Lin & Yue (1990) are included for comparison. The non-dimensional forms of the magnitudes are given by

$$\begin{cases} F_3' = amplitude\ of\ \ F_3 \times L / \rho g A \nabla \\ F_5' = amplitude\ of\ \ F_5 / \rho g A \nabla \end{cases} \tag{5.32}$$

where A is the amplitude of incident wave, ∇ is the volume of the ship. The phase angles are measured relative to the occurrence of wave peak.

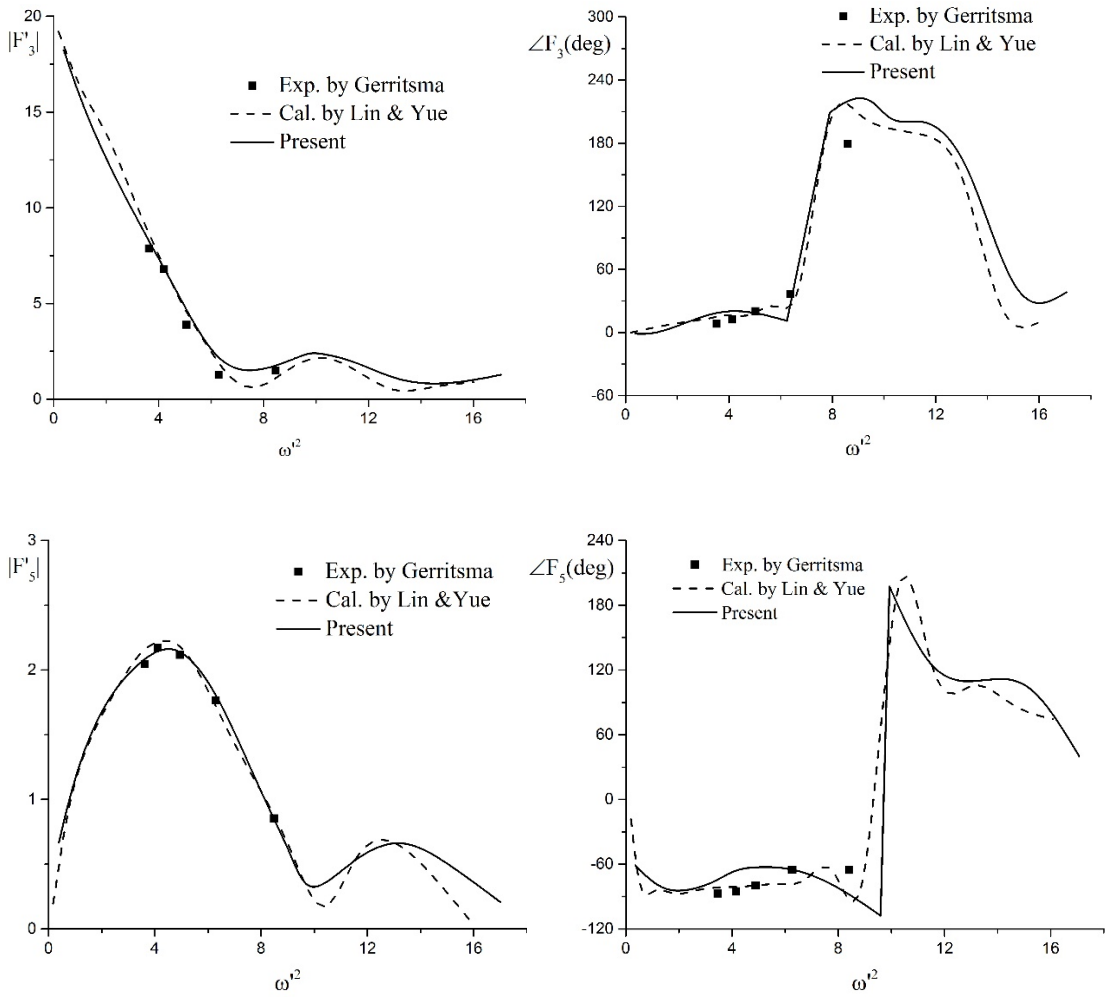

Fig. 5.25 Magnitude and phase of the wave exciting force and moment on the S60 advancing at $F_n = 0.2$

From comparison, the results by the present approach and by the 3D method by Lin & Yue (1990) all tend to agree with the measured experimental data nicely.

5.8 **Validation of RAO**

After presenting the results of hydrodynamic coefficients in radiation problems and wave exciting forces in diffraction problems, validations will be finally carried out on the wave induced motions. The recommended S175 container ship by the ITTC seakeeping committee will be used for calculations. RAOs of 5-DOF motions under different incident wave angles χ are presented. The Froude number F_n used is set at 0.275. And the range of the wave length is $0.5 < \lambda/L < 2.5$, corresponding to the non-dimensional natural frequency of the incident wave $1.58 < \omega_0\sqrt{L/g} < 3.54$. The results from the ITTC report (1978) as a set of statistic values, named "Quartiles" are included for comparison.

From Fig. 5.26, the results given by the present approach basically agree with the data provided by ITTC as well. Apparent deviations can be observed in sway, roll and yaw motions when the incident angle $\chi = -60^o$. Less good agreement is achieved in the case of the amplitudes, while the phases agree reasonably well. In the roll motion, the difference is present because the estimation of the equivalent roll damping coefficient is different from the one specified by ITTC. In the sway and yaw motions, the deviations of the amplitudes would be due to indirect approximation of the lift force appeared in lateral motions.

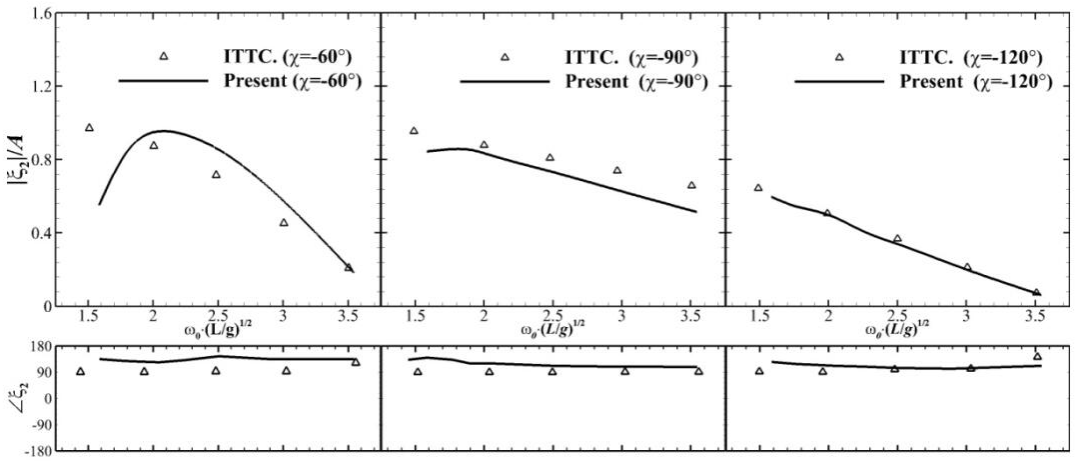

(a) Sway

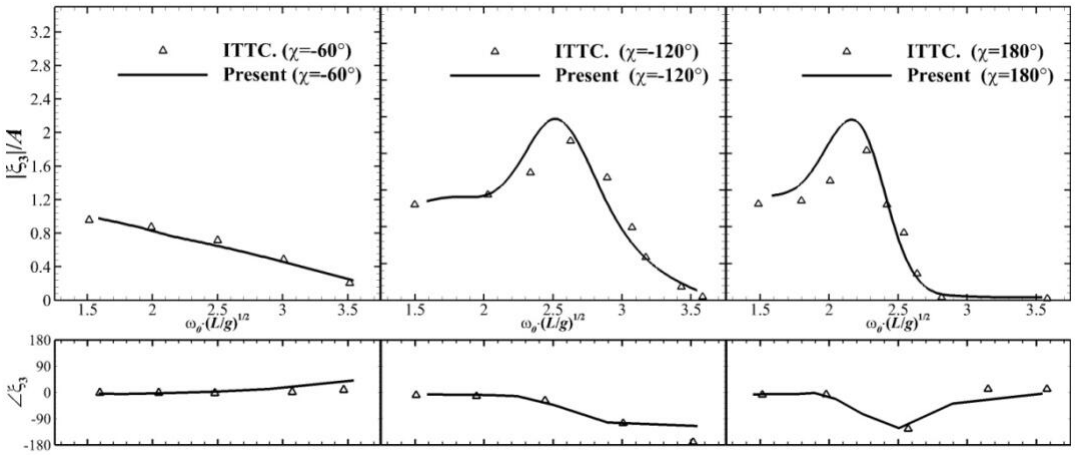

(b) Heave

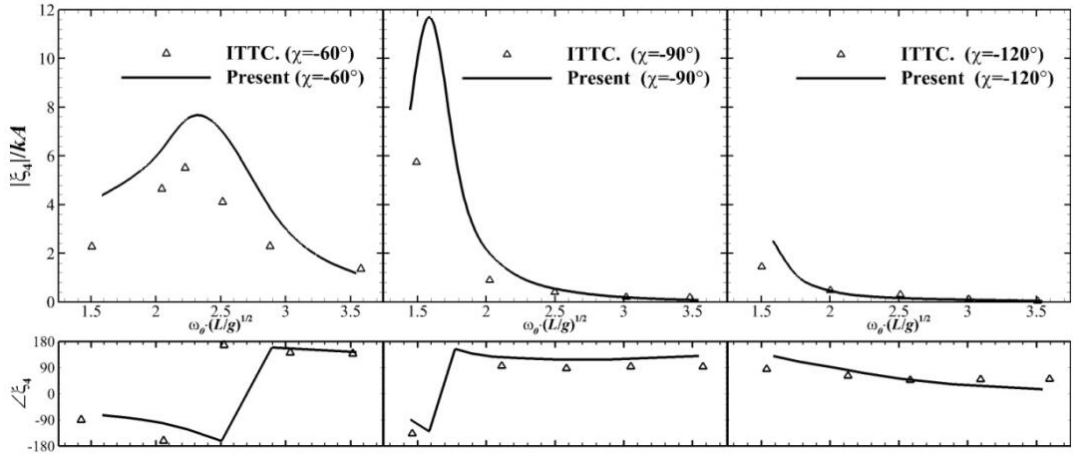

(c) Roll

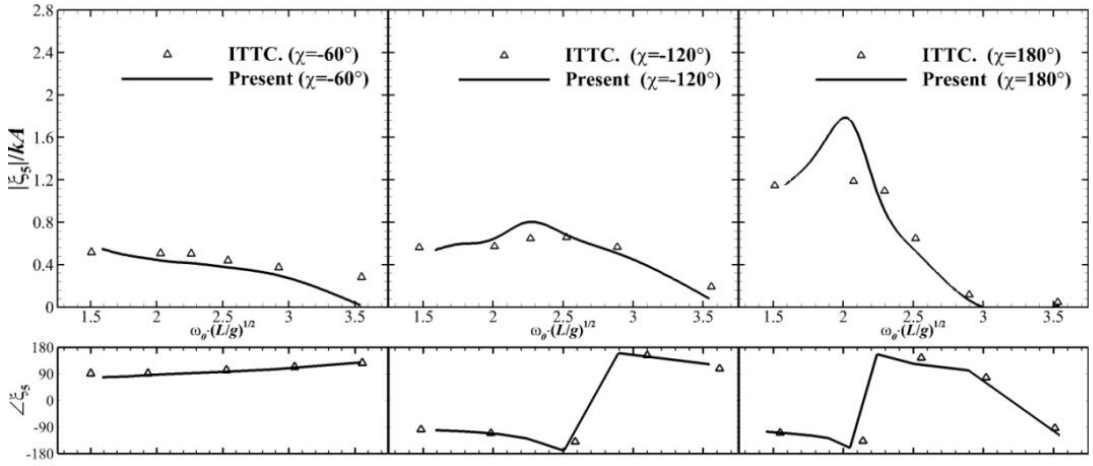

(d) Pitch

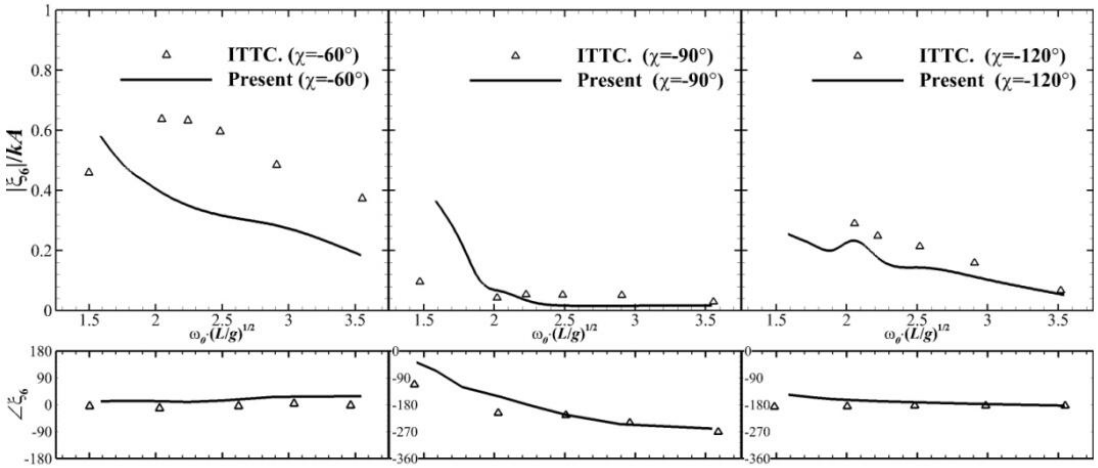

(e) Yaw

Fig. 5.26 RAOs for the S-175 container ship advancing at $F_n = 0.275$ *under different incident wave angles*

5.9 **Summary of the chapter**

Following the development of the 2.5D approach for seakeeping analysis already described in Chapter 3, the NURBS is first introduced for geometry modelling of the hulls including the fundamental algorithms applied in the present numerical tool been given. Verifications of the tool on the unit circle and mathematical ship hulls are carried out together with validations on the two common real ship types, i.e., a Series 60 ($C_B = 0.7$) ship and a S175 container ship. Then the NURBS based BEM is

proposed by applying the tool in expressing the distributions of the variables on the boundary.

Next, validations of the approach on the radiation problems by calculating the frequency dependent hydrodynamic coefficients are carried out on the WigleyIII and the Series 60 ($C_B = 0.7$) ship advancing in calm water coupled with forced vertical motions and lateral motions respectively. Validations on the diffraction problems are also carried out on the Series 60 ship by presenting the magnitude and phase of the wave exciting forces in heave and pitch. Regarding the wave induced motions, calculations of RAOs are carried out on the S175 ship recommended by the ITTC which will also be applied for manoeuvring simulations in the next Chapter. In all these validations presented above, results are compared with available experimental measured data or numerical results and good agreements have been achieved, thereby demonstrate that the present established 2.5D NURBS based numerical tool for seakeeping analysis is reliable. And it put a good foundation for the next analysis of a ship manoeuvring in waves which also involving high frequency wave induced motions.

6 Manoeuvring in waves

In this chapter, we will carry out the final objective of the present study which is analyzing the manoeuvring behaviour of a displacement ship advancing with forward speed in regular deep water waves. As stated before, the analysis is described by considering combined seakeeping and manoeuvring as a two time scales problem. The linear wave induced motions of a ship are assumed to occur on a more rapidly varying time scale than the manoeuvring. When the ship has a mean forward speed and does a manoeuvring in a seaway, the wave induced motions is affected by the slowly varying manoeuvring according to the changing kinematic parameters of the ship and the relative incident wave angle. On the other hand, the effect of the seakeeping on the manoeuvring analysis is in terms of slowly varying mean second order wave drift loads. In the proceeding discussion, a two time scales combined seakeeping and manoeuvring model will be shown applying a sequential procedure and followed by its implementation in case of typical maneuvers of a selected ship.

The mathematical model of the manoeuvring motions in horizontal plane will be formulated firstly based on the modular concept. Evaluations of each external force component will be given in detail. The mean drift force which cannot be considered properly by the methods based on the unified theory utilizing convolution integral will be estimated by the direct pressure integration method. After that, a whole flow chart of the simulation system based on the two time scales model will be presented. Finally, validation of the model will be carried out on the selected ship executing two typical maneuvers, namely turning circle and Zig-zag, in calm water and regular waves respectively. The simulation results will be compared with the available experimental measurements. Note that the simulations here are limited to the assumptions that the water depth and the horizontal extent are infinite which means the shallow water and bank effects are not considered.

6.1 The mathematical model

6.1.1 Coordinate system

Firstly, the procedure starts with an introduction of the manoeuvring body fixed coordinate system shown in Fig. 6.1. It should be noted that Fig. 6.1 represents the Fig. 4.1 in the horizontal plane as seen from above. The Earth fixed coordinate system $(O_0 - x_0 y_0 z_0)$ is still used to keep track of the global position of the ship and its heading angle. The incident wave direction is also described in this frame. The hydrodynamic frame $(O - xyz)$ translating in the horizontal calm water plane at the mean forward speed U is fixed with respect to the mean oscillatory position of the ship. Its x axis is coincide with the direction of U. This is the frame in which the BVPs are formulated as described in Chapter 4 for seakeeping analysis. Another manoevuring body fixed frame $(O' - x'y'z')$ is employed with its origin set in the plane of undisturbed free surface and z' axis pointing upwards passes through the center of gravity as well, whereas positive direction of x' axis is always pointing to the bow, y' axis is pointing to the portside. The frame translates and rotates in all 6-DOF with the body. Apparently, this frame is a non-inertia frame which is used to describe the forces and moments acting on the ship in manoeuvring motions for its convenience of time independent characteristic. Besides, it is also convenient for the description of the hull surface.

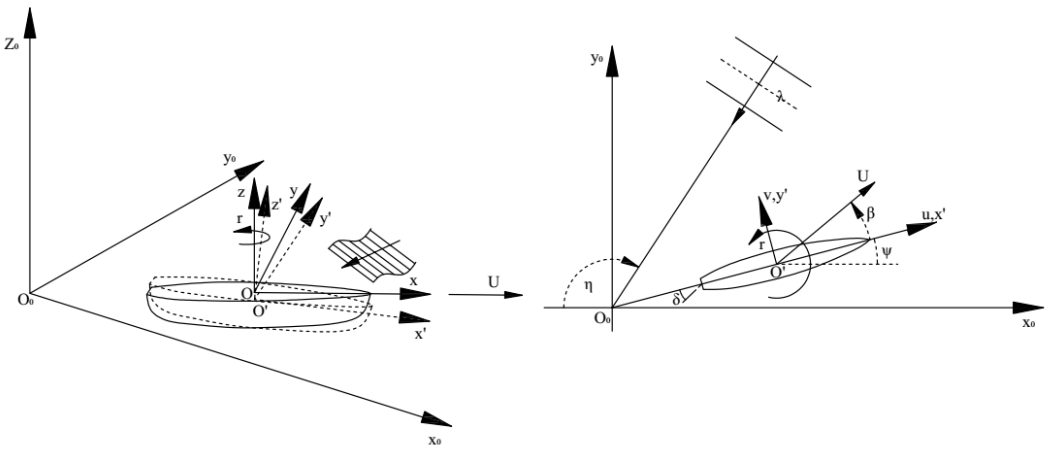

Fig. 6.1 Coordinate systems in manoeuvring analysis

Similar to those in the hydrodynamic frame, in the body fixed frame, u, v, w are defined as surge, sway and heave velocities respectively and p, q, r are rolling, pitching and yaw rates. The Euler angles between the body fixed frame and the earth fixed frame are ψ, θ, ϕ which denote the heading angle, pitching angle and rolling angle respectively. Noting that, in general $\dot{\psi} \neq r$, $\dot{\theta} \neq q$, $\dot{\phi} \neq p$. In addition, β, δ, η are the drift angle, rudder angle and incident wave angle respectively with the positive direction shown in Fig. 6.1.

Normally, motions of a rigid body can be described in the earth fixed frame, which is an inertial frame, according to the Newton's second law. However, for the purpose of manoeuverability analysis, it is more convenient to establish the motion equations in the body fixed frame, thereby a transformation of the kinematic variables from the earth fixed frame to the body fixed frame has to be conducted. By following the roll-pitch-yaw rotation convention as follow,

$$\begin{bmatrix} x_0 \\ \hat{y} \\ \hat{z} \end{bmatrix} = \begin{bmatrix} 1 & 0 & 0 \\ 0 & \cos\phi & \sin\phi \\ 0 & -\sin\phi & \cos\phi \end{bmatrix} \begin{bmatrix} x_0 \\ y_0 \\ z_0 \end{bmatrix}$$
$$\begin{bmatrix} \hat{x} \\ \hat{y} \\ z' \end{bmatrix} = \begin{bmatrix} \cos\theta & 0 & -\sin\theta \\ 0 & 1 & 0 \\ \sin\theta & 0 & \cos\theta \end{bmatrix} \begin{bmatrix} x_0 \\ \hat{y} \\ \hat{z} \end{bmatrix} \tag{6.1}$$
$$\begin{bmatrix} x' \\ y' \\ z' \end{bmatrix} = \begin{bmatrix} \cos\psi & \sin\psi & 0 \\ -\sin\psi & \cos\psi & 0 \\ 0 & 0 & 1 \end{bmatrix} \begin{bmatrix} \hat{x} \\ \hat{y} \\ z' \end{bmatrix}$$

in which $(\hat{x}, \hat{y}, \hat{z})$ is the interim frame during the rotation, the relationship between linear velocities in the body fixed and the earth fixed frames can be derived in the form of Euler matrix.

$$\begin{bmatrix} \dot{x}_0 \\ \dot{y}_0 \\ \dot{z}_0 \end{bmatrix} = \begin{bmatrix} \cos\psi\cos\theta & \cos\psi\sin\theta\sin\phi - \sin\psi\cos\phi & \sin\psi\sin\phi + \cos\psi\sin\theta\cos\phi \\ \sin\psi\cos\theta & \cos\psi\cos\phi + \sin\psi\sin\theta\sin\phi & \sin\psi\sin\theta\cos\phi - \cos\psi\sin\phi \\ -\sin\theta & \cos\theta\sin\phi & \cos\theta\cos\phi \end{bmatrix} \begin{bmatrix} u \\ v \\ w \end{bmatrix} \tag{6.2}$$

Similarly, the relationship between the angular velocities can be given as

$$\begin{bmatrix} \dot{\phi} \\ \dot{\theta} \\ \dot{\psi} \end{bmatrix} = \begin{bmatrix} 1 & \sin\phi\tan\theta & \cos\phi\tan\theta \\ 0 & \cos\phi & -\sin\phi \\ 0 & \sin\phi\sec\theta & \cos\phi\sec\theta \end{bmatrix} \begin{bmatrix} p \\ q \\ r \end{bmatrix} \tag{6.3}$$

If assuming small manoeuvring angles, then, $\cos\psi \approx 1$, $\sin\psi \approx \psi$ etc. and neglecting their products, e.g., $\psi\phi \approx 0$ etc., the linearized Euler matrix can be given as follow.

$$\begin{bmatrix} \dot{x}_0 \\ \dot{y}_0 \\ \dot{z}_0 \end{bmatrix} = \begin{bmatrix} 1 & -\psi & \theta \\ \psi & 1 & -\phi \\ -\theta & \phi & 1 \end{bmatrix} \begin{bmatrix} u \\ v \\ w \end{bmatrix} \tag{6.4}$$

$$\begin{bmatrix} \dot{\phi} \\ \dot{\theta} \\ \dot{\psi} \end{bmatrix} = \begin{bmatrix} 1 & 0 & \theta \\ 0 & 1 & -\phi \\ 0 & \phi & 1 \end{bmatrix} \begin{bmatrix} p \\ q \\ r \end{bmatrix} \tag{6.5}$$

It should be noted that the finite angular velocity transformation matrix is singular for the pitch angle, $\theta = \pm 90^{o}$, but this is not a problem for the ships since they never operate close to this singularity.

In the manoeuvring analysis, we are more concerned about the changing of the heading angle and the trajectory of the ship in horizontal plane. For most of conventional ships, the heave, pitch and roll motions would have weak influences on the horizontal motions which means ψ, x_0, y_0 are dependent of u, v, r only. This is the classical 3-DOF ship manoeuvring motions problem. However, for some modern ship types, e.g., container ship, ro-ro ship and high speed craft, having higher COG, the turning motion and wave effect may induce considerable values of heeling angle, thereby leads to pressure changes over the ship surface which will result significant different horizontal motions. Therefore, 4-DOF ship motions problem by considering u, v, r coupled with rolling velocity p should be established for the analysis of ship manoeuvring in waves. By setting $w = 0, q = 0$ and neglecting the pitching angle θ as stated above, following 4-DOF motions relationships can be derived.

$$\begin{cases} \dot{x}_0 = u\cos\psi - v\cos\phi\sin\psi \\ \dot{y}_0 = u\sin\psi + v\cos\phi\cos\psi \\ \dot{\psi} = r\cos\phi \\ \dot{\phi} = p \end{cases} \tag{6.6}$$

The time histories of the velocities and angular velocities can be first analysed in the body fixed frame. Then according to the relation (6.6), the position and attitude of the ship can be easily obtained by integrating the time derivatives in earth fixed frame numerically. In consequence, to establish the motion equations in the body fixed frame would be the first task.

6.1.2 Motion equations

A ship maneuvers in horizontal plane can be regarded as a special case of the generalized rigid body motions in infinite medium. By applying momentum theorem and moment of momentum theorem based on mechanics of rigid body, the motion equations can be derived for system dynamic analysis. In particular, there are mainly two ways for this derivation, one is the vector mechanics based on the Newton's laws of motion and the other one is the analytical mechanics which considering the system as a whole and making use of the kinetic energy and potential energy to derive the motion equations without calculating the force components. Theoretically, these two ways would derive the same set of the motion equations. The first way by vector mechanics will be applied for the current derivation.

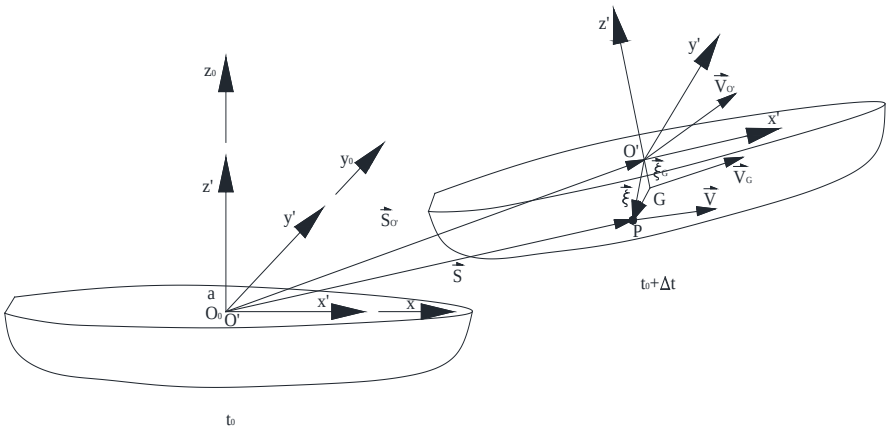

Fig. 6.2 Sketch map of the rigid body (ship) motion

The momentum theorem and moment of momentum theorem of a rigid body are expressed as follow.

$$\begin{cases} \sum \vec{F} = \dfrac{d\vec{G}}{dt} \\ \sum \vec{M}_a = \dfrac{d\vec{H}_a}{dt} \end{cases} \tag{6.7}$$

where $\sum \vec{F}$ is the total external force, $\sum \vec{M}_a$ is the total moment about a space fixed point a, $\vec{G}$ is the total momentum of the rigid body, then $\vec{H}_a$ is the total moment of momentum about the fixed point. For convenience, the origin of the earth fixed frame O_0 can be set on this fixed point. Meanwhile, the origin of the body fixed frame O' is also set on this point at an arbitrary time instance instantaneously as shown in Fig. 6.2.

Defining $G_{x'}, G_{y'}, G_{z'}$ as the coordinate components of the total momentum.

$$\vec{G} = G_{x'}\vec{i} + G_{y'}\vec{j} + G_{z'}\vec{k} \tag{6.8}$$

Then,

$$\frac{d\vec{G}}{dt} = \dot{G}_{x'}\vec{i} + \dot{G}_{y'}\vec{j} + \dot{G}_{z'}\vec{k} + G_{x'}\dot{\vec{i}} + G_{y'}\dot{\vec{j}} + G_{z'}\dot{\vec{k}} \tag{6.9}$$

Obviously,

$$\dot{G}_{x'}\vec{i} + \dot{G}_{y'}\vec{j} + \dot{G}_{z'}\vec{k} = \frac{\partial G}{\partial t} \tag{6.10}$$

which represents the partial derivative without considering the rotation of the body fixed frame. On the other hand, according to vector analysis, we have

$$\begin{cases} \dot{\vec{i}} = \dfrac{d\vec{i}}{dt} = (r\vec{j} - q\vec{k}) \\ \dot{\vec{j}} = \dfrac{d\vec{j}}{dt} = (p\vec{k} - r\vec{i}) \\ \dot{\vec{k}} = \dfrac{d\vec{k}}{dt} = (q\vec{i} - p\vec{j}) \end{cases} \tag{6.11}$$

So,

$$G_{x'}\dot{\vec{i}} + G_{y'}\dot{\vec{j}} + G_{z'}\dot{\vec{k}} = \vec{\Omega} \times \vec{G} \tag{6.12}$$

where,

$$\vec{\Omega} = p\vec{i} + q\vec{j} + r\vec{k} \tag{6.13}$$

Thereby, the following momentum equation in the body fixed frame can be derived.

$$\sum \vec{F} = \frac{d\vec{G}}{dt} = \frac{\partial G}{\partial t} + \vec{\Omega} \times \vec{G} \tag{6.14}$$

According to the definition of the momentum of a rigid body,

$$\vec{G} = \int \vec{V} dm \tag{6.15}$$

where $\vec{V}$ represents the velocity of an arbitrary point P on the rigid body with respect to the earth fixed frame, and dm is the mass element around this point. If taking the COG as the reference point of the rigid body motion, then

$$\vec{V} = \vec{V}_G + \vec{\Omega} \times \vec{r} \tag{6.16}$$

where $\vec{r}$ represents the radius vector of the point with respect to the COG. By using the definition of the center of mass $\int \vec{r} dm = 0$ and m is the total mass of the body, we can get

$$\vec{G} = \int (\vec{V}_G + \vec{\Omega} \times \vec{r}) dm = m\vec{V}_G \tag{6.17}$$

Furtherly,

$$\vec{V}_G = \vec{V}_{O'} + \vec{\Omega} \times \vec{\xi}_G \tag{6.18}$$

$$\vec{\xi}_G = x'_G \vec{i} + y'_G \vec{j} + z'_G \vec{k} \tag{6.19}$$

where, $\vec{V}_{O'}$ is the velocity of the body fixed frame origin, $\vec{\xi}_G$ is the radius vector of COG with respect to the origin, (x'_G, y'_G, z'_G) is the coordinate of the COG. Thus,

$$\vec{G} = m\vec{V}_{O'} + m\vec{\Omega} \times \vec{\xi}_G \tag{6.20}$$

$$\vec{\Omega} \times \vec{G} = m\vec{\Omega} \times \vec{V}_{O'} + m\vec{\Omega} \times (\vec{\Omega} \times \vec{\xi}_G) \tag{6.21}$$

Substituting (6.20) and (6.21) into (6.14), the final momentum equations of the rigid body motion can be expressed in the body fixed frame as follow.

$$\begin{cases} \sum X = m\left\{ \dot{u}_{(I)} + (qw - rv)_{(II)} - \left[x'_G (q^2 + r^2) - y'_G (pq - \dot{r}) - z'_G (pr + \dot{q}) \right]_{(III)} \right\} \\ \sum Y = m\left\{ \dot{v}_{(I)} + (ru - pw)_{(II)} - \left[y'_G (r^2 + p^2) - z'_G (qr - \dot{p}) - x'_G (qp + \dot{r}) \right]_{(III)} \right\} \\ \sum Z = m\left\{ \dot{w}_{(I)} + (pv - qu)_{(II)} - \left[z'_G (p^2 + q^2) - x'_G (rp - \dot{q}) - y'_G (rq + \dot{p}) \right]_{(III)} \right\} \end{cases} \tag{6.22}$$

Where the left hand side of the equations represents the components of total external forces; while for the right hand side, the terms with subscript (I) represent the inertial force due to the acceleration of the rigid body, the subscript (II) represents the inertial force due to the rotation of the body fixed frame, which in fact is the centrifugal force, the subscript (III) represents the added inertial force due to the origin of the body fixed frame is different from the COG, this force can be partly categorized into centrifugal force and the rest part into tangential inertial force qualitatively.

The derivation of the moment of momentum equation would be a little more complicated due to the conversion of the center of the moment. In fact, the second equation of (6.7) is valid for a space fixed point *a* as the center of the moment. However, the moving point O' has to be chosen as this center for convenience. This is not a conflict since the origin of the body fixed frame can be set on the space fixed point a at a time instance, then

$$\sum \vec{M}_{O'} = \sum \vec{M}_a \tag{6.23}$$

Similarly,

$$\vec{H}_{O'} = \vec{H}_a = \int (\vec{S} \times \vec{V}) dm \tag{6.24}$$

where $\vec{S}$ denotes the radius vector from point *a* which is also the point O' at time instance t_0 to an arbitrary point P on the rigid body. The situation would be different from that of $d\vec{G}/dt$ when deriving $d\vec{H}_{O'}/dt$, since not only the variation of H_a and the rotation of the body fixed frame, but also the origin O' departing from the space fixed point *a* would contribute to the time derivative d/dt by producing additional inertial moment.

As shown in Fig. 6.2, at time t_0 the origin O' is coincide with the space fixed point a then the frame $(O' - x'y'z')_{t_0}$ is also coincide with the $O_0 - x_0 y_0 z_0$ frame. At time $t_0 + \Delta t$ the body fixed frame moves to the position $(O' - x'y'z')_{t_0+\Delta t}$. By setting $\vec{S}_{O'}$ as the radius vector of O' with respect to *a* and $\vec{\xi}$ as the radius vector of *P* with respect to O', then,

$$\vec{S}_{t_0+dt} = \vec{S}_{O'} + \vec{\xi} \tag{6.25}$$

$$\begin{aligned}\left(\vec{H}_a\right)_{t_0+dt} &= \int\left(\vec{S}\times\vec{V}\right)_{t_0+dt} dm \\ &= \left(\vec{S}_{O'}\times\int\vec{V}dm\right)_{t_0+dt} + \left(\int\left(\vec{\xi}\times\vec{V}\right)dm\right)_{t_0+dt} \\ &= \left(\vec{S}_{O'}\times\vec{G}\right)_{t_0+dt} + \left(\vec{H}_{O'}\right)_{t_0+dt}\end{aligned} \tag{6.26}$$

Taking the time derivatives of both sides of the equations (6.26), and noting that $d\vec{S}_{O'}/dt = \vec{V}_{O'}$, the following relation can be derived,

$$\frac{d\vec{H}_a}{dt} = \frac{d\vec{H}_{O'}}{dt} + \vec{V}_{O'}\times\vec{G} \tag{6.27}$$

This relation clearly shows the difference between $\dot{\vec{H}}_a$ and $\dot{\vec{H}}_{O'}$.

Similar to $d\vec{G}/dt$, we can further derive,

$$\frac{d\vec{H}_{O'}}{dt} = \frac{\partial\vec{H}_{O'}}{\partial t} + \vec{\Omega}\times\vec{H}_{O'} \tag{6.28}$$

Finally, the moment of momentum equation with respect to body fixed frame can be given,

$$\sum\vec{M}_{O'} = \frac{d\vec{H}_a}{dt} = \frac{\partial\vec{H}_{O'}}{\partial t} + \vec{\Omega}\times\vec{H}_{O'} + \vec{V}_{O'}\times\vec{G} \tag{6.29}$$

Take a further look at the terms $\vec{H}_{O'}$ and $\partial\vec{H}_{O'}/\partial t$, then

$$\begin{aligned}\vec{H}_{O'} &= \left(H_a\right)_x\vec{i} + \left(H_a\right)_y\vec{j} + \left(H_a\right)_z\vec{k} \\ &= \int\left(\vec{\xi}\times\vec{V}\right)dm = \int\vec{\xi}\times\left(\vec{V}_{O'} + \vec{\Omega}\times\vec{\xi}\right)dm \\ &= \int\left(\vec{\xi}\times\vec{V}_{O'}\right)dm + \int\vec{\xi}\times\left(\vec{\Omega}\times\vec{\xi}\right)dm \\ &= m\vec{\xi}_G\times\vec{V}_{O'} + \int\vec{\xi}\times\left(\vec{\Omega}\times\vec{\xi}\right)dm\end{aligned} \tag{6.30}$$

The second term can be expanded as follow,

$$\begin{aligned}\int \vec{\xi}\times\left(\vec{\Omega}\times\vec{\xi}\right)dm &= \left(I_{x'x'}p - I_{x'y'}q - I_{x'z'}r\right)\vec{i} \\ &+\left(-I_{y'x'}p + I_{y'y'}q - I_{y'z'}r\right)\vec{j} \\ &+\left(-I_{z'x'}p - I_{z'y'}q + I_{z'z'}r\right)\vec{k}\end{aligned} \tag{6.31}$$

where,

$$\begin{cases} I_{x'x'} = \int\left(y'^2 + z'^2\right)dm \\ I_{y'y'} = \int\left(z'^2 + x'^2\right)dm \\ I_{z'z'} = \int\left(x'^2 + y'^2\right)dm \end{cases} \tag{6.32}$$

are the moments of inertia with respect to x', y', z' axes respectively. And,

$$\begin{cases} I_{x'y'} = I_{y'x'} = \int x'y'dm \\ I_{y'z'} = I_{z'y'} = \int y'z'dm \\ I_{z'x'} = I_{x'z'} = \int z'x'dm \end{cases} \tag{6.33}$$

are the products of inertia with respect to $x'y', y'z', z'x'$ planes respectively. The final moment of momentum equations of the rigid body motion can be expressed from (6.29) in the body fixed frame as follow.

$$\begin{cases} \sum K = \left[I_{x'x'}\dot{p} - I_{x'y'}\dot{q} - I_{x'z'}\dot{r}\right]_{(I)} \\ \quad +\left[-\left(I_{y'y'} - I_{z'z'}\right)qr + I_{x'y'}rp - I_{x'z'}pq - I_{y'z'}\left(q^2 - r^2\right)\right]_{(II)} \\ \quad +\left[my'_G\left(\dot{w} + pv - qu\right) - mz'_G\left(\dot{v} + ru - pw\right)\right]_{(III)} \\ \sum M = \left[I_{y'y'}\dot{q} - I_{y'z'}\dot{r} - I_{y'x'}\dot{p}\right]_{(I)} \\ \quad +\left[-\left(I_{z'z'} - I_{x'x'}\right)rp + I_{y'z'}pq - I_{x'y'}qr - I_{x'z'}\left(r^2 - p^2\right)\right]_{(II)} \\ \quad +\left[mz'_G\left(\dot{u} + qw - rv\right) - mx'_G\left(\dot{w} + pv - qu\right)\right]_{(III)} \\ \sum N = \left[I_{z'z'}\dot{r} - I_{x'z'}\dot{p} - I_{y'z'}\dot{q}\right]_{(I)} \\ \quad +\left[-\left(I_{x'x'} - I_{y'y'}\right)qp + I_{x'z'}qr - I_{y'z'}rp - I_{x'y'}\left(p^2 - q^2\right)\right]_{(II)} \\ \quad +\left[mx'_G\left(\dot{v} + ru - pw\right) - my'_G\left(\dot{u} + qw - rv\right)\right]_{(III)} \end{cases} \tag{6.34}$$

Similar to (6.21), the left hand side of the equations represents the components of total external moments; while for the right hand side, the terms with subscript (I) represent the inertial moment due to the acceleration of the rotation of the rigid body, the subscript (II) represents the inertial moment due to the gyroscopic effect, the subscript (III) represents the added inertial moment due to the origin of the body fixed frame is different from the COG.

Concrete to the 4-DOF manoeuvring motions considered here, the equations (6.22) and (6.34) can be simplified by neglecting heave and pitch which have little influence on the horizontal motions, then the following motion equations can be derived.

$$\begin{cases} m\left(\dot{u} - rv - x'_G r^2 + z'_G rp\right) = \sum X \\ m\left(\dot{v} + ru + x'_G \dot{r} - z'_G \dot{p}\right) = \sum Y \\ I_{x'x'}\dot{p} - I_{x'z'}\dot{r} - mz'_G\left(\dot{v} + ru\right) = \sum K \\ I_{z'z'}\dot{r} - I_{x'z'}\dot{p} + mx'_G\left(\dot{v} + ru\right) = \sum N \end{cases}. \tag{6.35}$$

In which the mass of the ship can be determined by,

$$m = \rho\nabla \text{ or } m = \rho LBDC_B$$

where ρ is the density of water, ∇ is the displacement of the ship, L, B, D represents the length between perpendiculars, breadth and draft as usual, C_B is the block coefficient of the ship.

Normally a ship is a slender body and approximately symmetrical about the midship section ships, then the equations can be further simplified by assuming that $I_{x'z'} \approx 0$. Besides, the origin of the body fixed frame can be set at the COG as well, then, (6.35) can be rewritten in the following simplified expression.

$$\begin{cases} m\left(\dot{u} - rv\right) = \sum X \\ m\left(\dot{v} + ru\right) = \sum Y \\ I_{x'x'}\dot{p} = \sum K \\ I_{z'z'}\dot{r} = \sum N \end{cases} \tag{6.36}$$

(6.35) or (6.36) is the basic model of the manoeuvring motions which can be solved by numerical approach if all the external forces or moments on right hand side and the initial state of the ship motion are known. In the present study, $x_G = 0$ is substituted into (6.35) and the 4th order Runge-Kutta scheme is applied to solve the motion equations, then the time histories of kinematic variables and the trajectory of the ship can be obtained for the assessment of ship's manoeuverability.

The external forces and moments acting on a manoeuvring ship can be classified into three groups as shown in Fig. 6.3. Note that the gravity of the ship and the buoyancy induced by hydrostatic force are neglected in the figure since they are equalized by each other.

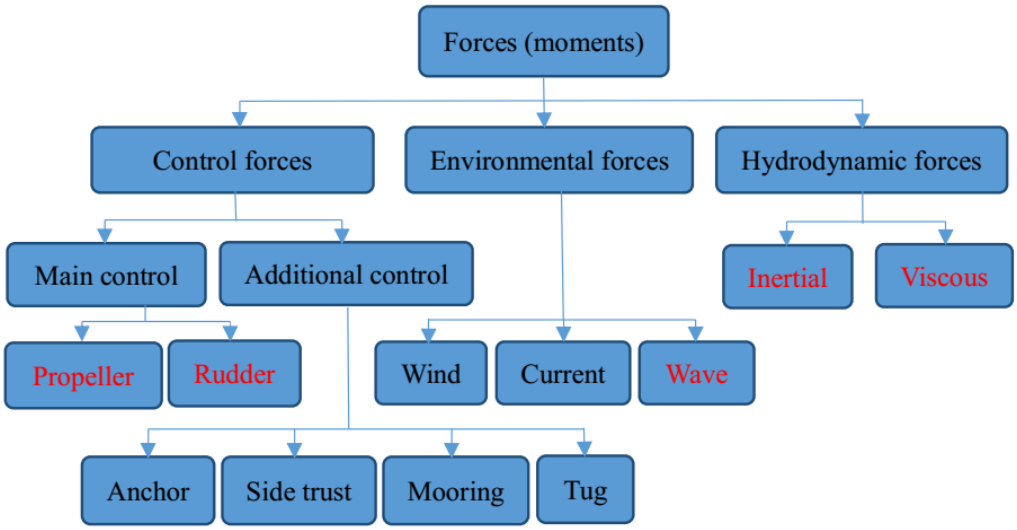

Fig. 6.3 Components of the force (moments) during maneuvers

The first group is the control forces including the main control forces by propeller and rudder, and the additional forces by other equipment like anchor chain, side thruster or mooring lines. It is the inducement of the ship executing expected maneuvers. The second group is the environmental forces including wind, current and wave effect. The wind force is acting on the superstructure of the ship and related to the Beaufort wind scale, encounter angle and the centroid of the lateral area of the superstructure. The current force depends on the characteristic of the current which means if the current is uniform it will cause the ship drifting along the current. Regarding the wave

force, apart from the first order high frequency oscillated forces been taken care of in Chapter 4 & 5, there are second order forces including mean drift forces which would lead to ship's deviation from its original course when advancing in regular waves and the low frequency slowly varying drift force if the wave condition is irregular. Under the action of control forces and environmental forces, the ship will start to execute manoeuvers in the water, then reaction force on the wetted hull surface provides the third group of external forces, namely the hydrodynamic forces on the hull, as the sum of the positive pressure and the shear stress. And it can be divided into an inertial part and a viscous part due to different causes. The present study only cover the force components from the propeller, the rudder, the wave and hydrodynamic forces on the hull, whereas other components are excluded.

6.2 **Modular concept**

As introduced in the literature review, the existing mathematical models related to the manoeuvring simulation of a single ship are nowadays mainly classified into two categories, i.e., the whole ship model and modular manoeuvring ship model (MMG model). Because of having a more clear physical explanation and more convenience in modification according to the imposed requirements from a simulation, the MMG model is the preferred choice instead of the whole ship model when the mathematical manoeuvring model needs to be constructed in a general and relatively simple way.

Therefore, the manoeuvring motion equation (6.35) can be rewritten as follow by decomposing the external forces and moments on the right hand side .

$$\begin{cases} m\left(\dot{u}-rv+z'_G rp\right)=X_P+X_R+X_H+X_W \\ m\left(\dot{v}+ru-z'_G\dot{p}\right)=Y_R+Y_H+Y_W \\ I_{x'x'}\dot{p}-mz'_G\left(\dot{v}+ru\right)=K_R+K_H+K_W \\ I_{z'z'}\dot{r}+mx'_G\left(\dot{v}+ru\right)=N_R+N_H+N_W \end{cases} \tag{6.37}$$

where the subscripts P,R,H denote the force components on the propeller, the rudder, the hull respectively, and W denote the wave drift forces. Note that the terms

Y_P, K_P, N_P are neglected in the model since they are relatively small and are included in the hull force part influenced by the propeller.

One more thing need to be mentioned is the nondimensionalization of terms for the purpose of eliminating the scale effect based on the analog principle. There are two categories of nondimensionalization. The first one named *Prime System* is proposed by the Society of Naval Architects & Marine Engineers (SNAME) in 1950. The other one is the *Bis System* proposed by the Swedish State Shipbuilding Experimental Tank (SSPA) in 1970. Moreover, in Prime System, there are two kinds of expressions for reference area, i.e., L^2 recommended by ITTC and LD widely adopted by Japanese MMG models. Details of these two ways are listed in Table 6.1.

Table 6.1 Standard measurement systems

Unit of measurement	Prime system	Bis system
Mass m	$\frac{1}{2}\rho L^3$; $\frac{1}{2}\rho L^2 D$	$\rho\nabla$
Length L	L	L
Time t	L/U	$\sqrt{L/g}$
Linear velocity V	U	$\sqrt{gL}$
Linear acceleration a	U^2/L	g
Angular velocity ω	U/L	$\sqrt{g/L}$
Angular acceleration α	U^2/L^2	g/L
Force F	$\frac{1}{2}\rho U^2 L^2$; $\frac{1}{2}\rho U^2 LD$	$\rho g\nabla$
Moment M	$\frac{1}{2}\rho U^2 L^3$; $\frac{1}{2}\rho U^2 L^2 D$	$\rho g\nabla L$
Reference area S	L^2 ; LD	$2\nabla/L$

In the present study, terms in (6.37) can be non-dimensionalized by adopting the Prime system as below,

$$\begin{cases} m' = m \Big/ \frac{1}{2}\rho L^2 D, I'_{x'x'} = I_{x'x'} \Big/ \frac{1}{2}\rho L^4 D, I'_{z'z'} = I_{z'z'} \Big/ \frac{1}{2}\rho L^4 D, I'_{x'z'} = I_{x'z'} \Big/ \frac{1}{2}\rho L^4 D \\ u' = u/U, v' = v/U, r' = rL/U \\ \dot{u}' = \dot{u}L/U^2, \dot{v}' = \dot{v}L/U^2, \dot{r}' = \dot{r}L^2/U^2, \dot{p}' = \dot{p}L^2/U^2 \\ X' = X \Big/ \frac{1}{2}\rho U^2 LD, Y' = Y \Big/ \frac{1}{2}\rho U^2 LD \\ K' = K \Big/ \frac{1}{2}\rho U^2 L^2 D, N' = N \Big/ \frac{1}{2}\rho U^2 L^2 D \end{cases} \tag{6.38}$$

The manoeuvring derivatives introduced later will follow the similar way to derive dimensionless values.

6.2.1 Hull force

As stated above, the forces and moments acting on the hull can be decomposed into an inertial part and a viscous part. Thereby,

$$\vec{F}_H = \vec{F}_I + \vec{F}_{HV} + \vec{F}_S + R(u) \tag{6.39}$$

where $\vec{F}_H$ represents the total hull force or moment, the subscripts I, HV denote the inertial force and the viscous force respectively. $R(u)$ is the longitudinal resistance on the ship which will be estimated in next subsection. In addition, $\vec{F}_S$ is the hydrostatic restoring force when the ship departs from its equilibrium position in roll, heave or pitch motion. In the present study, since only roll motion is considered in the 4-DOF manoeuvring motion this restoring roll moment is derived as follow.

$$K_S = -\rho g \nabla \overline{GM}_T \sin\phi \tag{6.40}$$

where $\overline{GM}_T$ is the transverse metacentric height of the ship.

Regarding the inertia force on the hull, it is caused by the ship accelerating the water around it during manoeuvring, thus the water provides the reaction force on the ship. This inertial force can be derived through the analysis same as derivation of the rigid body inertial force presented before. Then,

$$\begin{cases} \vec{F}_I = -\dfrac{d\vec{K}}{dt} = -\left[\dfrac{\partial \vec{K}}{\partial t} + \vec{\Omega} \times \vec{K}\right] \\ \vec{M}_I = -\dfrac{d\vec{I}_{O'}}{dt} = -\left[\dfrac{\partial \vec{I}_{O'}}{\partial t} + \vec{\Omega} \times \vec{I}_{O'} + \vec{V}_{O'} \times \vec{K}\right] \end{cases} \tag{6.41}$$

where $\vec{K}, \vec{I}_{O'}$ represent the added momentum and added moment of momentum of the water given as follow.

$$\vec{K} = \int_{S_0} \rho \varphi \vec{n} ds \tag{6.42}$$

$$\vec{I}_{O'} = \int_{S_0} \rho \varphi \left(\vec{\xi} \times \vec{n}\right) ds \tag{6.43}$$

Where φ is the velocity potential around the hull, $\vec{\xi}$ is the radius vector from the centroid to an arbitrary point on the hull, $\vec{n}$ is the unit normal vector on the hull boundary with positive orientation pointing out of the fluid domain.

By substituting the added inertial matrix

$$m_{kj} = \rho \int_{S_0} \varphi_j \frac{\partial \varphi_k}{\partial n} ds \tag{6.44}$$

into (6.42) and (6.43), the inertial forces and moments acting on the hull can be derived as follow by taking into account the symmetrical characteristic of a ship with respect to its central lateral plane.

$$\begin{cases} X_I = -m_{11}\dot{u} + m_{22} vr + m_{24} pr + m_{26} r^2 \\ Y_I = -m_{22}\dot{v} - m_{11} ur - m_{24}\dot{p} - m_{26}\dot{r} \\ K_I = -m_{44}\dot{p} - m_{42}\dot{v} - m_{46}\dot{r} \\ N_I = -m_{66}\dot{r} - m_{62}\dot{v} - m_{64}\dot{p} - m_{24} up + (m_{11} - m_{22}) uv - m_{62} ur \end{cases} \tag{6.45}$$

Here, added mass m_{ij} are corresponding to the limiting values as the frequency approaching zero which can be taken care of in the seakeeping analysis with the rigid

wall free surface condition as mentioned previously. In manoeuvring analysis, they are in accordance with the acceleration manoeuvring derivatives, which are,

$$\begin{cases} m_x = m_{11} = -X_{\dot{u}}, m_y = m_{22} = -Y_{\dot{v}}, J_{xx} = m_{44} = -K_{\dot{p}}, J_{zz} = m_{66} = -N_{\dot{r}} \\ m_{24} = -Y_{\dot{p}}, m_{26} = -Y_{\dot{r}} \\ m_{42} = -K_{\dot{v}}, m_{46} = -K_{\dot{r}} \\ m_{62} = -N_{\dot{v}}, m_{64} = -N_{\dot{p}} \end{cases} \tag{6.46}$$

If we neglect the added coupling terms which are believed small for a slender ship, the more common used inertial forces and moments are given as follow in view of practical purpose.

$$\begin{cases} X_I = -m_{11}\dot{u} + m_{22}vr \\ Y_I = -m_{22}\dot{v} - m_{11}ur \\ K_I = -m_{44}\dot{p} \\ N_I = -m_{66}\dot{r} + (m_{11} - m_{22})uv \end{cases} \tag{6.47}$$

By taking a further look on (6.45) and (6.47), if the ship is advancing stably in a straight line uniformly with a drift angle, which means $\dot{u} = \dot{v} = \dot{p} = \dot{r} = p = r = 0$, then,

$$X_I = Y_I = K_I = 0, N_I = (m_{11} - m_{22})uv \tag{6.48}$$

That is to say there is no force acting on the hull, namely the *d'Alembert* paradox as mentioned before, whereas a Munk moment is still experienced by the ship when it moves obliquely through the potential flow field. However, this Munk moment is usually omitted here but counted in the viscous moment part in order to avoid be double counted since the model test based on the viscous force evaluation model introduced later could not separate this Munk moment term from the total yaw moment.

In order to break the *d'Alembert* paradox occurred in the ideal flow, the manoeuvring simulation model should catch nature of manoeuvring motions so that it is necessary to predict the behaviour of the manoeuvring ship in real fluid by taking into account

the water viscosity. The water viscosity modifies the flow around an advancing ship causing a formation of the boundary layer and wake zone behind a ship thereby leads to fact the evaluation of viscous force and moment is essential. Moreover, this viscous part can be further divided into linear lift component and nonlinear component.

$$\vec{F}_{HV} = \vec{F}_{L} + \vec{F}_{NL} \tag{6.49}$$

where F_L, F_{NL} are the linear lift force and nonlinear force respectively.

As stated in Chapter 4, the linear lift force is the result of viscous effect when an elongated body travels in the fluid with an attacking angle similar like a wing. The lift force contains following components,

$$\begin{cases} Y_L = Y_v v + Y_r r \\ K_L = -z_H Y_L \\ N_L = N_v v + N_r r \end{cases} \tag{6.50}$$

where Y_v, Y_r, N_v, N_r are called linear velocity manoeuvring derivatives, z_H denotes the vertical position of the lateral force's acting point. Note that due to the symmetry of the ship, there is no linear term in the longitudinal direction.

When the amplitude of the maneuver is large such as involving large variation of the ship heading angle, e.g., a tight circle maneuver, only counting the linear lift force shown above which assumes small drift angle is inadequate. Therefore, the nonlinear viscous forces acting on the hull have to be evaluated.

There are several models to evaluate the nonlinear forces based on the modular concept such as the cross flow model for low speed manoeuvring, second or third order Taylor expansion polynomial model, Inoue model and Kijima model. With the demand of the present study, the third order polynomial model is applied as followed since it is superior to the other models in view of estimation accuracy and plenty of experimental results can be found in relevant publications on the selected ship for

validation. Therefore, the nonlinear viscous forces and moments are expressed as follow.

$$\begin{cases} X'_{NL} = X'_{vr} v'r' + X'_{vv} v'^2 + X'_{rr} r^2 \\ Y'_{NL} = Y'_{rrr} v'^3 + Y'_{vvr} v'^2 r' + Y'_{vrr} v' r'^2 \\ K'_{NL} = -z_H Y'_{NL} \\ N'_{NL} = N'_{rrr} r'^3 + N'_{vvr} v'^2 r' + N'_{vrr} v' r'^2 \end{cases} \tag{6.51}$$

where the nondimensionalization follows the Prime system as well which are

$$\begin{cases} X = (1/2)\rho LDU^2 X'(v', r') \\ Y = (1/2)\rho LDU^2 Y'(v', r') \\ N = (1/2)\rho L^2 DU^2 N'(v', r') \end{cases} \tag{6.52}$$

Subscripts are dropped which means all the force components are nondimensionalized in this way. All the above mentioned manoeuvring derivatives including the linear ones and nonlinear ones can be obtained by conducting PMM tests, details of processing the PMM data are given in Appendix C.

6.2.2 Resistance

Apart from above mentioned force components acting on the hull, an advancing ship at the desired constant speed on a straight course experiences a steady hydrodynamic resistance. The evaluation of the ship calm water resistance can be performed by several different methods, i.e., the direct model test, referring resistance charts, the regression based methods and CFD calculation.

The manoeuvring simulation of the behaviour of a ship advancing in waves which is the topic of the present study requires the optimal accuracy and the ability to be executed with as few computational resource as possible. These two requirements which need to be satisfied at the same time restrict our choice of the methods for the ship resistance estimation to the regression based methods.

As stated at the very beginning, the CFD based methods with higher accuracy in respect to the resistance charts or regression analysis methods are excluded simply

because they consume a lot of computational resource. Besides, in the view of the above requirements obviously the direct model test methods are also excluded from further considerations. The resistance charts have similarity with the regression analysis methods, i.e., both methods only need a few ship global design parameters such as block coefficient, prismatic coefficient, etc. to predict the ship resistance. However, they are not selected because of their limited accuracy in the estimation of the resistance for the modern ship hull forms.

Among various statistical regression analysis based methods for the ship resistance calculation, 'Holtrop-Mennen' method is one of the most popular and extensively used methods with general applicability. The method has been constantly improved through a series of papers by Holtrop & Mennen (1978, 1982) and Holtrop (1977, 1978 and 1984). With the improvements based on the results from 334 model tests in total, the resistance prediction became reliable for different types of ships with the operational speed even on the Froude numbers equal or above 0.55. Therefore, the present study will apply this method to estimate the calm water resistance of a single ship. During the implementation of the method certain modifications are introduced.

The total calm water resistance of a ship $R(u)$ is expressed as a sub division into parts

$$R(u) = R_F(1+k_1) + R_{APP} + R_W + R_B + R_{TR} + R_A \tag{6.53}$$

where R_F is the frictional resistance, $(1+k_1)$ is the hull form factor, R_{APP} is the hull form factor, R_W is the wave resistance, R_B is the additional pressure resistance of bulbous bow near the water surface, R_{TR} is the additional pressure resistance due to transom immersion, and R_A is the model-ship correlation resistance.

The formulation (6.53) is based on the Froude hypothesis where the frictional resistance R_F and the resistance due to the appendages R_{APP} have functional dependence on the Reynolds number $R_n = UL/\nu$, while the rest of the terms are

dependent on the Froude number $F_n = U/\sqrt{gL}$. Here $L = L_{wl}$ is the waterline length, and ν is the kinematic viscosity coefficient ($\nu = 1.35 \times 10^{-6} m^2 s^{-1}$ for sea water at $10^o C$).

The frictional resistance R_F is calculated as

$$R_F = 0.5 \rho C_f S_0 U^2 \tag{6.54}$$

with the friction coefficient $C_f = 0.075/\left(\log_{10} R_n - 2\right)^2$ according to the ITTC 1957.

The hull form factor $\left(1+k_1\right)$ is obtained from the regression analysis with the functional dependence on global ship parameters and given as

$$\begin{aligned}\left(1+k_1\right) = 0.93 + 0.487118\left(1+0.011 C_{stern}\right)\left(B/L\right)^{1.06806}\left(D/L\right)^{0.46106} \\ \cdot\left(L/L_R\right)^{0.121563}\left(L^3/\nabla\right)^{0.36486}\left(1-C_P\right)^{-0.604247}\end{aligned} \tag{6.55}$$

where L_R is a parameter defined as

$$L_R = L\left[1 - C_P + 0.06 C_P lcb/\left(4C_P - 1\right)\right] \tag{6.56}$$

with longitudinal position of the center of buoyancy *lcb* forward of 0.5L as a percentage of the waterline length. $C_P = \nabla/\left(S_M L\right)$ is the longitudinal prismatic coefficient, while S_M is the midship section area. In the expression (6.55) C_{stern} is defined as a stern shape parameter with values according to the Table 6.2.

Table 6.2 Stern shape parameter

Stern section form	C_{stern}
Pram with gondola	-25
V section	-10
Normal section	0
U section	10

The appendage resistance R_{APP} is determined from

$$R_{APP} = 0.5\rho C_f \left(1+k_2\right)_{eq} \sum S_{APP} U^2 + R_{BT} \tag{6.57}$$

in which S_{APP} is the wetted area of the particular ship appendage and

$$\left(1+k_2\right)_{eq} = \sum\left[\left(1+k_2\right) S_{APP}\right] / \sum S_{APP} \tag{6.58}$$

is the equivalent value for the appendages with the appendage form factors $\left(1+k_2\right)$ according to the Table 6.3.

Table 6.3 Appendage form factor

Appendage type	$\left(1+k_2\right)$
Rudder behind skeg	1.5-2.0
Rudder behind stern	1.3-1.5
Twin screw balanced rudders	2.8
Shaft brackets	3.0
Skegs	1.5-2.0
Strut bossing	3.0
Hull bossing	2.0
Shafts	2.0-4.0
Stabilizer fins	2.8
Dome	2.7
Bilge keels	1.4

The term R_{BT} stands for the resistance of the bow thruster openings.

$$R_{BT} = \pi d_T C_{BTO} U^2 \tag{6.59}$$

where d_T is the bow thruster tunnel diameter and the coefficient C_{BTO} in the range from 0.003 to 0.012.

The estimation of the wave resistance R_W does not follow the original procedure in 'Holtrop-Mennen' method. The main reason is that the original procedure calculates the wave resistance according to the three different expressions where each expression is valid in a particular range of Froude numbers. In order to overcome this practical difficulty the wave resistance R_W is estimated by Michell's integral

$$R_W = \frac{4}{\pi}\rho U^2 \tilde{v}^2 \int_1^\infty \frac{\tilde{\lambda}^2}{\sqrt{\tilde{\lambda}^2 - 1}} \left| -i\tilde{v}\tilde{\lambda} \iint_{cp} \zeta(x,z) e^{\tilde{v}z\tilde{\lambda}^2 + i\tilde{v}x\tilde{\lambda}} dz dx \right|^2 d\tilde{\lambda} \tag{6.60}$$

where $\tilde{v} = g/U^2$ and $\zeta(x,z)$ is the offset of the body surface, *cp* denotes the center plane of the hull. The derivation of the expression (6.60) can be found in Appendix D.

The Michell's integral based on the thin ship assumption can give satisfactory estimation of the wave resistance for very thin bodies, $B << D$, at an arbitrary Froude number, as well as, for slender ships, $B, D << L$, at a high Froude number. The application of the Michell's integral may be subjected to criticism due to fact that the real ships are not thin forms. However, in the scope of present study, the author believes that the Michell's integral is still a good choice compared to the statistical regression based methods or the computationally demanding and time consuming 3D methods.

The additional pressure resistance due to the bulbous bow near the free surface R_B is found from

$$R_B = 0.11 e^{\left(-3P_B^{-2}\right)} F_{ni}^3 A_{BT}^{1.5} \rho g \Big/ \left(1 + F_{ni}^2\right) \tag{6.61}$$

where,

$$P_B = 0.56\sqrt{A_{BT}} \Big/ \left(T_F - 1.5 h_B\right) \tag{6.62}$$

$$F_{ni} = U \Big/ \sqrt{g\left(T_F - h_B - 0.25 A_{BT}^{0.5}\right) + 0.15U^2} \tag{6.63}$$

are the bow emergence parameter and the immersion Froude number, respectively. Here A_{BT} is the transverse area of the bulbous bow above the keel line, T_F is the moulded draught on forward perpendicular and h_B is the height of the center of the transverse bulb area where $h_B = 0.6T_F$ is given as a recommended upper value.

If the ship has immersed transom stern the additional pressure resistance R_{TR} can be determined from

$$R_{TR} = 0.5\rho A_T U^2 c_6 \tag{6.64}$$

where,

$$c_6 = \begin{cases} 0.2\left(1-0.2F_{nT}\right) & for\ F_{nT} < 5 \\ 0 & for\ F_{nT} \geq 5 \end{cases} \tag{6.65}$$

$$F_{nT} = U \Big/ \sqrt{2gA_T\left(B + BC_{WP}\right)} \tag{6.66}$$

F_{nT} is the transom stern immersion Froude number. A_T denotes the immersed part of the transverse area of the transom at zero speed, while $C_{WP} = A_W \big/ \left(LB\right)$ is the water plane area coefficient with the water plane area A_W.

The model-ship correlation resistance R_A takes into account the air resistance with no wind R_{AA} and the additional frictional resistance due to the effects of the hull roughness ΔR_F. Therefore,

$$R_A = R_{AA} + \Delta R_F \tag{6.67}$$

where,

$$\begin{cases} R_{AA} = 0.5\rho_{air} C_{DAA} A_{\sup} U^2 \\ \Delta R_F = 0.5\rho \Delta C_F S_0 U^2 \\ \Delta C_F = \left[111\left(AHR \cdot U \right)^{0.21} - 404 \right] C_F^2 \end{cases} \tag{6.68}$$

ρ_{air} is the air density, $A_{\sup}$ represents the projected area of the superstructure, C_{DAA} is the aerodynamic drag coefficient with a range from 0.5 to 0.7. *AHR* means the average hull roughness in micrometers and chosen from the range of $75\mu m$ to $150\mu m$ which is common for new build ships.

The relative brief description of the 'Holtrop-Mennen' method presented here gives very limited insight into the physical features behind each component. This is because the main goal of this section is just to show the approach for the evaluation of the total resistance from a practical point of view.

6.2.3 Propeller force

The thrust forces provided by a single screw propeller can be estimated by following formulae.

$$\begin{cases} X_P = (1 - t_{p0}) \rho n_P^2 D_P^4 K_T (J_P) \\ Y_P = K_P = N_P = 0 \end{cases} \tag{6.69}$$

The lateral force component and moment here are neglected due to their relatively small quantities compared to the contributions from bare hull and rudder. Normally, they are included in the hull force module in a MMG model. Here, t_{p0} is the thrust deduction factor when the ship is advancing in a straight line, which can be assumed to be constant during the manoeuvring motions for simplicity. An estimation formula is also given by Holtrop (1984) as follow if no experimental data for use.

$$t_{p0} = \frac{0.25014\left(B/L \right)^{0.28956} \left[\sqrt{\left(BT \right)} / D \right]^{0.2624}}{\left(1 - C_P + 0.0225 lcb \right)^{0.01762}} + 0.0015 C_{stern} \tag{6.71}$$

Nomenclatures are given in the last subsection and will not be repeated here.

The thrust coefficient K_T can be derived by 2nd order polynomial fitting as follow according to the open water characteristic test results.

$$K_T(J_P) = a_0 + a_1 J_P + a_2 J_P^2 \tag{6.71}$$

where the advanced ratio J_P is defined as follow.

$$J_P = \frac{u(1-w_P)}{n_P D_P} \tag{6.72}$$

Here, n_P, D_P are the revolution speed and the propeller diameter respectively.

The wake coefficient w_P changes during the manoeuvring motions in general and can be evaluated as

$$w_P = w_{P0} \exp(-4\beta_P^2) \tag{6.73}$$

w_{P0} is the wake coefficient when ship advancing straightly and can be estimated as follow given by Holtrop (1984) if no experimental data for use.

$$w_{P0} = c_9 c_{20} C_V \frac{L}{T_A}\left(0.050776 + 0.93405 c_{11}\frac{C_V}{1-C_{P1}}\right) + 0.27915 c_{20}\sqrt{\frac{B}{L(1-C_{P1})}} + c_{19}c_{20} \tag{6.74}$$

where,

$$\begin{cases} C_V = (1+k_1)C_F + C_A \\ C_{P1} = 1.45C_P - 0.315 - 0.0225lcb \\ C_A = 0.006(L+100)^{-0.16} - 0.00205 + 0.003\sqrt{L/7.5}C_B^2 c_2 (0.04 - c_4) \end{cases} \tag{6.75}$$

The $c_i\,(i = 2,3,4,8,9,11,19,20)$ coefficients needed are given as follow.

$$
\begin{cases}
c_2 = e^{-1.89\sqrt{c_3}} \\
c_3 = 0.56 A_{BT}^{1.5} \Big/ \left[BT\left(0.31\sqrt{A_{BT}} + T_F - h_B\right)\right] \\
c_4 = \begin{cases} T_F/L & for\ \ T_F/L \le 0.04 \\ 0.04 & otherwise \end{cases} \\
c_8 = \begin{cases} BS_0 \big/ \left(LD_P T_A\right) & for\ \ B/T_A \le 5 \\ S_0\left(7B/T_A - 25\right) \big/ \left[LD_P\left(B/T_A - 3\right)\right] & otherwise \end{cases} \\
c_9 = \begin{cases} c_8 & for\ \ c_8 \le 28 \\ 32 - 16 \big/ \left(c_8 - 24\right) & otherwise \end{cases} \\
c_{11} = \begin{cases} T_A/D_P & for\ \ T_A/D_P \le 2 \\ 0.0833333\left(T_A/D_P\right)^3 + 1.33333 & otherwise \end{cases} \\
c_{19} = \begin{cases} 0.12997 \big/ \left(0.95 - C_B\right) - 0.11056 \big/ \left(0.95 - C_P\right) & for\ \ C_P \le 0.7 \\ 0.18567 \big/ \left(1.3571 - C_M\right) - 0.71276 + 0.38648 C_P & otherwise \end{cases} \\
c_{20} = 1 + 0.015 C_{stern}
\end{cases}
\tag{6.76}
$$

where $C_M = S_M \big/ \left(BD\right)$ is the midship section coefficient, T_A represents the moulded draught on aft perpendicular. Other nomenclatures have already been given in last subsection as well.

β_P in (6.73) is the geometrical inflow angle to the propeller which can be derived as follow.

$$
\beta_P = \beta - x'_P r' \tag{6.77}
$$

β is the drift angle, x'_P denotes the non-dimensional longitudinal coordinate of the propeller position.

6.2.4 Rudder forces and moments

Estimation of rudder forces is vital for accurate simulation of manoeuvring motions. Effective rudder forces and moment can be expressed as follows.

$$\begin{cases} X_R = -(1-t_R)F_N \sin\delta \\ Y_R = -(1+a_H)F_N \cos\delta \\ K_R = (1+a_H)z_R F_N \cos\delta \\ N_R = -(x_R + a_H x_H)F_N \cos\delta \end{cases} \tag{6.78}$$

Here x_R, z_R is the longitudinal and vertical coordinate of the acting point of the rudder normal force respectively, x_R usually take the value of $-0.5L_{PP}$, while t_R, a_H, x_H are the coefficients representing the interaction between the hull and rudder.

The rudder normal force F_N is expressed as follow.

$$F_N = \frac{1}{2}\rho A_R U_R^2 f_\alpha \sin\alpha_R \tag{6.79}$$

where A_R denotes the rudder area and f_α, denoting the rudder lift gradient coefficient, can be estimated by the common used formula as follow by Fujii & Tuda (1961).

$$f_\alpha = \frac{6.13\Lambda}{\Lambda + 2.25} \tag{6.80}$$

Here, Λ denotes the aspect ratio of the rudder. The non-dimensional effective rudder inflow velocity U_R' can be estimated by the model developed by Yoshimura & Nomoto (1978).

$$\begin{cases} U_R' = (1-w_R)\sqrt{1+CG(s)} \\ G(s) = \eta \cdot \dfrac{\kappa\left[2-(2-\kappa)s\right]}{(1-s)^2} \\ s = 1 - \dfrac{U\cos\beta(1-w_P)}{nP} \end{cases} \tag{6.81}$$

where w_R denotes the wake coefficient at the rudder position. The parameter C is the correction factor with different values for port side and starboard side rudder directions, 1.065 and 0.935 respectively according to the results given by Hirano

(1980), due to the asymmetric propeller slip stream effect. η is the ratio of the propeller diameter to the rudder height H_R and P is the propeller pitch. κ is an experimental constant to reflect the acceleration effect by the propeller.

Alternatively, based on the momentum theory the effective rudder inflow velocity can also be estimated as follow.

$$\begin{cases} U_R = \sqrt{u_R^2 + v_R^2} \\ v_R = U\gamma_R\beta_R \\ u_R = \varepsilon u\left(1-w_P\right)\sqrt{\eta\left[1+\kappa\left(\sqrt{1+\dfrac{8K_T}{\pi J_P^2}}-1\right)\right]^2+\left(1-\eta\right)} \end{cases} \tag{6.82}$$

Regarding the effective rudder inflow angle α_R, it can be derived by the following formulae.

$$\begin{cases} \alpha_R = \delta - \delta_0 - \gamma_R\beta_R(U/u_R) \\ \beta_R = \beta - \ell'_R r' \end{cases} \tag{6.83}$$

where δ_0 denotes the rudder angle with zero normal pressure on the rudder, γ_R is the flow straightening coefficient and β_R is the effective inflow angle to the rudder with ℓ'_R treated as an experimental constant and can be set as a default value of $2x'_R$ for simplicity if no accurate experimental value provided.

6.3 **Mean wave drift loads**

As discussed in the literature review, evaluation of the mean drift loads is very important to the simulations of a ship manoeuvring in waves. The methods usually applied for the theoretical prediction of the mean second order wave loads are basically categorized into two types. One type of methods is a direct pressure integration method and the other type uses conservation of fluid momentum. In the present study, a direct pressure integration method will be described in some more

details by giving the main steps of derivation which are used in a development of the method.

We start out with the expression for the fluid pressure given by the complete Bernoulli's equation

$$p = -\rho g z - \rho\left(\frac{\partial \phi}{\partial t} - U\frac{\partial \phi}{\partial x}\right) - \frac{\rho}{2}\left[\left(\frac{\partial \phi}{\partial x}\right)^2 + \left(\frac{\partial \phi}{\partial y}\right)^2 + \left(\frac{\partial \phi}{\partial z}\right)^2\right] \tag{6.84}$$

where $\phi = \phi(x, y, z)e^{i\omega_e t} = \left(\phi_I + \phi_D + \sum_{j=2}^{6}\xi_j\phi_j\right)e^{i\omega_e t}$ is the time dependent velocity potential decomposed into the incoming ϕ_I, diffracted ϕ_D and a radiated wave potential ϕ_j and ξ_j are the complex amplitudes of the j-th mode of motion ($j = 2,...,6$, neglected surge) as explained in Chapter 4. The pressure p given above using the total velocity potential $\Phi = -Ux + \phi(x, y, z, t)$ where the influence of the steady flow potential $\Phi_S(x, y, z)$ is neglected.

The pressure is now expanded up to the second order in the incident wave by using a perturbation expansion with introduction of a small perturbation slenderness parameter ε which is defined as beam to length ratio. This means that we will insert the expanded form of the time dependent velocity potential $\phi = \varepsilon\phi^{(1)} + \varepsilon^2\phi^{(2)}$ into the expression (6.84) and collect terms proportional to the ε^2. After some manipulations, it can be shown that the pressure p up to the order of ε^2 can be expressed as

$$\begin{aligned} p = -\rho g z &- \rho\left(\frac{\partial \phi^{(1)}}{\partial t} - U\frac{\partial \phi^{(1)}}{\partial x}\right) - \rho\left(\frac{\partial \phi^{(2)}}{\partial t} - U\frac{\partial \phi^{(2)}}{\partial x}\right)\Bigg|_m \\ &- \frac{\rho}{2}\left[\left(\frac{\partial \phi^{(1)}}{\partial x}\right)^2 + \left(\frac{\partial \phi^{(1)}}{\partial y}\right)^2 + \left(\frac{\partial \phi^{(1)}}{\partial z}\right)^2\right]\Bigg|_m \end{aligned} \tag{6.85}$$

where the subscript m indicates that the variables should be evaluated on the average position of the wetted hull surface S_0. Now, it is easy to see that the zero, first and second order pressure are given by

$$\begin{cases} p^{(0)} = -\rho g z \\ p^{(1)} = -\rho\left(\dfrac{\partial \phi^{(1)}}{\partial t} - U\dfrac{\partial \phi^{(1)}}{\partial x}\right) \\ p^{(2)} = -\rho\left(\dfrac{\partial \phi^{(2)}}{\partial t} - U\dfrac{\partial \phi^{(2)}}{\partial x}\right)\Bigg|_m - \dfrac{\rho}{2}\left[\left(\dfrac{\partial \phi^{(1)}}{\partial x}\right)^2 + \left(\dfrac{\partial \phi^{(1)}}{\partial y}\right)^2 + \left(\dfrac{\partial \phi^{(1)}}{\partial z}\right)^2\right]\Bigg|_m \end{cases} \tag{6.86}$$

The expression (6.85) for the pressure p and term $p^{(2)}$ within the expression (6.86) can be further simplified by noticing that $-\rho\left(\dfrac{\partial \phi^{(2)}}{\partial t} - U\dfrac{\partial \phi^{(2)}}{\partial x}\right)\Bigg|_m$ has no contribution to the mean wave loads as shown by Faltinsen & Løken (1979). Therefore we can write

$$p = -\rho g z - \rho\left(\frac{\partial \phi^{(1)}}{\partial t} - U\frac{\partial \phi^{(1)}}{\partial x}\right) - \frac{\rho}{2}\left[\left(\frac{\partial \phi^{(1)}}{\partial x}\right)^2 + \left(\frac{\partial \phi^{(1)}}{\partial y}\right)^2 + \left(\frac{\partial \phi^{(1)}}{\partial z}\right)^2\right]\Bigg|_m \tag{6.87}$$

and

$$p^{(2)} = -\frac{\rho}{2}\left[\left(\frac{\partial \phi^{(1)}}{\partial x}\right)^2 + \left(\frac{\partial \phi^{(1)}}{\partial y}\right)^2 + \left(\frac{\partial \phi^{(1)}}{\partial z}\right)^2\right]\Bigg|_m \tag{6.88}$$

The force and moment acting on the instantaneous wetted ship hull surface S^* are given by

$$\vec{F} = \int_{S^*} p\vec{n}\,ds \tag{6.89}$$

$$\vec{M} = \int_{S^*} p\left(\vec{r}\times\vec{n}\right)ds \tag{6.90}$$

Here, $\vec{n}$ is the instantaneous unit normal vector to the surface element ds in respect to the seakeeping coordinate system defined positively out of fluid domain. '×' denotes vector product and $\vec{r} = x\vec{i} + y\vec{j} + z\vec{k}$ is the position vector of arbitrary fixed point on the hull surface.

Expanding the force and moment as a perturbation expansion series, by using

$$\begin{cases} S^* = S_0 + \varepsilon S_1 + \varepsilon^2 S_2 \\ p = p^{(0)} + \varepsilon p^{(1)} + \varepsilon^2 p^{(2)} \\ \vec{n} = \vec{n}^{(0)} + \varepsilon \vec{n}^{(1)} + \varepsilon^2 \vec{n}^{(2)} \end{cases} \tag{6.91}$$

the forces and moments from zero to second order can be calculated by collecting terms of the same order in parameter ε. Performing this step, one will find that the zero, first and second order force can be expressed respectively as

$$\vec{F}^{(0)} = \int_{S_0} p^{(0)} \vec{n}^{(0)} ds \tag{6.92}$$

$$\vec{F}^{(1)} = \int_{S_0} p^{(0)} \vec{n}^{(1)} ds + \int_{S_0} p^{(1)} \vec{n}^{(0)} ds + \int_{S_1} p^{(0)} \vec{n}^{(0)} ds \tag{6.93}$$

$$\begin{aligned} \vec{F}^{(2)} = & \int_{S_0} p^{(0)} \vec{n}^{(2)} ds + \int_{S_0} p^{(1)} \vec{n}^{(1)} ds + \int_{S_0} p^{(2)} \vec{n}^{(0)} ds \\ & + \int_{S_1} p^{(0)} \vec{n}^{(1)} ds + \int_{S_1} p^{(1)} \vec{n}^{(0)} ds + \int_{S_2} p^{(0)} \vec{n}^{(0)} ds \end{aligned} \tag{6.94}$$

Similar type of expressions can be derived for moment from the expression (6.90).

The expanded instantaneous normal vector $\vec{n}$ can be expressed as

$$\vec{n} = \vec{n}'\left(x', y', z'\right) + R_1 \vec{n}'\left(x', y', z'\right) + R_2 \vec{n}'\left(x', y', z'\right) + O\left(\varepsilon^3\right) \tag{6.95}$$

from which it follows that

$$\begin{cases} \vec{n}^{(0)} = \vec{n}'\left(x', y', z'\right) \\ \vec{n}^{(1)} = R_1\vec{n}'\left(x', y', z'\right) = R_1\vec{n}^{(0)} \\ \vec{n}^{(2)} = R_2\vec{n}'\left(x', y', z'\right) = R_2\vec{n}^{(0)} \end{cases} \tag{6.96}$$

Here, $\vec{n}^{(0)}$ is the normal vector relative to the seakeeping coordinate system, $\vec{n}^{(1)}$ is an oscillatory component of $\vec{n}^{(0)}$ due to the first order oscillatory angular motions and $\vec{n}^{(2)}$ is an oscillatory component of $\vec{n}^{(0)}$ due to the second order oscillatory angular motions.

In a similar way, for any point on the hull surface with position vector $\vec{r}'\left(x', y', z'\right)$ in the manoeuvring body fixed coordinate system, its motions from the 'at rest' position in the seakeeping coordinate system can be expressed as

$$\vec{\alpha} = \vec{\alpha}^{(1)} + \vec{\alpha}^{(2)} = \vec{\xi} + R_1\vec{r}' + R_2\vec{r}' + O\left(\varepsilon^3\right) = \vec{r}' + \overrightarrow{\xi_T} + \overrightarrow{\xi_R} \times \vec{r}' + R_2\vec{r}' + O\left(\varepsilon^3\right) \tag{6.97}$$

where,

$$\begin{cases} \vec{\alpha}^{(1)} = \vec{\xi} + R_1\vec{r}' \\ \vec{\alpha}^{(2)} = R_2\vec{r}' \end{cases} \tag{6.98}$$

$\overrightarrow{\xi_T}$ and $\overrightarrow{\xi_R}$ are the translatory and angular motions respectively.

In the expressions (6.96) and (6.97), R_1 represents the first order transformation matrix from the body fixed coordinate system to seakeeping coordinate system given by

$$R_1 = \begin{bmatrix} 1 & -\xi_6 & \xi_5 \\ \xi_6 & 1 & -\xi_4 \\ -\xi_5 & \xi_4 & 1 \end{bmatrix} \tag{6.99}$$

The matrix R_1 is a linear Euler matrix for small first order angular motions, and is independent of the sequence of rotation, which means that it is irrelevant if we follow roll-pitch-yaw or yaw-pitch-roll rotation convention in the formulation of the matrix.

However, the sequence of rotation becomes important in the case of second order transformation matrix R_2. So that, if we follow roll-pitch-yaw rotation convention we will have

$$R_2 = \begin{bmatrix} -\frac{1}{2}\left(\xi_5^2 + \xi_6^2\right) & 0 & 0 \\ \xi_4\xi_5 & -\frac{1}{2}\left(\xi_4^2 + \xi_6^2\right)1 & 0 \\ \xi_4\xi_6 & \xi_5\xi_6 & -\frac{1}{2}\left(\xi_4^2 + \xi_5^2\right) \end{bmatrix} \tag{6.100}$$

whereas if we follow yaw-pitch-roll rotation convention, then

$$R_2 = \begin{bmatrix} -\frac{1}{2}\left(\xi_5^2 + \xi_6^2\right) & \xi_4\xi_5 & \xi_4\xi_6 \\ 0 & -\frac{1}{2}\left(\xi_4^2 + \xi_6^2\right)1 & \xi_5\xi_6 \\ 0 & 0 & -\frac{1}{2}\left(\xi_4^2 + \xi_5^2\right) \end{bmatrix} \tag{6.101}$$

A difference in the expressions for the transformation matrix R_2 will have a consequence on the estimation of the mean second order force in heave. This means that one additional term which accounts for the second order motion effect in rotation of the axis will appear if we follow roll-pitch-yaw rotation convention, which is otherwise absent if we follow yaw-pitch-roll rotation convention as shown by Pinkster (1980). However, in the present study, this will not be present due to the fact that we are considering the mean wave loads in the horizontal plane.

Now, before proceeding further, it is important to notice that the integral over the instantaneous wetted surface requires two kinds of adjustment. One is on the part of

the mean wetted hull surface S_0 up to the static waterline on the hull, while the other kind of adjustment is on the additional wetted area due to the wave elevation. So that,

$$\begin{aligned}\int_{S^*} p\vec{n}ds &= \int_{S_0} \left(\vec{\alpha}\cdot\nabla p\right)\vec{n}ds + \int_{L_0} dl \int_0^{\zeta_r} p\frac{\vec{n}}{h}dz + O\left(\varepsilon^3\right) \\ &\approx \int_{S_0} \left(\vec{\alpha}\cdot\nabla p\right)\vec{n}ds + \int_{L_0} dl \int_0^{\zeta_r} p\vec{n}dz + O\left(\varepsilon^3\right)\end{aligned} \tag{6.102}$$

where ∇ denotes the Laplace operator here, L_0 is the waterline contour of the ship in its equilibrium position in calm water. The inclination of the hull surface at the waterline $h = \sin\mu$ is set equal to 1, since we assume that the ship hull is wall sided near the free surface.

The relative wave elevation along the ship ζ_r is given as

$$\zeta_r \equiv \zeta_r^{(1)} = \zeta^{(1)} - \left(\xi_3 - x\xi_5 + y\xi_4\right) \tag{6.103}$$

Here, $\zeta^{(1)}$ includes the incident wave elevation as well as the unsteady contribution of the free surface elevation caused by the ship.

Now the zero, first and second order force will be derived, respectively. The zero order force is the hydrostatic force due to the ship buoyancy actually.

$$\vec{F}^{(0)} = \int_{S_0} p^{(0)}\vec{n}^{(0)}ds = \rho g\int_{S_0} z\vec{n}^{(0)}ds = \left(0,0,\rho gV\right) \tag{6.104}$$

Here V is the displaced volume of the ship. Using (6.102), the first order force is

$$\begin{aligned}\vec{F}^{(1)} &= \int_{S_0} p^{(0)}\vec{n}^{(1)}ds + \int_{S_0} p^{(1)}\vec{n}^{(0)}ds + \int_{S_1} p^{(0)}\vec{n}^{(0)}ds \\ &= \int_{S_0} p^{(0)}\vec{n}^{(1)}ds + \int_{S_0} p^{(1)}\vec{n}^{(0)}ds + \int_{S_0} \left(\vec{\alpha}^{(1)}\cdot\nabla p^{(0)}\right)\vec{n}^{(0)}ds + \int_{L_0} dl \int_0^{\zeta_r^{(1)}} p^{(0)}\vec{n}^{(0)}dz\end{aligned} \tag{6.105}$$

The last term of (6.105) is order $O(\varepsilon^2)$ which need to be transferred into the expression for the second order force. Omitting this term we have the first order force up to the order of $O(\varepsilon)$

$$\vec{F}^{(1)} = \int_{S_0} p^{(0)}\vec{n}^{(1)}ds + \int_{S_0} p^{(1)}\vec{n}^{(0)}ds + \int_{S_0}\left(\vec{\alpha}^{(1)}\cdot\nabla p^{(0)}\right)\vec{n}^{(0)}ds \tag{6.106}$$

Now, by using the above expressions for the $\vec{\alpha}^{(1)}$, $\vec{n}^{(0)}$, $\vec{n}^{(1)}$, $p^{(0)}$ and $p^{(1)}$, (6.106) can be rewritten as

$$\vec{F}^{(1)} = -\rho\int_{S_0}\left(\frac{\partial\phi^{(1)}}{\partial t} - U\frac{\partial\phi^{(1)}}{\partial x}\right)\vec{n}^{(0)}ds - \rho g\int_{S_0}\left\{zR_1\vec{n}^{(0)} + \left[\left(\vec{\xi} + R_1\vec{r}'\right)\nabla z\right]\vec{n}^{(0)}\right\}ds \tag{6.107}$$

The complete derivation of the second order force $\vec{F}^{(2)}$ is too extensive to be presented here. Therefore, we will only give some guidance steps about how to arrive on the final form for $\vec{F}^{(2)}$ which is suitable for further calculation.

First of all, integral of order $O(\varepsilon^2)$ which appears in the expression (6.105) for the first order force needs to be added to the second order force given by the expression (6.94). So that, the second order force $\vec{F}^{(2)}$ becomes

$$\begin{aligned}\vec{F}^{(2)} = &\int_{S_0} p^{(0)}\vec{n}^{(2)}ds + \int_{S_0} p^{(1)}\vec{n}^{(1)}ds + \int_{S_0} p^{(2)}\vec{n}^{(0)}ds \\ &+ \int_{S_1} p^{(0)}\vec{n}^{(1)}ds + \int_{S_1} p^{(1)}\vec{n}^{(0)}ds + \int_{S_2} p^{(0)}\vec{n}^{(0)}ds + \int_{L_0} dl\int_0^{\zeta_r^{(1)}} p^{(0)}\vec{n}^{(0)}dz\end{aligned} \tag{6.108}$$

By substituting expressions for the $\vec{n}^{(0)}$, $\vec{n}^{(1)}$, $\vec{n}^{(2)}$, and $p^{(0)}$, $p^{(1)}$, $p^{(2)}$, together with (6.102), the second order force can be written as

$$\begin{aligned}\vec{F}^{(2)} = & \frac{\rho g}{2}\int_{L_0}\left(\zeta_r^{(1)}\right)^2\vec{n}^{(0)}dl-\frac{\rho}{2}\int_{S_0}\left[\left(\frac{\partial\phi^{(1)}}{\partial x}\right)^2+\left(\frac{\partial\phi^{(1)}}{\partial y}\right)^2+\left(\frac{\partial\phi^{(1)}}{\partial z}\right)^2\right]_m\vec{n}^{(0)}ds \\ & -\rho\int_{S_0}\left[\vec{\alpha}^{(1)}\cdot\nabla\left(\frac{\partial\phi^{(1)}}{\partial t}-U\frac{\partial\phi^{(1)}}{\partial x}\right)\right]\vec{n}^{(0)}ds-\rho\int_{S_0}\left(\frac{\partial\phi^{(1)}}{\partial t}-U\frac{\partial\phi^{(1)}}{\partial x}\right)R_1\vec{n}^{(0)}ds \\ & -\rho g\int_{S_0}\left(\vec{\alpha}^{(1)}\cdot\nabla z\right)R_1\vec{n}^{(0)}ds-\rho g\int_{S_0}\left(\vec{\alpha}^{(2)}\cdot\nabla z\right)\vec{n}^{(0)}ds-\rho g\int_{S_0}zR_2\vec{n}^{(0)}ds+O\left(\varepsilon^3\right)\end{aligned} \tag{6.109}$$

Noticing that $\vec{\alpha}^{(2)} = R_2\vec{r}'$ and recalling the discussion about the matrix R_2, following roll-pitch-yaw rotation convention, the last two integrals in (6.109) equal zero. Then,

$$\begin{aligned}\vec{F}^{(2)} = & \frac{\rho g}{2}\int_{L_0}\left(\zeta_r^{(1)}\right)^2\vec{n}^{(0)}dl-\frac{\rho}{2}\int_{S_0}\left[\left(\frac{\partial\phi^{(1)}}{\partial x}\right)^2+\left(\frac{\partial\phi^{(1)}}{\partial y}\right)^2+\left(\frac{\partial\phi^{(1)}}{\partial z}\right)^2\right]_m\vec{n}^{(0)}ds \\ & -\rho\int_{S_0}\left[\vec{\alpha}^{(1)}\cdot\nabla\left(\frac{\partial\phi^{(1)}}{\partial t}-U\frac{\partial\phi^{(1)}}{\partial x}\right)\right]\vec{n}^{(0)}ds-R_1\vec{F}^{(1)}\end{aligned} \tag{6.110}$$

Here, the first order force $\vec{F}^{(1)}$ is substituted and can be written as follow according to the Newton's second law.

$$R_1\vec{F}^{(1)} = m\begin{bmatrix}\ddot{\xi}_1+z_G\ddot{\xi}_5-\ddot{\xi}_2\xi_6+z_G\ddot{\xi}_4\xi_6+\ddot{\xi}_3\xi_5 \\ \ddot{\xi}_1\xi_6+z_G\ddot{\xi}_5\xi_6+\ddot{\xi}_2-z_G\ddot{\xi}_4-\ddot{\xi}_3\xi_4 \\ -\ddot{\xi}_1\xi_5-z_G\ddot{\xi}_5\xi_5+\ddot{\xi}_2\xi_4-z_G\ddot{\xi}_4\xi_4+\ddot{\xi}_3\end{bmatrix} \tag{6.111}$$

Further substituting the and $\vec{\alpha}^{(1)} = \vec{\xi}+R_1\vec{r}'$, which can be expressed as

$$\vec{\alpha}^{(1)} = \begin{bmatrix}\xi_1-\xi_6y+\xi_5z \\ \xi_2+\xi_6x-\xi_4z \\ \xi_3-\xi_5x+\xi_4y\end{bmatrix} \tag{6.112}$$

the second order force $\vec{F}^{(2)}$ can be given in the form of three components as follow.

$$\vec{F}^{(2)} = \begin{bmatrix} F_1^{(2)} \\ F_2^{(2)} \\ F_2^{(2)} \end{bmatrix} = \frac{\rho g}{2} \int_{L_0} \left[\zeta^{(1)} - \left(\xi_3 - x\xi_5 + y\xi_4 \right) \right]^2 \begin{bmatrix} n_1 \\ n_2 \\ n_3 \end{bmatrix} dl$$

$$- \frac{\rho}{2} \int_{S_0} \left[\left(\frac{\partial \phi^{(1)}}{\partial x} \right)^2 + \left(\frac{\partial \phi^{(1)}}{\partial y} \right)^2 + \left(\frac{\partial \phi^{(1)}}{\partial z} \right)^2 \right]_m \begin{bmatrix} n_1 \\ n_2 \\ n_3 \end{bmatrix} ds$$

$$- \rho \int_{S_0} \begin{bmatrix} \left(\xi_1 - \xi_6 y + \xi_5 z \right) \frac{\partial}{\partial x} \left(\frac{\partial \phi^{(1)}}{\partial t} - U \frac{\partial \phi^{(1)}}{\partial x} \right) \\ + \left(\xi_2 + \xi_6 x - \xi_4 z \right) \frac{\partial}{\partial y} \left(\frac{\partial \phi^{(1)}}{\partial t} - U \frac{\partial \phi^{(1)}}{\partial x} \right) \\ + \left(\xi_3 - \xi_5 x + \xi_4 y \right) \frac{\partial}{\partial z} \left(\frac{\partial \phi^{(1)}}{\partial t} - U \frac{\partial \phi^{(1)}}{\partial x} \right) \end{bmatrix}_m \begin{bmatrix} n_1 \\ n_2 \\ n_3 \end{bmatrix} ds$$

$$- m \begin{bmatrix} \ddot{\xi}_1 + z_G \ddot{\xi}_5 - \ddot{\xi}_2 \xi_6 + z_G \ddot{\xi}_4 \xi_6 + \ddot{\xi}_3 \xi_5 \\ \ddot{\xi}_1 \xi_6 + z_G \ddot{\xi}_5 \xi_6 + \ddot{\xi}_2 - z_G \ddot{\xi}_4 - \ddot{\xi}_3 \xi_4 \\ -\ddot{\xi}_1 \xi_5 - z_G \ddot{\xi}_5 \xi_5 + \ddot{\xi}_2 \xi_4 - z_G \ddot{\xi}_4 \xi_4 + \ddot{\xi}_3 \end{bmatrix} \tag{6.113}$$

where the relation (6.103) is used.

By taking the time average (bar over the expressions) and assuming that the ship hull is slender, i.e., $\partial/\partial x << \partial/\partial y, \partial/\partial z$, we can write

- Mean second order surge force (added resistance in waves)

$$\overline{F_x^{(2)}} = \frac{\rho g}{2} \overline{\int_{L_0} \left[\zeta^{(1)} - \left(\xi_3 - x\xi_5 + y\xi_4 \right) \right]^2 n_1 dl} - \frac{\rho}{2} \overline{\int_{S_0} \left[\left(\frac{\partial \phi^{(1)}}{\partial y} \right)^2 + \left(\frac{\partial \phi^{(1)}}{\partial z} \right)^2 \right]_m n_1 ds}$$

$$- \rho \overline{\int_{S_0} \begin{bmatrix} \left(\xi_2 + \xi_6 x - \xi_4 z \right) \frac{\partial}{\partial y} \left(\frac{\partial \phi^{(1)}}{\partial t} - U \frac{\partial \phi^{(1)}}{\partial x} \right) \\ + \left(\xi_3 - \xi_5 x + \xi_4 y \right) \frac{\partial}{\partial z} \left(\frac{\partial \phi^{(1)}}{\partial t} - U \frac{\partial \phi^{(1)}}{\partial x} \right) \end{bmatrix}_m n_1 ds} \tag{6.114}$$

$$- m \overline{\left[-\ddot{\xi}_2 \xi_6 + z_G \ddot{\xi}_4 \xi_6 + \ddot{\xi}_3 \xi_5 \right]}$$

- Mean second order sway force

$$\overline{F_y^{(2)}} = \frac{\rho g}{2}\int_{L_0}\overline{\left[\zeta^{(1)} - \left(\xi_3 - x\xi_5 + y\xi_4\right)\right]^2 n_2 dl} - \frac{\rho}{2}\int_{S_0}\overline{\left[\left(\frac{\partial\phi^{(1)}}{\partial y}\right)^2 + \left(\frac{\partial\phi^{(1)}}{\partial z}\right)^2\right]_m n_2 ds}$$
$$-\rho\int_{S_0}\overline{\left[\begin{array}{l}\left(\xi_2 + \xi_6 x - \xi_4 z\right)\dfrac{\partial}{\partial y}\left(\dfrac{\partial\phi^{(1)}}{\partial t} - U\dfrac{\partial\phi^{(1)}}{\partial x}\right)\\ +\left(\xi_3 - \xi_5 x + \xi_4 y\right)\dfrac{\partial}{\partial z}\left(\dfrac{\partial\phi^{(1)}}{\partial t} - U\dfrac{\partial\phi^{(1)}}{\partial x}\right)\end{array}\right]_m n_2 ds} \qquad (6.115)$$
$$-m\overline{\left[\ddot{\xi}_1\xi_6 + z_G\ddot{\xi}_5\xi_6 - \ddot{\xi}_3\xi_4\right]}$$

where it should be noticed that the time average of the terms $\left(\ddot{\xi}_1 + z_G\ddot{\xi}_5\right)$ and $\left(\ddot{\xi}_2 - z_G\ddot{\xi}_4\right)$ are zero. In addition, the mean second order heave force can be also obtained from the expression (6.113), but it is omitted here because the present study does not use the mentioned force.

The second order moments in roll, pitch and yaw can be derived in a similar way if one carries out in principle the same steps which are outlined above for the second order force. The details of this process are extremely lengthy, and therefore they are omitted here. After the time average and the slender assumption, $\partial/\partial x << \partial/\partial y, \partial/\partial z$ the final expressions for mean second order yaw moment is directly presented as follow.

- Mean second order roll moment

$$\overline{M_x^{(2)}} = \frac{\rho g}{2}\int_{L_0}\overline{\left[\zeta^{(1)} - \left(\xi_3 - x\xi_5 + y\xi_4\right)\right]^2 n_4 dl} - \frac{\rho}{2}\int_{S_0}\overline{\left[\left(\frac{\partial\phi^{(1)}}{\partial y}\right)^2 + \left(\frac{\partial\phi^{(1)}}{\partial z}\right)^2\right]_m n_4 ds}$$
$$-\rho\int_{S_0}\overline{\left[\begin{array}{l}\left(\xi_2 + \xi_6 x - \xi_4 z\right)\dfrac{\partial}{\partial y}\left(\dfrac{\partial\phi^{(1)}}{\partial t} - U\dfrac{\partial\phi^{(1)}}{\partial x}\right)\\ +\left(\xi_3 - \xi_5 x + \xi_4 y\right)\dfrac{\partial}{\partial z}\left(\dfrac{\partial\phi^{(1)}}{\partial t} - U\dfrac{\partial\phi^{(1)}}{\partial x}\right)\end{array}\right]_m n_4 ds} \qquad (6.116)$$
$$-\overline{\left[\xi_6\left(-I_{22}\ddot{\xi}_5 - mz_G\ddot{\xi}_1\right) + \xi_5\left(-I_{31}\ddot{\xi}_4 + I_{33}\ddot{\xi}_6\right)\right]}$$

with $n_4 = yn_3 - zn_2$.

- Mean second order yaw moment

$$\overline{M_z^{(2)}} = \frac{\rho g}{2}\int_{L_0}\overline{\left[\zeta^{(1)} - \left(\xi_3 - x\xi_5 + y\xi_4\right)\right]^2 n_6 dl} - \frac{\rho}{2}\int_{S_0}\overline{\left[\left(\frac{\partial\phi^{(1)}}{\partial y}\right)^2 + \left(\frac{\partial\phi^{(1)}}{\partial z}\right)^2\right]_m n_6 ds}$$
$$-\rho\int_{S_0}\overline{\left[\begin{array}{l}\left(\xi_2 + \xi_6 x - \xi_4 z\right)\dfrac{\partial}{\partial y}\left(\dfrac{\partial\phi^{(1)}}{\partial t} - U\dfrac{\partial\phi^{(1)}}{\partial x}\right)\\ +\left(\xi_3 - \xi_5 x + \xi_4 y\right)\dfrac{\partial}{\partial z}\left(\dfrac{\partial\phi^{(1)}}{\partial t} - U\dfrac{\partial\phi^{(1)}}{\partial x}\right)\end{array}\right]_m n_6 ds} \qquad (6.117)$$
$$-\overline{\left[\xi_5\left(-I_{11}\ddot{\xi}_4 + mz_G\ddot{\xi}_2 + I_{13}\ddot{\xi}_6\right) + \xi_4\left(I_{22}\ddot{\xi}_5 + mz_G\ddot{\xi}_1\right)\right]}$$

with $n_6 = xn_2 - yn_1$. Here, one should be aware that the expression (6.116) for the mean second order roll moment is not utilized in the numerical calculations of combined seakeeping and maneuvering. The expression for the mean second order pitch moment can be written in a similar way, but it is omitted as it is not needed.

The main characteristics of the direct pressure integration method can be summarized as follows. First of all, the method accounts for the complete Bernoulli's equation expanded up to the second order. Further, it accounts for the second order effects due to the instantaneous vessel position and the wetted surface. Because the effect of the second order potential is neglected, the theory only needs information about linear flow variables. In the evaluation, three different quantities, i.e., the water line integral, the body surface integral and the hydrostatic contributions due to the rotational transformations between the body-fixed and seakeeping coordinate system are needed. All the three quantities are of similar magnitudes. Because the contributions have different signs, relatively small inaccuracies in each term will cause a relatively larger inaccuracy in the final result for the mean wave loads. Therefore, the direct pressure integration method is more numerically sensitive than the method based on conservation of energy and fluid momentum to calculate mean horizontal loads.

6.4 Flow chart of the two time scales model

After the methods to obtain all the external force components acting on the ship been introdunced, the two time scales combined seakeeping and manoeuvring simulation system can be briefly illustrated in Fig. 6.4 by summarizing the interaction between the two sets of motion equations associated with seakeeping performance analysis and manoeuvring simulation respectively through data exchange.

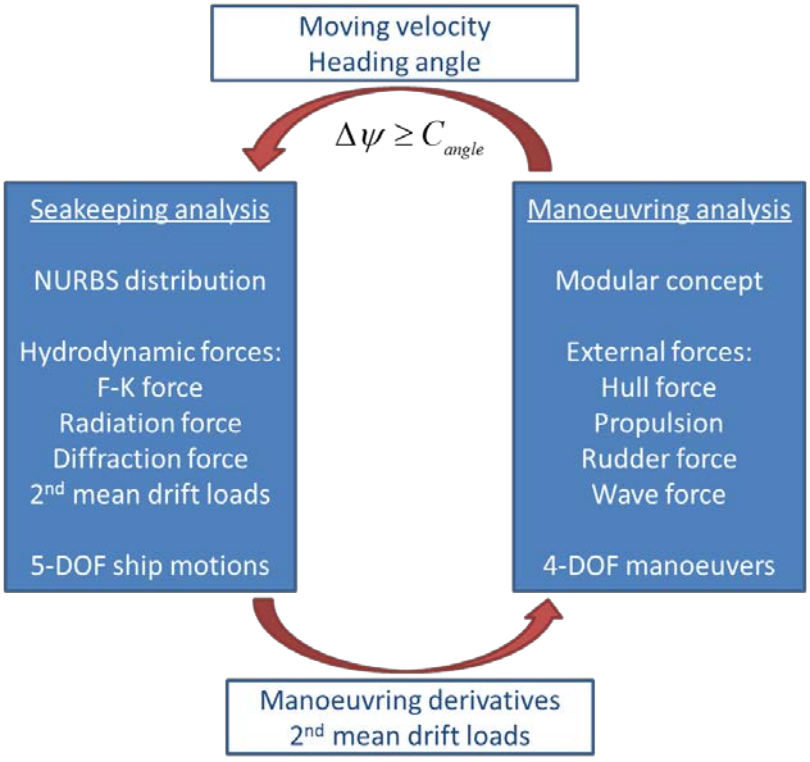

Fig. 6.4 Data exchange between seakeeping and manoeuvring

A more detailed flow chart describing the implementation of the whole simulation system is presented in Fig. 6.5. Firstly, the main particulars of an investigated ship together with its equipped propeller and rudder are inputted for pre-processing. The transverse contours of the hull in all cross sections along the ship length are modeled with the NURBS for later use in solving BVPs in seakeeping calculations. The regular deep water wave characteristics and prefixed difference in the heading angle C_{angle} are specified. Then, the initial conditions concerning the manoeuvring analysis are given including the approach speed of the ship to the chosen maneuver, the ship position in respect to the Earth fixed coordinate system, rudder steering rate, etc. At the first time

step, $t = 0$, the seakeeping calculations by the 2.5D approach will provide the linear calm water manoeuvring derivatives and continue with the estimation of the slowly varying mean second order wave loads. Meanwhile, the resistance, propulsion, rudder and nonlinear viscous loads modules will give the rest of coefficients, such as resistance, thrust, rudder forces and moment, nonlinear manoeuvring derivatives which are needed to complete the manoeuvring equation system. In this way, the maneuvering equation system can proceed and give, among other manoeuvring parameters, the instantaneous ship heading angle ψ which is summed up and compared with the prefixed difference in the heading angle C_{angle}. If the total sum of ship heading angle is greater than the prefixed difference, the integer value 1 will be assigned to the indication parameter *Act* and the instantaneous ship speed and ship heading angle will be recorded, otherwise we stay in the manoeuvring simulation system with the old wave loads input. As the time continues, the *Act* parameter will initiate the new estimation of the mean second order wave loads depending on the integer value. The time loop terminates until the end of the simulation. The manoeuvring equation system is solved with a time integration algorithm based on the explicit 4^{th} order Runge-Kutta scheme with constant time steps.

By applying this two time scales model, not only the nature of the wave induced motions and manoeuvring motions in different frequencies is captured, but also the calculation amount is significantly reduced.

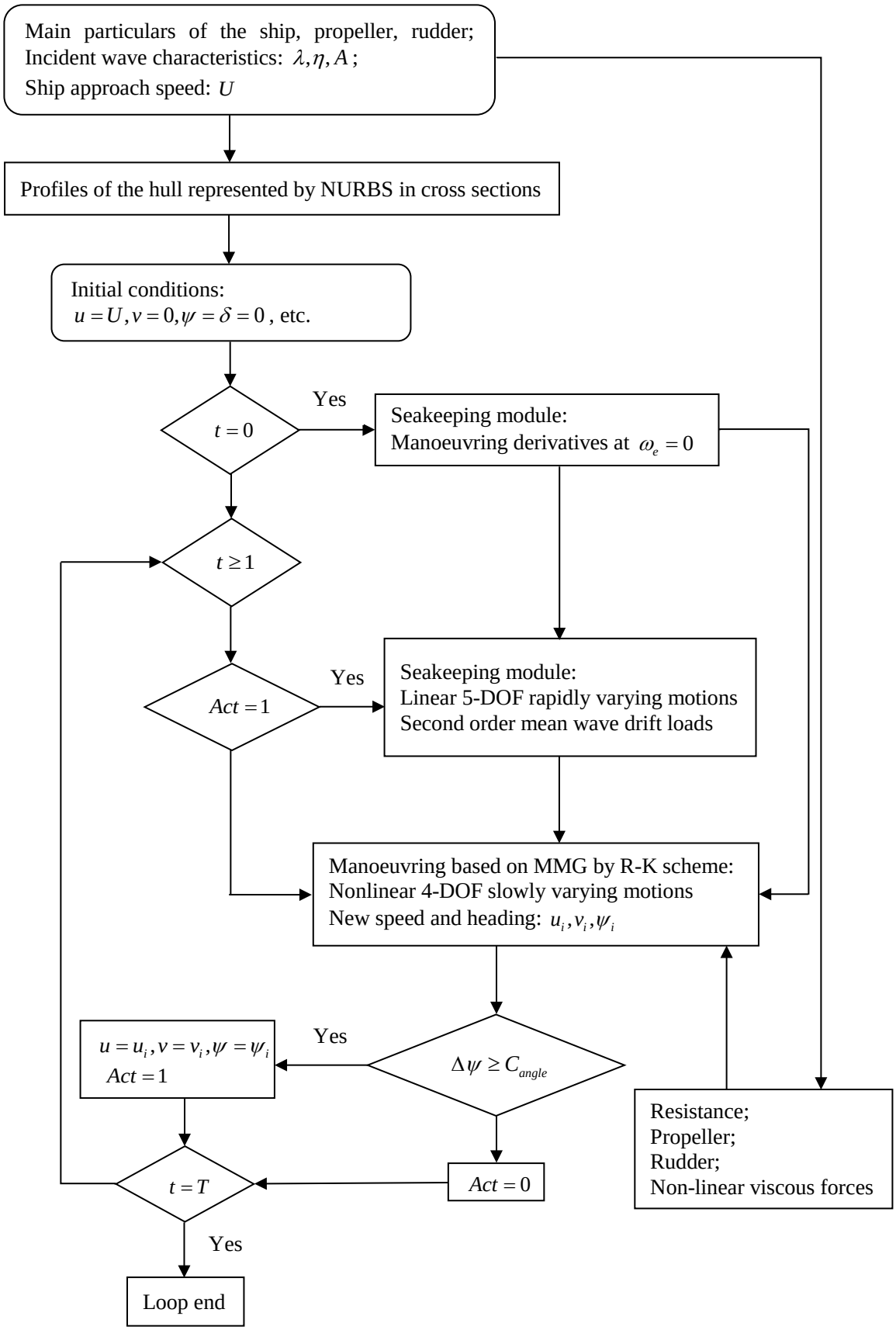

Fig. 6.5 Flow chart of the whole simulation system

6.5 **Validation of the simulation system**

The S175 container ship is selected for the following validations of the present simulation tool based on the two time scales model by carrying out two standard maneuvers, namely $\pm 35^{o}$ turning circle and Zig-zag at $\pm 10^{o}/10^{o}$ and $\pm 20^{o}/20^{o}$. The main particulars of the full scale ship and its equipped propeller and rudder are listed below in Table 6.4.

Table 6.4 Main particulars of the S175 container ship

	Parameters	S175
Hull	Length, $L(m)$	175
	Breath, $B(m)$	25.4
	Draft, $D(m)$	9.5
	Block coefficient, C_B	0.572
	Volume of displacement, $\nabla(ton)$	24742
	Transverse metacentric height, $\overline{GM_T}(m)$	1.0
	Radius of inertia for roll, k_{xx}	$0.33\,B$
	Radius of inertia for pitch, k_{yy}	$0.25\,L$
	Radius of inertia for yaw, k_{zz}	$0.269\,L$
	Wetted surface area, $S_0(m^2)$	5396
Propeller	Diameter, $D_p(m)$	6.5064
	Pitch ratio	0.7348
Rudder	Rudder area, $A_R(m^2)$	32.46
	Rudder height, $H_R(m)$	7.7
	Aspect ratio	1.8268

The approach speed of the ship is set at the Froude number $F_n = 0.15$, and the propeller rpm is assumed to be constant during simulations according to the balance between the propulsion and resistance when the ship moving on a straight course.

For turning motions, experimental measurements conducted by Shanghai Jiao Tong University (SJTU) cited from Zhu (2015)'s work on a $1/57.686$ scaled model with a rudder steering rate at 13^{o}/s are presented for comparison, whereas for Zig-zag motions the experimental measurements obtained by Yasukawa (2008) on a $1/50$ scaled model with a rudder steering rate at 12^{o}/s are used for comparison.

6.5.1 Validation in calm water

Simulations will be first carried out in calm water for standard maneuvers. In order to avoid the scale effects, the same scaled models as the ones used in the model tests are chosen in the simulations. The coefficients applied in the simulations are listed in Table 6.5 from Yasukawa (2006).

Table 6.5 Coefficients used in manoeuvring simulations

	Coefficients	Values	Coefficients	Values	Coefficients	Values
Hull	m_x'	0.0044	Y_{vvv}'	-2.008	N_{vvv}'	0.0275
	X_{vv}'	-0.0711	Y_{vvr}'	0.3942	N_{vvr}'	-0.7811
	X_{rr}'	0.0037	Y_{vrr}'	-0.7461	N_{vrr}'	0.0287
	X_{vr}'	-0.0573	Y_{rrr}'	0.0326	N_{rrr}'	-0.0422
	X_{uu}'	0.01563	z_H/D	0.5		
Propeller	t_{p0}	0.175	w_{P0}	0.1684	x_P'	-0.47
	a_0	0.2932	a_1	-0.1971	a_2	-0.0481
Rudder	t_R	0.29	x_H'	-0.48	ℓ_R'	-1.0
	a_H	0.237	ε	0.921	$\gamma_R(v<0)$	0.088
	κ	0.631	z_R/D	0.7	$\gamma_R(v\geq 0)$	0.193

Fig. 6.6 shows the trajectories of the ship performing standard $\pm 35^{o}$ turning motions. Good agreements with the experimental measurements have been achieved if the lift effect correction been considered which indicate that the lift force is an important component in the force analysis during manoeuvers and the indirect way for this 3D effect correction is reasonable. Besides, the good results also verify that the other

coefficients applied in the present study are accurate and the 4th order Runge-Kutta scheme for the manoeuvring motion simulation is reliable.

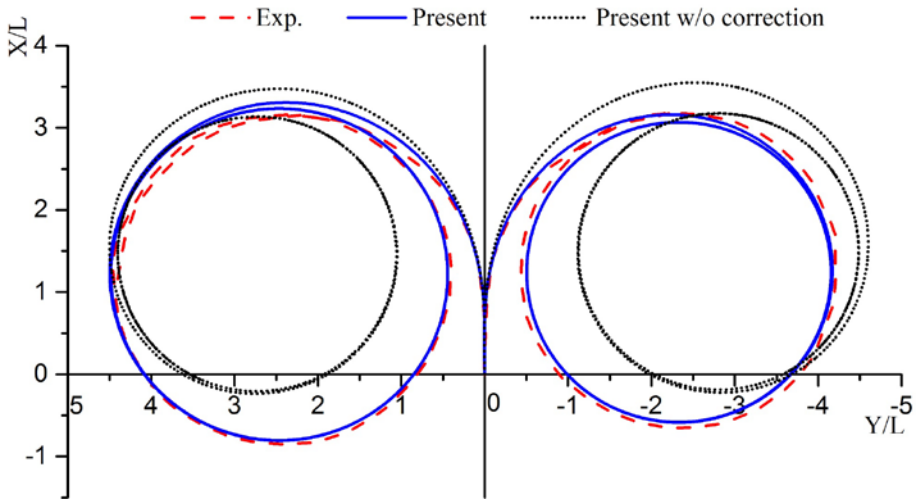

Fig. 6.6 Comparison of turning trajectories of the S175 in calm water

Fig. 6.7 shows the time history of the heel angle during the starboard side turning. As seen, the angle is varying from negative values at the beginning to the positive values in the end which agrees with the phenomena appeared in reality.

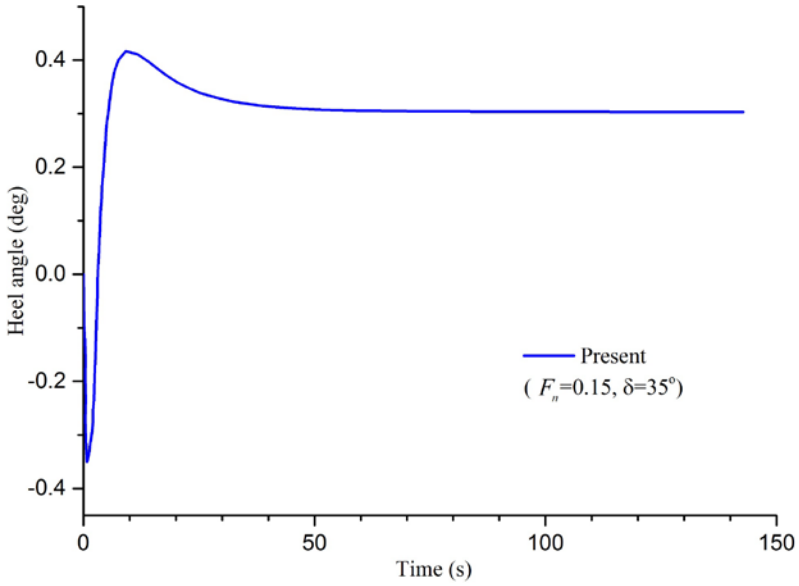

Fig. 6.7 Heel angle of the S175 in starboard side turning

Next, Zig-zag tests at ±10°/10° and ±20°/20° are carried out. Except for intuitive comparison in Fig. 6.8, detailed manoeuvring parameters of the 1st and 2nd overshoot angles are listed in Table 6.6.

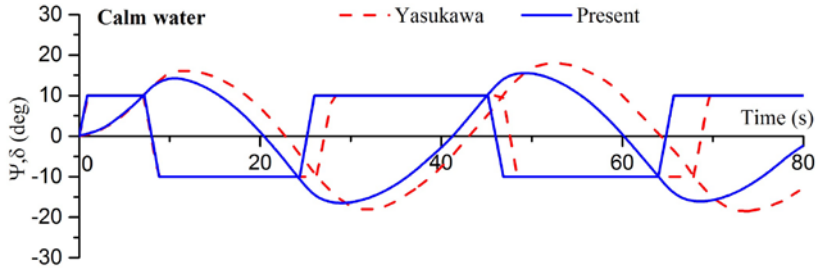

(a) 10°/10°

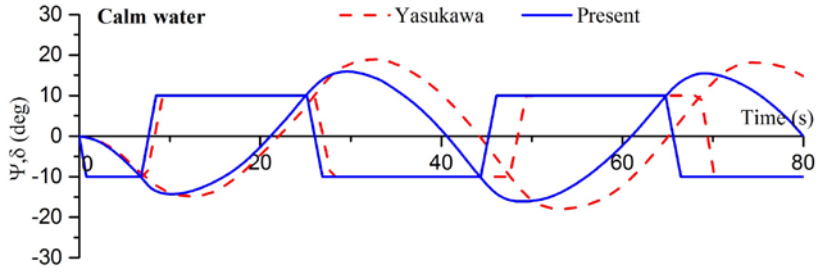

(b) -10°/-10°

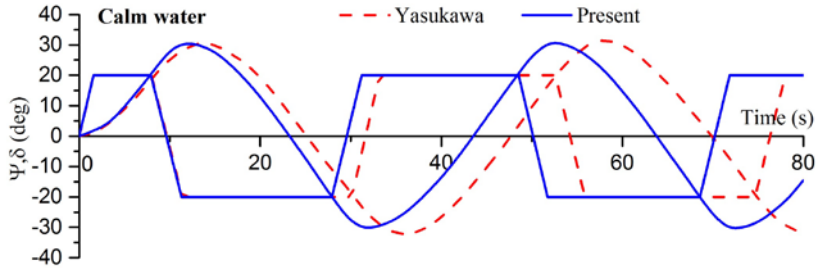

(c) 20°/20°

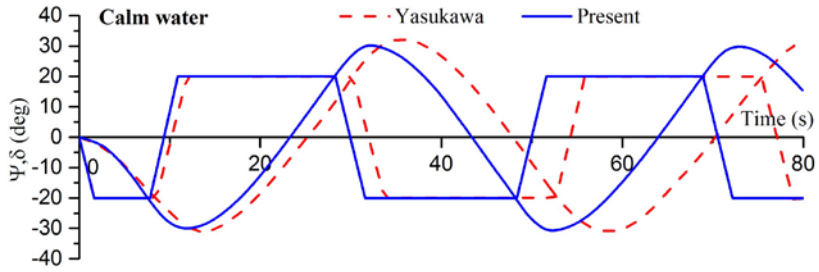

(d) -20°/-20°

Fig. 6.8 Time histories of rudder and heading angles during Zig-zag motions of the S175 in calm water

Table 6.6 Comparison of overshoot angles in calm water

	1st overshoot			2nd overshoot		
	Cal.	Exp.	Error	Cal.	Exp.	Error
10°/10°	5.5°	6.3°	12.6%	6.0°	8.1°	25.9%
-10°/-10°	5.5°	5.6°	1.7%	6.7°	8.6°	22.1%
20°/20°	10.7°	11.1°	3.6%	10.4°	10.6°	1.8%
-20°/-20°	10.5°	10.6°	1.0%	10.4°	12.1°	14.0%

From comparison, the simulation results roughly agree with the measurements, and can capture the overall tendency of the Zig-zag maneuvers. However, relative big deviations can be observed in the 2nd overshoot angle at $\pm 10^o/10^o$ Zig-zag motions. First of all, it is difficult to ensure the accuracy in a few degrees. Secondly, all the results calculated by the present method are smaller than the test results. There is a possibility that hull damping force used in the simulations is a bit too larger than actual one. Moreover, the estimation formulae for rudder force is based on an approximated rectangle rudder which is different from the actual rudder profile, thereby further reduce the accuracy.

6.5.2 Validation of mean second order loads

Before further simulations of the standard maneuvers in waves, validation of the mean second order loads are carried out on the S175 ship in head sea $\left(\chi = 180^o\right)$ and beam sea $\left(\chi = 90^o\right)$, respectively. The incident wave length is chosen in the range of $0.5 < \lambda/L < 1.5$. In the head sea case, the added resistance results are compared with the experimental results by Fuji & Takahashi (1975), while in the beam sea case, results are compared with the experimental results by Yasukawa & Adnan (2006).

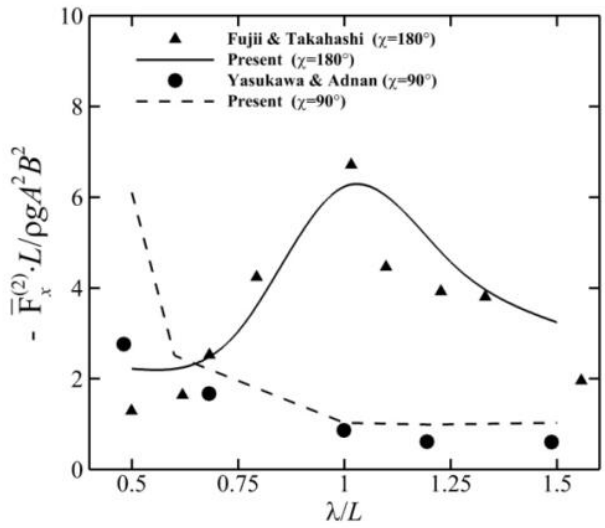

Fig. 6.9 The added resistance on the S175 ship advancing in head and beam sea

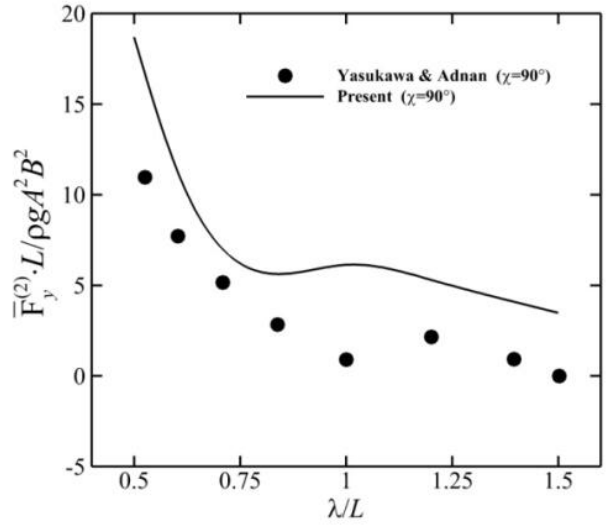

Fig. 6.10 The mean 2nd order sway force on the S175 ship advancing in beam sea

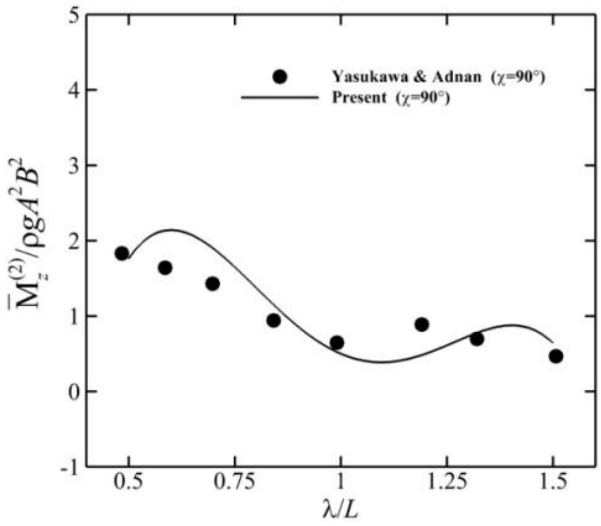

Fig. 6.11 The mean 2nd order yaw moment on the S175 ship advancing in beam sea

From the Fig. 6.9 to Fig. 6.11, the tendency of the calculated results basically agree with the experimental measurements. Deviations are mainly observed at short wave lengths. Except for the sensitivity of the method already stated in subsection 6.3, the deviations can be explained by the fact that the direct integration method is applicable in the range of wavelengths which are longer than the cross sectional beam in the solution of diffraction potential. Besides, the S175 has large flare profiles at the bow and stern regions which conflict the assumption of wall sided body surface near free surface applied in the method thereby increase the deviation of the results.

6.5.3 Validation in waves

Turning circle

Finally, validation are carried out on the S175 ship manoeuvring in waves with different wavelengths and incident angles. Fig. 6.12 and Fig. 6.13 are the trajectories of the ship conducting $\pm 35^{o}$ turning motions in head sea, while Fig. 6.14 and Fig. 6.15 are the trajectories of the ship manoeuvring in beam sea.

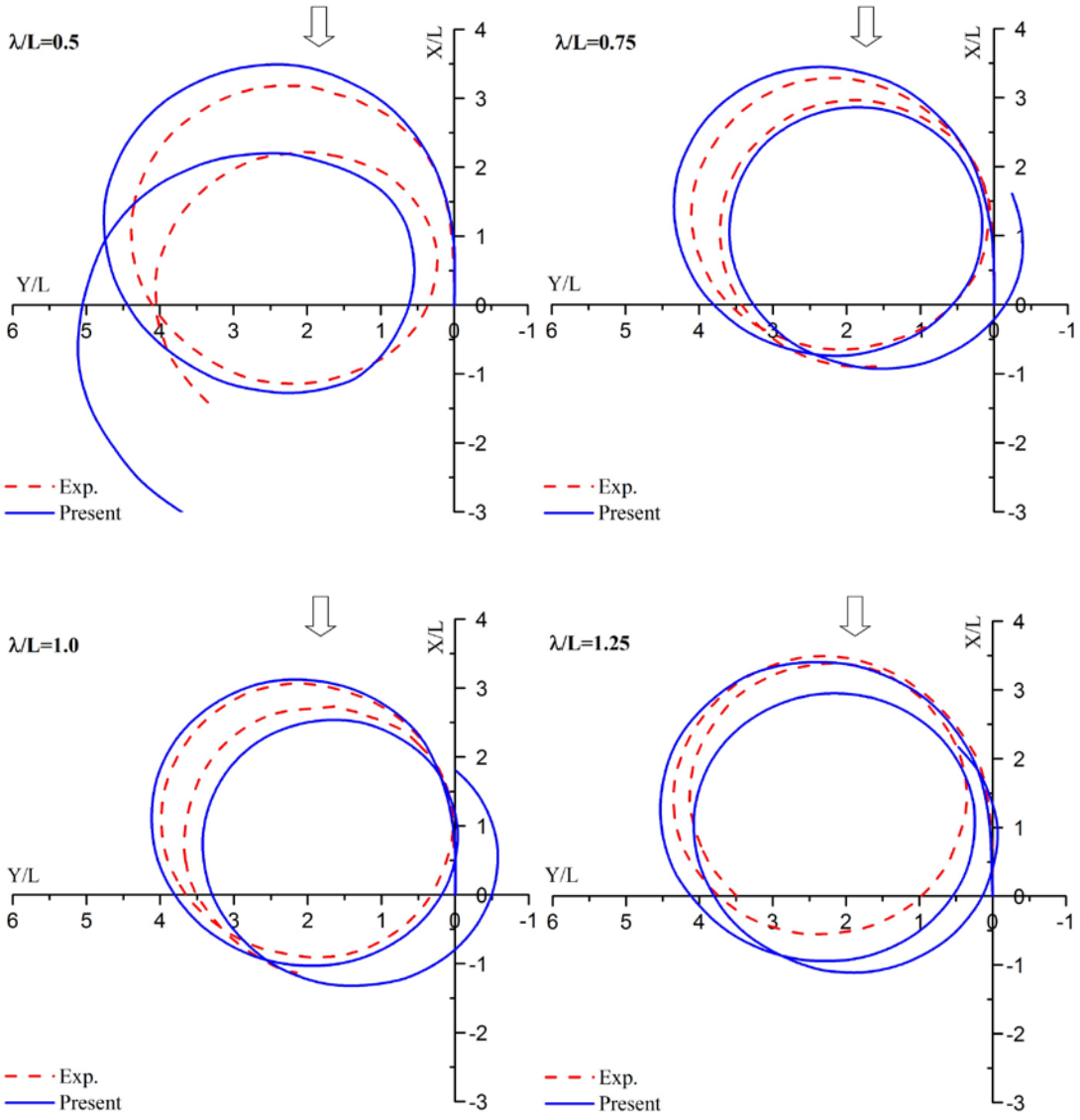

Fig. 6.12 Comparison of portside 35º turning trajectories of the S175 in head sea

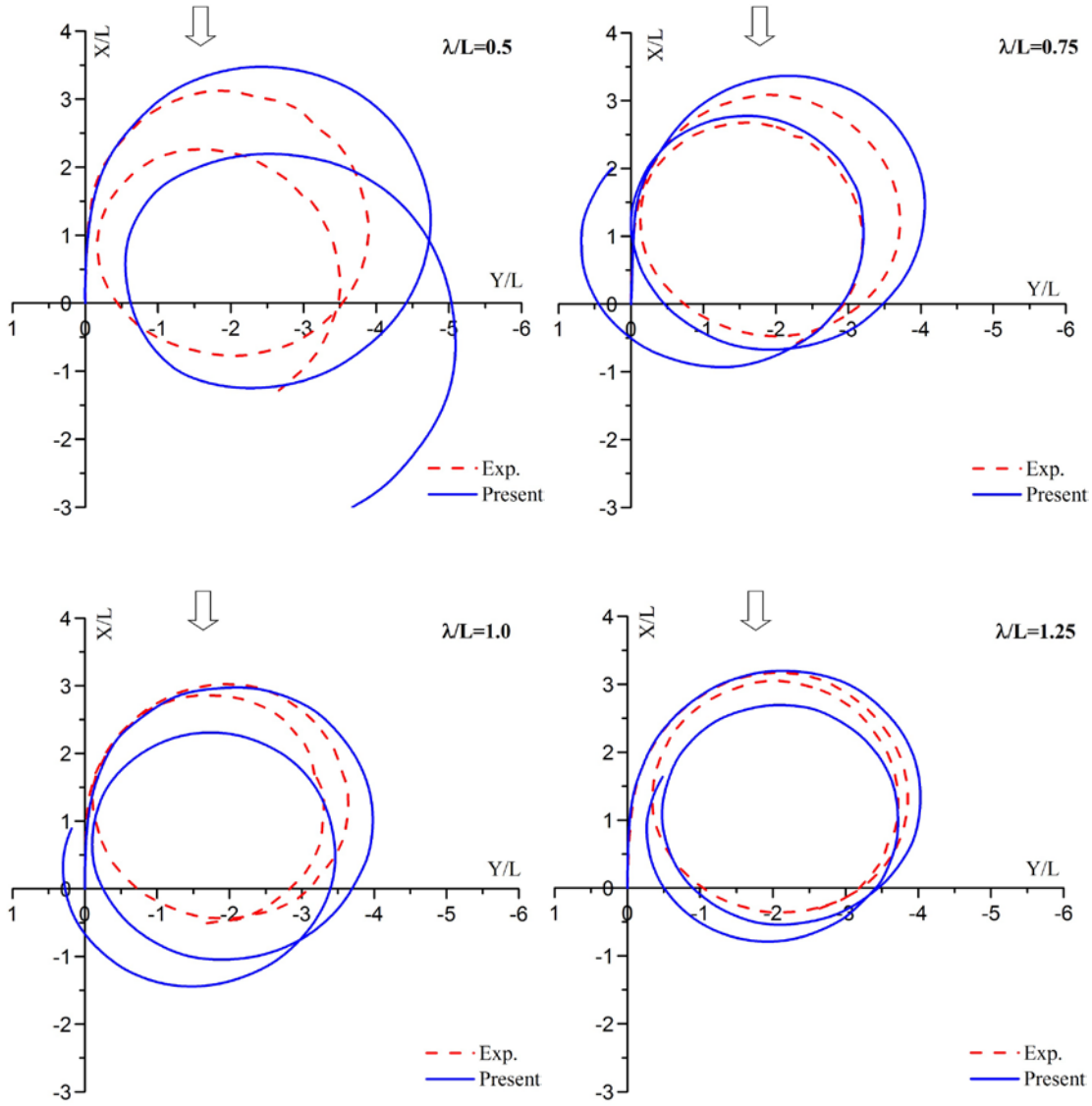

Fig. 6.13 Comparison of starboardside 35^o turning trajectories of the S175 in head sea

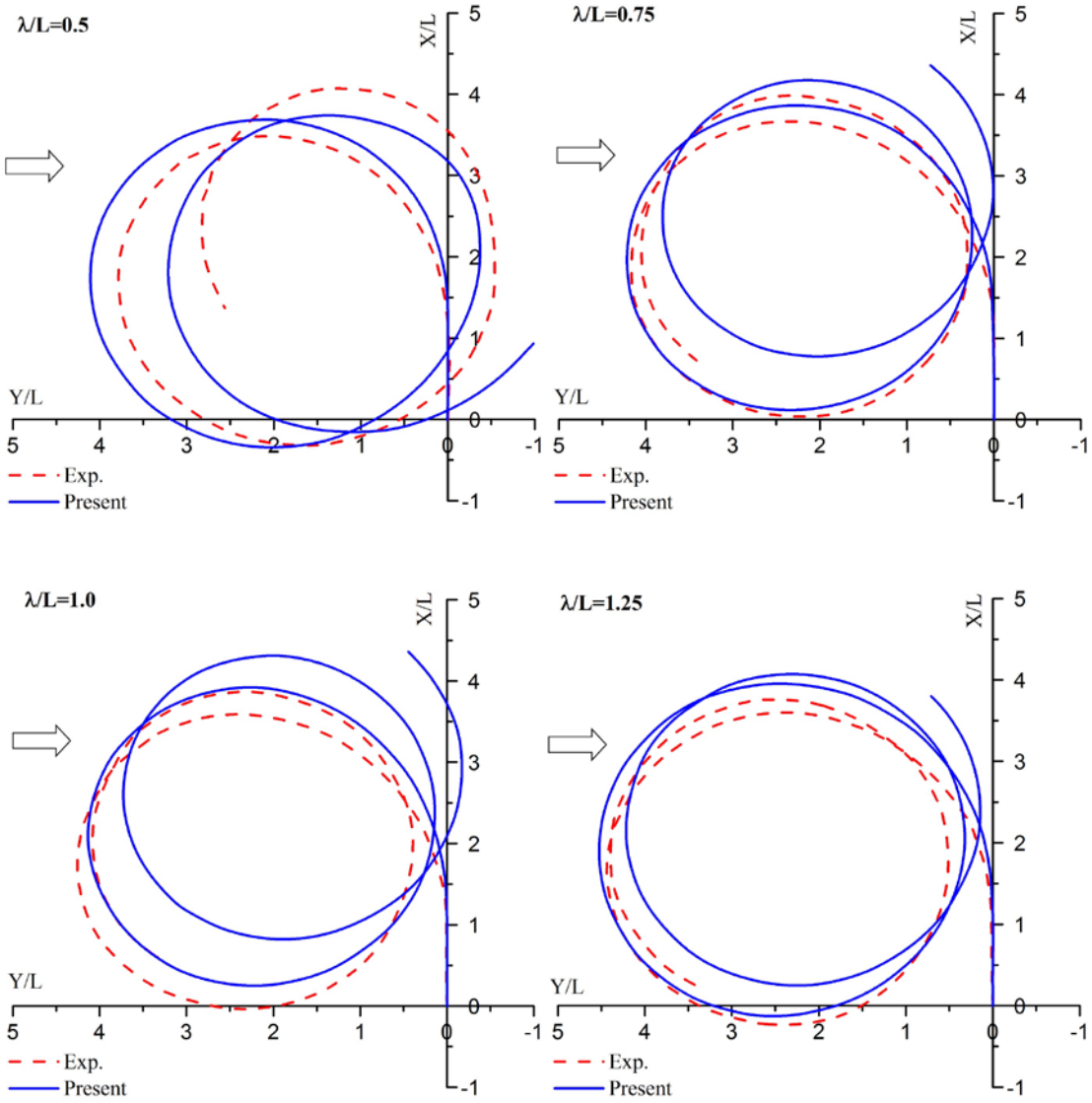

Fig. 6.14 Comparison of portside 35º turning trajectories of the S175 in beam sea

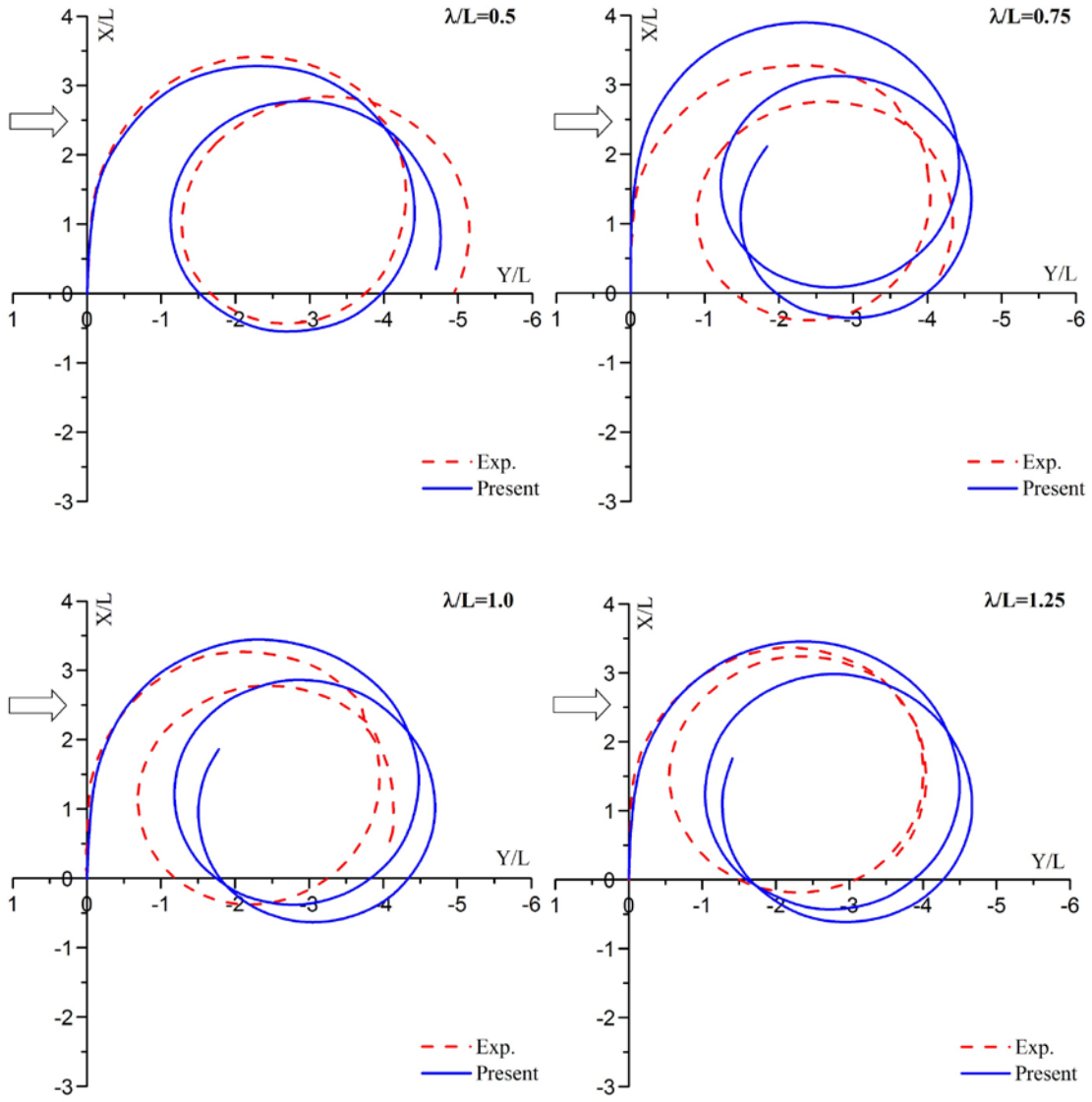

Fig. 6.15 Comparison of starboardside 35^o turning trajectories of the S175 in beam sea

From the figures, we can learn that there is a drift motion during the turning manoeuver no matter in which the direction the wave is incoming. And the results by the present simulations fairly catch the tendency of the drifting measured by model tests. The drift distance becomes bigger with the shorter wave length which can be easily understood as the mean second order sway force and yaw moment are tend to increase according to the results already shown in Fig. 6.10 and Fig. 6.11. Besides, it should be noticed that the difference of the drift distance between the $\lambda/L = 0.75$ and $\lambda/L = 1$ is small. A possible explanation would be the added resistance at $\lambda/L = 1$ is

bigger than that at $\lambda/L = 0.75$ when in head sea moments, though the sway force and yaw moment are smaller, thereby even the wave effects.

Zig-zag

From Fig. 6.16 to Fig. 6.23, the time histories of rudder and heading angle of the ship conducting series of Zig-zag motion tests in head sea and beam sea are presented. In each sea state, four wave lengths are imposed.

For the head sea cases, satisfied agreement is only achieved at $\lambda/L = 0.5$, whereas obvious deviations can be observed at the other three wave lengths. Similar deviations also appear in the results by Yasukawa (2008). Again, the inaccuracy of the wave drift would always be the primary cause. Besides, we should notice that the heave and pitch motions would have remarkable amplitudes in head sea, especially at the wavelength around $\lambda/L = 1$. Assuming a time, the bow is penetrating a wave crest, while the stern is just lying on the wave trough. This will induce relative bigger amplitude oscillation, thereby the rudder force would be significantly affected due to the changing inflow speed. Beside, even partly emergence of the rudder would occur in the oscillation which leads to smaller rudder area in the water.

For the beam sea cases, better agreements are achieved in contrast to the head sea cases. The changing of the heading deviation times is well captured by the simulation results especially at the wavelength $\lambda/L = 0.5$ as relative bigger mean second order sway force and yaw moment occurred.

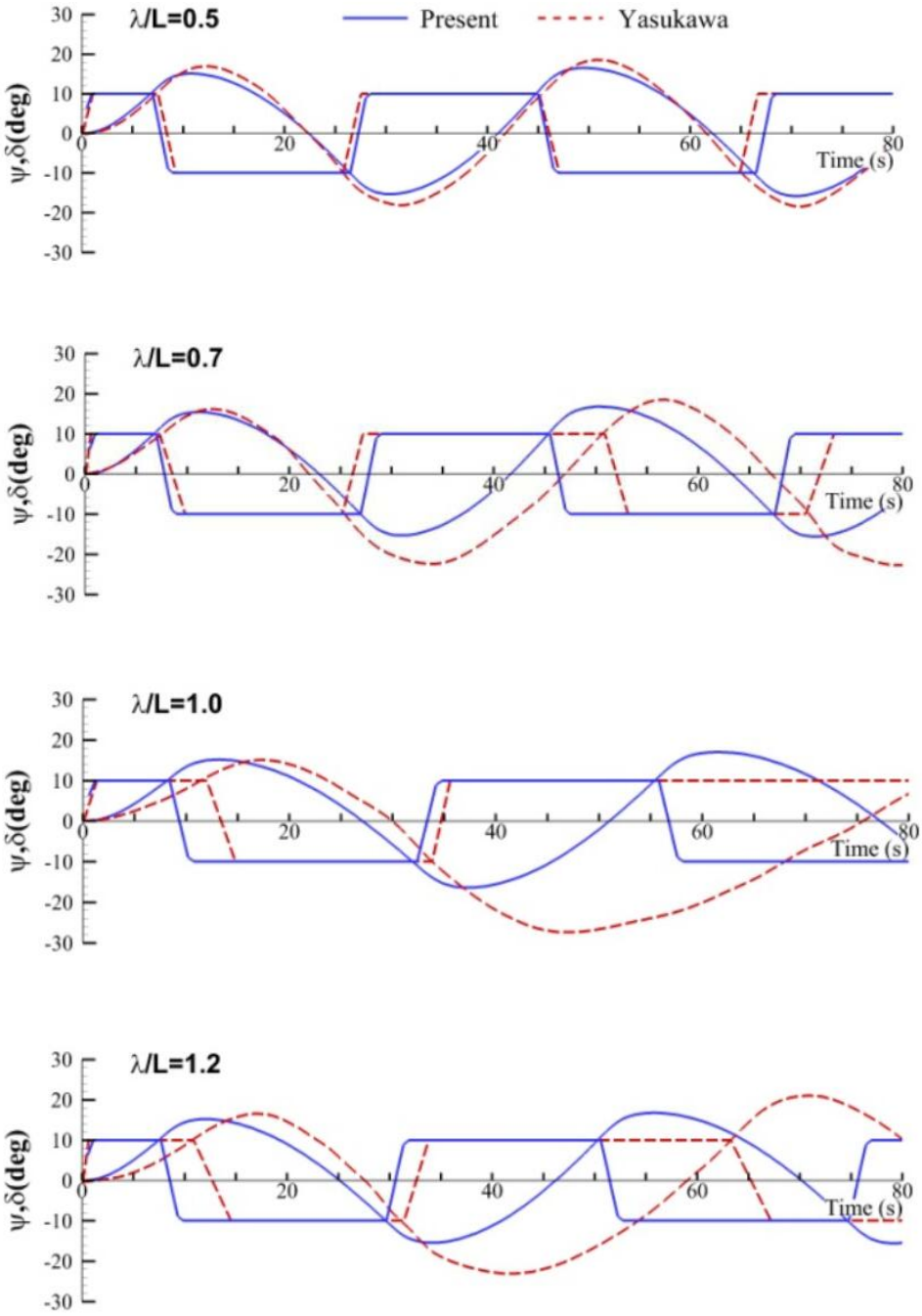

Fig. 6.16 Time histories of rudder and heading angles during $10^o/10^o$ Zig-zag of the S175 in head sea

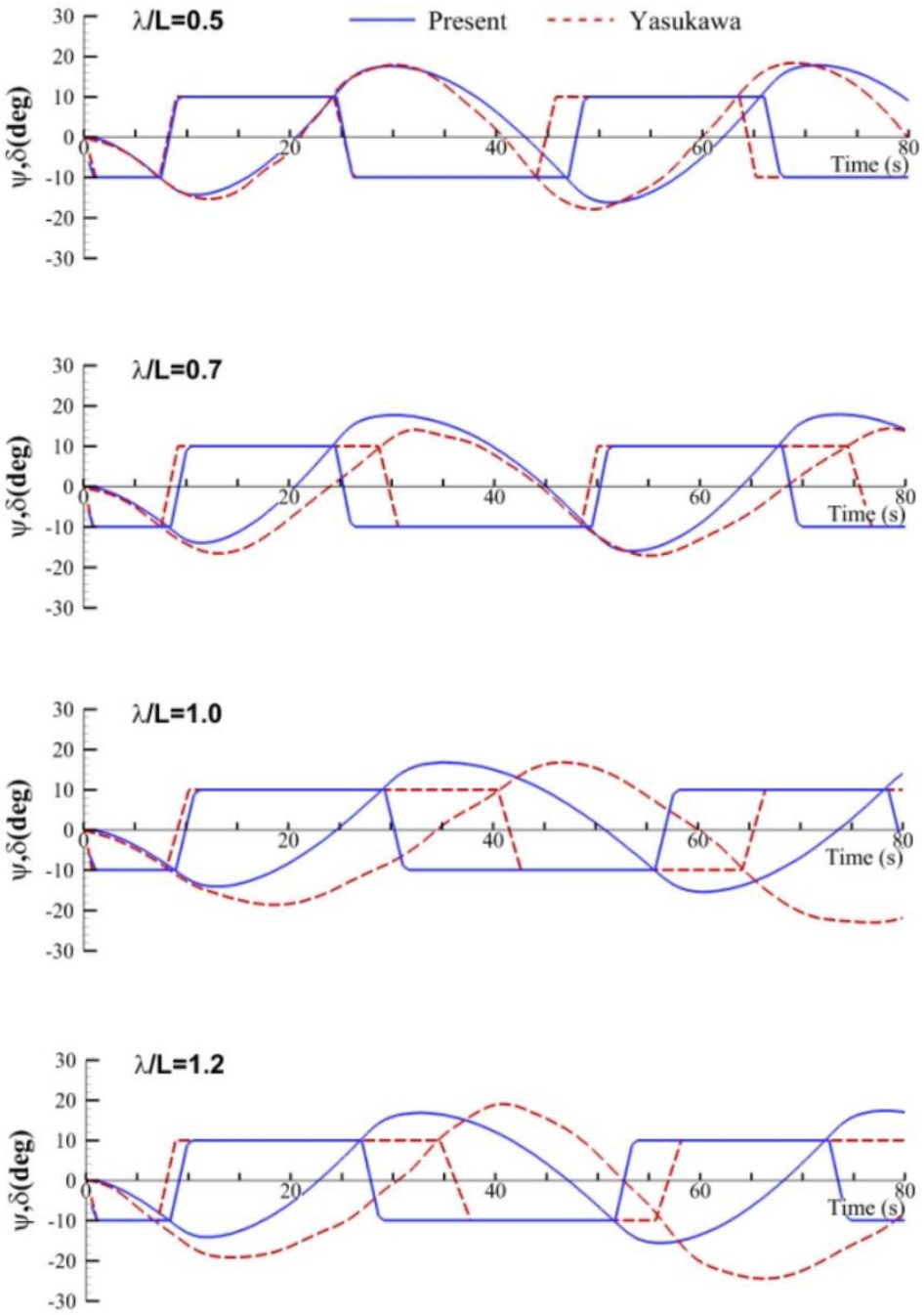

Fig. 6.17 Time histories of rudder and heading angles during -10º/-10º Zig-zag of the S175 in head sea

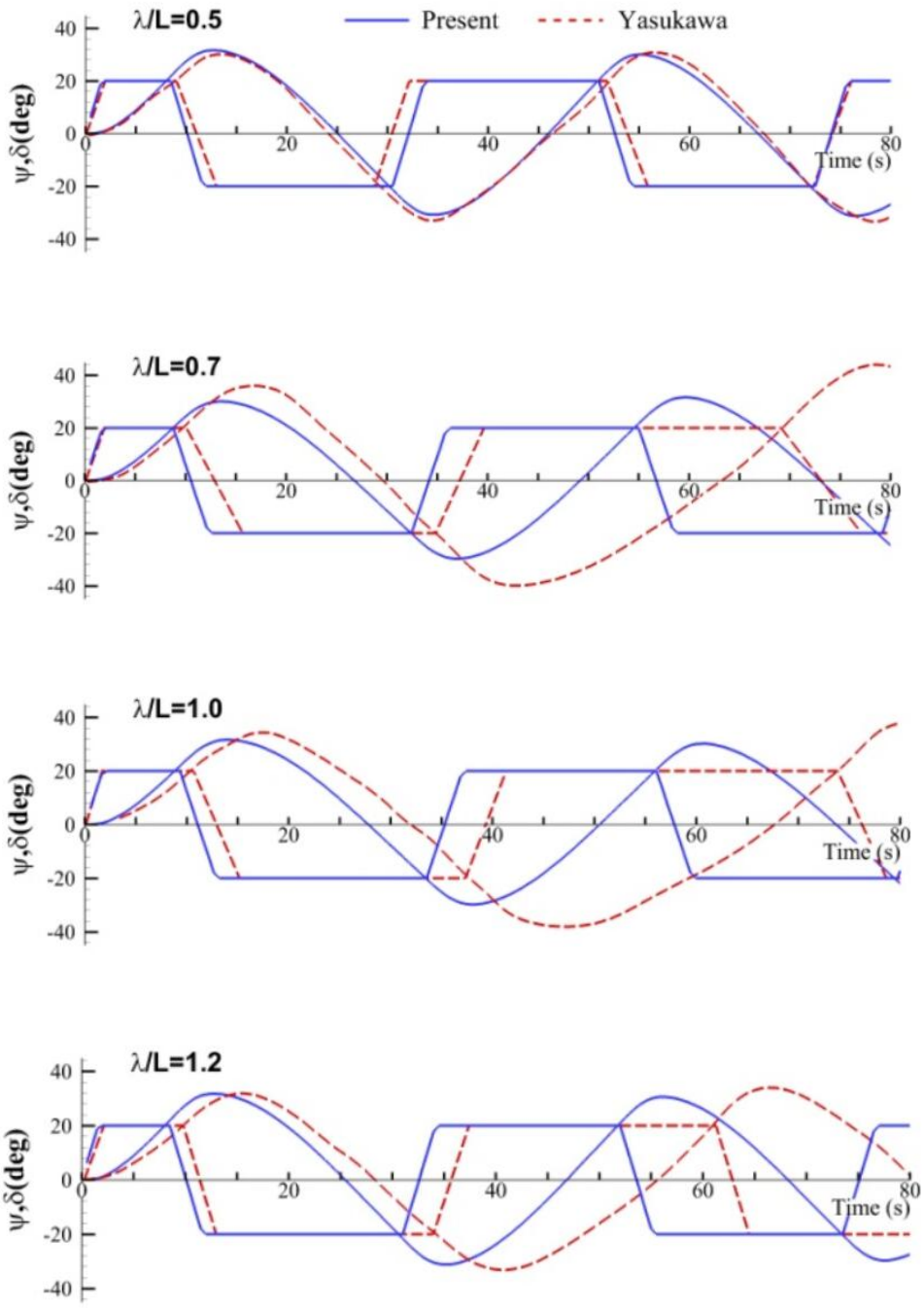

Fig. 6.18 Time histories of rudder and heading angles during 20º/20º Zig-zag of the S175 in head sea

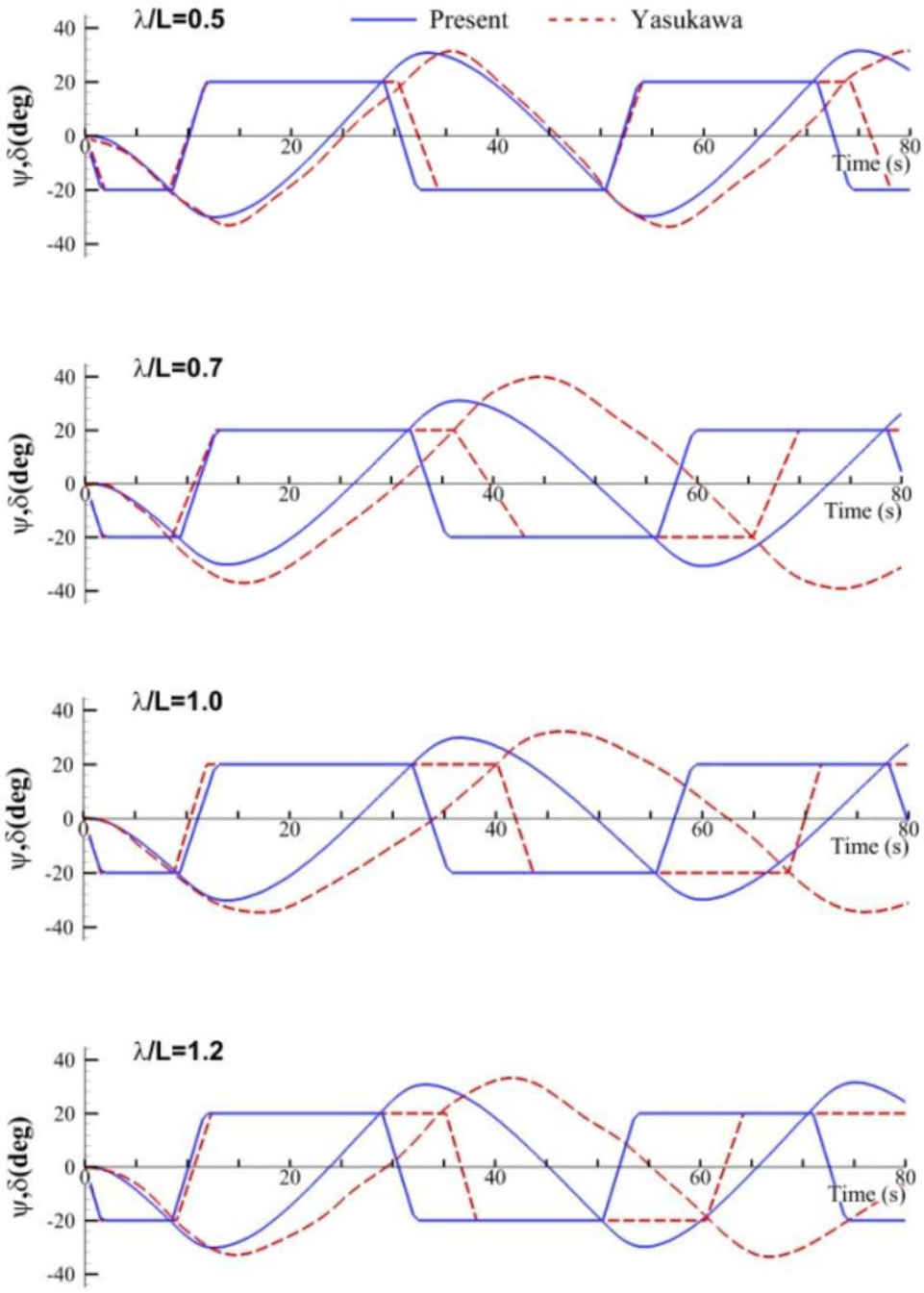

Fig. 6.19 Time histories of rudder and heading angles during -20^o/-20^o Zig-zag of the S175 in head sea

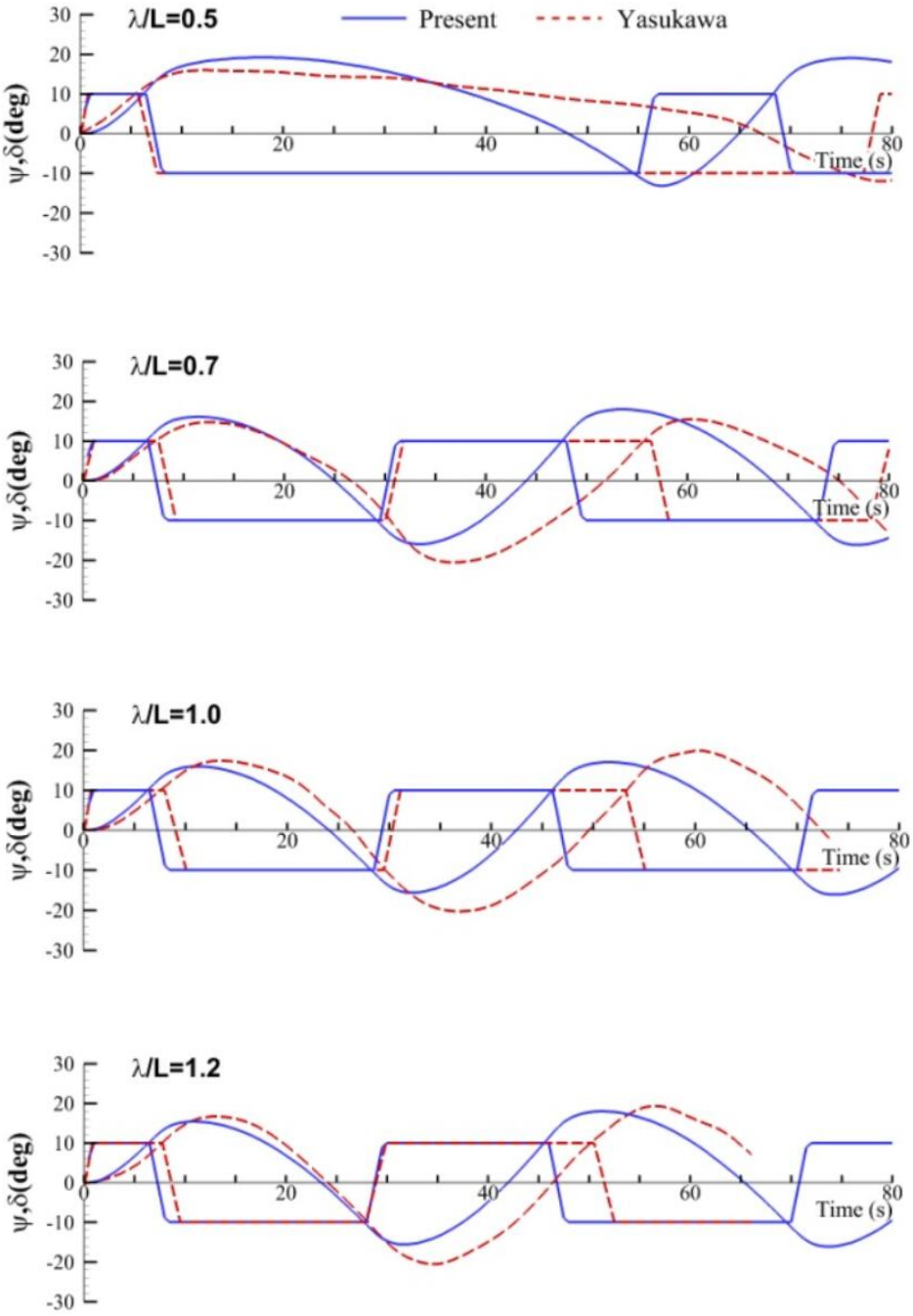

Fig. 6.20 Time histories of rudder and heading angles during $10^o/10^o$ Zig-zag of the S175 in beam sea

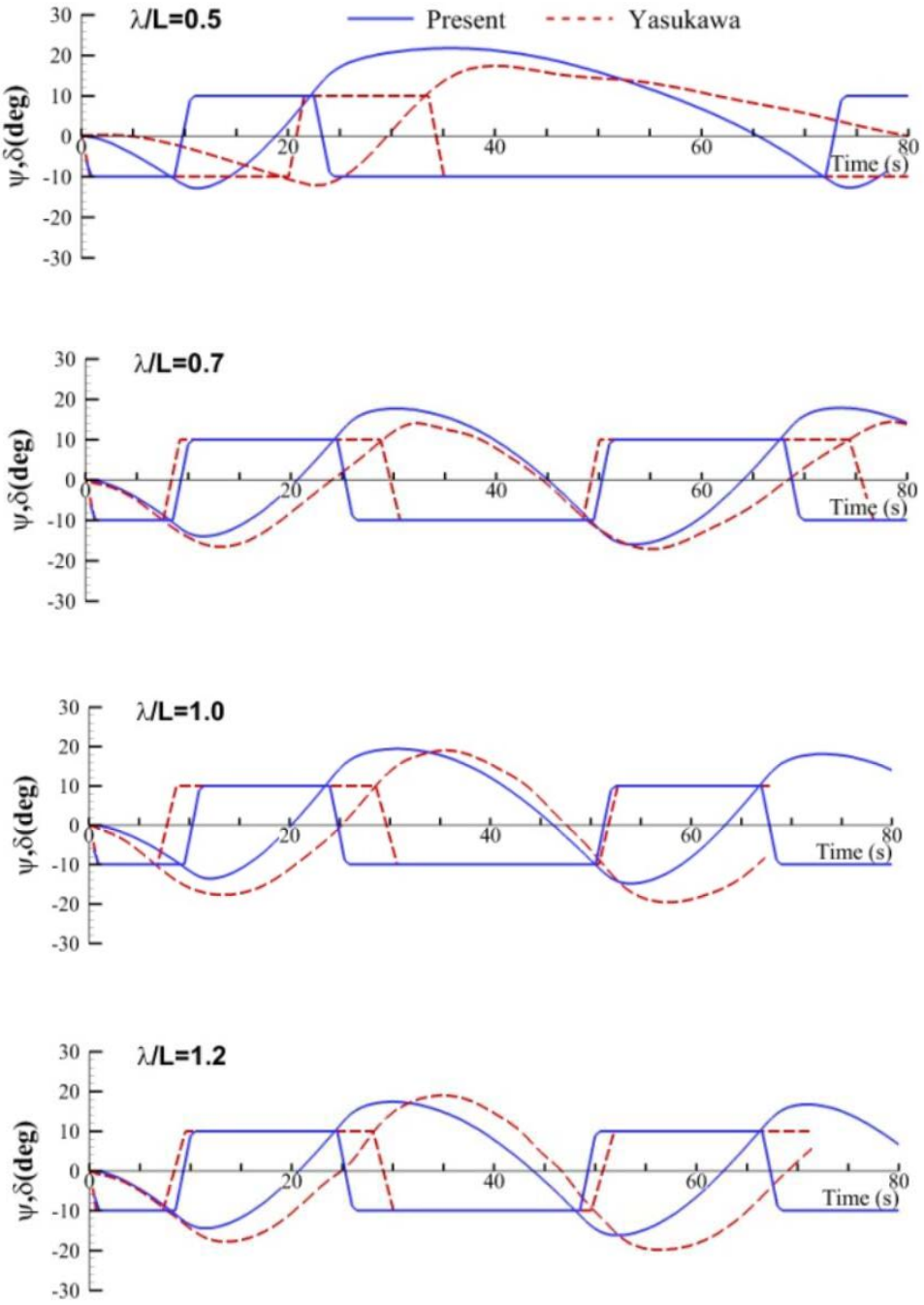

Fig. 6.21 Time histories of rudder and heading angles during -10º/-10º Zig-zag of the S175 in beam sea

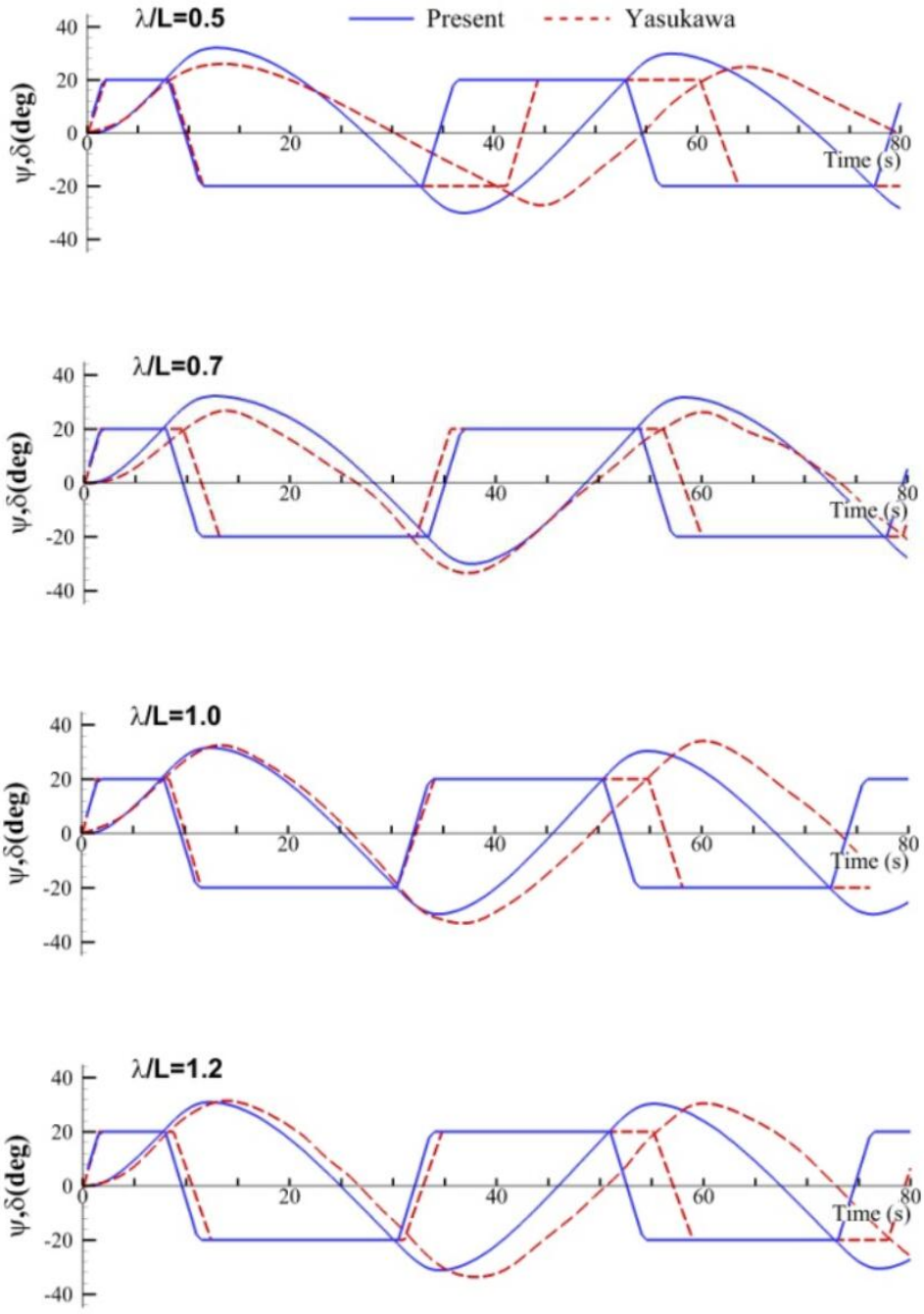

Fig. 6.22 Time histories of rudder and heading angles during 20º/20º Zig-zag of the S175 in beam sea

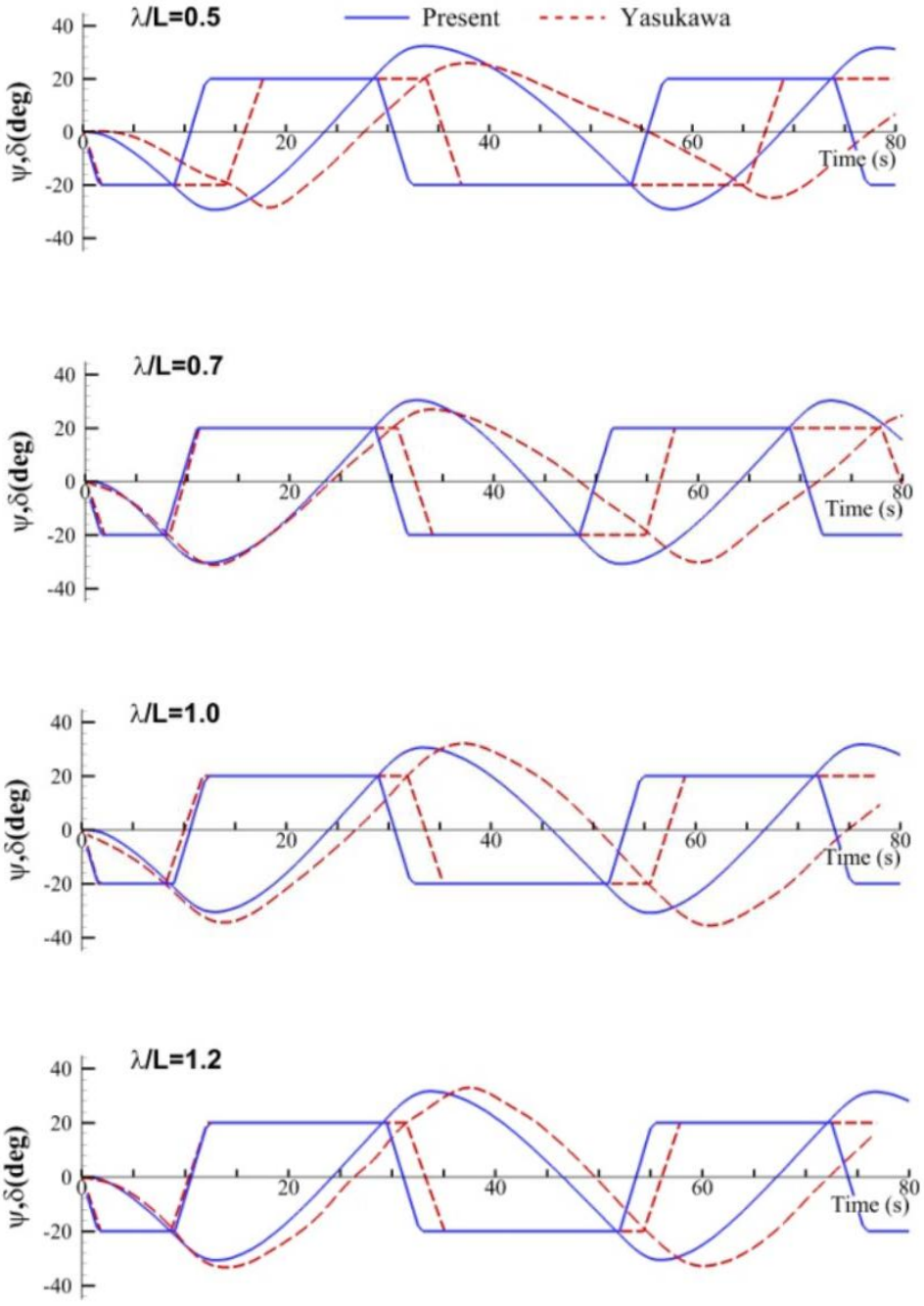

Fig. 6.23 Time histories of rudder and heading angles during -20º/-20º Zig-zag of the S175 in beam sea

6.6 Summary of the chapter

In this chapter, the two time scales model is introduced for the combined seakeeping and manoeuvring analysis. The formation of the manoeuvring equation system is first established in a body fixed frame. Then, the external forces and moments acting on the ship are divided into several components based on the modular concept. The hull force, resistance, propeller force, rudder force and mean wave drift force are modeled as separate modules by allowing possibility to replace or update the existing numerical procedures in a module without affecting the other modules. The theoretical or semi-empirical methods covering the force components are employed with details presented. These methods are commonly used within the manoeuvring research field. Special attention is paid on the derivation of the mean wave drift force according to perturbation expansion. Finally, the computational algorithm for the whole simulation system is illustrated by a flow chart.

Validations of the system are carried out on the S175 manoeuvring in calm water and waves with different incident angles and wavelengths. Validations of the mean second order wave loads are also carried out on the S175 in head and beam sea respectively. From the results, the overall satisfying agreements with the experimental results demonstrate that the present numerical simulation system for a ship manoeuvring in waves is fairly reliable. However, further improvements are required to increase the accuracy of the simulations.

7 Conclusions and future works

7.1 Achievements and conclusions

The behaviour of a single slender ship manoeuvring in regular waves is studied by numerical prediction. For this purpose, a systematic model combining the linear seakeeping analysis and the nonlinear manoeuvring analysis is developed on a two time scales approach. The approach uses the fact that the manoeuvring, in general, occurs at more slowly varying time scale than the linear wave induced ship motions. The seakeeping analysis affects the manoeuvring behaviour of a ship by introducing the regular wave effects with the slowly varying mean second order wave loads. On the other hand, the slowly time varying manoeuvring analysis affects the wave frequency problem by accounting for the changes in ship speed and wave direction during the execution of maneuver.

The seakeeping analysis on the high frequency linear wave induced motions is carried out by the developed approach based on the 2.5D theory. Rankine type singularities are applied in the BEM to solve the established 2D BVPs in each cross station plane along the ship length direction. The contours of body plans and the unknown variables on the boundary are accurately expressed with the help of the modelling tool, i.e., NURBS. The BVPs are solved by a time stepping procedure from the bow to stern with the kinematic and dynamic conditions on the free surface implemented in a finite difference scheme and the radiation condition on the open boundary fulfilled by a second order MTF scheme. Viscous correction on the roll damping is taken into account by adopting a set of semi-empirical formulae. Approximation for lift force in lateral motion are addressed indirectly with the help of the slender wing theory and the low aspect ratio wing theory.

Validation of the NURBS modelling tool is implemented on a unit circle, two Wigley hulls and two real ship types, i.e., Series 60 ship and S175 container ship. The satisfactory results of the plotted contours demonstrate the tool is perfect for geometry representing. Then, the 2.5D approach based on the NURBS is validated by solving

the radiation problem and the diffraction problem on the Wigley III and the Series 60 ship. Furthermore, the S175 container ship is used for the validation of the free ship motions in waves. From all the above validation results, the present developed 2.5D NURBS based BEM tool is reliable for the seakeeping analysis of a slender ship advancing in waves with forward speed.

Regarding the manoeuvring analysis, the motion equations are established in a body fixed coordinate system with the external forces and moments acting on the ship been treated under the modular concept. The linear manoeuvring derivatives required in the analysis can be taken care of by the 2.5D seakeeping analysis tool with the rigid wall free surface condition. Semi-empirical or empirical methods commonly used within the manoeuvring research field are employed to cover the estimation of resistance on the hull, thrust from the propeller and the steering force from the rudder. The mean wave drift loads are accounted for by the direct pressure integration based on the first order velocity potential already obtained in the seakeeping analysis of the linear wave induced motions. According to the validation on the S175 container ship advancing in head sea and beam sea, the present numerical tool can give reasonable estimated values for the mean wave drift loads.

Finally, the developed system based on the two time scales model is applied on two scaled S175 ship models to investigate their manoeuvring characteristics under imposed regular deep water wave conditions. The simulations of two typical standard maneuvers, namely turning circle and Zig-zag maneuvers, in calm water and in regular wave field are carried out. The obtained calm water results concerning the ship's trajectory and selected manoeuvring parameters are compared with available experimental measurements. Good agreement is achieved. Then, by keeping the same simulation conditions, the regular waves at different incident angles and wavelengths are imposed. Generally speaking, all the numerical simulations are satisfactory by comparing with the experimental measurements. A common fact of incident waves having a significant influence on the manoeuvring performance of a ship is captured by the present simulations. Relatively better results are obtained in the turning circle tests and can catch the tendency of the drifting in the maneuvers, while some differences are observed in the Zig-zag maneuvers. In comparison with the cases in the head sea state, Zig-zag maneuvers in beam sea show more promising results.

According to the presented work, the main objectives of the subject have been achieved which providing a practical numerical tool to study the behaviour of a slender ship manoeuvring in waves and can be considered as a basic platform for the further study in the relative field.

7.2 Recommendations for Future work

Due to the complexity of the problem and time constraint, the present work has just completed a slice of the whole subject. There are several things which should be done in order to make a better analysis of a manoeuvring ship in seaway.

Firstly, the 2.5D theory applied in the present work is a classical 5-DOF theory for a single hull same as the strip theories which neglects the surge mode. Although the surge mode is considered to be negligible in context of the seakeeping analysis, it will be required to investigate its influence on the manoeuvring behaviour of a ship in waves concerning in particular the involuntary speed reduction and ship trajectory. Secondly, the present study is still in the scope of the linear potential flow theory such as the model does not account for the instantaneous wetted surface of the hull and the influence of the steady flow on the unsteady flow is also neglected. Considering these effects will improve the accuracy of the predictions. Further, an accurate evaluation of the mean second order wave loads is important. On one hand, contribution from the second order velocity potential is suggested to be included. On the other hand, scenario of a ship manoeuvring in a sea state where the wavelength is shorter than the sectional beam requires a more adequate method for the mean wave drift loads evaluation as the reflection of the incident wave plays an important role. Moreover, the present study only take into account the wave effects on the bare hull, whereas neglect the influence on the propeller and rudder. This leads to the improper estimations of the propulsive efficiency and steering ability especially in the head sea condition.

The ultimate improvement of the present model can be achieved by using a 3D approach even a CFD method in solving the low frequency lateral motions instead of the 2.5D approach. Although, it is well known that a 3D approach will be time consuming, it will fundamentally make up the deficiencies of the 2.5D approach in

dealing with the 3D effects such as the lift force problem provided the computational time problem can be overcome in the future.

Finally, the present model should be extended to include the shallow water effects in order to be able to simulate ship maneuvers in waters of restricted depth. In addition, wind, current and irregular waves are also in the range of consideration for the next step work.

Appendix A: Estimations of the equivalent roll damping components

Bilge keel damping

Bilge keel damping is usually the largest component in the roll damping which contributes more than 50% of the total value. It can be divided into two components, i.e., the normal force component B_{BKN} and the hull pressure component B_{BKH}. Both components are created by the same vortices from the edge of bilge keels. The former one is created by the force acting on bilge keels, and the latter by the pressure over the hull surfaces in front and back sides of the bilge keel. They can be estimated as follow.

$$B_{BKN} = \int_{L_b} \frac{8}{3\pi} \rho r_b^3 b_{BK} \omega_e \phi_a f^2 \left(22.5 \frac{b_{BK}}{\pi r_b \phi_a f} + 2.4 \right) dl \tag{A.1}$$

$$B_{BKH} = \int_{L_b} \frac{4}{3\pi} \rho r_b^2 D_s^2 \omega_e \phi_a f^2 \left[-\left(-22.5 \frac{b_{BK}}{\pi r_b f \phi_a} - 1.2 \right) A_{coeff} + 1.2 B_{coeff} \right] dl \tag{A.2}$$

where,

$$\begin{cases} r_b = D_s \sqrt{\left(H_0 - 0.293 \frac{R_b}{D_s} \right)^2 + \left(1 - \frac{\overline{OG}}{D_s} - 0.293 \frac{R_b}{D_s} \right)^2} \\ f = 1 + 0.3 e^{-160(1-\sigma)} \\ H_0 = \frac{B_s}{2D_s},\ \sigma = \frac{A_{\sec}}{B_s D_s} \\ R_b = \begin{cases} 2D_s \sqrt{\frac{H_0(\sigma - 1)}{\pi - 4}} & for\ R_b < D_s, R_b < \frac{B_s}{2} \\ D_s & for\ H_0 \geq 1, \frac{R_b}{D_s} > 1 \\ \frac{B_s}{2} & for\ H_0 < 1, \frac{R_b}{D_s} > H_0 \end{cases} \end{cases} \tag{A.3}$$

ρ is the density of the fluid, ω_e is the frequency of excitation equal to the encounter frequency in waves. B_s, D_s are the breadth and the draft of the underwater cross section under consideration respectively, L_b is the length of the bilge keel. $\overline{OG}$ is the distance between the roll center of the ship and the center of gravity. b_{BK} is the breadth of the bilge keel and r_b is the mean distance from the roll axis to the bilge keel. ϕ_a is the roll amplitude, R_b is the bilge radius. H_0, σ represent the half the beam draft ratio and area coefficient at the underwater cross section under consideration respectively. Furthermore,

$$\begin{cases} A_{coeff} = (m_3 + m_4) m_8 - m_7^2 \\ B_{coeff} = \dfrac{m_3^2}{3(H_0 - 0.215 m_1)} + \dfrac{(1-m_1)^2 (2m_3 - m_2)}{6(1-0.215 m_1)} + (m_3 m_5 + m_4 m_6) m_1 \end{cases} \tag{A.4}$$

$$\begin{cases} m_1 = \dfrac{R_b}{D_s} \\ m_2 = \dfrac{\overline{OG}}{D_s} \\ m_3 = 1 - m_1 - m_2 \\ m_4 = H_0 - m_1 \\ m_5 = \dfrac{0.414 H_0 + 0.0651 m_1^2 - (0.382 H_0 + 0.0106) m_1}{(H_0 - 0.215 m_1)(1 - 0.215 m_1)} \\ m_6 = \dfrac{0.414 H_0 + 0.0651 m_1^2 - (0.382 + 0.0106 H_0) m_1}{(H_0 - 0.215 m_1)(1 - 0.215 m_1)} \\ m_7 = \begin{cases} \dfrac{L_0'}{D_s} - 0.25\pi m_1 & for\ L_0' > 0.25\pi R_b \\ 0 & otherwise \end{cases} \\ m_8 = \begin{cases} m_7 + 0.414 m_1 & for\ L_0' > 0.25\pi R_b \\ m_7 + m_1 \sqrt{2} \left[1 - \cos\left(\dfrac{L_0'}{R_b} \right) \right] & otherwise \end{cases} \end{cases} \tag{A.5}$$

where L_0' is the constant pressure distribution length given by

$$L_0' = 0.3\pi\, fr_b \phi_a + 1.95 b_{BK} \tag{A.6}$$

Eddy damping

Eddy damping is estimated by

$$B_E = \left[\frac{\left(0.04\omega_e L/U\right)^2}{1+\left(0.04\omega_e L/U\right)^2}\right]\cdot \int_L \frac{4}{3\pi}\rho D^2 \omega_e \phi_a r_{\max}^2 C_p \left\{\left(1-f_1\frac{R_b}{D_s}\right)\left(1-\frac{\overline{OG}}{D_s}-f_1\frac{R_b}{D_s}\right)+f_2\left(H_0-f_1\frac{R_b}{D_s}\right)^2\right\}dl \tag{A.7}$$

where,

$$\begin{cases} f_1 = \frac{1}{2}\left[1+\tanh\left\{20\left(\sigma-0.7\right)\right\}\right] \\ f_2 = \frac{1}{2}\left(1-\cos\pi\sigma\right)-1.5\left(1-e^{-5(1-\sigma)}\right)\sin^2\pi\sigma \\ C_p = \frac{1}{2}\left(0.87e^{-\gamma}-4e^{-0.187\gamma}+3\right) \end{cases} \tag{A.8}$$

The relative velocity ratio γ is estimated by

$$\gamma = \frac{\sqrt{\pi}\,f_3}{2D_s\left(1-\frac{\overline{OG}}{D_s}\right)\sqrt{H_0'\sigma'}}\left(r_{\max}+\frac{2M_s}{H_s}\sqrt{a^2+b^2}\right) \tag{A.9}$$

where

$$\begin{cases} H_0' = \frac{H_0 D_s}{D_s-\overline{OG}};\sigma' = \frac{\sigma D_s-\overline{OG}}{D_s-\overline{OG}} \\ f_3 = 1+4e^{-1.65\times10^5(1-\sigma)^2} \\ a = -2a_3\cos5\psi'+a_1\left(1-a_3\right)\cos3\psi'+\left[\left(6-3a_1\right)a_3^2+\left(a_1^2-3a_1\right)a_3+a_1^2\right]\cos\psi' \\ b = -2a_3\sin5\psi'+a_1\left(1-a_3\right)\sin3\psi'+\left[\left(6+3a_1\right)a_3^2+\left(a_1^2+3a_1\right)a_3+a_1^2\right]\sin\psi' \\ H_s = 1+a_1^2+9a_3^2+2a_1\left(1-a_3\right)\cos2\psi'-6a_3\cos4\psi' \\ M_s = \frac{B_s}{2\left(1+a_1+a_3\right)} \\ r_{\max} = M_s\sqrt{\left[\left(1+a_1\right)\sin\psi'-a_3\sin3\psi'\right]^2+\left[\left(1-a_1\right)\cos\psi'+a_3\cos3\psi'\right]^2} \end{cases} \tag{A.10}$$

The value of ψ' is determined by

$$\psi' = \begin{cases} \psi_1' = 0 & for\ r_{\max}(\psi_1') \geq r_{\max}(\psi_2') \\ \psi_2' = \frac{1}{2}\cos^{-1}\frac{a_1(1+a_3)}{4a_3} & otherwise \end{cases} \tag{A.11}$$

The coefficient a_1, a_3 are the Lewis form parameters corresponding to the modified cylinder which can be determined according to the formulae given in the manual by Journée & Adegeest (2003).

Friction damping

Friction damping is estimated by

$$B_F = \frac{4}{3\pi}\rho S_0 r_f^3 \phi_a \omega_e C_f \left(1 + 4.1\frac{U}{\omega_e L}\right) \tag{A.12}$$

where,

$$\begin{cases} C_f = 1.328\sqrt{\dfrac{2\pi\nu}{3.22 r_f^2 \phi_a^2 \omega_e}} \\ r_f = \dfrac{1}{\pi}\left[(0.887 + 0.145C_B)\dfrac{S_0}{L} - 2\overline{OG}\right] \\ S_0 = L(1.7D + C_B B) \end{cases} \tag{A.13}$$

L, B, D are the length, the breath and draft of the ship respectively, C_B is the block coefficient of the ship. C_f is the friction coefficient, r_f is the effective bilge radius, S_0 is the empirically estimated wetted surface area. ν is the kinematic viscosity of fluid.

Lift damping

Lift damping is estimated by

$$B_L = 0.075\rho ULD^3 k_N \left[1 - 2.8\frac{\overline{OG}}{D} + 4.667\left(\frac{\overline{OG}}{D} \right)^2 \right] \tag{A.14}$$

where,

$$k_N = 2\pi \frac{D}{L} + \kappa' \left(4.1\frac{B}{L} - 0.045 \right) \tag{A.15}$$

$$\begin{cases} \kappa' = 0.0 \quad for\ C_M \le 0.92 \\ \kappa' = 0.1 \quad for\ 0.92 < C_M \le 0.97 \\ \kappa' = 0.3 \quad for\ 0.97 < C_M \le 0.99 \end{cases} \tag{A.16}$$

C_M represents the midship cross section coefficient.

Appendix B: Fundamental algorithms for NURBS curve

Since only the contours of ship's cross sections are needed to be modeled for the 2D boundary value problem analysis in present study, the algorithms for 2D NURBS curve are presented.

Evaluation of the curve

In brief, the evaluation problem of NURBS, which is to plot a curve with a set of control points and corresponding weight factors already known, can be achieved directly by the recursion formulae (5.8) and the definition expression (5.12) with stable results. However, for a degree *k* curve, this method requires to call the recursion formulae $(2^{k-1}-1)$ times for one basis function $N_{i,k}(u)$. And for each point on the curve, values of $(k+1)$ basis functions are needed to be given, then leads to a total $(k+1)(2^{k-1}-1)$ times calculations of the formulae thus results in low computational efficiency relatively. An alternative to reduce calculation amount is using the *de Boor* algorithm for B-spline which could also be applied to NURBS according to the homogeneous coordinate expression as follow.

$$\begin{aligned} Q(u) &= H\left\{P(u)\right\} = H\left\{\sum_{i=0}^{n} D_i N_{i,k}(u)\right\} \\ &= H\left\{\sum_{i=j-k}^{j-l} D_i^l N_{i,k-l}(u)\right\} = \ldots = H\left\{D_{j-k}^k\right\}, u \in [u_j, u_{j+1}] \subset [u_k, u_{n+1}] \end{aligned} \tag{B.1}$$

where,

$$\begin{cases} D_i^l = \begin{cases} D_i & l = 0 \\ (1-a_i^l)D_i^{l-1} + a_i^l D_{i+1}^{l-1} & i = j-k, j-k+1, \ldots, j-l; l = 1,2,\ldots,k \end{cases} \\ a_i^l = \dfrac{u-u_{i+l}}{u_{i+k+1}-u_{i+l}} \\ define \dfrac{0}{0} = 0 \end{cases} \tag{B.2}$$

Derivatives of the curve

The differentiability of NURBS or B-spline are essential for curve modelling to fulfill the smoothness requirement at the first place which refers to the derivatives of the curve. Similar to the above, there are also two ways for the derivatives, the direct one and one based on *de Boor* algorithm. Firstly, rewrite the definition expression (5.12) as follow.

$$Q(u)=\frac{\sum_{i=0}^{n} w_i d_i N_{i,k}(u)}{\sum_{i=0}^{n} w_i N_{i,k}(u)}=\frac{A(u)}{w(u)} \tag{B.3}$$

Here, $A(u)$ and $w(u)$ can be considered as two special B-splines. Then, the m-th order derivative of the curve can be presented according to *Leibniz*'s rule.

$$Q^{(m)}(u)=\frac{A^{(m)}(u)-\sum_{i=1}^{m}\binom{m}{i} w^{(i)} Q^{(m-i)}(u)}{w(u)} \tag{B.4}$$

where, following iterative formulae are applied directly.

$$\begin{cases} w^{(m)}(u)=\sum_{i=0}^{n} N_{i,k}^{(m)}(u) w_i \\ A^{(m)}(u)=\sum_{i=0}^{n} N_{i,k}^{(m)}(u) w_i d_i \\ N_{i,k}^{(m)}(u)=k\left(\frac{N_{i,k-1}^{(m-1)}(u)}{u_{i+k}-u_i}-\frac{N_{i+1,k-1}^{(m-1)}(u)}{u_{i+k+1}-u_{i+1}}\right) \\ \binom{m}{i}=\frac{m!}{(m-i)!i!}=\binom{m-1}{i}+\binom{m-1}{i-1} \end{cases} \tag{B.5}$$

Particularly, the first order derivative of NURBS is

$$Q'(u)=\frac{\sum_{i=0}^{n} w_i N_{i,k}(u)\sum_{i=0}^{n} w_i d_i N'_{i,k}(u)-\sum_{i=0}^{n} w_i N'_{i,k}(u)\sum_{i=0}^{n} w_i d_i N_{i,k}(u)}{\left(\sum_{i=0}^{n} w_i N_{i,k}(u)\right)^2} \tag{B.6}$$

On the other hand, based on *de Boor* algorithm, the formula for r-th order derivatives of B-spline can be derived.

$$P^{(r)}(u) = \frac{d^r}{du^r}\sum_{i=0}^{n} d_i N_{i,k}(u) = \sum_{i=j-k}^{j-r} d_i^r N_{i,k-r}(u), u \in [u_j, u_{j+1}] \subset [u_k, u_{n+1}] \tag{B.7}$$

$$d_i^l = \begin{cases} d_i & l = 0 \\ (k-l+1)\dfrac{d_{i+1}^{l-1} - d_i^{l-1}}{u_{i+k+1} - u_{i+l}} & i = j-k, j-k+1, \ldots, j-r; l = 1, 2, \ldots, k \end{cases} \tag{B.8}$$

As shown, the r-th order derivatives of degree k B-spline is reduced to $(k-r)$ degree. Keep this in mind and further consider the NURBS, we can similarly derive

$$\begin{cases} D_i^m = \begin{cases} w_i d_i & m = 0 \\ \dfrac{k-m+1}{u_{i+k+1} - u_{i+m}}(w_{i+1}^{m-1} d_{i+1}^{m-1} - w_i^{m-1} d_i^{m-1}) & m > 0 \end{cases} \\ w_i^m = \begin{cases} w_i & m = 0 \\ \dfrac{k-m+1}{u_{i+k+1} - u_{i+m}}(w_{i+1}^{m-1} - w_i^{m-1}) & m > 0 \end{cases} \end{cases} \tag{B.9}$$

Replace the terms in the formula (B.7) with (B.9), $A^{(m)}(u)$ and $w^{(m)}(u)$ can be derived instead of using the iterative formulae (B.5). Then the derivatives of NURBS can also be given by formula (B.4).

Curve fitting

In practical ship design, coordinates of discrete data points on the ship profiles are usually provided instead of control points which are mostly not on the profiles. Then a curve fitting procedure is necessary to create a demanded NURBS or B-spline curve through all these data points. Therefore, to derive the control points of the convex polygon would be the key step. This step can also be called as inverse computation which requires boundary conditions and parameterization of the data points. Normally, cubic curve is fairly enough for modelling application.

According to the relation shown in Fig. 5.3, in order to let the curve pass through the given data points $q_i (i = 0,1,\cdots,n)$, $(n+3)$ control points $d_j (j = 0,1,\cdots,n+2)$ are required with the knot vector $\boldsymbol{u} = [u_0, u_1, \cdots u_i, \cdots u_{n+6}] \subset [0,1]$. Firstly, the multiplicities at both ends of the knot vector should be 4 to ensure the first and last control points are coincide with the endpoints of the curve, which implies $u_0 = u_1 = u_2 = u_3 = 0$, $u_{n+3} = u_{n+4} = u_{n+5} = u_{n+6} = 1$. Other internal knots can be determined by adopting certain parameterization method. To be specific, there are four parameterization methods, i.e., uniform, accumulating chord length, centripetal and Foley's as introduced by Piegl & Tiller (1997). In present study, the accumulating chord length parameterization is chosen because it is believed that it can reflect the geometric distribution of the data points more accurately. In this way, the knots spacing is proportional to the distance between the points. Thus,

$$\begin{cases} v_0 = 0 \\ v_i = v_{i-1} + \dfrac{|q_i - q_{i-1}|}{D}, i = 1,\cdots,n-1 \\ v_n = 1 \end{cases} \tag{B.10}$$

where knots $u_0 = u_1 = u_2 = u_3 = v_0 = 0$, $u_{n+3} = u_{n+4} = u_{n+5} = u_{n+6} = v_n = 1$, and $u_i = v_{i-3}$, $D = \sum_{i=1}^{n} |q_i - q_{i-1}|$ represents the sum of chords length. Besides, the data points and knots have one to one correspondence, $q_i \Rightarrow u_{i+3}, i = 0,\cdots,n$.

With the help of the homogeneous coordinate expression, the inverse computation can be transferred into non-rational B-spline category again. In addition, because of the local control property, only 4 adjacent control points would affect the value of the point on the curve. In this way, the point on the corresponding B-spline in 3D space can be expressed as follow.

$$P(u) = \sum_{j=i-3}^{i} D_j N_{j,3}(u), i = 3,\cdots,n+2 \tag{B.11}$$

Substituting the weighted data points $P_i = \left[h_i q_i, h_i\right](i = 0,1,\cdots,n)$ with their weight factors h_i already known into expression (B.11), $(n+1)$ linear equations can be established as follow.

$$\begin{cases} P(u_{i+3}) = \sum_{j=i}^{i+3} D_j N_{j,3}(u_{i+3}) = P_i, u \in [u_{i+3}, u_{i+4}] \subset [u_3, u_{n+3}], i = 0,1,\cdots,n-1 \\ P(u_{n+3}) = \sum_{j=n-1}^{n+2} D_j N_{j,3}(u_{n+3}) = P_n \end{cases} \tag{B.12}$$

Besides, for an open curve, end points conditions, $D_0 = P_0, D_{n+2} = P_n$, should be fulfilled as mentioned above. Therefore, the linear equations can be further expressed in matrix form as follow.

$$n+1\left\{\begin{bmatrix} 1 & & & & & \\ N_{1,3}(u_4) & N_{2,3}(u_4) & N_{3,3}(u_4) & N_{4,3}(u_4) & & \\ & \ddots & \ddots & \ddots & & \\ & N_{n-1,3}(u_{n+2}) & N_{n,3}(u_{n+2}) & N_{n+1,3}(u_{n+2}) & N_{n+2,3}(u_{n+2}) & \\ & & & & & 1 \end{bmatrix}\right. \begin{bmatrix} D_0 \\ D_1 \\ \vdots \\ D_n \\ D_{n+1} \\ D_{n+2} \end{bmatrix} = \begin{bmatrix} P_0 \\ P_1 \\ \vdots \\ P_n \end{bmatrix} \tag{B.13}$$

However, $(n+1)$ equations cannot uniquely determine $(n+3)$ unknowns, two more boundary conditions should be added which leads to specific requirements at the endpoints such as clamped ends, natural ends, parabolically terminated, virtual knots or so called not-a-knot. According to the transverse profiles of ships to be modelled, the parabolically terminated and the clamped ends conditions are adopted here respectively. For the mathematical ship types, the parabolically terminated condition is selected, while the clamped ends condition is suitable for real ships with straight line ends.

For the parabolically terminated condition or so called Bezier condition, the tangent vectors should be determined as follow.

$$\begin{cases} \dot{P}_0 = 2\dfrac{\Delta P_0}{\Delta_3} - \dot{P}_1 = 2\dfrac{P_1 - P_0}{u_4} - \dot{P}_1 \\ \dot{P}_n = 2\dfrac{\Delta P_{n-1}}{\Delta_{n+2}} - \dot{P}_{n-1} = 2\dfrac{P_n - P_{n-1}}{1-u_{n+2}} - \dot{P}_{n-1} \end{cases} \tag{B.14}$$

where, $\Delta_i = u_{i+1} - u_i$, and,

$$\begin{aligned} \dot{P}_i &= \frac{\Delta_i}{\Delta_{i-1}+\Delta_i}\frac{\Delta P_{i-1}}{\Delta_{i-1}} + \frac{\Delta_{i-1}}{\Delta_{i-1}+\Delta_i}\frac{\Delta P_i}{\Delta_i} \\ &= \frac{v_{i+1}-v_i}{v_{i+1}-v_{i-1}}\frac{P_i - P_{i-1}}{v_i - v_{i-1}} + \frac{v_i - v_{i-1}}{v_{i+1}-v_{i-1}}\frac{P_{i+1}-P_i}{v_{i+1}-v_i}, \qquad i = 1 \ \ or \ \ n-1 \end{aligned} \tag{B.15}$$

On the other hand, the clamped ends condition can be given as follow.

$$\begin{cases} \dot{P}_0 = \dot{P}(u_3) = \dfrac{3}{\Delta_3}(D_1 - D_0) = \dfrac{3}{u_4}(D_1 - D_0) \\ \dot{P}_n = \dot{P}(u_{n+3}) = \dfrac{3}{\Delta_{n+2}}(D_{n+2} - D_{n+1}) = \dfrac{3}{1-u_{n+2}}(D_{n+2} - D_{n+1}) \end{cases} \tag{B.16}$$

Note that the tangent vectors at the endpoints of the NURBS curve in 2D plane and the corresponding B-spline in 3D space have following relations according to perspective projection.

$$\begin{cases} \dot{P}_0 = \left[(w_0\dot{q}_0 + \dot{w}_0 q_0), \dot{w}_0\right] \\ \dot{P}_n = \left[(w_{n+2}\dot{q}_n + \dot{w}_{n+2} q_n), \dot{w}_{n+2}\right] \end{cases} \tag{B.17}$$

Here, the unknown first order derivatives $\dot{w}_0, \dot{w}_{n+2}$ can be derived by interpolating the B-spline $w(u)$ with the weight factors h_i of the data points firstly, and then calculating its derivatives by the *de Boor* algorithm introduced before.

Assuming the clamped ends condition is chosen, the matrix equations can be rewritten as follow finally by combining (B.13) and (B.16) without the first and last control points for $D_0 = P_0, D_{n+2} = P_n$ already applied, that is,

$$\begin{bmatrix} 1 & & & & \\ a_2 & b_2 & c_2 & & \\ & \ddots & \ddots & \ddots & \\ & & a_n & b_n & c_n \\ & & & & 1 \end{bmatrix} \begin{bmatrix} D_1 \\ D_2 \\ \vdots \\ D_n \\ D_{n+1} \end{bmatrix} = \begin{bmatrix} e_1 \\ e_2 \\ \vdots \\ e_n \\ e_{n+1} \end{bmatrix} \tag{B.18}$$

where,

$$\begin{cases} a_i = \dfrac{(\Delta_{i+2})^2}{\Delta_i + \Delta_{i+1} + \Delta_{i+2}} = \dfrac{(u_{i+3} - u_{i+2})^2}{u_{i+3} - u_i} \\ b_i = \dfrac{\Delta_{i+2}(\Delta_i + \Delta_{i+1})}{\Delta_i + \Delta_{i+1} + \Delta_{i+2}} + \dfrac{\Delta_{i+1}(\Delta_{i+2} + \Delta_{i+3})}{\Delta_{i+1} + \Delta_{i+2} + \Delta_{i+3}} \\ \quad = \dfrac{(u_{i+3} - u_{i+2})(u_{i+2} - u_i)}{u_{i+3} - u_i} + \dfrac{(u_{i+2} - u_{i+1})(u_{i+4} - u_{i+2})}{u_{i+4} - u_{i+1}} \\ c_i = \dfrac{(\Delta_{i+1})^2}{\Delta_{i+1} + \Delta_{i+2} + \Delta_{i+3}} = \dfrac{(u_{i+2} - u_{i+1})^2}{u_{i+4} - u_{i+1}} \\ e_i = (\Delta_{i+1} + \Delta_{i+2}) P_{i-1} = (u_{i+3} - u_{i+1}) P_{i-1} \\ i = 2, \cdots, n \end{cases} \tag{B.19}$$

$$\begin{cases} e_1 = P_0 + \dfrac{\Delta_3}{3} \dot{P}_0 = P_0 + \dfrac{u_4}{3} \dot{P}_0 \\ e_{n+1} = P_n - \dfrac{\Delta_{n+2}}{3} \dot{P}_n = P_n - \dfrac{1 - u_{n+2}}{3} \dot{P}_n \end{cases} \tag{B.20}$$

By solving the equations (B.18), all the weighted control points of the B-spline in 3D space can be obtained. Sequentially, the original control points of the NURBS in 2D plane can be derived by perspective projection according to the relation (5.14).

Knot insertion

The flexibility of the curve is another important desirable property for modelling. In order to increasing the flexibility of a NURBS curve or non-rational B-spline, knot insertion is an alternative way without changing the shape of the curve. It is a key basic algorithm of many advanced algorithms such as local modification, subdivision and degree elevation which will be introduced later for generating complex curves.

For a NURBS curve of degree k with $(n+1)$ control points and $(n+k+2)$ knots, inserting another knot $u \in \left[u_j, u_{j+1}\right) \subset \left[u_k, u_{n+1}\right]$, the curve can be expressed by the rational polynomial of definition with new $(n+2)$ control points.

$$Q(u) = \frac{\sum_{i=0}^{n+1} w_i^* d_i^* N_{i,k}^*(u)}{\sum_{i=0}^{n+1} w_i^* N_{i,k}^*(u)} \tag{B.21}$$

where the new control points d_i^* and weight factor w_i^* could be derived by following formulae developed from the knot insertion algorithm of B-spline curve according to the homogeneous coordinate expression and perspective projection as well. Thus,

$$\begin{cases} d_i^* = \dfrac{(1-a_i)w_{i-1}d_{i-1} + a_i w_i d_i}{(1-a_i)w_{i-1} + a_i w_i} \\ w_i^* = (1-a_i)w_{i-1} + a_i w_i \end{cases} \tag{B.22}$$

where,

$$a_i = \begin{cases} 1 & i = 0,1,\ldots, j-k \\ \dfrac{u-u_i}{u_{i+k}-u_i} & i = j-k+1, j-k+2,\ldots, j-r \\ 0 & i = j-r+1, j-r+2,\ldots, n+1 \end{cases} \tag{B.23}$$

Here, r is the multiplicity of the knot to be inserted. If the inserted knot u is a new one which means it does not lie on any existed knots, then $r = 0$; while if the inserted knot already has multiplicity p, then $r = p$.

Degree elevation

Furthermore, ship profiles would be commonly consist of straight lines, conics and free form curves together such as the transverse profiles of parallel middle body or bulbous bow. Then a uniform expression of NURBS is required to describe the combined curve precisely with degree elevation technique. In addition, degree

elevation operation can also increase the flexibility of the curve like knot insertion, it requires larger amount of calculation but without reducing the continuity of the curve.

As previous stated, the curve (5.12) has the differentiability class of C^{k-p} at a knot position with multiplicity p. Raising the curve degree to $(k+1)$, the curve should be expressed by $(k+1)$ degree B-spline basis functions. In order to keep the curve unchanged geometrically which means the differentiability class remains C^{k-p}, the multiplicity of the knot should be raised to $(p+1)$. The original knot vector has the form expressed as follow.

$$\boldsymbol{u} = \left[u_0, u_1, \ldots, u_{n+k+1}\right] = \left[\underbrace{\tau_0, \ldots, \tau_0}_{p_0}, \ldots, \underbrace{\tau_l, \ldots, \tau_l}_{p_l}\right] \tag{B.24}$$

Here, p_i represents the multiplicity of the knot τ_i which satisfies $\sum_{i=0}^{l} p_i = n+k+2$. Particularly, for the knots at the ends, $p_0 = p_l = k+1$. So after one degree elevation, the new knot vector should be

$$\boldsymbol{u}^* = \left[u_0, u_1^*, \ldots, u_{n^*+k+2}^*\right] = \left[\underbrace{\tau_0, \ldots, \tau_0}_{p_0+1}, \ldots, \underbrace{\tau_l, \ldots, \tau_l}_{p_l+1}\right] \tag{B.25}$$

with $\sum_{i=0}^{l}\left(p_i+1\right) = n^*+k+3$. Thus, the number of new unknown control points would be $(n^*+1) = (n+l+1)$. Accordingly, the new knot vector determines a set of B-spline basis functions of degree $(k+1)$, $N_{i,k+1}(u)(i = 0,1,\ldots,n+l)$. Then, the original curve can be expressed as follow.

$$Q(u) = \frac{\sum_{i=0}^{n+l} w_i^* d_i^* N_{i,k+1}(u)}{\sum_{i=0}^{n+l} w_i^* N_{i,k+1}(u)} \tag{B.26}$$

With the help of the homogeneous coordinate expression one more time, the solutions of the new control points d_i^* and weight factor w_i^* can be derived by the formulae as follow equivalent to a corner cutting process of the control polygon.

$$\begin{cases} d_i^* = \dfrac{(1-a_i)w_i d_i + a_i w_{i-1} d_{i-1}}{w_i^*} \\ w_i^* = (1-a_i)w_i + a_i w_{i-1} \end{cases} \tag{B.27}$$

where $a_i = i/(k+1), i = 0,1,\ldots,k+1$.

Appendix C: PMM tests

Planar motion mechanism (PMM) test is a kind of captive model test conducted in a long and narrow towing tank for manoeuvring hydrodynamic derivatives by using harmonic analysis.

Coordinate system and definitions

Define U_C is the speed of carriage, ω is the frequency of motion, a is the amplitude of lateral motion of the carriage. u_0, v_0, r_0 are the speed components in Earth fixed coordinate, u, v, r are the speed components in body fixed coordinate, V is the total speed of the ship ($\neq$ carriage), $\beta = -\arctan(v/u)$ is the drift angle, ψ is the heading angle, ψ_0 is the angle of velocity vector in Earth fixed coordinate, and $\psi = \psi_0 + \beta$. Then,

$$\begin{cases} x_0 = U_C t \\ y_0 = a \sin \omega t \\ \psi_0 = \arctan(a\omega \cos \omega t / U_C) = \arctan(\varepsilon \cos \omega t) \qquad define \;\; \varepsilon = a\omega / U_C \end{cases} \tag{C.1}$$

Fig. C-1 shows the four test motions usually being conducted in PMM tests.

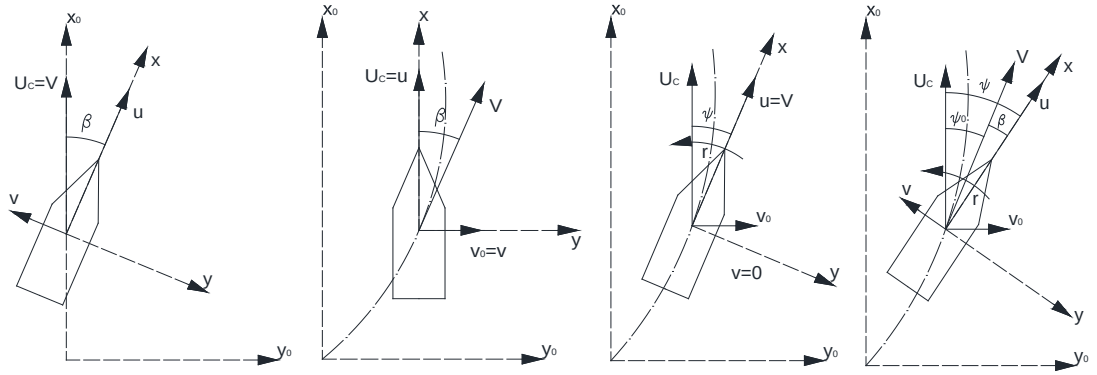

(a) (b) (c) (d)

Fig. C-1. a)Oblique towing test b)Pure sway c)Pure yaw d)Yaw plus drift

Kinematic analysis

From Fig. C-1, we can first derive the values of kinematic parameters in each coordinate system.

In earth fixed coordinate,

Table C-1.

Parameters	OTT	Pure sway	Pure yaw	Yaw plus drift
u_0	U_C	U_C	U_C	U_C
$\dot{u}_0$	0	0	0	0
v_0	0	$a\omega\cos\omega t$	$a\omega\cos\omega t$	$a\omega\cos\omega t$
$\dot{v}_0$	0	$-a\omega^2\sin\omega t$	$-a\omega^2\sin\omega t$	$-a\omega^2\sin\omega t$
r_0	0	0	$-\dfrac{\varepsilon\omega\sin\omega t}{1+\varepsilon^2\cos^2\omega t}$	$-\dfrac{\varepsilon\omega\sin\omega t}{1+\varepsilon^2\cos^2\omega t}$
$\dot{r}_0$	0	0	$-\varepsilon\omega^2\cos\omega t\dfrac{1+\varepsilon^2\left(1+\sin^2\omega t\right)}{\left(1+\varepsilon^2\cos^2\omega t\right)^2}$	$-\varepsilon\omega^2\cos\omega t\dfrac{1+\varepsilon^2\left(1+\sin^2\omega t\right)}{\left(1+\varepsilon^2\cos^2\omega t\right)^2}$

In body fixed coordinate,

Table C-2.

Parameters	OTT	Pure sway	Pure yaw	Yaw plus drift
u	$U_C\cos\beta$	U_C	$U_C\sqrt{1+\varepsilon^2\cos^2\omega t}$	$U_C\sqrt{1+\varepsilon^2\cos^2\omega t}\cos\beta$
$\dot{u}$	0	0	$-U_C\omega\dfrac{\varepsilon^2\sin 2\omega t}{2\sqrt{1+\varepsilon^2\cos^2\omega t}}$	$-U_C\omega\dfrac{\varepsilon^2\sin 2\omega t}{2\sqrt{1+\varepsilon^2\cos^2\omega t}}\cos\beta$
v	$-U_C\sin\beta$	$a\omega\cos\omega t$	0	$-U_C\sqrt{1+\varepsilon^2\cos^2\omega t}\sin\beta$
$\dot{v}$	0	$-a\omega^2\sin\omega t$	0	$U_C\omega\dfrac{\varepsilon^2\sin 2\omega t}{2\sqrt{1+\varepsilon^2\cos^2\omega t}}\sin\beta$
r	0	0	$-\dfrac{\varepsilon\omega\sin\omega t}{1+\varepsilon^2\cos^2\omega t}$	$-\dfrac{\varepsilon\omega\sin\omega t}{1+\varepsilon^2\cos^2\omega t}$
$\dot{r}$	0	0	$-\varepsilon\omega^2\cos\omega t\dfrac{1+\varepsilon^2\left(1+\sin^2\omega t\right)}{\left(1+\varepsilon^2\cos^2\omega t\right)^2}$	$-\varepsilon\omega^2\cos\omega t\dfrac{1+\varepsilon^2\left(1+\sin^2\omega t\right)}{\left(1+\varepsilon^2\cos^2\omega t\right)^2}$

However, even for the tests to determine nonlinear derivatives, the drift angle or heading angle is up to 20 degrees, so ε can still be treated as a small value, then we can omit the $O\left(\varepsilon^2\right)$ terms.

In this way, following simplified motion equations of pure yaw and yaw plus drift can be derived.

Pure yaw: $\begin{cases} u \approx U_C, \dot{u} \approx 0 \\ v = \dot{v} = 0 \\ r \approx -a\omega^2 \sin \omega t / U_C \\ \dot{r} \approx -a\omega^3 \cos \omega t / U_C \end{cases}$ Yaw plus drift: $\begin{cases} u \approx U_C \cos \beta, \dot{u} \approx 0 \\ v \approx -U_C \sin \beta, \dot{v} \approx 0 \\ r \approx -a\omega^2 \sin \omega t / U_C \\ \dot{r} \approx -a\omega^3 \cos \omega t / U_C \end{cases}$

Hydrodynamic models

Total hydrodynamic forces and moment including the inertial components are

$$\begin{cases} F_x = -m_x \dot{u} + m_y vr - Y_{\dot{r}} r^2 + X_H \\ F_y = -m_y \dot{v} - m_x ur + Y_{\dot{r}} \dot{r} + Y_H \\ M_z = -J_z \dot{r} + N_{\dot{v}} \dot{v} + Y_{\dot{r}} ur + N_H \end{cases} \tag{C.2}$$

where, $m_x = -X_{\dot{u}}, m_y = -Y_{\dot{v}}, J_z = -N_{\dot{r}}$.

Kijima model

Based on Kijima model, the viscous force components yaw moment would be

$$\begin{cases} X_H = X(u) + X_{vv} v^2 + X_{vr} vr + X_{rr} r^2 + X_{vvvv} v^4 \\ Y_H = Y_v v + Y_r r + Y_{|v|v} |v| v + Y_{|r|r} |r| r + Y_{vvr} v^2 r + Y_{vrr} vr^2 \\ N_H = N_v v + N_r r + N_{|v|v} |v| v + N_{|r|r} |r| r + N_{vvr} v^2 r + N_{vrr} vr^2 \end{cases} \tag{C.3}$$

$X(u)$ is the straight forward resistance at speed u. Therefore,

1. In oblique towing test

$$\begin{cases} F_x = X(u) + X_{vv} v^2 + X_{vvvv} v^4 \\ F_y = Y_v v + Y_{|v|v} |v| v \\ M_z = N_v v + N_{|v|v} |v| v \end{cases} \tag{C.4}$$

Conduct the test at different drift angles up to 20 degrees, then the derivatives can be obtained by the least square fit.

2. In pure sway

$$\begin{cases} F_x = X(u) + X_{vv}v^2 + X_{vvvv}v^4 \\ F_y = -m_y\dot{v} + Y_v v + Y_{|v|v}|v|v \\ M_z = N_{\dot{v}}\dot{v} + N_v v + N_{|v|v}|v|v \end{cases} \tag{C.5}$$

Substitute the motion from Table A-2 into the equations,

$$\begin{cases} F_x = X(U_C) + X_{vv}a^2\omega^2\cos^2\omega t + X_{vvvv}a^4\omega^4\cos^4\omega t \\ F_y = m_y a\omega^2\sin\omega t + Y_v a\omega\cos\omega t + Y_{|v|v}a^2\omega^2|\cos\omega t|\cos\omega t \\ M_z = -N_{\dot{v}}a\omega^2\sin\omega t + N_v a\omega\cos\omega t + N_{|v|v}a^2\omega^2|\cos\omega t|\cos\omega t \end{cases} \tag{C.6}$$

Here, we only need to consider the side force and yaw moment, as the surge force component has already been derived in oblique towing test. However, for the purpose of completeness, surge force is still given. With simple transformation, the forces and moments can be expressed as follow.

$$\begin{cases} F_x = X_0 + X_{C2}\cos 2\omega t + X_{C4}\cos 4\omega t \\ F_y = Y_0 + Y_{C1}\cos\omega t + Y_{S1}\sin\omega t + Y_{C2}\cos 2\omega t \\ M_z = N_0 + N_{C1}\cos\omega t + N_{S1}\sin\omega t + N_{C2}\cos 2\omega t \end{cases} \tag{C.7}$$

Where,

$$\begin{cases} X_0 = X(U_C) + \dfrac{X_{vv}a^2\omega^2}{2} + \dfrac{3X_{vvvv}a^4\omega^4}{8}, X_{C2} = \dfrac{X_{vv}a^2\omega^2 + X_{vvvv}a^4\omega^4}{2}, X_{C4} = \dfrac{X_{vvvv}a^4\omega^4}{8}; \\ Y_{C1} = Y_v a\omega, Y_{S1} = m_y a\omega^2; N_{C1} = N_v a\omega, N_{S1} = -N_{\dot{v}}a\omega^2; \\ for\ \ 2k\pi - \dfrac{\pi}{2} < \omega t < 2k\pi + \dfrac{\pi}{2},\ k \in Z^+ : \\ Y_0 = Y_{C2} = \dfrac{Y_{|v|v}a^2\omega^2}{2}; N_0 = N_{C2} = \dfrac{N_{|v|v}a^2\omega^2}{2} \\ for\ \ 2k\pi + \dfrac{\pi}{2} < \omega t < (2k+1)\pi + \dfrac{\pi}{2},\ k \in Z^+ : \\ Y_0 = Y_{C2} = -\dfrac{Y_{|v|v}a^2\omega^2}{2}; N_0 = N_{C2} = -\dfrac{N_{|v|v}a^2\omega^2}{2} \end{cases} \tag{C.8}$$

In order to derive all these coefficients, Fourier integration could be applied based on the characteristics of trigonometric functions, namely Fourier series. Any periodic function can be treated as linear superposition of several simple harmonic functions with different amplitudes and phrases. So it can be expressed as follow.

$$\begin{aligned} f(t) &= \frac{a_0}{2} + \sum_{n=1}^{\infty} A_n \sin\left(n\omega t + \varphi_n\right) \\ &= \frac{a_0}{2} + \sum_{n=1}^{\infty} \left(a_n \cos n\omega t + b_n \sin n\omega t\right) \end{aligned} \tag{C.9}$$

Where,

$$A_n = \sqrt{a_n^2 + b_n^2}, \sin\varphi_n = \frac{a_n}{A_n}, \cos\varphi_n = \frac{b_n}{A_n} \tag{C.10}$$

Therefore, the coefficients are derived according to following formulae.

$$\begin{cases} a_0 = \dfrac{2}{T}\displaystyle\int_0^T f(t)\,dt \\ a_n = \dfrac{2}{T}\displaystyle\int_0^T f(t)\cos n\omega t\,dt \\ b_n = \dfrac{2}{T}\displaystyle\int_0^T f(t)\sin n\omega t\,dt \end{cases} \tag{C.11}$$

Here T is the period. Choose a stable period from 0 to T including N time steps, we have $F_k = f(t_k)$; $t_k = k \cdot \Delta t$, $k = 0,1,2,\ldots,N-1$, Then the coefficients can be rewritten as follow.

$$\begin{cases} a_0 = \dfrac{2}{N}\displaystyle\sum_{k=0}^{N-1} F_k \\ a_n = \dfrac{2}{N}\displaystyle\sum_{k=0}^{N-1} F_k \cos\dfrac{2\pi kn}{N} \\ b_n = \dfrac{2}{N}\displaystyle\sum_{k=0}^{N-1} F_k \sin\dfrac{2\pi kn}{N} \end{cases} \tag{C.12}$$

Finally the derivatives can be obtained

$$
\begin{cases}
X(U_C) = X_0 - \left(\dfrac{X_{vv} a^2 \omega^2}{2} + \dfrac{3X_{vvvv} a^4 \omega^4}{8} \right), X_{vv} = \dfrac{2X_{C2} - X_{vvvv} a^4 \omega^4}{a^2 \omega^2}, X_{vvvv} = \dfrac{8X_{C4}}{a^4 \omega^4}; \\
Y_v = \dfrac{Y_{C1}}{a\omega}, m_y = \dfrac{Y_{S1}}{a\omega^2}; N_v = \dfrac{N_{C1}}{a\omega}, N_{\dot{v}} = -\dfrac{N_{S1}}{a\omega^2}; \\
\textit{choose period } 2k\pi - \dfrac{\pi}{2} < \omega t < 2k\pi + \dfrac{\pi}{2}, k \in Z^+ : \\
\int_{\frac{2k\pi - \pi/2}{\omega}}^{\frac{2k\pi + \pi/2}{\omega}} F_y(t)dt = \dfrac{2Y_{C1}}{\omega} + Y_{|v|v} \dfrac{a^2 \omega \pi}{2} \Rightarrow Y_{|v|v} = \dfrac{2\left(\int_{\frac{2k\pi - \pi/2}{\omega}}^{\frac{2k\pi + \pi/2}{\omega}} F_y(t)dt - \dfrac{2Y_{C1}}{\omega} \right)}{a^2 \omega \pi}; \\
\int_{\frac{2k\pi - \pi/2}{\omega}}^{\frac{2k\pi + \pi/2}{\omega}} M_z(t)dt = \dfrac{2N_{C1}}{\omega} + N_{|v|v} \dfrac{a^2 \omega \pi}{2} \Rightarrow N_{|v|v} = \dfrac{2\left(\int_{\frac{2k\pi - \pi/2}{\omega}}^{\frac{2k\pi + \pi/2}{\omega}} M_z(t)dt - \dfrac{2N_{C1}}{\omega} \right)}{a^2 \omega \pi}; \\
\textit{or choose period } 2k\pi + \dfrac{\pi}{2} < \omega t < (2k+1)\pi + \dfrac{\pi}{2}, k \in Z^+ : \\
\int_{\frac{2k\pi + \pi/2}{\omega}}^{\frac{2k\pi + 3\pi/2}{\omega}} F_y(t)dt = -\dfrac{2Y_{C1}}{\omega} - Y_{|v|v} \dfrac{a^2 \omega \pi}{2} \Rightarrow Y_{|v|v} = \dfrac{-2\left(\int_{\frac{2k\pi + \pi/2}{\omega}}^{\frac{2k\pi + 3\pi/2}{\omega}} F_y(t)dt + \dfrac{2Y_{C1}}{\omega} \right)}{a^2 \omega \pi}; \\
\int_{\frac{2k\pi + \pi/2}{\omega}}^{\frac{2k\pi + 3\pi/2}{\omega}} M_z(t)dt = -\dfrac{2N_{C1}}{\omega} - N_{|v|v} \dfrac{a^2 \omega \pi}{2} \Rightarrow N_{|v|v} = \dfrac{-2\left(\int_{\frac{2k\pi + \pi/2}{\omega}}^{\frac{2k\pi + 3\pi/2}{\omega}} M_z(t)dt + \dfrac{2N_{C1}}{\omega} \right)}{a^2 \omega \pi};
\end{cases} \quad \text{(C.13)}
$$

3. In pure yaw

$$
\begin{cases}
F_x = -Y_{\dot{r}} r^2 + X(u) + X_{rr} r^2 \\
F_y = -m_x u r + Y_{\dot{r}} \dot{r} + Y_r r + Y_{|r|r} |r| r \\
M_z = -J_z \dot{r} + Y_{\dot{r}} u r + N_r r + N_{|r|r} |r| r
\end{cases} \quad \text{(C.14)}
$$

Again substitute the motion from Table C-2 into the equations,

$$
\begin{cases}
F_x = -Y_{\dot{r}} a^2 \omega^4 \sin^2 \omega t / U_C^2 + X(U_C) + X_{rr} a^2 \omega^4 \sin^2 \omega t / U_C^2 \\
F_y = m_x a \omega^2 \sin \omega t - Y_{\dot{r}} a \omega^3 \cos \omega t / U_C - Y_r a \omega^2 \sin \omega t / U_C - Y_{|r|r} a^2 \omega^4 |\sin \omega t| \sin \omega t / U_C^2 \\
M_z = J_z a \omega^3 \cos \omega t / U_C - Y_{\dot{r}} a \omega^2 \sin \omega t - N_r a \omega^2 \sin \omega t / U_C - N_{|r|r} a^2 \omega^4 |\sin \omega t| \sin \omega t / U_C^2
\end{cases} \quad \text{(C.15)}
$$

According to transformation, we have

$$\begin{cases} F_x = X_0 + X_{C2}\cos 2\omega t \\ F_y = Y_0 + Y_{C1}\cos\omega t + Y_{S1}\sin\omega t + Y_{C2}\cos 2\omega t \\ M_z = N_0 + N_{C1}\cos\omega t + N_{S1}\sin\omega t + N_{C2}\cos 2\omega t \end{cases} \tag{C.16}$$

Same as the procedure used in pure sway, the derivatives can be obtained as follow.

$$\begin{cases} X(U_C) = X_0 + X_{C2}, X_{rr} = -\dfrac{2X_{C2}U_C^2}{a^2\omega^4} + Y_{\dot r}; \\ Y_{\dot r} = \dfrac{-Y_{C1}U_C}{a\omega^3}, Y_r = \dfrac{\left(m_x a\omega^2 - Y_{S1}\right)U_C}{a\omega^2}; J_z = \dfrac{N_{C1}U_C}{a\omega^3}, N_r = -\dfrac{\left(N_{S1} + Y_{\dot r}a\omega^2\right)U_C}{a\omega^2}; \\ \textit{choose period } 2k\pi < \omega t < (2k+1)\pi,\ k \in Z^+: \\ \int_{\frac{2k\pi}{\omega}}^{\frac{(2k+1)\pi}{\omega}} F_y(t)dt = \dfrac{2Y_{S1}}{\omega} - Y_{|r|r}\dfrac{a^2\omega^3\pi}{2U_C^2} \Rightarrow Y_{|r|r} = \dfrac{2U_C^2\left(\dfrac{2Y_{S1}}{\omega} - \int_{\frac{2k\pi}{\omega}}^{\frac{(2k+1)\pi}{\omega}} F_y(t)dt\right)}{a^2\omega^3\pi}; \\ \int_{\frac{2k\pi}{\omega}}^{\frac{(2k+1)\pi}{\omega}} M_z(t)dt = \dfrac{2N_{S1}}{\omega} - N_{|r|r}\dfrac{a^2\omega^3\pi}{2U_C^2} \Rightarrow N_{|r|r} = \dfrac{2U_C^2\left(\dfrac{2N_{S1}}{\omega} - \int_{\frac{2k\pi}{\omega}}^{\frac{(2k+1)\pi}{\omega}} M_z(t)dt\right)}{a^2\omega^3\pi}; \\ \textit{or choose period } (2k+1)\pi < \omega t < (2k+2)\pi,\ k \in Z^+: \\ \int_{\frac{(2k+1)\pi}{\omega}}^{\frac{(2k+2)\pi}{\omega}} F_y(t)dt = -\dfrac{2Y_{S1}}{\omega} + Y_{|r|r}\dfrac{a^2\omega^3\pi}{2U_C^2} \Rightarrow Y_{|r|r} = \dfrac{2U_C^2\left(\dfrac{2Y_{S1}}{\omega} + \int_{\frac{(2k+1)\pi}{\omega}}^{\frac{(2k+2)\pi}{\omega}} F_y(t)dt\right)}{a^2\omega^3\pi}; \\ \int_{\frac{(2k+1)\pi}{\omega}}^{\frac{(2k+2)\pi}{\omega}} M_z(t)dt = -\dfrac{2N_{S1}}{\omega} + N_{|r|r}\dfrac{a^2\omega^3\pi}{2U_C^2} \Rightarrow N_{|r|r} = \dfrac{2U_C^2\left(\dfrac{2N_{S1}}{\omega} + \int_{\frac{(2k+1)\pi}{\omega}}^{\frac{(2k+2)\pi}{\omega}} M_z(t)dt\right)}{a^2\omega^3\pi}; \end{cases} \tag{C.17}$$

4. In yaw plus drift

$$\begin{cases} F_x = m_y vr - Y_{\dot r}r^2 + X(u) + X_{vv}v^2 + X_{vr}vr + X_{rr}r^2 + X_{vvvv}v^4 \\ F_y = -m_x ur + Y_{\dot r}\dot r + Y_v v + Y_r r + Y_{|v|v}|v|v + Y_{|r|r}|r|r + Y_{vvr}v^2 r + Y_{vrr}vr^2 \\ M_z = -J_z\dot r + Y_{\dot r}ur + N_v v + N_r r + N_{|v|v}|v|v + N_{|r|r}|r|r + N_{vvr}v^2 r + N_{vrr}vr^2 \end{cases} \tag{C.18}$$

In the same manner, we have

$$
\begin{cases}
F_x = m_y a\omega^2 \sin\omega t \sin\beta - Y_r a^2\omega^4 \sin^2\omega t / U_C^2 + X(U_C \cos\beta) \\
\quad + X_{vv} U_C^2 \sin^2\beta + X_{vr} a\omega^2 \sin\omega t \sin\beta + X_{rr} a^2\omega^4 \sin^2\omega t / U_C^2 + X_{vvv} U_C^4 \sin^4\beta \\
F_y = m_x a\omega^2 \sin\omega t \cos\beta - Y_r a\omega^3 \cos\omega t / U_C \\
\quad - Y_v U_C \sin\beta - Y_r a\omega^2 \sin\omega t / U_C - Y_{|v|v} U_C^2 \left|\sin\beta\right| \sin\beta - Y_{|r|r} a^2\omega^4 \left|\sin\omega t\right| \sin\omega t / U_C^2 \\
\quad - Y_{vvr} U_C \sin^2\beta \cdot a\omega^2 \sin\omega t - Y_{vrr} \sin\beta \cdot a^2\omega^4 \sin^2\omega t / U_C \\
M_z = J_z a\omega^3 \cos\omega t / U_C - Y_r a\omega^2 \sin\omega t \cos\beta \\
\quad - N_v U_C \sin\beta - N_r a\omega^2 \sin\omega t / U_C - N_{|v|v} U_C^2 \left|\sin\beta\right| \sin\beta - N_{|r|r} a^2\omega^4 \left|\sin\omega t\right| \sin\omega t / U_C^2 \\
\quad - N_{vvr} U_C \sin^2\beta \cdot a\omega^2 \sin\omega t - N_{vrr} \sin\beta \cdot a^2\omega^4 \sin^2\omega t / U_C
\end{cases}
\tag{C.19}
$$

Then, again rewrite the equations as follow

$$
\begin{cases}
F_x = X_0 + X_{S1} \sin\omega t + X_{C2} \cos 2\omega t \\
F_y = Y_0 + Y_{C1} \cos\omega t + Y_{S1} \sin\omega t + Y_{C2} \cos 2\omega t \\
M_z = N_0 + N_{C1} \cos\omega t + N_{S1} \sin\omega t + N_{C2} \cos 2\omega t
\end{cases}
\tag{C.20}
$$

Finally, the derivatives would be

$$
\begin{cases}
X_{vr} = \dfrac{X_{S1}}{a\omega^2 \sin\beta} - m_y ; Y_{vvr} = \dfrac{m_x a\omega^2 \cos\beta - \dfrac{Y_r a\omega^2}{U_C} - Y_{S1}}{U_C \sin^2\beta \cdot a\omega^2} ; N_{vvr} = \dfrac{-N_{S1} - \left(Y_r a\omega^2 \cos\beta + \dfrac{N_r a\omega^2}{U_C} \right)}{U_C \sin^2\beta \cdot a\omega^2} ; \\
choose\ \ period\ \ 2k\pi < \omega t < (2k+1)\pi,\ k \in Z^+ : \\
\displaystyle\int_{\frac{2k\pi}{\omega}}^{\frac{(2k+1)\pi}{\omega}} F_y(t)dt = \frac{2Y_{S1}}{\omega} - \left(Y_v U_C \sin\beta + Y_{|v|v} U_C^2 \left|\sin\beta\right| \sin\beta + \frac{Y_{vrr} \sin\beta \cdot a^2\omega^4}{2U_C} + \frac{Y_{|r|r} a^2\omega^4}{2U_C^2} \right) \frac{\pi}{\omega} \\
\Rightarrow Y_{vrr} = \dfrac{2U_C\omega \left(\dfrac{2Y_{S1}}{\omega} - \displaystyle\int_{\frac{2k\pi}{\omega}}^{\frac{(2k+1)\pi}{\omega}} F_y(t)dt - \left(Y_v U_C \sin\beta + Y_{|v|v} U_C^2 \left|\sin\beta\right| \sin\beta + \dfrac{Y_{|r|r} a^2\omega^4}{2U_C^2} \right) \dfrac{\pi}{\omega} \right)}{\sin\beta \cdot a^2\omega^4\pi} ; \\
\displaystyle\int_{\frac{2k\pi}{\omega}}^{\frac{(2k+1)\pi}{\omega}} M_z(t)dt = \frac{2N_{S1}}{\omega} - \left(N_v U_C \sin\beta + N_{|v|v} U_C^2 \left|\sin\beta\right| \sin\beta + \frac{N_{vrr} \sin\beta \cdot a^2\omega^4}{2U_C} + \frac{N_{|r|r} a^2\omega^4}{2U_C^2} \right) \frac{\pi}{\omega} \\
\Rightarrow N_{vrr} = \dfrac{2U_C\omega \left(\dfrac{2N_{S1}}{\omega} - \displaystyle\int_{\frac{2k\pi}{\omega}}^{\frac{(2k+1)\pi}{\omega}} M_z(t)dt - \left(N_v U_C \sin\beta + N_{|v|v} U_C^2 \left|\sin\beta\right| \sin\beta + \dfrac{N_{|r|r} a^2\omega^4}{2U_C^2} \right) \dfrac{\pi}{\omega} \right)}{\sin\beta \cdot a^2\omega^4\pi} ;
\end{cases}
$$

$$
\begin{cases}
or\ \ choose\ \ period\ \ (2k+1)\pi < \omega t < (2k+2)\pi,\ k \in Z^+ : \\
\int_{\frac{(2k+1)\pi}{\omega}}^{\frac{(2k+2)\pi}{\omega}} F_y(t)dt = -\dfrac{2Y_{S1}}{\omega} - \left(Y_v U_C \sin\beta + Y_{|v|v} U_C^2 \left|\sin\beta\right| \sin\beta + \dfrac{Y_{vrr} \sin\beta \cdot a^2\omega^4}{2U_C} - \dfrac{Y_{|r|r} a^2\omega^4}{2U_C^2} \right) \dfrac{\pi}{\omega} \\
\Rightarrow Y_{vrr} = \dfrac{2U_C\omega \left(-\dfrac{2Y_{S1}}{\omega} - \int_{\frac{(2k+1)\pi}{\omega}}^{\frac{(2k+2)\pi}{\omega}} F_y(t)dt - \left(Y_v U_C \sin\beta + Y_{|v|v} U_C^2 \left|\sin\beta\right| \sin\beta - \dfrac{Y_{|r|r} a^2\omega^4}{2U_C^2} \right) \dfrac{\pi}{\omega} \right)}{\sin\beta \cdot a^2\omega^4\pi}; \\
\int_{\frac{(2k+1)\pi}{\omega}}^{\frac{(2k+2)\pi}{\omega}} M_z(t)dt = -\dfrac{2N_{S1}}{\omega} - \left(N_v U_C \sin\beta + N_{|v|v} U_C^2 \left|\sin\beta\right| \sin\beta + \dfrac{N_{vrr} \sin\beta \cdot a^2\omega^4}{2U_C} - \dfrac{N_{|r|r} a^2\omega^4}{2U_C^2} \right) \dfrac{\pi}{\omega} \\
\Rightarrow N_{vrr} = \dfrac{2U_C\omega \left(-\dfrac{2N_{S1}}{\omega} - \int_{\frac{(2k+1)\pi}{\omega}}^{\frac{(2k+2)\pi}{\omega}} M_z(t)dt - \left(N_v U_C \sin\beta + N_{|v|v} U_C^2 \left|\sin\beta\right| \sin\beta - \dfrac{N_{|r|r} a^2\omega^4}{2U_C^2} \right) \dfrac{\pi}{\omega} \right)}{\sin\beta \cdot a^2\omega^4\pi};
\end{cases}
\tag{C.21}
$$

3rd order polynominal model

Similarly, based on 3rd order model, the viscous side force and yaw moment would be:

$$
\begin{cases}
Y_H = Y_v v + Y_r r + Y_{vvv} v^3 + Y_{rrr} r^3 + Y_{vvr} v^2 r + Y_{vrr} v r^2 \\
N_H = N_v v + N_r r + N_{vvv} v^3 + N_{rrr} r^3 + N_{vvr} v^2 r + N_{vrr} v r^2
\end{cases}
\tag{C.22}
$$

Other force components keep the same as in the Kijima model, then

1. In oblique test

$$
\begin{cases}
F_x = X(u) + X_{vv} v^2 + X_{vvvv} v^4 \\
F_y = Y_v v + Y_{vvv} v^3 \\
M_z = N_v v + N_{vvv} v^3
\end{cases}
\tag{C.23}
$$

Again, the derivatives can be obtained by the least square fit.

2. In pure sway

$$
\begin{cases}
F_x = X(u) + X_{vv} v^2 + X_{vvvv} v^4 \\
F_y = -m_y \dot{v} + Y_v v + Y_{vvv} v^3 \\
M_z = N_{\dot{v}} \dot{v} + N_v v + N_{vvv} v^3
\end{cases}
\tag{C.24}
$$

By substituting the motion equations into the formulae

$$\begin{cases} F_x = X(U_C) + X_{vv}a^2\omega^2\cos^2\omega t + X_{vvv}a^4\omega^4\cos^4\omega t \\ F_y = m_y a\omega^2\sin\omega t + Y_v a\omega\cos\omega t + Y_{vvv}a^3\omega^3\cos^3\omega t \\ M_z = -N_{\dot{v}}a\omega^2\sin\omega t + N_v a\omega\cos\omega t + N_{vvv}a^3\omega^3\cos^3\omega t \end{cases} \quad \text{(C.25)}$$

Rewrite the formulae in following expressions.

$$\begin{cases} F_x = X_0 + X_{C2}\cos 2\omega t + X_{C4}\cos 4\omega t \\ F_y = Y_{C1}\cos\omega t + Y_{S1}\sin\omega t + Y_{C3}\cos 3\omega t \\ M_z = N_{C1}\cos\omega t + N_{S1}\sin\omega t + N_{C3}\cos 3\omega t \end{cases} \quad \text{(C.26)}$$

So the derivatives would be

$$\begin{cases} X(U_C) = X_0 - \left(\dfrac{X_{vv}a^2\omega^2}{2} + \dfrac{3X_{vvvv}a^4\omega^4}{8}\right), \\ X_{vv} = \dfrac{2X_{C2} - X_{vvvv}a^4\omega^4}{a^2\omega^2}, X_{vvvv} = \dfrac{8X_{C4}}{a^4\omega^4}; \\ Y_v = \dfrac{Y_{C1} - \dfrac{3}{4}Y_{vvv}a^3\omega^3}{a\omega}, m_y = \dfrac{Y_{S1}}{a\omega^2}, Y_{vvv} = \dfrac{4Y_{C3}}{a^3\omega^3}; \\ N_v = \dfrac{N_{C1} - \dfrac{3}{4}N_{vvv}a^3\omega^3}{a\omega}, N_{\dot{v}} = -\dfrac{N_{S1}}{a\omega^2}, N_{vvv} = \dfrac{4N_{C3}}{a^3\omega^3} \end{cases} \quad \text{(C.27)}$$

3. In pure yaw

$$\begin{cases} F_x = -Y_{\dot{r}}r^2 + X(u) + X_{rr}r^2 \\ F_y = -m_x ur + Y_{\dot{r}}\dot{r} + Y_r r + Y_{rrr}r^3 \\ M_z = -J_z\dot{r} + Y_{\dot{r}}ur + N_r r + N_{rrr}r^3 \end{cases} \quad \text{(C.28)}$$

$$\begin{cases} F_x = -Y_{\dot{r}}a^2\omega^4\sin^2\omega t/U_C^2 + X(U_C) + X_{rr}a^2\omega^4\sin^2\omega t/U_C^2 \\ F_y = m_x a\omega^2\sin\omega t - Y_{\dot{r}}a\omega^3\cos\omega t/U_C - Y_r a\omega^2\sin\omega t/U_C \\ \qquad - Y_{rrr}a^3\omega^6\sin^3\omega t/U_C^3 \\ M_z = J_z a\omega^3\cos\omega t/U_C - Y_{\dot{r}}a\omega^2\sin\omega t - N_r a\omega^2\sin\omega t/U_C \\ \qquad - N_{rrr}a^3\omega^6\sin^3\omega t/U_C^3 \end{cases} \quad \text{(C.29)}$$

Then,

$$\begin{cases} F_x = X_0 + X_{C2}\cos 2\omega t \\ F_y = Y_{C1}\cos\omega t + Y_{S1}\sin\omega t + Y_{S3}\sin 3\omega t \\ M_z = N_{C1}\cos\omega t + N_{S1}\sin\omega t + N_{S3}\sin 3\omega t \end{cases} \tag{C.30}$$

The derivatives would be

$$\begin{cases} X(U_C) = X_0 + X_{C2}, X_{rr} = -\dfrac{2U_C^2 X_{C2}}{a^2\omega^4} + Y_{\dot r}; \\ Y_{\dot r} = \dfrac{-Y_{C1}U_C}{a\omega^3}, Y_r = \dfrac{U_C}{a\omega^2}\left(m_x a\omega^2 - Y_{S1} - \dfrac{3Y_{rrr}a^3\omega^6}{4U_C^3}\right), Y_{rrr} = \dfrac{4U_C^3 Y_{S3}}{a^3\omega^6}; \\ J_z = \dfrac{U_C N_{C1}}{a\omega^3}, N_r = -\dfrac{U_C}{a\omega^2}\left(Y_{\dot r}a\omega^2 + N_{S1} + \dfrac{3N_{rrr}a^3\omega^6}{4U_C^3}\right), N_{rrr} = \dfrac{4U_C^3 N_{S3}}{a^3\omega^6} \end{cases} \tag{C.31}$$

4. In yaw plus drift

$$\begin{cases} F_x = m_y vr - Y_{\dot r}r^2 + X(u) + X_{vv}v^2 + X_{vr}vr + X_{rr}r^2 + X_{vvvv}v^4 \\ F_y = -m_x ur + Y_{\dot r}\dot r + Y_v v + Y_r r + Y_{vvv}v^3 + Y_{rrr}r^3 + Y_{vvr}v^2 r + Y_{vrr}vr^2 \\ M_z = -J_z\dot r + Y_{\dot r}ur + N_v v + N_r r + N_{vvv}v^3 + N_{rrr}r^3 + N_{vvr}v^2 r + N_{vrr}vr^2 \end{cases} \tag{C.32}$$

$$\begin{cases} F_x = m_y a\omega^2\sin\omega t\sin\beta - Y_{\dot r}a^2\omega^4\sin^2\omega t/U_C^2 + X(U_C\cos\beta) \\ \quad + X_{vv}U_C^2\sin^2\beta + X_{vr}a\omega^2\sin\omega t\sin\beta + X_{rr}a^2\omega^4\sin^2\omega t/U_C^2 + X_{vvvv}U_C^4\sin^4\beta \\ F_y = m_x a\omega^2\sin\omega t\cos\beta - Y_{\dot r}a\omega^3\cos\omega t/U_C \\ \quad - Y_v U_C\sin\beta - Y_r a\omega^2\sin\omega t/U_C - Y_{vvv}U_C^3\sin^3\beta - Y_{rrr}a^3\omega^6\sin^3\omega t/U_C^3 \\ \quad - Y_{vvr}U_C\sin^2\beta\cdot a\omega^2\sin\omega t - Y_{vrr}\sin\beta\cdot a^2\omega^4\sin^2\omega t/U_C \\ M_z = J_z a\omega^3\cos\omega t/U_C - Y_{\dot r}a\omega^2\sin\omega t\cos\beta \\ \quad - N_v U_C\sin\beta - N_r a\omega^2\sin\omega t/U_C - N_{vvv}U_C^3\sin^3\beta - N_{rrr}a^3\omega^6\sin^3\omega t/U_C^3 \\ \quad - N_{vvr}U_C\sin^2\beta\cdot a\omega^2\sin\omega t - N_{vrr}\sin\beta\cdot a^2\omega^4\sin^2\omega t/U_C \end{cases} \tag{C.33}$$

So, we have

$$\begin{cases} F_x = X_0 + X_{S1}\sin\omega t + X_{C2}\cos 2\omega t \\ F_y = Y_0 + Y_{C1}\cos\omega t + Y_{S1}\sin\omega t + Y_{C2}\cos 2\omega t + Y_{S3}\sin 3\omega t \\ M_z = N_0 + N_{C1}\cos\omega t + N_{S1}\sin\omega t + N_{C2}\cos 2\omega t + N_{S3}\sin 3\omega t \end{cases} \tag{C.34}$$

The cross coupling derivatives would be

$$\begin{cases} X_{vr} = \dfrac{X_{S1}}{a\omega^2 \sin\beta} - m_y; \\ Y_{vrr} = \dfrac{-2U_C\left(Y_0 + Y_v U_C \sin\beta + Y_{vvv} U_C^3 \sin^3\beta\right)}{\sin\beta \cdot a^2\omega^4} \; or \; Y_{vrr} = \dfrac{2U_C Y_{C2}}{\sin\beta \cdot a^2\omega^4} \\ Y_{vvr} = \dfrac{m_x a\omega^2 \cos\beta - \dfrac{Y_r a\omega^2}{U_C} - Y_{S1} - \dfrac{3Y_{rrr} a^3\omega^6}{4U_C^3}}{U_C \sin^2\beta \cdot a\omega^2}; \\ N_{vrr} = \dfrac{-2U_C\left(N_0 + N_v U_C \sin\beta + N_{vvv} U_C^3 \sin^3\beta\right)}{\sin\beta \cdot a^2\omega^4} \; or \; N_{vrr} = \dfrac{2U_C N_{C2}}{\sin\beta \cdot a^2\omega^4} \\ N_{vvr} = -\dfrac{\left(Y_{\dot{r}} a\omega^2 \cos\beta + \dfrac{N_r a\omega^2}{U_C} + N_{S1} + \dfrac{3N_{rrr} a^3\omega^6}{4U_C^3}\right)}{U_C \sin^2\beta \cdot a\omega^2}; \end{cases} \tag{C.35}$$

For both models, the only unknowns is the surge added mass m_x, in that case, a pure surge test can be carried out for the purpose of deriving a more accurate value instead of estimation by empirical formula, which is

$$\begin{cases} x_0 = U_C t + a\sin\omega t \\ u_0 = U_C + a\omega\cos\omega t \\ \dot{u}_0 = -a\omega^2 \sin\omega t \\ y_0 = v_0 = \dot{v}_0 = \psi = r_0 = \dot{r}_0 = 0 \end{cases} \quad and \begin{cases} u = U_C + a\omega\cos\omega t \\ \dot{u} = -a\omega^2 \sin\omega t \\ y = v = \dot{v} = r = \dot{r} = 0 \end{cases}$$

Thus, there is only surge force measured

$$\begin{aligned} F_x &= -m_x\dot{u} + X\left(u\right) \\ &= X\left(u\right) + m_x a\omega^2 \sin\omega t \\ &= X_0^* + X_{S1}\sin\omega t \end{aligned} \tag{C.36}$$

Note here, X_0^* is not a constant as previous since $u = U_C + a\omega\cos\omega t$, but we are only concern about the X_{S1} which can derive the surge added mass

$$m_x = \frac{X_{S1}}{a\omega^2} \tag{C.37}$$

Finally, all the derivatives need to be nondimensionalized according to the Prime System proposed by SNAME with the reference area of L^2 or LD. That is to say

$$\begin{cases}
m_x', m_y' = \dfrac{m_x, m_y}{\frac{1}{2}\rho L^3}, J_z' = \dfrac{J_z}{\frac{1}{2}\rho L^5}; \\
Y_v' = \dfrac{Y_v}{\frac{1}{2}\rho U_C L^2}, Y_r' = \dfrac{Y_r}{\frac{1}{2}\rho U_C L^3}, Y_{\dot{r}}' = \dfrac{Y_{\dot{r}}}{\frac{1}{2}\rho L^4}; \\
N_v' = \dfrac{N_v}{\frac{1}{2}\rho U_C L^3}, N_r' = \dfrac{N_r}{\frac{1}{2}\rho U_C L^4}, N_{\dot{v}}' = \dfrac{N_{\dot{v}}}{\frac{1}{2}\rho L^4}; \\
X_{vv}' = \dfrac{X_{vv}}{\frac{1}{2}\rho L^2}, X_{vr}' = \dfrac{X_{vr}}{\frac{1}{2}\rho L^3}, X_{rr}' = \dfrac{X_{rr}}{\frac{1}{2}\rho L^4}, X_{vvvv}' = \dfrac{X_{vvvv}}{\frac{1}{2}\rho L^2 \Big/ U_C^2}; \\
Y_{|v|v}' = \dfrac{Y_{|v|v}}{\frac{1}{2}\rho L^2}, Y_{|r|r}' = \dfrac{Y_{|r|r}}{\frac{1}{2}\rho L^4}, Y_{vvv}' = \dfrac{Y_{vvv}}{\frac{1}{2}\rho L^2 \Big/ U_C}, Y_{rrr}' = \dfrac{Y_{rrr}}{\frac{1}{2}\rho L^5 \Big/ U_C}; \\
N_{|v|v}' = \dfrac{N_{|v|v}}{\frac{1}{2}\rho L^3}, N_{|r|r}' = \dfrac{N_{|r|r}}{\frac{1}{2}\rho L^5}, N_{vvv}' = \dfrac{N_{vvv}}{\frac{1}{2}\rho L^3 \Big/ U_C}, N_{rrr}' = \dfrac{N_{rrr}}{\frac{1}{2}\rho L^6 \Big/ U_C}; \\
Y_{vvr}' = \dfrac{Y_{vvr}}{\frac{1}{2}\rho L^3 \Big/ U_C}, Y_{vrr}' = \dfrac{Y_{vrr}}{\frac{1}{2}\rho L^4 \Big/ U_C}, N_{vvr}' = \dfrac{N_{vvr}}{\frac{1}{2}\rho L^4 \Big/ U_C}, N_{vrr}' = \dfrac{N_{vrr}}{\frac{1}{2}\rho L^5 \Big/ U_C};
\end{cases} \tag{C.38}$$

Appendix D: Michell's integral

The wave resistance R_W of a thin ship, beam $B <<$ draft D, in calm and deep water can be calculated by the well-known Michell's integral.

$$R_W = \frac{\pi}{2}\rho U^2 \int_{-\pi/2}^{\pi/2} \left|A(\theta)\right|^2 \cos^3\theta d\theta \tag{D.1}$$

where the complex wave amplitude function $A(\theta)$ is given as

$$A(\theta) = \frac{2}{\pi}\tilde{\nu}\sec^3\theta \iint_{cp} \frac{\partial\zeta(x,z)}{\partial x} e^{\tilde{\nu}z\sec^2\theta + i\tilde{\nu}x\sec^2\theta\cos\theta} dzdx \tag{D.2}$$

Here, $\tilde{\nu} = g/U^2$ is the wave number of pure transverse waves at wave propagation direction angle $\theta = 0$. The mean forward ship speed is U and *cp* denotes the center plane of the hull. Term $\partial\zeta(x,z)/\partial x$ is the longitudinal slope of the mean submerged hull surface $y = \pm\zeta(x,z)$. The wave propagation direction angles θ are positively defined for waves which propagate to the port side of the ship hull.

Due to the lateral symmetry of the hull and the surrounding flow the complex wave amplitude function $A(\theta)$ is an even function and needs only to be computed for positive wave propagation angles. Therefore, the expression (D.1) can be rewritten as

$$R_W = 2\frac{\pi}{2}\rho U^2 \int_0^{\pi/2} \left|A(\theta)\right|^2 \cos^3\theta d\theta = \pi\rho U^2 \int_0^{\pi/2} \left|A(\theta)\right|^2 \cos^3\theta d\theta \tag{D.3}$$

In order to derive a variation of the above expression of the Michell's integral which will be applicable for a case of the real ship offset, the wave amplitude function $A(\theta)$ is transferred as follow.

$$A(\theta)=\frac{2}{\pi}\tilde{\nu}\sec^3\theta\iint_{cp}\frac{\partial\zeta(x,z)}{\partial x}e^{\tilde{\nu}z\sec^2\theta+i\tilde{\nu}x\sec^2\theta\cos\theta}dzdx=$$

$$=\frac{2}{\pi}\tilde{\nu}\sec^3\theta\iint_{cp}\zeta_x(x,z)e^{\tilde{\nu}z\sec^2\theta+i\tilde{\nu}x\sec\theta}dzdx=$$

$$=\frac{2}{\pi}\tilde{\nu}\sec^3\theta\int_{-D}^{0}e^{\tilde{\nu}z\sec^2\theta}\int_{x_S}^{x_B}\zeta_x(x,z)e^{i\tilde{\nu}x\sec\theta}dxdz=$$

$$=\frac{2}{\pi}\tilde{\nu}\sec^3\theta\int_{-D}^{0}e^{\tilde{\nu}z\sec^2\theta}\int_{x_S}^{x_B}\zeta_x(x,z)\left[\cos(\tilde{\nu}x\sec\theta)+i\sin(\tilde{\nu}x\sec\theta)\right]dxdz=$$

$$=\frac{2}{\pi}\tilde{\nu}\sec^3\theta\int_{-D}^{0}e^{\tilde{\nu}z\sec^2\theta}\left[\underbrace{\int_{x_S}^{x_B}\zeta_x(x,z)\cos(\tilde{\nu}x\sec\theta)dx}_{AA}+i\underbrace{\int_{x_S}^{x_B}\zeta_x(x,z)\sin(\tilde{\nu}x\sec\theta)dx}_{BB}\right]dz \tag{D.4}$$

where x_B, x_s denotes the longitudinal positions of bow and stern respectively. The integrals in the bracket can be obtained by integration by parts as follow.

$$\mathrm{AA}=\int_{x_S}^{x_B}\zeta_x(x,z)\cos(\tilde{\nu}x\sec\theta)dx=\cos(\tilde{\nu}x\sec\theta)\zeta(x,z)\Big|_{x_S}^{x_B}+\int_{x_S}^{x_B}\zeta(x,z)\sin(\tilde{\nu}x\sec\theta)\tilde{\nu}\sec\theta dx$$

$$\mathrm{BB}=\int_{x_S}^{x_B}\zeta_x(x,z)\sin(\tilde{\nu}x\sec\theta)dx=\sin(\tilde{\nu}x\sec\theta)\zeta(x,z)\Big|_{x_S}^{x_B}-\int_{x_S}^{x_B}\zeta(x,z)\cos(\tilde{\nu}x\sec\theta)\tilde{\nu}\sec\theta dx$$

Multiplying the part of expression (D.4) outside of bracket with $-i$, while i is multiplied into the bracket, we have

$$A(\theta)=-\frac{2i}{\pi}\tilde{\nu}\sec^3\theta\int_{-D}^{0}e^{\tilde{\nu}z\sec^2\theta}(\text{-BB}+i\mathrm{AA})dz=$$

$$=-\frac{2i}{\pi}\tilde{\nu}\sec^3\theta\int_{-D}^{0}e^{\tilde{\nu}z\sec^2\theta}\left[-\sin(\tilde{\nu}x\sec\theta)\zeta(x,z)\Big|_{x_S}^{x_B}+\int_{x_S}^{x_B}\zeta(x,z)\cos(\tilde{\nu}x\sec\theta)\tilde{\nu}\sec\theta dx\right.$$

$$\left.+i\cos(\tilde{\nu}x\sec\theta)\zeta(x,z)\Big|_{x_S}^{x_B}+i\int_{x_S}^{x_B}\zeta(x,z)\sin(\tilde{\nu}x\sec\theta)\tilde{\nu}\sec\theta dx\right]dz$$

$$=-\frac{2i}{\pi}\tilde{\nu}\sec^3\theta\left\{\int_{-D}^{0}e^{\tilde{\nu}z\sec^2\theta}\left[-\sin(\tilde{\nu}x\sec\theta)\zeta(x,z)\Big|_{x_S}^{x_B}+i\cos(\tilde{\nu}x\sec\theta)\zeta(x,z)\Big|_{x_S}^{x_B}\right]dz\right.$$

$$\left.+\int_{\text{-D}}^{0}e^{\tilde{\nu}z\sec^2\theta}\left[\int_{x_S}^{x_B}\zeta(x,z)\cos(\tilde{\nu}x\sec\theta)\tilde{\nu}\sec\theta dx+i\int_{x_S}^{x_B}\zeta(x,z)\sin(\tilde{\nu}x\sec\theta)\tilde{\nu}\sec\theta dx\right]dz\right\}$$

$$
\begin{aligned}
&= -\frac{2i}{\pi}\tilde{\nu}^2 \sec^4\theta \int_{-D}^{0} e^{\tilde{\nu}z\sec^2\theta} \int_{x_S}^{x_B} \zeta(x,z) e^{i\tilde{\nu}x\sec\theta} dxdz \\
&-\frac{2i}{\pi}\tilde{\nu}\sec^3\theta \int_{-D}^{0} e^{\tilde{\nu}z\sec^2\theta} \left[-\sin(\tilde{\nu}x\sec\theta)\zeta(x,z)\Big|_{x_S}^{x_B} + i\cos(\tilde{\nu}x\sec\theta)\zeta(x,z)\Big|_{x_S}^{x_B} \right](-ii)\, dz \\
&= -\frac{2i}{\pi}\tilde{\nu}^2 \sec^4\theta \int_{-D}^{0} e^{\tilde{\nu}z\sec^2\theta} \int_{x_S}^{x_B} \zeta(x,z) e^{i\tilde{\nu}x\sec\theta} dxdz \\
&-\frac{2i^2}{\pi}\tilde{\nu}\sec^3\theta \int_{-D}^{0} e^{\tilde{\nu}z\sec^2\theta} \left[\cos(\tilde{\nu}x\sec\theta)\zeta(x,z)\Big|_{x_S}^{x_B} + i\sin(\tilde{\nu}x\sec\theta)\zeta(x,z)\Big|_{x_S}^{x_B} \right] dz \\
&= -\frac{2i}{\pi}\tilde{\nu}^2 \sec^4\theta \int_{-D}^{0} e^{\tilde{\nu}z\sec^2\theta} \int_{x_S}^{x_B} \zeta(x,z) e^{i\tilde{\nu}x\sec\theta} dxdz + \frac{2}{\pi}\tilde{\nu}\sec^3\theta \int_{-D}^{0} e^{\tilde{\nu}z\sec^2\theta} e^{i\tilde{\nu}x\sec\theta} \zeta(x,z)\Big|_{x_S}^{x_B} dz \\
&= -\frac{2i}{\pi}\tilde{\nu}^2 \sec^4\theta \int_{-D}^{0} \int_{x_S}^{x_B} \zeta(x,z) e^{\tilde{\nu}z\sec^2\theta + i\tilde{\nu}x\sec\theta} dxdz + \frac{2}{\pi}\tilde{\nu}\sec^3\theta \int_{-D}^{0} e^{\tilde{\nu}z\sec^2\theta + i\tilde{\nu}x\sec\theta} \zeta(x,z)\Big|_{x_S}^{x_B} dz \\
&= -\frac{2i}{\pi}\tilde{\nu}^2 \sec^4\theta \iint_{cp} \zeta(x,z) e^{\tilde{\nu}z\sec^2\theta + i\tilde{\nu}x\sec\theta} dzdx + \frac{2}{\pi}\tilde{\nu}\sec^3\theta \int_{-D}^{0} e^{\tilde{\nu}z\sec^2\theta + i\tilde{\nu}x\sec\theta} \zeta(x,z)\Big|_{x_S}^{x_B} dz
\end{aligned}
\tag{D.5}
$$

The expression can be further simplified if the ship has pointed bow and stern which means the second integral of the last line of (D.5) equal zero, then,

$$
A(\theta) = -\frac{2i}{\pi}\tilde{\nu}^2 \sec^4\theta \iint_{cp} \zeta(x,z) e^{\tilde{\nu}z\sec^2\theta + i\tilde{\nu}x\sec\theta} dzdx \tag{D.6}
$$

In this way, the resistance (D.3) can be rewritten as follow.

$$
\begin{aligned}
R_w &= \pi\rho U^2 \int_0^{\pi/2} \left|A(\theta)\right|^2 \cos^3\theta d\theta \\
&= \pi\rho U^2 \int_0^{\pi/2} \left| \frac{2}{\pi}\tilde{\nu}\sec^3\theta \left[-i\tilde{\nu}\sec\theta \iint_{cp} \zeta(x,z) e^{\tilde{\nu}z\sec^2\theta + i\tilde{\nu}x\sec\theta} dzdx \right] \right|^2 \cos^3\theta d\theta \\
&= \frac{4}{\pi}\rho U^2 \tilde{\nu}^2 \int_0^{\pi/2} \sec^6\theta \left| -i\tilde{\nu}\sec\theta \iint_{cp} \zeta(x,z) e^{\tilde{\nu}z\sec^2\theta + i\tilde{\nu}x\sec\theta} dzdx \right|^2 \cos^3\theta d\theta
\end{aligned}
\tag{D.7}
$$

Introducing $\tilde{\lambda} = \sec\theta$, then, $d\theta = \dfrac{1}{\sqrt{\tilde{\lambda}^2\left(\tilde{\lambda}^2 - 1\right)}} d\tilde{\lambda}$. Therefore, the final Michell's integral can be rewritten as follow.

$$R_w = \frac{4}{\pi}\rho U^2 \tilde{v}^2 \int_0^{\pi/2} \sec^6\theta \left| -i\tilde{v}\sec\theta \iint_{cp} \zeta(x,z) e^{\tilde{v}z\sec^2\theta + i\tilde{v}x\sec\theta} dzdx \right|^2 \cos^3\theta d\theta$$

$$= \frac{4}{\pi}\rho U^2 \tilde{v}^2 \int_1^{\infty} \tilde{\lambda}^6 \left(1/\tilde{\lambda}^3\right) \frac{1}{\sqrt{\tilde{\lambda}^2\left(\tilde{\lambda}^2 - 1\right)}} \left| -i\tilde{v}\tilde{\lambda} \iint_{cp} \zeta(x,z) e^{\tilde{v}z\tilde{\lambda}^2 + i\tilde{v}x\tilde{\lambda}} dzdx \right|^2 d\tilde{\lambda} \qquad \text{(D.8)}$$

$$= \frac{4}{\pi}\rho U^2 \tilde{v}^2 \int_1^{\infty} \frac{\tilde{\lambda}^2}{\sqrt{\tilde{\lambda}^2 - 1}} \left| -i\tilde{v}\tilde{\lambda} \iint_{cp} \zeta(x,z) e^{\tilde{v}z\tilde{\lambda}^2 + i\tilde{v}x\tilde{\lambda}} dzdx \right|^2 d\tilde{\lambda}$$

Bibliography

Abkowitz M.A., (1964). Lectures on ship hydrodynamics-steering and manoeuvrability. Hydro- and Aerodynamics Laboratory, Lyngby, Denmark.

Abkowitz M.A., (1980). Measurement of hydrodynamic characteristics from ship maneuvering trials by system identification. *Transaction of SNAME*, 1980, No.88, pp.283-318.

Alessandrini B., Delhommeau G., (1998). Viscous free surface flow past a ship in drift and in rotating motion. *22nd Symposium on Naval Hydrodynamics*, Washington D.C., U.S.A.

Ando J., Yamamoto T., Maita S., Nakatake K., (1997). An estimation of hydrodynamic forces acting on a ship in oblique towing by a simple surface panel method (SQCM). *Transaction of the West-Japan Society of Naval Architects*, No.94, pp.13-20.

Aoki I., Kijima K., Furukawa Y., Nakiri Y., (2006). On the prediction method for maneuverability of a full scale ship. *Journal of the Japan Society of Naval Architects and Ocean Engineers*, No.3, pp.157-165.

Ayaz Z., Vassalos D., (2003). Towards an improved mathematical model for ship manoeuvring in astern Seas. *MARSIM*, Kanazawa, Japan.

Ayaz Z., Vassalos D., Spyrou K.J., (2006). Manoeuvring behaviour of ships in extreme astern seas. *Ocean Engineering*, Vol.33(17), pp.2381-2434.

Bailey P., Price W., Temarel P., (1997). A unified mathematical model describing the manoeuvring of a ship travelling in a seaway. *Transaction of RINA*, Vol.140, pp.131-149.

Bech M., (1966). Alternative procedure for carrying out spiral tests. The Scandinavian Ship Technical Symposium.

Beck R.F., Magee A.R., (1990). Time-domain analysis for predicting ship motions. *International Symposium on the Dynamics of Marine Vehicles and Structures in Waves*, Uxbridge, U.K., pp.49-64.

Bertram V., (1990). Rankine source approach to forward speed diffraction problem. *5th International Workshop on Water Waves and Floating Bodies*, Manchester, U.K.

Bertram V., (2000). *Practical Ship Hydrodynamics*. Butterworth Heinemann, Oxford.

Bingham H.B., (1994). Simulating ship motions in the time domain. Massachusetts Institute of Technology, U.S.A.

Bollay W., (1939). A non-linear wing theory and its application to rectangular wings of small aspect ratio. *Journal of Applied Mathematics and Mechanics*, Vol.19(1), pp.21-35.

Brard R., (1972). The representation of a given ship form by singularity distributions when the boundary condition on the free surface is linearized. *Journal of Ship research*, Vol.16, pp.79-92.

Carrica P.M., Wilson R.V., Noack R., Xing T., Kandasamy M., Shao J., Sakamoto N., Stern F., (2006). A dynamic overset, single-phase level set approach for viscous ship flows and large amplitude motions and maneuvering. *26th Symposium on Naval Hydrodynamics*, Rome, Italy.

Chang M.S., (1977). Computations of three-dimensional ship motions with forward speed. *2nd International Conference on Numerical Ship Hydrodynamics*, California, U.S.A., pp.124-135.

Chang M.S., Pien P.C. (1976). Velocity potentials of submerged bodies near a free surface application to wave excited forces and motions. *11th Symposium on Naval Hydrodynamics*, London

Chapman R. B., (1975). Free surface effects for hydrodynamic forces on a surface piercing plate oscillating in yaw and sway. *1st International Conference on Numerical Ship Hydrodynamics*, Bethesda, Maryland, pp.333-350.

Chapman R.B., (1976). Free surface effects for yawed surface piercing plates. *Journal of Ship research*, Vol.20, No.3, pp.125-136.

Chasnow J.R., (2012). *Introduction to numerical methods*. The Hong Kong University of Science and Technology.

Chen J.P, Zhu D.X., (2010 a). Numerical simulations of wave-induced ship motions in time domain by a Rankine panel method. *Journal of Hydrodynamics*, Vol.22, No.3, pp.373-380.

Chen J.P., Zhu D.X., (2010 b). Numerical simulations of wave-induced ship motions in regular oblique waves by a time domain panel method. *Journal of Hydrodynamics*, Vol.22, No.5, pp.419-426.

Chen X.B., Diebold L., Doutreleau Y., (2000). New Green function method to predict wave-induced ship motions and loads. *23rd Symposium on Naval Hydrodynamics*, Val de Reuil, France.

Chen X.B., Noblesse F., (1998). Super Green functions. *22nd Symposium on Naval Hydrodynamics*, Washington D.C., U.S.A.

Chislett M.S., Strøm-Tejsen J., (1965). Planar motion mechanism tests and full scale steering maneuvering predictions for a mariner class vessel. Hydro- and Aerodynamics Laboratory, Lyngby, Denmark. Report No. Hy A6.

Clarke D., (1971). A new non-linear equation for ship manoeuvring. *International Shipbuilding Progress*, Vol.18, No.201, pp.181-197.

Clarke D., Gedling P., Hine G., (1982). The application of manoeuvring criteria in hull design using linear theory. *Transaction of RINA*, pp.45-68.

Cummins W. E., (1962). The impulse response function and ship motions. Schiffstechnik, Vol.9, pp.101-109.

Dai Y.S., (1998). *Potential flow theory of ship motions in waves in frequency and time domain*. National Defense Industry Press, Beijing.

Danmeier, D.G., (1999). A higher-order panel method for large-amplitude simulation of bodies in waves. Massachusetts Institute of Technology, U.S.A.

Das S., Cheung K.F., (2012). Scattered waves and motions of marine vessels advancing in a seaway. *Wave Motion*, Vol.49(1), pp.181-197.

Datta R., Sen D., (2006). A B-spline-based method for radiation and diffraction problems. *Ocean Engineering*, Vol.33(17), pp.2240-2259.

Davidson K. S., Schiff L., (1946). Turning and course keeping qualities of ships. *Transaction of SNAME*, Vol.54, pp.152-200.

Davis M.R., Holloway D.S., (2003). Motion and passenger discomfort on high speed catamarans in oblique seas. *International Shipbuilding Progress*, Vol.50, No.4, pp.317-332.

Dawson C.W., (1977). A practical computer method for solving ship wave problems. *2nd International Conference on Numerical Ship Hydrodynamics*, pp.30-38.

Duan W.Y., (1995). Nonlinear hydrodynamic forces acting on a ship undergoing large amplitude motion. Harbin Engineering University, China.

Duan W.Y., Dai Y.S., (1999). Time domain calculation of hydrodynamic forces on ships with large flare. *International Shipbuilding Progress*, Vol.46, No.446, pp.209-221.

Duan W.Y., He W.Z., (2001). Motion characteristics of fast displacement vessels. *Journal of Tsinghua University*, Vol.41(12), pp.82-85.

Faltinsen O.M., Løken A.E., (1979). Slow drift oscillations of a ship in irregular waves. *Applied Ocean Research*, Vol.1(1), pp.21-31.

Faltinsen O.M., Michelsen F.C., (1974). Motions of large structure in waves at zero Froude number. *International symposium on the dynamics of marine vehicles and structure in waves*, London, U.K.

Faltinsen O.M., Minsaas K., Liapis N., Skjørdal S.O., (1980). Prediction of resistance and propulsion of a ship in a seaway. *13th Symposium on Naval Hydrodynamics*, Tokyo, Japan, pp.505-529.

Faltinsen O.M., Zhao R., (1991). Numerical prediction of ship motions at high forward speed. *Physical Sciences and Engineering*, Vol.334, No.1634, pp.241-252.

Faltinsen O.M., (2005). *Hydrodynamics of high speed marine vehicles*. Cambridge University Press, New York.

Fang M.C., Luo J.H., Lee M.L., (2005). A nonlinear mathematical model for ship turning circle simulation in waves. *Journal of Ship Research*, Vol.49(2), pp.69-79.

Fathi D., Hoff J.R., (2004). Theory manual of ShipX Vessel Responses. MARINTEK A/S.

Fossen T.I., (2005). A nonlinear unified state space model for ship manoeuvring and control in a seaway. *International Journal of Bifurcation and Chaos*, Vol.15, pp.2717-2746.

Frank W., (1967). Oscillation of cylinders in or below the free surface of deep fluids. Report No.2375, Naval Ship Research and Development Center.

Froude W., (1861). On the rolling of ships. *Transaction of Institution of Naval Architects*, pp.180-229.

Fujii H., Takahashi T., (1975). Experimental study on the resistance increase of a ship in regular oblique waves. *14th ITTC*, Ottawa, Canada, pp.351-360.

Fujii H., Tuda T., (1961). Experimental research on rudder performance. *Journal of the Society of Naval Architects of Japan*, No.110, pp.31-42.

Fujino M., Ohmori T., Usami S., Eguchi S., Miyata H., (1995). A study of flow field around full ship forms in maneuvering motion: 2nd report: hydrodynamic forces and pressure distribution on ship's hull in steady turning condition. *Journal of the Society of Naval Architects of Japan*, No.177, pp.13-28.

Furukawa Y., Nakiri Y., Kijima K., Ibaragi H., (2008). The prediction of the manoeuvrability of KVLCC1 and KVLCC2. *SIMMAN*, part E, pp.9-14.

Fuwa T., (1973). Hydrodynamic forces acting on a ship in oblique towing. *Journal of the Society of Naval Architects of Japan*, No.134, pp.135-147.

Gadd G.E., (1976). A method of computing the flow and surface wave pattern around full forms. *Transaction of RINA*, Vol. 113, pp. 207-219.

Gao Z.L., Zou Z.J., (2008). A NURBS based high order panel method for three dimensional radiation and diffraction problems with forward speed. *Ocean Engineering*, Vol. 35(11-12), pp.1271-1282.

Garrison C.J., (1978). Hydrodynamic loading of large offshore structures: three dimensional source distribution methods. *Numerical methods on offshore engineering*, pp.87-140.

Gerritsma J., (1960). Ship motions in longitudinal waves. *International Shipbuilding Progress*, Vol.66, pp.42-95.

Gerritsma J., Beukelman V., (1971). Analysis of the resistance increase in waves of a fast cargo ship. Laboratory for Ship Hydrodynamics, Delft, Netherlands, Report No.334.

Hamamoto M., (1977). MMG Report - II, the theoretical background of the mathematical model of ship maneuverability. *The Bulletin of Society of Naval Architects of Japan*, No.577, pp.322-329.

Hamamoto M., (1992). A new coordinate system and the equations describing manoeuvring motion of a ship in waves. *Workshop on prediction of ship manoeuvrability*, the West Japan society of Naval Architects, pp.61-76.

Haraguchi T., (2000). Simple estimating method on ship manoeuvrability by means of manoeuvring performance database. *MARSIM*, Orlando, U.S.A., pp.289-299.

Haskind M.D., (1946). The oscillation of a ship in still water. *Izv. Akad. Nauk SSSR. Otd. Tekh. Nauk*, Vol.1, pp.23-34.

Hess J.L., (1979). A higher order panel method for three-dimensional potential flow. Naval Air Development Center, Report No. NADC 77166-30, pp.517-520.

Hess J.L., Smith A.M.O., (1964). Calculation of nonlifting potential flow about arbitrary three dimensional bodies. *Journal of Ship Research*, Vol.8, No.2, pp.22-44.

Himeno Y., (1981). Prediction of ship roll damping – state of the art. University of Michigan, Department of Naval Architecture and Marine Engineering, Report No.239.

Hirano M., (1980). On calculation method of ship maneuvering motion at initial design phase. *Journal of the Society of Naval Architects of Japan*, No.147, pp.144-153.

Hirano M., Takashina J., Takaishi Y., Saruta T., (1980). Ship turning trajectory in regular waves. *Transactions of the West-Japan Society of Naval Architects*, No.60, pp.17-31.

Hochbaum A.C., (1998). Computation of the turbulent flow around a ship model in steady turn and in steady oblique motion. *22nd Symposium on Naval Hydrodynamics*, Washing D.C., pp.550-567.

Hochbaum A.C., (2006). Virtual PMM tests for manoeuvring prediction. *26th Symposium on Naval Hydrodynamics*, Rome, Italy.

Hochbaum A.C., Vogt M., (2002). Towards the simulation of seakeeping and manoeuvring based on the computation of the free surface viscous ship flow. *24th Symposium on Naval Hydrodynamics*, Fukuoka, Japan.

Holtrop J., (1977). A statistical analysis of performance test results. *International Shipbuilding Progress*, Vol.24, pp23-28.

Holtrop J., (1978). Statistical data for the extrapolation of model performance. *International Shipbuilding Progress*, Vol.14, pp.122-126.

Holtrop J., (1984). A statistical re-analysis of resistance and propulsion data. *International Shipbuilding Progress*, Vol.31, pp.272-276.

Holtrop J., Mennen G.G.J., (1978). A statistical power prediction method. *International Shipbuilding Progress*, Vol.25, pp.253-256.

Holtrop J., Mennen G.G.J., (1982). An approximate power prediction method. *International Shipbuilding Progress*, Vol.29, pp.166-170.

Hsin C.Y., Kerwin J.E., Kinnas S.A., (1991). A panel method for the analysis of the flow around highly skewed propellers. *The Propellers & Shafting'91 Symposium*, Virginia Beach, U.S.A., pp.1-13.

Hsin C. Y., Kerwin J.E., Newman J.N., (1993). A higher order panel method based on B-Splines. *6th International Conference on Numerical Ship Hydrodynamics*, Iowa, U.S.A., pp.133-151.

Hwang W.Y., (1980). Application of system identification to ship maneuvering. Massachusetts Institute of Technology, U.S.A.

Ikeda Y., Himeno Y., Tanaka N., (1978). A prediction method for ship roll damping. Department of Naval Architecture, Technical report No. 00405, University of Osaka Prefecture, Japan.

IMO, (1985). Interim guidelines for estimating manoeuvring performance in ship design. MSC/Circ.389.

IMO, (2002). Explanatory notes to the standards for ship manoeuvrability. MSC/Circ.1053.

IMO, (2002). Standards for ship manoeuvrability. Resolution MSC.137(76).

Inglis R.B., Price W.G., (1982). A three-dimensional ship motion theory: comparison between theoretical predictions and experimental data of the hydrodynamic coefficients with forward speed. *Transaction of RINA*, Vol.124, pp.141-157.

Inoue S., (1956). On the turning of ships. *Memoirs of the Faculty of Engineering*, Kyushu University, Vol.16, No.2, pp.49-110.

Inoue S., (1981). Hydrodynamic derivatives on ship manoeuvring. *International Shipbuilding Progress*, Vol.28, No.321, pp.112-125.

Inoue S., Hirano M., Kijima K., Takashina J., (1981). A practical calculation method of ship maneuvering motion. *International Shipbuilding Progress*, Vol.28, No.325, pp.207-222.

Inoue S., Murahashi T., (1966). A calculation of turning motion in regular waves. *Transactions of the West-Japan Society of Naval Architects*, No.31, pp.77-99.

Israeli M., Orszag S.A., (1981). Approximation of radiation boundary conditions. *Journal of Computational Physics*, Vol.41(1), pp.115-135.

ITTC Manoeuvring Committee, (2005). Final report and recommendations to the 24th ITTC. Edinburgh, U.K.

ITTC Manoeuvring Committee, (2011). Manoeuvring and course keeping in waves. In Final report and recommendations to the 26th ITTC, Rio de Janeiro, Brazil, pp.147-150.

ITTC Manoeuvring Committee, (2014 a). Manoeuvring and course keeping in waves. In Final report and recommendations to the 27th ITTC, Copenhagen, Denmark, pp.156-160.

ITTC Manoeuvring Committee, (2014 b). Recommended procedures and guidelines of free running model tests. *27th ITTC*, Copenhagen, Denmark.

ITTC Seakeeping Committee, (1978). Comparison of results obtained with computer programs to predict ship motions in six degrees of freedom. In Report of the Seakeeping Committee to the 15th ITTC, Hague, Netherlands, pp. 79-92.

Jensen G., Söding H., Mi Z.X., (1986). Rankine source methods for numerical solutions of steady wave resistance problem. *16th Symposium on Naval Hydrodynamics*, Berkeley, U.S.A., pp.575-582.

Joncquez S.A.G., (2009). Second-order forces and moments acting on ships in waves. Technical University of Denmark, Denmark.

Journée J.M.J., (1992). Experiments and calculations on 4 Wigley hull forms in head waves. TU Delft, Report No.0909.

Journée J.M.J., Adegeest L.J.M., (2003). Theoretical manual of 'SEAWAY for Windows'. TU Delft, Report No.1370.

Kasai H., Yumuro A., (1977). MMG report-III, the forces on the rudder and their interactions with hull and propeller, *The Bulletin of Society of Naval Architects of Japan*, No.578, pp.358-372.

Kashiwagi M., (1992). Added Resistance, wave-induced steady sway force and yaw moment on an advancing ship. *Ship Technology Research*, Vol.39, pp.3-16.

Kashiwagi M., (1997). Numerical seakeeping calculations based on the slender ship theory. *Ship Technology Research*, Vol.44, No.4, pp.167-192.

Katz J., Plotkin A., (1991). *Low-speed aerodynamics*, Inc. McGraw-Hill, pp.212-222.

Kijima K., (2003). Some studies on the prediction for ship manoeuvrability. *International Conference of Ship Simulation and Ship Manoeuvrability*, pp.26-35.

Kijima K., Katsuno T., Nakiri Y., Furukawa Y., (1990). On the manoeuvring performance of a ship with the parameter of loading condition. *Journal of the Society of Naval Architects of Japan*, No.168, pp141-148.

Kijima K., Nakiri Y., (1999). Approximate expression for hydrodynamic derivatives of ship manoeuvring motion taking into account of the effect of stern shape. *Transactions of the West-Japan Society of Naval Architects*, No.98, pp.67-77.

Kijima K., Takazumi T., (2000). Study on method for hydrodynamic force acting on a ship hull by cross flow model. *Transaction of the West-Japan Society of Naval Architects*, No.99, pp.135-143.

Kim K.H., Kim Y., (2010). Comparative study on ship hydrodynamics based on Neumann-Kelvin and double-body linearizations in time-domain analysis. *International Journal of Offshore and Polar Engineering*, Vol.20, No.4, pp.265-274.

Kim K.H., Kim Y., (2011). Numerical study on added resistance of ships by using a time-domain Rankine panel method. Ocean Engineering, Vol.38, pp.1357-1367.

Kim Y.H., Kim K.H., Kim J.H., Seo M.G., Kim Y., (2011). Time-domain analysis of nonlinear motion responses and structural loads on ships and offshore structures: development of WISH programs. *International Journal of Naval Architecture and Ocean Engineering*, Vol.3(1), pp.37-52.

Kim B., Shin Y.S., (2003). A NURBS panel method for three-dimensional radiation and diffraction problems. *Journal of Ship Research*, Vol.47, No.2, pp.117-186.

King B., (1987). Time-domain analysis of wave exciting forces on ships and bodies. University of Michigan, U.S.A.

Kinoshita T., Bao W., Yoshida M., Nihei Y., Xu Y., Itakura H., (2008). Effects of wave drift forces on maneuvering of ship. *27th International Conference on Offshore Mechanics and Arctic Engineering*, Estoril, Portugal, pp.407-413.

Korvin-Kroukovsky B.V., (1955). Investigation of ship motions in regular waves. *Transaction of SNAME*, Vol.63, pp.386-435.

Korvin-Kroukovsky B.V., Jacobs W.R., (1957). Pitching and heaving motions of a ship in regular waves. *Transaction of SNAME*, Vol.65, pp.590-630.

Kose K., Kijima K., (1977). MMG report-IV, the methods of the captive mode test and the test installations. *The Bulletin of Society of Naval Architects of Japan*, No.579, pp.404-413.

Kose K., Yumuro A., Yoshimura Y., (1981). Concrete of mathematical model for ship manoeuvring. *3rd Symposium on Ship Maneuverability*, Society of Naval Architects of Japan, pp.27-80.

Kouh J.S., Ho C.H., (1996). A high order panel method based on source distribution and Gaussian quadrature. *Ship Technology Research*, Vol.43, No.1, pp.38-47.

Kouh J.S., Suen J.B., (2001). A 3D potential-based and desingularized high order panel method. *Ocean Engineering*, Vol.28(11), pp.1499-1561.

Kreuzer E.J., Sichermann W.M., (2005). Slender body theory approach to nonlinear ship motions. *International Workshop on Water Waves and Floating Bodies*, Longyearbyen, Norway.

Kring D.C., (1994). Time domain ship motions by a three-dimensional Rankine panel method. Massachusetts Institute of Technology, U.S.A.

Krylov A., (1896). A new theory of the pitching motions of a ship on waves and the stresses produced by this motion. *Transaction of Institution of Naval Architects*, Vol.37, pp.326-368.

Lee C.H., (1995). WAMIT theory manual. Report No.95-2, Massachusettes Institute of Technology, U.S.A.

Lee S., Hwang S., Yun S., Rhee K., Seong W., (2009). An experimental study of a ship manoeuvrability in regular waves. *MASIM*, Panama City, Panama.

Lewis F.M., (1929). The inertia of the water surrounding a vibrating ship. *Transaction of SNAME*, Vol.37, pp.1-20.

Liao Z.P., (1996). Extrapolation non-reflecting boundary conditions. *Wave Motion*, Vol.24, pp.117-138.

Liapis S., (1986). Time domain analysis of ship motions. University of Michigan, U.S.A.

Lin W.M., Yue D., (1990). Numerical solutions for large amplitude ship motions in the time domain. *18th Symposium on Naval Hydrodynamics*, Ann Arbor, U.S.A., pp.41-66.

Lin W.M., Zhang S., Yue D., (1996). Linear and nonlinear analysis of motions and loads of a ship with forward speed in large-amplitude waves. *11th International Workshop on Water Waves and Floating Bodies*, Hamburg, Germany.

Lin W.M., Zhang S., Weems K., Liut D., (2006). Numerical simulations of ship maneuvering in waves. *26th Symposium on Naval Hydrodynamics*, Rome, Italy.

Lin W.M., Zhang S., Weems K., Yue D., (1999). A mixed source formulation for nonlinear ship motion and wave load simulations. *7th International Conference on Numerical Ship Hydrodynamics*, Nantes, France.

Loukakis T.A., Sclavounos P.D., (1978). Some extensions of the classical approach to strip theory of ship motions, including the calculation of mean added forces and moments. *Journal of Ship Research*, Vol.22(1), pp.1-19.

Lugni C., Colagrossi A., Landrini M., Faltinsen O.M., (2004). Experimental and numerical study of semi-displacement mono-hull and catamaran in calm water and incident waves. *25th Symposium on Naval Hydrodynamics*. St. John's, Canada.

Luo W.L., Zou Z.J., (2009). Parametric identification of ship maneuvering models by using support vector machines. *Journal of Ship Research*, Vol.53, No.1, pp.19-30.

Lyster C.A., Knights H.L., (1979). Prediction equations for ship's turning circles. *Transaction of Northeast Coast Institutions for Engineers and Shipbuilders*, Vol.95(4), pp.217-229.

Maruo H., (1960). The drift of a body floating on waves. *Journal of Ship Research*, Vol.4, No.3, pp.1-5.

Maruo H., (1989). Evolution of the theory of slender ships, *Ship Technology Research*, Vol.36(3), pp.107-133.

Maniar H.D., (1995). A three-dimensional higher order panel method based on B-splines. Massachusetts Institute of Technology, U.S.A.

Ma S., Duan W.Y., Song J.Z., (2005). An efficient numerical method for solving '2.5D' ship seakeeping problem. *Ocean Engineering*, Vol. 32, pp.937-960.

Ma S., Duan W.Y., Wang B., Wang R.F., (2012). Prediction of ship motions of trimaran in oblique regular wave. *Chinese Journal of Hydrodynamics*, Vol.27, No.2, pp.224-230.

Ma X.S., (2007). Study on the steering operations executed in Dashun shipwreck. Vol.2, *Tianjin Maritime*, pp.3-11.

Matsui S., Yang J.M., Tamashima M., Yamazaki R., (1994). Calculation of flow around a hull in turning motion and its hydrodynamic forces. *Transaction of the West-Japan Society of Naval Architects*, No.88, pp.57-72.

Matsumoto N., Suemitsu K (1980). The prediction of manoeuvring performances by captive model tests. *Journal of the Kansai Society of Naval Architects,* No.176, pp.11-22

Matsumoto N., Suemitsu K., (1981). Maneuvering performance test analysis by mathematical response model. *Journal of the Kansai Society of Naval Architects,* No.180, pp.87-95.

McCreight W.R., (1986). Ship maneuvering in waves. *16th Symposium on Naval Hydrodynamics,* pp.456-469.

Miao G.P., (1980). On the computation of ship motions in regular waves. Report No.58, Division of Ship Hydrodynamics, Chalmers University of Technology, Sweden.

Michell J.H., (1898). The wave resistance of a ship. *Philosophical Magazine,* Vol.45, pp.106-123.

Munk M.M., (1924). The aerodynamic forces on airship hulls. NACA Rep. 184.

Nakatake K., Ando J., Komura A., Kataoka K., (1990). On the flow field and the hydrodynamic forces of an obliquing ship. *Transactions of West-Japan Society of Naval Architects,* No.80, pp.1-12.

Nakatake K., Sekiguchi T., Ando J., (2001). Prediction of hydrodynamic forces acting on ship hull in oblique and turning motions by a simple surface panel method. *8th International Symposium on Practical Design of Ships and Other Floating Structures,* Shanghai, China, pp645-650.

Nakos D., (1990). Ship wave patterns and motions by a three dimensional Rankine panel method. Massachusetts Institute of Technology, U.S.A.

Nakos D., Kring D., Sclavounos P.D., (1993). Rankine panel methods for transient free surface flows. *6th International Conference on Numerical Ship Hydrodynamics,* Washington D.C., U.S.A.

Nakos D., Kring D., Sclavounos P.D., (1994). Rankine panel methods for transient free surface flows. *6th Internaltional Conference on Numerical Ship Hydrodynamics*, Iowa, U.S.A., pp.613-633.

Newman J.N., (1964). Slender body theory for ship oscillations in waves. *Journal of Fluid Mechanics*, Vol.18, pp.602-618.

Newman J. N., (1967). The drift force and moment on ships in waves. *Journal of Ship Research*, Vol.11, pp. 51–60.

Newman J.N., (1977). *Marine Hydrodynamics*. The MIT Press, Cambridge.

Newman J.N., (1978). The theory of ship motions. *Advances in Applied Mechanics*, Vol.18, pp.221-282.

Newman J.N., (1985). Algorithms for the free-surface Green function. *Journal of Engineering Mathematics*, Vol.19, No.1, pp.57-67.

Newman J.N., Sclavounos P.D., (1980). The unified theory of ship motions. *13th Symposium on Naval Hydrodynamics*, Tokyo, Japan, pp. 373-397.

Nishimura K., Hirayama T., (2003). Maneuvering and motion simulation of a small vessel in waves. *MASIM*, Kanazawa, Japan.

Noblesse F., (1982). The Green function in the theory of radiation and diffraction of regular water waves by a body. *Journal of Engineering Mathematics*, Vol.16, No.2, pp.137-169.

Nomoto K., Taguchi K., Honda K., Hirano S (1956). On the steering qualities of ships. *Journal of Zosen Kiokai*, No.99, pp.75-82.

Nomoto K., Taguchi K., (1957). On the steering qualities of ships (2). *Journal of the Society of Naval Architects of Japan*, No.101, pp.57-66.

Nonaka K., (1990). On the manoeuvring motion of a ship in waves. *Transactions of the West-Japan Society of Naval Architects*, No.80, pp.73-86.

Norrbin N.H., (1960). A Study of Course Keeping and Maneuvering Performance. SSPA Publication No.45, Göteborg, Sweden.

Norrbin N.H., (1970). Theory and observations on the use of a mathematical model for ship manoeuvring in deep and confined waters. *8th Symposium on Naval Hydrodynamics*.

Ogawa A., Koyama T., Kijima K., (1977). MMG report-I, on the mathematical model of ship manoeuvring. *The Bulletin of Society of Naval Architects of Japan*, No.575, pp.22-28.

Ogilvie T.F., (1967). Nonlinear high Froude number free surface problems. *Journal of Engineering Mathematics*, Vol.1, pp.215-235.

Ogilvie T.F., Tuck E.O., (1969). A rational strip theory of ship motions: Part I. Department of Naval Architecture and Marine Engineering, College of Engineering, University of Michigan, Report No.013.

Ohmori T., Fujino M., Miyata H., (1998). A study on flow field around full ship forms in maneuvering motion. *Journal of Marine Science and Technology*, Vol.3(1), pp.22-29.

Ohmori T., Fujino M., Miyata H., Kanai M., (1994). A study on flow field around full ship forms in maneuvering motion: 1st report: in oblique tow. *Journal of the Japan Society of Naval Architects and Ocean Engineers*, No.176, pp.241-250.

Ohrmori T., Fujino M., Tatsumi K., Kawamura T., Miyata H., (1996). A study on flow field around full ship forms in maneuvering motion: 3rd report: flow field around ship's hull in steady turning condition. *Journal of the Society of Naval Architects of Japan*, No.179, pp.125-138.

Orlanski I., (1976). A simple boundary condition for unbounded hyperbolic flows. *Journal of Computational Physics*, Vol.21, pp.251-269.

Ottosson P., Bystrom L., (1991). Simulation of the dynamics of a ship maneuvering in waves. *Transaction of SNAME*, Vol.99, pp.281-298.

Piegl L., Tiller W., (1997). *The NURBS book (second edition)*. Springer press.

Pinkster J.A., (1980). Low frequency second order wave exciting forces on floating structures. Netherlands Ship Model Basin, Publication No.650.

Qiu W., Hsiung C.C., (2002). A panel-free method for time-domain analysis of the radiation problem. *Ocean Engineering*, Vol.29(12), pp.1555-1561.

Quadvlieg F., Tonelli R., (2015). Scale effects on free running model tests. *MARSIM*, Newcastle, U.K.

Ronæss M., (2002). Wave induced motions of two ships advancing on parallel course. Department of Marine Hydrodynamics, NTNU, Trondheim.

Salvesen N., (1974). Second order steady state forces and moments on surface ships in oblique regular waves. *International Symposium on the Dynamics of Marine Vehicles and Structures in Waves*, London, U.K., pp.212-227.

Salvesen N., Tuck E.O., Faltinsen O.M., (1970). Ship motions and sea loads. *Transaction of SNAME*, Vol.78, pp.250-287.

Sato Y., Miyata H., Sato T., (1999). CFD Simulation of 3-dimensional motion of a ship in waves: application to an advancing ship in regular heading waves. *Journal of Marine Science and Technology*, Vol.4(3), pp.108-116.

Sclavounos P.D., (1984). The unified slender body theory: ship motions in waves. *15th Symposium on Naval Hydrodynamics*, Hamburg, Germany, pp.177-192.

Sclavounos P.D., Lee S., (2013). A fluid impulse nonlinear theory of ship motions and sea loads. *Interational Shipbuilding Progress*, Vol.60, No.1-4, pp.555-577.

Sen D., (2002). Time domain computation of large amplitude 3D ship motions with forward speed. *Ocean Engineering*, Vol.29(8), pp.973-1002.

Seo M.G., Kim Y., (2011). Numerical analysis on ship maneuvering coupled with ship motion in waves. *Ocean Engineering*, Vol.38, pp.1934-1945.

Seo M.G., Park D.M., Yang K.K., Kim Y., (2013). Comparative study on computation of ship added resistance in waves. *Ocean Engineering*, Vol.73, pp.1-15.

Seo M.G., Yang K.K., Park D.M., Kim Y., (2014). Numerical analysis of added resistance on ships in short waves. *Ocean Engineering*, Vol.87, pp.97-110.

SIMMAN website: https://simman2014.dk/

Simonsen C.D., (2004). PMM model test with DDG51 including uncertainty assessment. FORCE Technology, Department of Maritime Industry, Lyngby, Denmark.

Simonsen C.D., Stern F., Agdrup K., (2006). CFD with PMM test validation for manoeuvring VLCC2 tanker in deep and shallow water. *MARSIM*, Terschelling, Netherlands.

Simonsen C.D., Otzen J.F, Klimt C., Larsen N.L., Stern F., (2012). Maneuvering predictions in the early design phase using CFD generated PMM data. *29th Symposium on Naval Hydrodynamics*, Gothenburg, Sweden, pp.26-31.

Skejic R., (2013). Ships maneuvering simulations in a seaway: how close are we to reality? *International Workshop on Nautical Traffic Models*, Delft, Netherlands, pp.91-101.

Skejic R., Faltinsen O.M., A unified seakeeping and maneuvering analysis of ships in regular waves. *Journal of Marine Science and Technology*, Vol.13(4), pp.371-394.

Söding H., (1993). A method for accurate force calculations in potential flow. *Ship Technology Research*, Vol.40, No.3, pp.176-186.

Sommerfeld A., (1949). *Partial differential equations in physics*, Academic Press, New York.

Son K.H., Nomoto K., (1982). On the coupled motion of steering and rolling of a high speed container ship. *Naval Architecture and Ocean Engineering*, No.20, pp.73-83.

Song M.J., Kim K.H., Kim Y., (2011). Numerical analysis and validation of weakly nonlinear ship motions and structural loads on a modern containership. *Ocean Engineering*, Vol.38(1), pp.77-87.

St Denis M., Pierson W.J., (1953). On the motions of ships in confused seas. *Transaction of SNAME,* Vol.61, pp.280-354.

Stern F., Agdrup K., Kim S., Hochbaum A.C., Rhee K.P., Quadvlieg F., Perdon P., Hino T., Broglia R., Gorski J., (2011). Experience from SIMMAN 2008—the first workshop on verification and validation of ship maneuvering simulation methods. *Journal of Ship Research,* Vol.55, No.2, pp.135-147.

Sun H., Faltinsen O.M., (2007). The influence of gravity on the performance of planning vessels in calm water. *Journal of Engineering Mathematics,* Vol.58(1), pp.91-107.

Sutulo S., Guedes Soares C., (2006a). Numerical study of ship rolling in turning manoeuvres. *9th International Conference on Stability of Ships and Ocean Vehicles,* Rio de Janeiro, Brazil, pp.395-408.

Sutulo S., Guedes Soares C., (2006b). A unified nonlinear mathematical model for simulating ship manoeuvring and seakeeping in regular waves. *MARSIM,* Terschelling, Netherlands.

Sutulo S., Guedes Soares C., (2008). A generalized strip theory for curvilinear motion in waves. *27th International Conference on Offshore Mechanics and Arctic Engineering,* pp.1-10.

Tahara Y., Longo J., Stern F., (2002). Comparison of CFD and EFD for the Series 60 $C_B = 0.6$ in steady drift motion. *Journal of Marine Science and Technology,* Vol.7(1), pp.17-30.

Takaki M., Lin X., Gu X., Mori H., (1995). Theoretical prediction of seakeeping qualities of high speed vessels. *3rd International Conference on Fast Sea Transportation,* Lubeck Travemunde, Germany, pp.893-904.

Tasai F., (1967). On the swaying, yawing and rolling motions of ships in oblique waves. *International Shipbuilding Progress,* Vol.14, No. 153, pp.216-228.

Tasai F., Takaki M., (1969). Theory and calculation of ship responses in regular waves. *Symposium on Seaworthiness of Ships,* Japan Society of Naval Architects.

Timman R., Newman J.N., (1962). The coupled damping coefficients of symmetric ships. *Journal of Ship Research*, Vol.5, No.4, pp.1-7.

Toxopeus S., (2004). Simulation and validation of the viscous flow around the Series 60 hull form at 10° drift angle. *7th Numerical Towing Tank Symposium*, Hamburg, Germany.

Triantafyllou M.S., (1982). A consistent hydrodynamic theory for moored and positioned vessels. *Journal of Ship Research*, Vol.26, No.2, pp.97-105.

Tulin M.P., (1957). The theory of slender surfaces planning at high speeds. *Schiffstechnik*, Vol.4, No.21, pp.125-133.

Tulin M.P., Landrini M., (2001). Breaking waves in the ocean and around ships. *23rd Symposium on Naval Hydrodynamics*, Val de Reuil, France.

Ueno M, Nimura T, Miyazaki H, (2003). Experimental study on manoeuvrinc motion of a ship in waves. *MASIM*, Kanazawa, Japan.

Ursell F., (1949). On the heaving of a circular cylinder on the surface of a fluid. *Quarterly Journal of Mechanic and Applied Math*, Vol.2, pp.218-231.

Van Leeuwen G., (1956). The lateral damping and added mass of a horizontally oscillating ship model. Netherlands Ship Research Center, Delft, Report No.65.

Wang C.T., (1999). Vertical motions of slender bodies with forward speed. *Proceedings of National Science Council*, ROC, Vol.23, No.1, pp.31-41.

Wang H., Zou Z.J., (2008). Numerical research on wave-making resistance of trimaran. *Journal of Shanghai Jiao Tong University*, Vol.13(3), pp.348-351.

Wang X.G., Zou Z.J., Xu F., Ren R.Y., (2014). Sensitivity analysis and parametric identification for ship manoeuvring in 4 degrees of freedom. *Journal of Marine Science and Technology*, Vol.19(4), pp.394-405.

Webster W.C., (1975). The flow about arbitrary, three-dimensional smooth bodies. *Journal of Ship Research*, Vol.19, No.4, pp.206-218.

Wellicome J., Wilson P., Cheng X., (1995). Prediction of sway force and yaw moment on slender ships. *International Shipbuilding Progress*, Vol.42, No.431, pp.259-276.

Willis D.J., Peraire J., White J.K., (2006). A quadratic basis function, quadratic geometry, high order panel method. *44th AIAA Aerospace Sciences Meeting*, Reno, 2006, No. AIAA-2006-1253.

Wu G.X., Eatock Taylor R., (1987). A Green function for ship motions at forward speed. *International Shipbuilding Progress*, Vol.34, pp.189-196.

Xia Z.D., Fan S.M., (2008). Study progress on the prediction of ship manoeuvring in wind & wave current and restricted line. *Ship Engineering*, Vol.30, Supplement, pp. 1-11.

Xu C., (1998). Kutta condition for sharp edge flows. *Mechanics Research Communications*, Vol.25, No.4, pp.415-420.

Xu G., Duan W.Y., (2008). Time domain simulation of irregular wave diffraction. *8th International Conference on Hydrodynamics*, Nantes, France.

Xu Y., Bao W., Kinoshita T., Itakura H., (2007). A PMM experimental research on ship maneuverability in waves. *26th International Conference on Offshore Mechanics and Arctic Engineering*, San Diego, U.S.A., pp.11-16.

Yamasaki K., Fujino M., (1985). Linear hydrodynamic coefficients of ships with forward speed during harmonic sway, yaw and roll oscillations. *4th International Conference on Numerical Ship Hydrodynamics*, Washington D.C., U.S.A., pp.56-68.

Yang J.M., Matsui S., Tamashima M., Yamazaki R., (1994). On the mutual interaction between hull and propeller-rudder system of an obliquely sailing ship. *Transaction of the West-Japan Society of Naval Architects*, No.87, pp.61-79.

Yasukawa H., (2006). Simulations of ship maneuvering in waves: 1st report: turning motion. *Journal of the Japan Society of Naval Architects and Ocean Engineers*, No.4, pp.127-136.

Yasukawa H., (2008). Simulations of ship maneuvering in waves: 2nd report: zig-zag and stopping maneuvers. *Journal of the Japan Society of Naval Architects and Ocean Engineers*, No.7, pp.163-170.

Yasukawa H., Adnan F.A., (2006). Experimental study on wave-induced motions and steady drift forces of an obliquely moving ship. *Journal of the Japan Society of Naval Architects and Ocean Engineers*, No.3, pp.133-138.

Yasukawa H., Hirata N., Yonemasu I., Terada D., Matsuda A., (2015). Maneuvering simulation of a KVLCC2 tanker in irregular waves. *MASIM*, Newcastle, U.K.

Yasukawa H., Nakayama Y., (2009). 6-DOF motion simulations of a turning ship in regular waves. *MARSIM*, Panama City, Panama.

Yasukawa H., Yoshimura Y., (2015). Introduction of MMG standard method for ship maneuvering predictions. *Journal of Marine and Science Technology*, Vol.20, No.1, pp.37-52.

Yen T.G., Zhang S., Weems K., Lin W.M., (2010). Development and validation of numerical simulations for ship maneuvering in calm water and in waves. *28th Symposium on Naval Hydrodynamics*, Pasadena, U.S.A., pp.12-17.

Yeung R.W., Kim S.H., (1981). Radiation force on ships with forward speed. *3rd International Conference on Numerical Ship Hydrodynamics*, Paris, France, pp.499-515.

Yoon H.K, Rhee K.P. (2003). Identification of hydrodynamic coefficients in ship maneuvering equations of motion by estimation-before-modelling technique. *Ocean Engineering*, Vol.30, No.18, pp.2379-2404.

Yoshimura Y., Nomoto K., (1978). Modelling of manoeuvring behaviour of ships with a propeller ldling, boosting and reversing. *Journal of the Society of Naval Architects of Japan*, No.144, pp.57-69.

Young F., (1912). *Titanic*, Grant Richards LTD.

Yuan Z.M., He S., Paula K., Incecik A., Turan O., Boulougouris E., (2015). Ship-to-ship interaction during overtaking operation in shallow water. *Journal of Ship Research*, Vol.59, No.3, pp.1-16.

Yuan Z.M., Incecik A., Jia L., (2014). A new radiation condition for ships travelling with very low forward speed. *Ocean Engineering*, Vol.88, pp.298-309.

Yuan Z.M., Ji C.Y., Incecik A., Zhao W.H., Day S., (2016). Theoretical and numerical estimation of ship-to-ship hydrodynamic interaction effects. *Ocean Engineering*, Vol.121, pp.239-253.

Zhang X.G., Zou Z.J., (2011). Identification of response models of ship manoeuvring motion using support vector regression. *Journal of Shanghai Jiao Tong University*, Vol.45(4), pp.501-504.

Zhao C.B., Ma M., (2016). A hybrid 2.5 dimensional high speed strip theory method and its application to apply pressure loads to 3 dimensional full ship finite element models. *Journal of Ship Production and Design*, Vol.32, No.4, pp.216-225.

Zhou Z.M., Sheng Z.Y., Feng W.S., (1983). On manoeuvrability prediction for multipurpose cargo ship. *Ship Engineering*, Vol.6, pp.21-29.

Zhu D.J., (2015). Study on ship maneuvering and rolling prediction and course keeping control in waves. Shanghai Jiao Tong University, China.

Zou L., Larsson L., Orych M., (2010). Verification and validation of CFD predictions for a manoeuvring tanker. *Journal of Hydrodynamics*, Vol.22, No.5, pp.438-445.

Zou Z.J., (2006). Lecture notes on ship manoeuvring and seakeeping. Shanghai Jiao Tong University.

Zou Z.J., Söding H., (1994). A panel method for lifting potential flows around three dimensional surface piercing bodies. *20th Symposium on Naval Hydrodynamics*, Santa Barbara, California, U.S.A., pp.810-821.

Publications

The following papers have been published during the Ph.D. study. Some of them are not related to this work.

Conference:

S. He, A. Incecik: Lateral motions in shallow water by a 2.5D approach, *7th International Workshop on Ship Hydrodynamics,* Shanghai, 2011.

Z.M. Yuan, A. Incecik, **S. He**: Hydrodynamic interaction between two ships arranged side by side in shallow water, *33th International Conference on Ocean, Offshore and Arctic Engineering, OMAE2014-23325,* San Francisco, 2014.

P. Kellett, **S. He**, O. Turan, E. Boulougouris, A. Incecik: Manoeuvring prediction based on CFD generated derivatives. *9th International Workshop on Ship and Marine Hydrodynamics,* Glasgow, 2015.

Journal:

Z.M. Yuan, **S. He**, P. Kellett, A. Incecik, O. Turan, E. Boulougouris: Ship-to-ship interaction during overtaking operation in shallow water. *Journal of Ship Research* 59 (3), 1-16, 2015.

S. He, P. Kellett, Z.M. Yuan, A. Incecik, O. Turan, E. Boulougouris: Manoeuvring prediction based on CFD generated derivatives. *Journal of Hydrodynamics* 28 (2), 840-847, 2016.